

**Titre:** Rheological effects in film blowing of polyethylene blends  
Title:

**Auteur:** Yunli Fang  
Author:

**Date:** 2004

**Type:** Mémoire ou thèse / Dissertation or Thesis

**Référence:** Fang, Y. (2004). Rheological effects in film blowing of polyethylene blends [Thèse de doctorat, École Polytechnique de Montréal]. PolyPublie.  
Citation: <https://publications.polymtl.ca/7438/>

 **Document en libre accès dans PolyPublie**  
Open Access document in PolyPublie

**URL de PolyPublie:** <https://publications.polymtl.ca/7438/>  
PolyPublie URL:

**Directeurs de recherche:** Pierre Carreau, & Pierre Lafleur  
Advisors:

**Programme:** Non spécifié  
Program:

# NOTE TO USERS

This reproduction is the best copy available.

**UMI<sup>®</sup>**





UNIVERSITÉ DE MONTRÉAL

**RHEOLOGICAL EFFECTS IN FILM BLOWING OF  
POLYETHYLENE BLENDS**

YUNLI FANG

DÉPARTEMENT DE GÉNIE CHIMIQUE  
ÉCOLE POLYTECHNIQUE DE MONTRÉAL

THÈSE PRÉSENTÉE EN VUE DE L'OBTENTION  
DU DIPLÔME DE PHILOSOPHIAE DOCTOR  
(GÉNIE CHIMIQUE)

Juillet 2004



Library and  
Archives Canada

Bibliothèque et  
Archives Canada

Published Heritage  
Branch

Direction du  
Patrimoine de l'édition

395 Wellington Street  
Ottawa ON K1A 0N4  
Canada

395, rue Wellington  
Ottawa ON K1A 0N4  
Canada

*Your file    Votre référence*

*ISBN: 0-612-98177-0*

*Our file    Notre référence*

*ISBN: 0-612-98177-0*

#### NOTICE:

The author has granted a non-exclusive license allowing Library and Archives Canada to reproduce, publish, archive, preserve, conserve, communicate to the public by telecommunication or on the Internet, loan, distribute and sell theses worldwide, for commercial or non-commercial purposes, in microform, paper, electronic and/or any other formats.

The author retains copyright ownership and moral rights in this thesis. Neither the thesis nor substantial extracts from it may be printed or otherwise reproduced without the author's permission.

#### AVIS:

L'auteur a accordé une licence non exclusive permettant à la Bibliothèque et Archives Canada de reproduire, publier, archiver, sauvegarder, conserver, transmettre au public par télécommunication ou par l'Internet, prêter, distribuer et vendre des thèses partout dans le monde, à des fins commerciales ou autres, sur support microforme, papier, électronique et/ou autres formats.

L'auteur conserve la propriété du droit d'auteur et des droits moraux qui protègent cette thèse. Ni la thèse ni des extraits substantiels de celle-ci ne doivent être imprimés ou autrement reproduits sans son autorisation.

---

In compliance with the Canadian Privacy Act some supporting forms may have been removed from this thesis.

Conformément à la loi canadienne sur la protection de la vie privée, quelques formulaires secondaires ont été enlevés de cette thèse.

While these forms may be included in the document page count, their removal does not represent any loss of content from the thesis.

Bien que ces formulaires aient inclus dans la pagination, il n'y aura aucun contenu manquant.

UNIVERSITÉ DE MONTRÉAL

ÉCOLE POLYTECHNIQUE DE MONTRÉAL

Cette thèse intitulée:

**RHEOLOGICAL EFFECTS IN FILM BLOWING OF  
POLYETHYLENE BLENDS**

présentée par : YUNLI FANG

en vue de l'obtention du diplôme de : Philosophiae Doctor

a été dûment acceptée par le jury d'examen constitué de:

M. BERTRAND François, Ph.D., président

M. CARREAU Pierre J., Ph.D., membre et directeur de recherche

M. LAFLEUR Pierre G., Ph.D., membre et codirecteur de recherche

M. AJJI Abdellah, Ph.D., membre

M. CAMPBELL Gregory, Ph.D., membre

To my parents

To my family

## ACKNOWLEDGEMENTS

I am deeply grateful to my dissertation director Professor Pierre J. Carreau and co-director Professor Pierre G. Lafleur for providing me with the opportunity to study under their guidance. I am also very indebted to them for their patience, encouragement, financial support and supervision in this work. Without their extensive and comprehensive help, this dissertation would not have been possible

I am also grateful to all my fellow graduate students and staff of the “Centre de Recherche Appliquée sur les Polymères (CRASP)” for their assistance and friendship. I would like to give my thanks Mr. Luc Parent, Mr. Frédéric Cotton and Mr. Jacques Beausoleil for their considerable and continuous assistance with all aspects of film blowing and rheological experiments carried out. I also would like to acknowledge my co-workers, Mr. Salah Ymmel and Dr. Seungoh Kim, for their help.

I would like to express my sincere thanks to my parents for their continuous encouragement and my sister Cheng Fang, my brother-in-law Yusuo Chang for their kindly help. Finally, I would like to extend my appreciation to my wife, Huimin Tian, and my lovely daughter, Wendy Fang, for their love, care, passion and understanding.

## RÉSUMÉ

L'extrusion soufflage est l'un des principaux procédés de mise en oeuvre des polymères. Toutefois, les phénomènes qu'il entraîne sont encore mal compris, en particulier l'influence des propriétés rhéologiques des résines. Aussi loin que l'on remonte dans le passé, il n'y a pas dans la littérature d'équation constitutive qui peut décrire, d'une manière satisfaisante, les effets rhéologiques observés dans le procédé de soufflage de gaine. La modélisation du procédé reste surtout empirique. Tout d'abord, il y a lieu de noter que le procédé d'extrusion soufflage de film est un procédé complexe, fortement affecté par des effets simultanés du transfert thermique, de la rhéologie du fluide, de l'aérodynamique et de la cinématique de la bulle. Ensuite, on doit disposer de données sûres et complètes pour établir des modèles ; lesquels sont peu nombreux dans la littérature. L'objectif général de cette étude est donc de recueillir plus de données sûres pour développer des modèles.

En général, les effets de mémoire du polymère sont négligés et seuls les écoulements en sortie de filière sont considérés. Par contre, la plupart des études publiées sont consacrées à des mesures élongationnelles et uniaxiales. Cependant, le polymère fondu est non isotherme dès la sortie de la filière et soumise à un étirage élongationnel biaxial non uniforme. En utilisant le principe de superposition temps-température, on peut évaluer la viscosité élongationnelle le long de la bulle, pour une même température de référence.

Les instabilités de bulle, durant le procédé d'extrusion soufflage, ont été évaluée pour trois échantillons de polyéthylène de grade commercial ; le polyéthylène linéaire obtenu en présence d'un catalyseur à base de métallocène (LmPE), le polyéthylène basse densité linéaire (LLDPE) et le polyéthylène basse densité linéaire (LDPE). Des critères sûrs et objectifs, pour décrire les différentes instabilités de la bulle, ont été

proposés. On peut citer notamment l'instabilité hélicoïdale, l'instabilité de la hauteur de la ligne de figeage et le « draw resonance ». Des détails dynamiques de chaque type d'instabilité ont été soigneusement investigués en fonction du temps sur un large domaine de valeurs des taux d'étirage (TUR) et du taux de gonflage (BUR) et du FLH. De plus, les effets de la température du fluide et du débit massique sur les dynamiques des instabilités de bulle ont été discutés. Il est montré que le nouveau système permet d'obtenir les caractéristiques principales de toutes les instabilités de façon quantitative.

Le comportement rhéologique des différents polyéthylènes (PEs) avec de différentes structures moléculaires a été étudié, d'une manière détaillée, en utilisant un équipement complet. La viscosité élongationnelle biaxiale, non isotherme et non uniforme (NNBEV) a été déterminée. La technique de NNBEV a été confirmée en utilisant un échantillon de LDPE à différentes conditions opératoires. Des essais expérimentaux ont montré que la NNBEV est approximativement une fonction unique de la vitesse de déformation. Elle est indépendante des conditions opératoires. Ceci confirme la validité des hypothèses et les techniques utilisées pour le calcul de la NNBEV.

Les viscosités élongationnelles uniaxiales des différents PEs ont été obtenues dans le but de les relier à leur mise en œuvre « leur transformabilité ». La viscosité élongationnelle uniaxiale n'a pas pu être reliée directement à la stabilité de la bulle. La courbe de variation de  $\text{Log } G'$  en fonction de  $\text{Log } G''$  est indépendante de la température, pour tous les polymères étudiés. De plus, durant l'extrusion soufflage, la bulle est d'autant plus stable que la valeur de  $G'$  est plus large. En étudiant les rapports de Trouton pour le polyéthylène haute densité (HDPE), LLDPE, LDPEa, LDPEb et le polyéthylène branché polymérisé en présence d'un catalyseur au métallocène (mPE) en fonction de la vitesse de déformation, il est trouvé dans tous les cas que le rapport de Trouton que la valeur limite de 3, comme attendu pour les fluides newtoniens. Les rapports de Trouton pour LDPEa et LDPEb sont beaucoup plus élevés que ceux des



HDPE, LLDPE et mPE. Ceci laisse à penser que les valeurs élevées du rapport de Trouton sont intimement reliées à la stabilité de la bulle. Il apparaît, donc, que l'information sur la viscosité élongationnelle est pour le moins plus importante que les propriétés du fluide en cisaillement.

Les propriétés thermiques et rhéologiques de mélanges de PE ont été investiguées en vue de déterminer la miscibilité/l'immiscibilité et offrent des données rhéologiques à utiliser dans les calculs durant le procédé d'extrusion soufflage. Il est difficile de déterminer la miscibilité de mélanges de PE par les méthodes usuelles, à cause du faible contraste entre les phases et la faible différence des températures de transition vitreuse des PE. Les résultats des thermogrammes de DSC ont montrés que le LmPE, copolymère de l'éthylène avec l'hexène, est immiscible avec les deux LDPEs à l'état cristallin, alors que la résine mPE branchée (BmPE), copolymère de l'éthylène avec l'octène, est miscible quand il est mélangé avec les deux LDPE. Ceci suggère que l'augmentation de la longueur des ramifications courtes dans mPE favorise la miscibilité des mélanges mPE/LDPE. Les propriétés viscoélastiques linéaires confirment l'immiscibilité des mélanges de LmPE avec les résines de LDPE, à l'état fondu. De plus, le modèle en émulsion de Palierne montre de bonnes prédictions des données des propriétés de viscoélasticité linéaire, concernant les mélanges de PE miscibles et immiscibles. Comme attendu, les données aux faibles fréquences ont montré une influence claire de la tension interfaciale sur le module élastique des mélanges immiscibles.

La miscibilité/immiscibilité des mélanges mPE/LDPE ont été ensuite confirmé en utilisant les mesures en ligne de la biréfringence durant le procédé d'extrusion du film. Les résultats expérimentaux montrent qu'avant le début de la cristallisation la variation de la biréfringence des mélanges du BmPE avec le LDPE-2 avec la composition est linéaire, suggérant ainsi la miscibilité des deux résines en toute proportion. Cependant, la variation de la biréfringence des mélanges de LmPE avec

LDPE-1 en fonction de la composition est non linéaire, ce qui indiquerait une immiscibilité entre les résines de LmPE et de LDPE-2.

## ABSTRACT

Film blowing is a major plastic transformation process and yet, the phenomena involved are far from being understood, mainly with respect to the influence of the rheological properties of the resins. As far as we are aware, no known constitutive equation can satisfactorily describe the rheological effects observed in film blowing and modeling of the process remains an empirical exercise. First of all, film blowing is a very complex process with simultaneous effects of heat transfer, melt rheology, aerodynamics and free surface kinematics. Secondly, one needs complete and reliable data, which are rather sparse in the open literature, to assess the different models. Therefore, the general objective of this study is to offer more reliable data for modeling purposes.

Due to the fact that polymer has fading memory, only flows after die exit are concerned. Therefore, most of the study in the literature focused on uniaxial elongational measurement. However, the polymer melt after die exit experiences highly non-isothermal, non-uniform biaxial elongational stretch during film blowing process. By using time-temperature superposition principle, we may shift and compare the elongational viscosity along the bubble to the same reference temperature.

The bubble instabilities during film blowing were critically evaluated using three commercial film-grade polyethylenes, linear metallocene catalyzed polyethylene (LmPE), linear low density polyethylene (LLDPE) and low density polyethylene (LDPE). Reliable and objective criteria for differentiating various bubble instabilities such as draw resonance, helicoidal instability, frost line height instability are proposed by using a new in-line scanning camera system. Detailed dynamics of each bubble instability was carefully investigated as a function of time in a broad range of the take-up ratio (TUR), blow-up ratio (BUR) and frost line height (FLH). In addition, effects of

melt temperature and mass flow rates on dynamics of the bubble instabilities are also discussed. It was found that the new system could capture the main characteristics of all bubble instabilities quantitatively and offer a better and easier way to obtain more reliable stability data.

The rheological behavior of different polyethylenes (PEs) with different molecular structures has been extensively studied using fully equipped instrument. The non-isothermal non-uniform biaxial elongational viscosity (NNBEV) has been determined. The technique to NNBEV was further confirmed using one LDPE at different operating conditions. Experimental trials showed that NNBEV is approximately a unique function of the deformation rate and independent of operating conditions, confirming the validity of the assumptions and technique used for NNBEV calculation.

The complex, shear and uniaxial elongational viscosities of different PEs were also obtained in order to be correlated to their processabilities. The uniaxial elongational viscosity can not be correlated to the bubble stability directly.  $\log G'$  versus  $\log G''$  plot was observed to be virtually independent of temperature for all the polymers investigated. Furthermore, the larger the  $G'$  value was, the more stable the bubble was during film blowing. By investigating the Trouton ratios for the high density polyethylene (HDPE), LLDPE, LDPEa, LDPEb and metallocene catalyzed polyethylene (mPE) versus deformation rate, we found that in all cases, the ratio exceeds the limiting value of 3, expected for Newtonian fluids. The Trouton ratios of the LDPEa and LDPEb are much larger than those of the HDPE, LLDPE and mPE. The high values of the Trouton ratio are believed to be closely related to the bubble stability in film blowing. Hence, it appears that information on the elongational viscosity is at least as important information as the shear flow properties.

The thermal and rheological properties of the PE blends have been investigated in order to determine the miscibility/immiscibility and offer rheological data for the calculation during film blowing process. Due to the low contrast, low and closer glass transition temperatures of PE blend components, it is quite difficult to determine the blend miscibility using routine ways. Our DSC results showed that the LmPE based on hexene comonomer is immiscible with both LDPEs in crystalline states whereas the branched mPE (BmPE) based on octene comonomer is miscible with the LDPEs. This suggests that increasing the length of short chains in mPEs can promote the miscibility of mPE/LDPE blends. The linear viscoelastic properties confirmed the immiscibility of the LmPE with the LDPEs in the molten state and miscibility of BmPE with LDPEs. In addition, the Palierne emulsion model showed good predictions of the linear viscoelastic data for both miscible and immiscible polyethylene blends. However, as expected the low frequency data showed a clear influence of the interfacial tension on the elastic modulus of the blends for the immiscible blends. This miscibility/immiscibility of mPE/LDPE blend was further confirmed using inline birefringence measurement during film blowing. Experimental data show that before the crystallization starts the birefringence of the BmPE/LDPE-2 blends is a linear function of blend composition, suggesting miscibility of the BmPE/LDPE-2 blends. However, the birefringence of LmPE/LDPE-1 is not a linear function of blend composition, which indicates the existence of form birefringence, suggesting immiscibility of the LmPE/LDPE-1 blends.

## CONDENSÉ EN FRANÇAIS

L'extrusion soufflage est un important procédé de transformation des matériaux plastiques et les phénomènes qu'il entraîne sont loin d'être compris, particulièrement l'influence des propriétés rhéologiques des résines de polymère. Aussi loin que l'on remonte dans le passé, il n'y a pas dans la littérature d'équation constitutive qui peut décrire, d'une manière satisfaisante, les effets rhéologiques observés dans le procédé de soufflage de gaine et la modélisation du procédé reste empirique. De prime abord, il y a lieu de noter que le procédé d'extrusion soufflage de film est un procédé complexe, fortement affecté par des effets simultanés du transfert thermique, de la rhéologie du fluide, de l'aérodynamique et de la cinématique de la bulle. En second lieu, on doit disposer de données sûres et complètes pour établir des modèles ; lesquels sont peu nombreux dans la littérature. L'objectif général de cette étude est donc d'offrir plus de données sûres pour développer des modèles.

En général, les effets de mémoire du polymère sont négligés et seuls les écoulements en sortie de filière sont considérés. Par contre, la plupart des études publiées sont consacrées à des mesures élongationnelles et uniaxiales. Cependant durant le procédé d'extrusion soufflage de gaine, la bulle est non isotherme dès la sortie de la filière et soumise à un étirage élongationnel biaxial non uniforme. En utilisant le principe de superposition temps- température, on peut évaluer la viscosité élongationnelle le long de la bulle, pour une même température de référence. Le premier article est le premier essai pour valider cette idée.

Le premier article est consacré aux effets rhéologiques sur la cinématique et la dynamique de la bulle gonflée pour différentes résines de polyéthylène dont deux de polyéthylène basse densité (LDPEa, LDPEb), un polyéthylène haute densité (HDPE), un polyéthylène basse densité linéaire (LLDPE) et un polyéthylène polymérisé en

présence d'un catalyseur à base d'un métallocène (mPE). Pour l'étude, une unité d'extrusion soufflage de laboratoire complètement équipée a été utilisée. Des courbes maîtresse pour les cinq résines ont été déterminées, en utilisant le principe de superposition temps –température. Les viscosités complexes et en cisaillement des différentes résines ont été étudiées. La règle de Cox-Merz s'applique bien dans le cas de mPE et LLDPE. Cependant, elle montre une déviation pour les résines de LDPE et HDPE. La stabilité de la bulle de mPE a été étudiée et comparée avec les résultats des travaux antérieurs de notre laboratoire (Ghaneh-Fard et al., 1997). Les bulles de mPE et de LLDPE étaient beaucoup plus instables comparées à celles des LDPE et HDPE, durant l'extrusion soufflage. Les viscosités élongationnelles uniaxiales des trois résines, HDPE, LDPEb et mPE, ont été déterminées à l'aide de deux filières convergentes et des techniques d'analyse de Cogswell et Binding. La viscosité élongationnelle uniaxiale n'a pas pu être reliée la stabilité de la bulle. Les profils de vitesse et du diamètre des bulles de LDPEb et mPE ont été utilisés pour déterminer la vitesse de déformation. La vitesse et le diamètre de la bulle ont été mesurés, respectivement, au moyen d'un *vélocimètre* au Laser Doppler (VLD) et d'une caméra vidéo. La technique de mesure de la biréfringence a été également présentée. Les données en ligne de biréfringence ont été utilisées pour calculer les contraintes le long de la bulle des résines de mPE et de LDPEb. Pour la résine de mPE, la valeur de biréfringence observée est très faible dans la zone fondue (fluide) et augmente rapidement dans la zone de cristallisation. Les contraintes dans les directions longitudinale (MD) et transversale (TD) pour les résines de mPE et de LDPEb sont similaires dans la zone de striction. Cependant, elles sont assez différentes dans la zone d'expansion. Il n'y pas de relation simple entre les contraintes et les vitesses de déformation dans le procédé d'extrusion soufflage. La courbe de variation de  $\text{Log } G'$  en fonction de  $\text{Log } G''$  est indépendante de la température, pour tous les polymères étudiés. Durant l'extrusion soufflage, la bulle est d'autant plus stable que la valeur de  $G'$  est plus large. Les variations du rapport de Trouton pour HDPE, LLDPE, LDPEa, LDPEb et mPE en fonction de la vitesse de déformation ont été rapportées. Dans tous les cas, le rapport dépasse la valeur de 3,

attendue pour les fluides newtoniens. Les rapports de Trouton pour LDPEa et LDPEb sont beaucoup plus élevés que ceux des HDPE, LLDPE et mPE. Ceci laisse à penser que les valeurs élevées du rapport de Trouton sont intimement reliées à la stabilité de la bulle. Il apparaît, donc, que l'information sur la viscosité élongationnelle est pour le moins plus importante que les propriétés du fluide en cisaillement.

Le premier article a quand même conduit à quelques conclusions qualitatives. Les résultats ont été évalués, en détails, pour améliorer la qualité des données. Dans le second article, une nouvelle méthode en ligne (« inline ») est introduite pour mesurer quantitativement la stabilité de la bulle.

Dans cet article, la performance d'un nouveau système de balayage par caméra vidéo, en ligne, pour l'étude d'instabilité de bulles dans l'extrusion soufflage a été évaluée d'une manière critique en utilisant trois résines de polyéthylène, de grade commercial, LmPE, LLDPE et LDPE. Des critères objectifs et sûrs pour différents types d'instabilité incluant le « draw resonance », l'instabilité hélicoïdale et l'instabilité de la hauteur de la ligne de figeage (instabilité du FLH), ont été proposés en utilisant un nouveau système. Des détails dynamiques de chaque type d'instabilité ont été soigneusement en fonction du temps sur un large domaine de valeurs des taux d'étirage (TUR) et du taux de gonflage (BUR) et du FLH. De plus, les effets de la température du fluide et du débit massique sur les dynamiques des instabilités de bulle ont été discutés. Il est montré que le nouveau système permet d'obtenir les caractéristiques principales de toutes les instabilités de façon quantitative.

Après avoir évalué, d'une manière satisfaisante, la mise en œuvre des différents polyéthylènes, la technique proposée dans le premier article a été réexaminée, pour calculer la viscosité élongationnelle biaxiale, non uniforme et non isotherme (NNBEV). La NNBEV à la température de référence de 175°C évaluée en utilisant LDPE-1, à différents BUR, TUR et FLH a été rapportée dans l'article 4. Les résultats montrent que



la NNBEV est approximativement une fonction unique de la vitesse de déformation, confirmant la validité des hypothèses et de la technique utilisée pour le calcul du NNBEV. Donc, l'utilisation de l'unité d'extrusion soufflage comme un rhéomètre en ligne (« inline ») est possible. L'article 4 présente les données rhéologiques en utilisant les mesures en ligne durant l'extrusion soufflage pour les polyéthylènes de différentes structures ainsi que leurs mélanges. Cependant, il est indispensable d'investiguer la miscibilité des mélanges avant d'examiner leur comportement en extrusion soufflage. Toutefois, le faible contraste en microscopie et les températures de transition vitreuse faibles et rapprochées des mélanges de PE rendent l'étude de leur miscibilité, par les méthodes usuelles, très difficile. Le troisième article est principalement dédié à la miscibilité et l'immiscibilité des mélanges de PE. De plus, il offre des données rhéologiques pour le calcul de la NNBEV présentée dans l'article 4.

Dans l'article 3, deux polyéthylènes polymérisés en présence d'un catalyseur à base de métallocène (les résines mPE) et deux polyéthylènes basse densité (les résines LDPE) ainsi que leurs mélanges ont été étudiés, utilisant la calorimétrie différentielle (DSC) et la rhéométrie. Les résultats de DSC ont montré que la résine mPE linéaire (LmPE), copolymère de l'éthylène avec l'hexène, est immiscible avec les deux LDPEs à l'état cristallin, alors que la résine mPE branchée (BmPE), copolymère de l'éthylène avec l'octène, est miscible dans les deux LDPEs. Ceci suggère que l'augmentation de la longueur des ramifications courtes dans mPE favorise la miscibilité des mélanges mPE/LDPE. Les propriétés viscoélastiques linéaires confirment l'immiscibilité des mélanges de LmPE avec les résines de LDPE. De plus, le modèle en émulsion de Palierne montre de bonnes prédictions des données des propriétés de viscoélasticité linéaire, concernant les mélanges de PE miscibles et immiscibles. Comme attendu, les données aux faibles fréquences ont montré une influence claire de la tension interfaciale sur le module élastique des mélanges immiscibles.

De cet article, deux systèmes de mélanges, LmPE/LDPE-1 et BmPE/LDPE-2, sont soupçonnés d'être immiscible et miscible, respectivement. Cette conclusion a été confirmée par les mesures de biréfringence, rapportées dans l'article 4. Les résultats expérimentaux montrent qu'avant le début de la cristallisation la variation de la biréfringence des mélanges du BmPE avec le LDPE-2 avec la composition est linéaire, suggérant ainsi la miscibilité des deux résines en toute proportion. Cependant, la variation de la biréfringence des mélanges de LmPE avec LDPE-1 en fonction de la composition est non linéaire, ce qui indiquerait une immiscibilité entre les résines de LmPE et de LDPE-2.

## TABLE OF CONTENTS

<i>Dédiace</i>	<i>10</i>
ACKNOWLEDGEMENTS .....	V
RÉSUMÉ.....	VI
ABSTRACT.....	X
CONDENSÉ EN FRANÇAIS .....	XIII
TABLE OF CONTENTS.....	XVIII
LIST OF TABLES .....	XXII
LIST OF FIGURES .....	XXIII
NOMENCLATURE.....	XXIX
INTRODUCTION .....	1
CHAPTER 1. LITERATURE REVIEW .....	5
1.1. Modeling Film Blowing Process.....	5
1.1. Rheological Properties and Their Effects of on Film Process and Film Properties .....	10
1.1.1. Strain, Strain Rates and Stress .....	10
1.1.2. Molecular Structure and Elongational Viscosities.....	12
1.1.2.1. Uniaxial Elongational Viscosity .....	12
1.1.2.2. Biaxial Elongational Viscosity.....	14
1.2. Bubble Stability.....	15
1.3. Birefringence Measurements .....	17
1.4. PE Blends.....	18
CHAPTER 2. OBJECTIVES AND ORGANIZATION OF THE ARTICLES.....	22
2.1. Objectives.....	22
2.2. Organization of the Articles.....	23
CHAPTER 3. RHEOLOGICAL EFFECTS OF POLYETHYLENES IN FILM BLOWING.....	27
3.1. Introduction.....	28
3.1.1. Determination of Stresses in Film.....	29

3.1.2.	Determination of Non-uniform Biaxial Elongational Viscosity .....	31
3.1.3.	Bubble Stability .....	32
3.2.	Experimental .....	33
3.2.1.	Materials .....	33
3.2.2.	Film Blowing In-line Measurements .....	33
3.2.3.	Rheological Measurements .....	34
3.3.	Results and Discussion .....	35
3.3.1.	Complex and Shear Viscosities .....	35
3.3.2.	Apparent Uniaxial Elongational Viscosity .....	36
3.3.3.	Temperature, Diameter, Velocity and Thickness Profiles .....	37
3.3.4.	Strain Rates .....	38
3.3.5.	Birefringence and Stresses .....	40
3.3.6.	Non-uniform Biaxial Elongational Viscosity and Deformation Rate .....	41
3.3.7.	Bubble Stability .....	41
3.3.8.	The Role of Rheology in Film Blowing .....	42
3.3.9.	$G'$ , $G''$ and Relationship to Bubble Stability .....	42
3.3.10.	Elongational Behavior .....	43
3.4.	Concluding Remarks .....	44
3.5.	References .....	46
CHAPTER 4. DYNAMICS AND CRITERIA FOR BUBBLE INSTABILITIES IN A SINGLE LAYER FILM BLOWING EXTRUSION .....		69
4.1.	Introduction .....	70
4.2.	Experimental .....	75
4.2.1.	Film Blowing Unit .....	75
4.2.2.	In-line Measurements .....	76
4.2.3.	Polymers Studied .....	78
4.3.	Characteristics of various bubbles .....	79
4.4.	Results and Discussion .....	85
4.4.1.	Dynamics of Unstable Bubbles .....	85

4.4.2.	Quantification of Stable Region in Bubble Stability Map .....	87
4.5.	Conclusions.....	90
4.6.	References .....	91
CHAPTER 5. THERMAL AND RHEOLOGICAL PROPERTIES OF MPE/LDPE		
	BLENDS .....	128
5.1.	Introduction.....	129
5.2.	Experimental .....	131
5.2.1.	Materials and Blend Preparation.....	131
5.2.2.	Thermal Analysis .....	132
5.2.3.	Rheological Measurements .....	133
5.3.	Results and Discussion.....	133
5.3.1.	Thermal Properties .....	133
5.3.2.	Rheological Properties .....	135
5.4.	Conclusions.....	141
5.5.	References .....	143
CHAPTER 6. PROPERTIES OF MPE/LDPE BLENDS IN FILM BLOWING .....		
6.1.	Introduction.....	164
6.2.	Experimental .....	167
6.2.1.	Materials.....	167
6.2.2.	Blending Procedure.....	168
6.2.3.	Film Blowing Unit .....	168
6.2.4.	Birefringence and Stress Optical Rule (SOR).....	169
6.3.	Results and Discussion.....	171
6.3.1.	LDPE-1 .....	171
6.3.2.	LmPE/LDPE-1 Blends .....	175
6.3.3.	BmPE/LDPE-2 Blends.....	177
6.4.	Concluding Remarks.....	178
6.5.	References .....	180
CHAPTER 7. SCIENTIFIC CONTRIBUTIONS.....		
		200

CHAPTER 8. CONCLUSIONS AND RECOMMENDATIONS .....	201
8.1.    Conclusions.....	201
8.2.    Recommendations for Future Work.....	203
REFERENCES.....	204

## LIST OF TABLES

Table 3.1. Materials used in this study and main characteristics.....	48
Table 3.2. Geometries of the dies for the piston-driven capillary rheometer (INSTRON) and for the in-line capillary rheometer (mounted on a Killion extruder).....	49
Table 4.1. Processing conditions for a mass flow rate of 2.0 kg/h. ....	93
Table 4.2. Molecular parameters of polymers used .....	94
Table 4.3. Summary of proposed criteria for bubble instabilities.....	95
Table 5.1. Polymers used in this study and their main characteristics.....	145
Table 5.2. Values of $\alpha/R_V$ for the best fits of the Palierne model predictions. ....	146
Table 6.1. Polymers used and their main characteristics .....	182
Table 6.2. Activation energy and pressure inside the bubble of LmPE, BmPE, LDPE-1, LDPE-2 and their blends.....	183

## LIST OF FIGURES

## Chapter 3

Figure 3. 1. Comparison of complex and steady shear viscosity data for five resins at 200°C. ....	50
Figure 3. 2. Temperature shift factors at a reference temperature of 170°C.....	51
Figure 3. 3. Apparent uniaxial elongational viscosity versus elongational rate at 200°C. (a) calculated from two different techniques using two different dies for LDPEb.....	52
Figure 3. 4. Bubble temperature along the axial distance for mPE and LDPEb. The mass flow rate = 3.0 kg/h, TUR = 13.6, BUR = 2.0, temperature = 200°C.....	54
Figure 3. 5. Comparison of bubble diameter profile of LDPE with 1% colorant measured both by the line-scan camera method and by the traditional video method (operating conditions: mass flow rate = 5.0 kg/h, BUR = 2.7, TUR = 5.0, temperature = 200°C).....	55
Figure 3. 6. Bubble velocity profiles measured by the video method for LDPE (operating conditions: mass flow rate = 5.0kg/h, BUR = 2.0, TUR = 10, temperature = 200°C).....	56
Figure 3. 7. Bubble diameter and velocity profiles along the axial distance for (a) mPE and (b) LDPEb. The film blowing conditions are the same as in Figure 3.4.	57
Figure 3. 8. Strain rates in MD and TD along the axial distance for mPE and LDPEb. The film blowing conditions are the same as in Fig. 3.4. ....	59
Figure 3. 9. (a) Birefringence along the axial distance for LDPEb and mPE. (b) Stress profiles along the axial distance for mPE and LDPEb. The film blowing conditions are the same as in Fig. 3.4. ....	60
Figure 3. 10. Deformation rate and non-uniform biaxial elongational viscosity along the bubble for LDPEb and mPE. The film blowing conditions are the same as in Fig. 3.4. ....	62



Figure 3.11. Biaxial elongational viscosity versus deformation rate for mPE and LDPEb at reference temperature of 170°C. ....	63
Figure 3.12. Bubble stability behavior of mPE and LLDPE under the extrusion temperature of 200°C, mass flow rate = 5.4 kg/h (He: Helical; PH: Partially Helical; FI: Frost Line Height Instable; BI: Bubble Instable); (a) TUR = 4.7 (b) TUR = 6.2.....	64
Figure 3.13. $G'$ versus $G''$ for all polyethylenes at five different temperatures: (a) LDPEb. (b) HDPE, LLDPE, LDPEa, LDPEb, and mPE.....	66
Figure 3. 14. Comparison of the Trouton ratio for five polyethylenes at a reference temperature of 170°C. ....	68

## Chapter 4

Figure 4. 1. Schematic views of typical bubble instabilities (a) draw resonance (DR), (b)FLH combined with DR, (c) FLH instability, (d) Helicoidal instability. ....	96
Figure 4. 2. Variations of BUR and air cooling rate as functions of TUR while holding an approximately constant similar FLH of 180mm (LDPE, targeted BUR around 1.5). ....	97
Figure 4. 3. (a) Schematic view of the new system and (b) geometrical variables of bubble and die. ....	98
Figure 4. 4. Typical responses for a stable bubble of LmPE (FLH = 180 mm, BUR = 1.5, TUR = 42); a) radius variations, b) variations of eccentricity and rotation angle, c) variations of pressure inside the bubble and radius ratio as a function of time. (FLH = 180 mm, BUR = 1.5, TUR = 18.6).....	100
Figure 4. 5. Typical responses for draw resonance of LDPE (FLH = 100 mm, BUR = 1.0, TUR = 18.6); a) radius variations and radius ratio, b) variations of eccentricity and rotation angle, c) variations of pressure inside the bubble and radius as a function of time. ....	103
Figure 4. 6. Typical responses for helicoidal instability of LLDPE (FLH = 180 mm, BUR = 2.0, TUR = 30.5); a) radius variations and rotation angle, b)	

eccentricity and radius ratio, c) variations of pressure inside the bubble and eccentricity as a function of time. ....	106
Figure 4. 7. Typical responses for FLH instability of LmPE (FLH = 250 mm, BUR = 2.2, TUR = 18.6); a) variations of eccentricity and rotation angle, b) radius variations and radius ratio, c) variations of pressure inside the bubble and rotational angle as functions of time. ....	109
Figure 4. 8. Schematic views of additional bubble instability from two different points of view.....	112
Figure 4. 9. Responses for additional bubble instability of LmPE (FLH = 180 mm, BUR = 1.98, TUR = 6); a) radius variations and radius ratio, b) variations of eccentricity and rotation angle as functions of time.....	113
Figure 4. 10. Evolution of draw resonance as a function of TUR of LDPE (FLH = 100 mm, BUR = 0.9, $Q = 2.0 \pm 0.1$ kg/h, $T_{melt} = 185^{\circ}\text{C}$ ). ....	115
Figure 4. 11. Variations of amplitude and periodicity for draw resonance as functions of TUR. All conditions are the same as in Fig. 4.10. ....	116
Figure 4. 12. Radius ratio and eccentricity as functions of time with various TUR values under helicoidal instability of LLDPE. (FLH = 180 mm, BUR = 2.0, $Q = 2.0 \pm 0.1$ kg/h, $T_{melt} = 186^{\circ}\text{C}$ ).....	117
Figure 4. 13. Rotational angle and radius variations as functions of TUR under helicoidal instability of LDPE. All conditions are the same as in Fig. 4.12.	118
Figure 4. 14. Bubble stability map for LDPE as functions of BUR and TUR (FLH = 180 mm, $Q = 2.0 \pm 0.1$ kg/h, $T_{melt} = 185^{\circ}\text{C}$ ). ....	119
Figure 4. 15. Bubble stability map for LLDPE as functions of BUR and TUR (FLH = 180 mm, $Q = 2.0 \pm 0.1$ kg/h, $T_{melt} = 186^{\circ}\text{C}$ ).....	120
Figure 4. 16. Bubble stability map for LLDPE as functions of BUR and TUR (FLH = 250 mm, $Q = 2.0 \pm 0.1$ kg/h, $T_{melt} = 187^{\circ}\text{C}$ ). ....	121
Figure 4. 17. Typical example of graphical quantification of stable region in the bubble stability map of LLDPE. All conditions are the same as in Fig. 4.15.....	122

Figure 4. 18. Summary of bubble stability of samples used as a function of FLH ( $Q = 2.0 \pm 0.1$ kg/h, $T_{\text{melt}} = 186 \sim 187^\circ\text{C}$ ). .....	123
Figure 4. 19. Bubble stability map of LDPE as functions of BUR and TUR (FLH = 250mm, $Q = 4.5 \pm 0.1$ kg/h, $T_{\text{melt}} = 185^\circ\text{C}$ ). .....	124
Figure 4. 20. Summary of bubble stability map of LDPE as a function of mass flow rate (FLH = 250 mm, $T_{\text{melt}} = 185^\circ\text{C}$ ). .....	125
Figure 4. 21. Bubble stability map of LDPE as functions of BUR and TUR (FLH = 250 mm, $Q = 2.0 \pm 0.1$ kg/h, $T_{\text{melt}} = 204^\circ\text{C}$ ). .....	126
Figure 4. 22. Summary of bubble stability map of LDPE as a function of melt temperature (FLH = 250 mm, $Q = 2.0 \pm 0.1$ kg/h). .....	127

## Chapter 5

Figure 5. 1. DSC thermograms for the LmPE, LDPE-1 and their blends: (a) Heating,..	147
Figure 5. 2. DSC thermograms for the LmPE, LDPE-2 and their blends: (a) Heating,..	148
Figure 5.3. Composition dependence of the melting temperature, $T_m$ , and the crystallization temperature, $T_c$ , for (a) LmPE/LDPE-1, (b) LmPE/LDPE-1 blends. ....	149
Figure 5. 4. DSC thermograms for the BmPE, LDPE-1 and their blends: (a) Heating, .	150
Figure 5. 5. DSC thermograms for the BmPE, LDPE-2 and their blends: (a) Heating, .	151
Figure 5.6. Composition dependence of the melting temperature, $T_m$ , and the crystallization temperature, $T_c$ , for (a) BmPE/LDPE-1 blends and (b) BmPE/LDPE-2 blends. ....	152
Figure 5.7. Complex viscosity versus frequency for LmPE/LDPE-1 blends at $175^\circ\text{C}$ (solid line is curve fitting using Carreau-Yasuada model). .....	153
Figure 5. 8. Composition dependence on complex viscosity at different frequencies for: (a) LmPE/LDPE-1, (b) LmPE/LDPE-2, (c) BmPE/LDPE-1 and (d) BmPE/LDPE-2 blends at $150^\circ\text{C}$ . ....	154
Figure 5.9. Zero-shear viscosity versus blend composition for the LmPE/LDPE-1, LmPE/LDPE-2, BmPE/LDPE-1, BmPE/LDPE-2 blends at $200^\circ\text{C}$ . .....	156

Figure 5. 10. Weighted relaxation spectra of (a) LmPE/LDPE-1 blends at 150°C (b) BmPE/LDPE-1 blends at 175°C. ....	157
Figure 5. 11. Storage modulus $G'$ versus frequency of (a) LmPE/LDPE-1, (b) BmPE/LDPE-2 blends at 175°C. ....	158
Figure 5. 12. Sensitivity of Palierne model predictions of $G'$ for the (10/90)LmPE/LDPE-1 blend to different values of $\alpha/R_V$ at 175°C. ....	160
Figure 5. 13. Sensitivity of Palierne model predictions of $G'$ for the 20/90 blends to different values of $\alpha/R_V$ at 175°C: (a) LmPE/LDPE-1, (b) LmPE/LDPE-2, (c) BmPE/LDPE-1 and (d) BmPE/LDPE-2 blends. ....	161

## Chapter 6

Figure 6. 1. Diameter and temperature profiles of the LDPE-1 at a mass flow rate of 2.0 kg/h and die temperature of 200°C for different other operation conditions. ....	184
Figure 6. 2. Velocity profiles of the LDPE-1 for the conditions indicated in Fig. 6.1. ...	185
Figure 6.3. Strain rates of the LDPE-1 in machine and transverse directions for the conditions indicated in Fig. 6.1 (T = TUR, B = BUR, F = FLH). ....	186
Figure 6. 4. Anisotropy profiles of the LDPE-1 for the conditions indicated in Fig. 6.1. ....	187
Figure 6.5. Thickness and birefringence profiles of the LDPE-1 for the conditions indicated in Fig. 6.1. ....	188
Figure 6. 6. Non-uniform, non-isothermal biaxial elongational viscosity versus effective deformation rate for the LDPE-1 at 175°C for the conditions indicated in Fig.6.1. ....	189
Figure 6. 7. Diameter and velocity profiles for the LmPE/LDPE-1 blends at a mass flow rate = 2.0kg/h, BUR = 1.5, TUR $\approx$ 60, FLH $\approx$ 180mm, die temperature = 200°C. ....	190
Figure 6. 8. Temperature profiles for the LmPE/LDPE-1 blends. The operating conditions are the same as for Fig. 6.7. ....	191
Figure 6. 9. Strain rates along the bubble for the LmPE/LDPE-1 blends in machine and transverse directions. The operating conditions are the same as for Fig. 6.7. ....	192

Figure 6.10. Birefringence profile for the LmPE/LDPE-1 blends. The operating conditions are the same as for Fig. 6.7.....	193
Figure 6. 11. Non-uniform, non-isothermal, biaxial elongational viscosity versus effective deformation rate at the reference temperature of 175°C for the LmPE/LDPE-1 blends. The operating conditions are the same as for Fig. 6.7.....	194
Figure 6. 12. Diameter and velocity profiles for the BmPE/LDPE-2 blends at a mass flow rate = 2.0kg/h, BUR = 1.5, TUR $\approx$ 40, FLH $\approx$ 180mm, and die temperature = 200°C. ....	195
Figure 6.13. Temperature profiles for the BmPE/LDPE-2 blends. The operation conditions are the same as shown in Fig. 6.12.....	196
Figure 6. 14. Strain rates in machine and transverse directions for the BmPE/LDPE-2 blends along the bubble. The operation conditions are the same as shown in Fig. 6. 12. ....	197
Figure 6.15. Birefringence profile for the BmPE/LDPE-2 blends. The operating conditions are the same as in Fig. 6.12. ....	198
Figure 6. 16. Non-uniform, non-isothermal, biaxial elongational viscosity and Biaxial Trouton ratio versus effective deformation rate at a reference temperature of 175°C for the BmPE/LDPE-2 blends. The operating conditions are the same as in Fig. 6.12.....	199

## NOMENCLATURE

$a_T$	Temperature shift factor
$C$	Stress-optical coefficient ( $m^2 / N$ )
$d$	Bubble diameter (mm)
$d$	Eccentricity (mm)
$h$	Film thickness (mm)
$h_0$	Die gap (mm)
$D_0$	Outer diameter of the die (mm)
$D_p$	Scaling factor
$DR$	Draw resonance
$E_a$	Activation energy for flow ( $J$ )
$F_z$	Bubble drawdown force at frost line ( $N$ )
$G'$	Storage modulus ( $Pa$ )
$G''$	Loss modulus ( $Pa$ )
$I$	Light intensity
$I_0$	Incident light intensity
$l_d$	Length of convergent die (mm)
$k$	Boltzmann constant ( $1.381 \times 10^{-23} J / K$ )
$L$	Parameter of elongational viscosity ( $Pa \cdot s'$ )
$m$	Power-law parameter of shear viscosity ( $Pa \cdot s^n$ )

$n$	Power-law index of shear viscosity
$\Delta n$	Birefringence
$P$	Degree of polymerization
$\Delta P$	Pressure difference across the bubble ( $Pa$ )
$\Delta P_{ent}$	Entry Pressure drop ( $Pa$ )
$\Delta P_{elongational}$	Entry pressure drop due to elongation ( $Pa$ )
$\Delta P_{shear}$	Entry pressure drop due to shear ( $Pa$ )
$Q_f$	Volumetric flow rate ( $m^3 / s$ )
$r$	Bubble radius (m)
$R_0$	Outlet radius of nozzle die (m)
$R_1$	Inlet radius of nozzle die (m)
$R_L$	Radius of curvature in machine direction (m)
$R_H$	Radius of curvature in transverse direction (m)
$T_0$	Reference temperature ( $K$ )
$t$	Power-law index of elongational viscosity
$w$	Mass flow rate of molten polymer ( $kg^3 / s$ )
$z$	Axial distance (m)

### Abbreviation

BI	Bubble instability
----	--------------------

BUR	Blow –up-ratio
BmPE	Branched metallocene-catalyzed polyethylene
DHI	Degree of helical instability
FI	Freeze line height instability
FLH	Frost line height
HDPE	High density polyethylene
LCB	Long chain branching
LDPE	Low density polyethylene
LLDPE	Linear low density polyethylene
LmPE	Linear metallocene-catalyzed polyethylene
MD	Machine direction
MDW	Molecular weight distribution
MI	Melt index
mPE	Metallocene-catalyzed polyethylene
MS	Melt strength
MW	Molecular weight
MWD	Molecular weight distribution
NNBEV	non-isothermal non-uniform biaxial elongational viscosity
NNBT(R)	non-isothermal non-uniform biaxial Trouton ratio ( $\eta_{fb} / \eta$ )
PE	Polyethylene
PH	Partially helical
PS	Polystyrene



SAXS	Small angle X-ray scattering
SCB	Short chain branching
SEM	Scanning electron microscopy
TD	Transverse direction
TEM	Transmission electron microscopy
TUR	Take-up ratio
WAXS	Wide angle X-ray scattering
XRS	X-ray scattering

### Greek Letters

$\beta$	Inverse of the contraction ratio
$\eta, \eta(\dot{\gamma})$	Shear Viscosity ( $Pa \cdot s$ )
$\eta^*$	Complex viscosity ( $Pa \cdot s$ )
$\eta_e$	Uniaxial elongational viscosity ( $Pa \cdot s$ )
$\eta_{be}$	Apparent biaxial elongational viscosity ( $Pa \cdot s$ )
$\eta_{fb}$	Apparent non-uniform biaxial elongational viscosity ( $Pa \cdot s$ )
$\lambda$	Relaxation time ( $s$ )
$\lambda$	Wavelength (m)
$a$	Length characteristic of the chemical structure of the molecule
$\sigma$	Shear stress tensor ( $Pa$ )
$\dot{\epsilon}$	Uniaxial elongational strain rate ( $s^{-1}$ )

$\dot{\varepsilon}_B$	Rate of deformation ( $s^{-1}$ )
$\rho$	Density ( $kg / m^3$ )
$\dot{\gamma}$	Shear rate tensor ( $s^{-1}$ )
$\bar{\dot{\gamma}}$	Effective deformation rate ( $s^{-1}$ )
$\omega$	Frequency ( $s^{-1}$ )
$\theta$	Bubble inflation angle
$\delta$	Retardation

## INTRODUCTION

### General

Film blowing is one of the most important polymer processes. This technology, which can be dated back to 1915 (Kang et al, 1990), was first applied to cellulosic derivatives. Now, tubular film production is the most important application area to produce bags for conventional low density polyethylenes (LDPEs), linear low density polyethylenes (LLDPEs), high density polyethylenes (HDPEs), and likewise is the major outlet for the new families of metallocene-catalyzed polyethylenes (mPEs).

It is well-known that LLDPE has superior mechanical properties but relatively poor processability due to its narrow MWD and lack of LCB whereas LDPE has very good processability but relatively poor mechanical properties due to its broad MWD and a large amount of LCB. mPE was designed and expected to have the combined properties of LLDPE and LDPE due to its tailored structure, with narrow molecular weight distribution (MWD) and sparse long-chain branches (LCB). However, the amount of LCB in mPEs is not sufficient to give good processability even though the superior properties of mPE have been widely recognized. Hence, the use of mPEs has been largely limited.

### The Description of Film Blowing Process

A schematic diagram of film blowing process can be seen in Fig. 1.1. A thin film is produced by means of the extrusion of a polymer melt through an annular die. The molten polymer, in the form of a tube, exiting from the die is drawn upward by a take-up

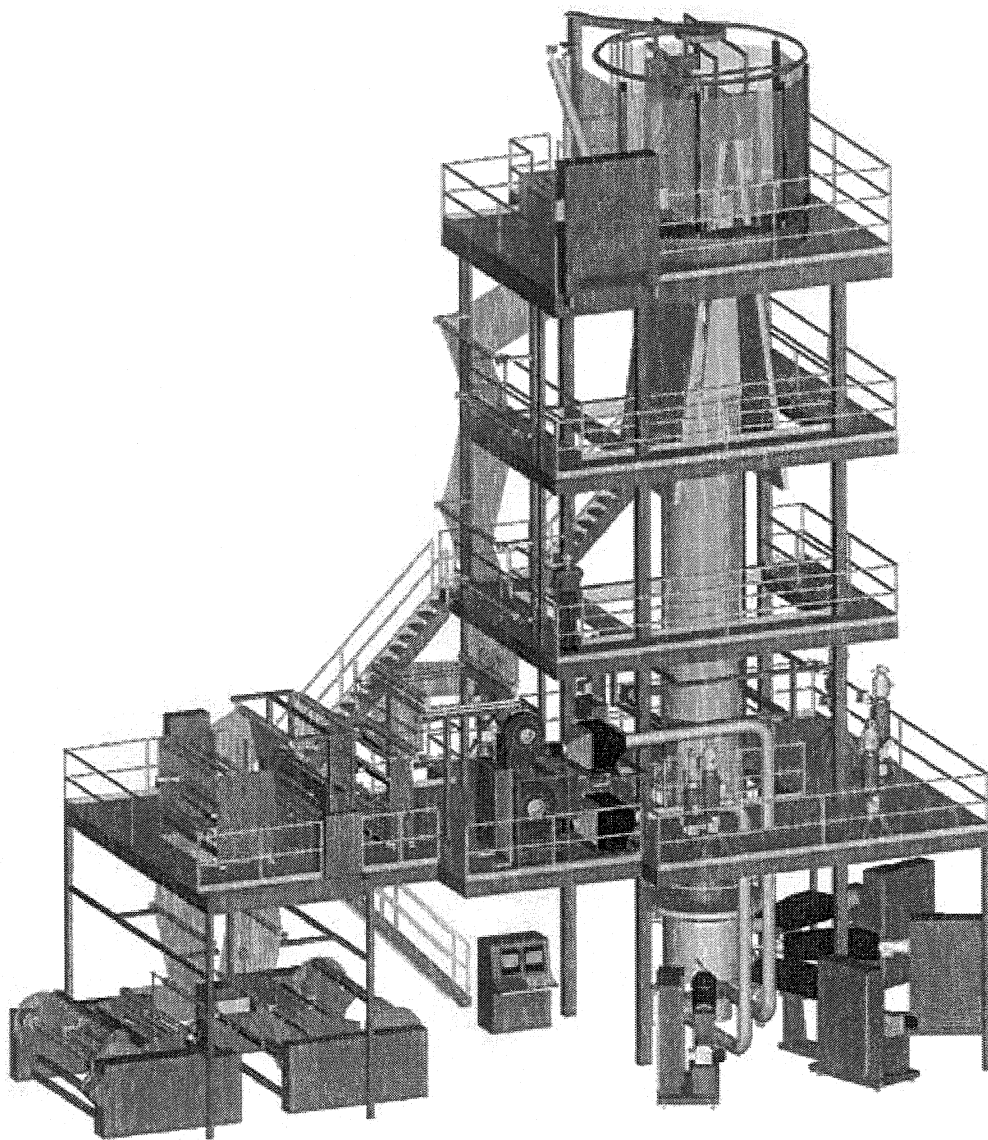


Figure 1. Schematic diagram of film blowing process.

device. When the process starts up, air is introduced at the bottom of the die to inflate the tube and form a bubble. An air ring is also used to rapidly cool the hot bubble and solidify it at some distance above the die exit. This distance is usually called Frost Line Height (FLH). The inflated, solidified bubble is then flattened as it passes through the nip rolls. The nip rolls, driven by a variable-speed motor, provided the axial tension needed to pull the film upward, and they form an airtight seal to keep a constant pressure inside the bubble. The pressure is controlled by the air supply to the bottom of the die. The bubble is then wound onto cylindrical cores and sold or used as 'lay-flat' tubing; alternatively, the edges can be trimmed off after passing through the nip rolls and two rolls of flat sheet can be wound from the lay-flat tube. This process is usually carried out vertically upward, sometimes vertically downward, and occasionally horizontally.

As the polymer film moves towards the nip rolls, it is being drawn longitudinally by the nip rolls and stretched transversely by the internal pressure. Therefore, the thickness of the molten polymer tube will decrease progressively as the polymer is drawn away from the die. At some distance from the die, a point will be reached whereby the pressure inside the bubble will exceed the melt strength of the thin walled tube and this will cause the tube to expand radially. The transition of the molten polymer to a solid film is accelerated and localized by a jet of cold air directed onto the outer surface of the film from an annular ring just above the die. The height above the die at which solidification occurs can be controlled through the airflow rate and negligible deformation of the bubble occurs beyond the frost line in most processes. The film dimensions are determined by the blow-up ratio (BUR), which is the ratio of the bubble radius at the frost line to the die radius, and the take-up ratio (TUR), which is the ratio of the take-up velocity to the extrudate velocity at the die exit.

### **Rheological View of the Process**

The film blowing process is a complex manufacturing process involving interactions between melt rheology, heat transfer, and free surface kinematics. The film

blowing process is kinematically similar to film casting and fiber spinning. The flow in all three processes is primarily elongational and under free surfaces. The major difference is that the processes of casting and spinning result in a uniaxially oriented product and therefore increased strength in one direction whereas film blowing provides biaxial orientation and therefore increased strength in two directions. This two-directional orientation is one of the primary attractions of the film blowing process, since it allows for precise control of the mechanical properties of the product sheet by variation of the axial draw velocity and blow-up pressure.

During the film blowing process, the molten polymer is subjected to different stress fields that develop at various stages of the process. First, as the melt flows through the annular die, it is subjected to shearing stresses, resulting in a partial molecular orientation in the machine direction (MD). Upon leaving the die, where the melt is suddenly free of the constraints imposed by the contact with the die wall, this orientation may be partially relaxed but further orientation of the macromolecules will occur as a result of biaxial stretching. The level of extensional stresses will then increase with increasing viscosity due to cooling. Depending on the cooling rate of the melt a second relaxation process may also take place, causing reorientation of macromolecules. In the vicinity of the frost line height the melt under stress starts to crystallize (Ghaneh-Fard *et al.*, 1997c; Maddams and Preddy, 1978a).

The film processability of a polymer is intimately related to its rheological behavior, which in turn, depends on the molecular parameters, namely, molecular weight (MW), molecular weight distribution (MWD), and the degree of long chain branching (LCB). What makes the matter more complicated is that, whereas the rheological behavior of a polymer is a direct response to molecular parameters, it also depends on many other factors, which includes: 1) the types of flow field (i.e., kinematics); 2) the intensity of the rate of deformation; 3) the deformation and thermal histories.

## CHAPTER 1. LITERATURE REVIEW

### 1.1. Modeling Film Blowing Process

The analysis of tubular film blowing was first proposed by Alfrey (1965). Based on his analysis, Pearson and Petrie (1970a, 1970b) gave a detailed description of modeling the flow of the molten polymer between the die exit and the frost line, even though they assumed the flow to be isothermal, and the polymer to be an incompressible Newtonian fluid with constant viscosity. A thin-shell theory, which could use local rectangular Cartesian coordinates, was also employed. Their analysis of the film kinematics and dynamics provided a theoretical framework for most subsequent studies and has been universally recognized and extensively utilized in all succeeding investigation. Most subsequent literatures can be characterized as an evaluation of the incorporation of rheological models into Pearson and Petrie's kinematic and dynamic analysis.

Petrie (1973b) numerically showed the bubble for different Maxwell-type models. He predicted that the radius and thickness of the bubble decrease with increasing the elasticity of the polymer. Later (1975), he extended the calculation to a non-isothermal Newtonian fluid. Agreement between theoretical predictions and experimental measurement was sought by Wagner (1976), but he assumed an average Newtonian viscosity for the process, which due to viscoelastic effects, was of course found to depend strongly on the TUR.

Han and Park (1975) employed a power-law model dependent melt viscosity without taking the temperature effects into consideration to successfully predict stresses and the shape of the bubble. However, it was of less value as a fully predictive model.

Luo and Tanner (1985) extended Petrie's work on film blowing to cover viscoelastic isothermal and non-isothermal flow for both the convected Maxwell and the Leonov models. They showed that the Leonov model had poor agreement with experimental data since it did not stiffen enough with increasing elongational rate to model the bubble well. Owing to numerical instability, they did not get any results for cases in which  $BUR < 1$ . However, for  $BUR > 1$ , they obtained a good agreement between the predictions of the Maxwell model and Gupta's data (1982) on PS by modifying the relevant mean relaxation time. It is worth mentioning that the variation of properties due to temperature was seen as dominant effect.

Cain and Denn (1988) considered the Newtonian and two viscoelastic models: the upper convected Maxwell model and Marrucci model and compared their predictions to the data of Gupta (1982). Moreover, they assumed the convective heat transfer coefficients were constant along the bubble length. They predicted that multiple solutions for the bubble were possible and it was impossible to determine the bubble profile by simply defining pressure difference and take-up force.

Petrie (1975) was the first one who considered the heat transfer during the film blowing process in his analysis. Kanai and White (1985) have also used the Newtonian model in the non-isothermal simulation of film blowing.

Gupta (1982) et al. considered the general non-isothermal process and reported measurements of PS bubble shapes, velocities, stretch rates, stresses and temperatures in the melt region. The viscoelastic nature of the melt was described by the White-Metzner equation.

Alaie and Papanastasiou (1993) analyzed the melt film-blowing by means of a nonlinear integral constitutive equation that incorporates shear history effects, spectrum of relaxation times, shear thinning and extension thinning or thickening. The



temperature history, as predicted by the simultaneously solved energy equation, was introduced into the constitutive equation by means of the appropriate shift factor incorporated in the linear modulus of the constitutive equation. The resulting system of integro-differential equations is solved by finite element discretization and Newton iteration. The model predicts that with increasing elasticity, both the bubble radius and film thickness decrease but the velocity of film increases. Moreover, the thickness, radius, temperature, and MD stress profiles show a good agreement with experimental data of Gupta (1982). However, the stress in transverse direction (TD) is slightly overestimated near the die exit and underestimated in the vicinity of FLH. It is worth noting that they mistakenly reported that the stress in TD is greater than that in MD for a Gupta's experiment due to an error in unit conversion.

In the above analyses, computations were primarily based on trial and error and proceed up to the frost line. Two-phase model, which is the combination of modified Maxwell model and modified Hookean model, was first introduced by Campbell and Cao (1987) who proposed that the film, in the tube forming area, was composed of two layers. This idea was supported by the experimental evidence that the surface temperature of the film differs from the bulk average (through thickness) by as much as 15 to 20°C in the tube forming area. (Cao et al., 1990). In a another publication, Cao and Campbell (1990) introduced yield stress as a criterion for the cessation of radial deformation beyond the frost line, leading to a plastic-elastic transition and thus successfully extended the model above this line. They have predicted blown film process from die exit to nip roll and compared their predictions to the experimental data of Gupta. Their model is the first to yield qualitatively correct predictions of all process variables, even though it slightly overestimates the film thickness above the FLH. Later, Ashok and Campbell (1992) have used an upper convected Maxwell equation of state with a single relaxation time and the Oldroyd model and applied derivative to the amorphous or liquid-like phase while a perfect plastic model with yield was used to describe the deformation of crystallized phase. The model is in qualitative agreement for

the bubble radius and axial velocity profiles. However, contradictory results, as in the Pearson and Petrie model, were predicted. This may be due to assumptions – there is no extrudate swell and no temperature gradient across the film, which has been demonstrated by Cao et al. (1990) to be substantial.

Yeow (1975) used a linear hydrodynamic stability theory to examine the stability of the film blowing process. Infinitesimal disturbances were superimposed on the steady Pearson and Petrie model. Both axisymmetric and non-axisymmetric bubbles were considered in their study.

Liu et al. (1995a) gave detailed experimental data on film blowing process. Most of their description is contradictory to modeling on tubular film blowing that appeared in the literature. Later (1995b), they used “quasi-cylindrical” model for the tubular film blowing geometry, using a deformation-thinning viscosity equation, which satisfactorily explains the essential features of the experimental data. However, the assumptions are only satisfactory in the solid mechanics problem but not in the fluid mechanics problem.

Seo and Wissler (1989) considered the extrudate swell effect in modeling the film blowing process in addition to Pearson and Petrie’s work. Their prediction was in good agreement with experimental data of Wagner when TUR was low. For the case that TUR is high, the die swelling effect is not significant. However, they did not attempt to model non-Newtonian behavior due the high Weissenberg number.

All the experiments mentioned above have been performed on a small scale machine and a small amount of resin. Kanai et al. (1986) have presented a study on scale-up of the tubular film process and suggested that the melt behavior in tubular film process, the orientation factors of film, and physical properties of film were independent on film width and thickness under the scale-up conditions.

Due to the facts that the authors mentioned above neglected the effect of crystallization on the process dynamics and rheological behavior, they cannot predict the occurrence of the frost line naturally. Only a few authors took this effect into account. Kanai and White (1984) presented a basic study of the kinematics, dynamics, and heat transfer occurring during tubular film extrusion of three kinds of polyethylenes – LDPE, HDPE and LLDPE by using a crystallization model. However, they did not include an explicit transformation rate equation and their constitutive formulation is not molecularly based, thus their model could not precisely predict evolution of the microstructure. Campbell and his coworkers [Campbell and Cao (1987); Ashok and Campbell (1992)] introduced a two-phase model to describe the deformation of the crystallized phase. Even though their approach could fit experimental velocity and radius data, it did not include an explicit coupling to the crystallization kinetics. More recently, Doufas and Mchugh (2001) developed a two phase microstructural flow-induced crystallization model, which can predict the locked-in system stresses at the frost line.

In summary, numerous efforts have been put on modeling film blowing process. However, it cannot be denied that there is no model which can be quite successful. Because the film blowing is very complicated process, where melt rheology, heat transfer and aerodynamics are involved, as mentioned before. Furthermore, the reliable data published for film blowing models to be examined are rather sparse.

## **1.1. Rheological Properties and Their Effects of on Film Process and Film Properties**

### **1.1.1. Strain, Strain Rates and Stress**

Huang and Campbell (1985, 1986) have measured the strain rates and bubble temperature in blown film of LLDPE and LDPE and found that the peak strain rates occur closer to the die exit. The strain rates of LDPE are higher than those of LLDPE. Moreover, they also found that the addition of a small amount of LDPE to LLDPE could cause a significant increase in the strain rates at lower axial positions.

Farber and Dealy (1974) were the first to postulate that the orientation in the film resulted from the plastic strain in the immediate vicinity of the FLH and they got the conclusion that melt rheology did not play an important role in the generation of the orientation which was observed in blown films. However, Babel and Campbell (1993a) have attempted to correlate the mechanical properties of blown films with the kinematics and dynamics of the process. They suggested that the plastic strain, defined as the strain put in the film after the onset of crystallization, could be a correlating variable, even though their experimental data were too scattered to claim any clear correlation. Later, Babel and Campbell (1993a, 1995) have attempted to correlate the film properties with both plastic strain and strain rates based on a limited set of experimental data. Since the quantitative determination of velocity and diameter profiles still remain a very difficult task, their results are easily questionable. Tas (1994) calculated the MD stress of blown film at the freeze line using the PTT model and correlated MD stress with the mechanical properties. He concluded that the equal MD stresses at the freeze line resulted in the same mechanical properties, regardless of the type of LDPE, equipment and processing conditions as well. However, he was not successful in correlating the TD stresses with film properties due to the fact that the PTT model did not predict the TD

stresses at all well. However, the influence of the TD stresses on final film properties can not be neglected.

Agassant *et al.* (1991) have analyzed the film blowing process for a Newtonian fluid. They calculated the pulling force and then predicted that the entire stress history in the film is independent of any hypothesis on the material behavior.

Kuijk *et al.* (1998) have presented a comprehensive model for film blowing of PE, whereby film properties (optical and mechanical) can be calculated starting from the relevant PE properties (rheological characteristics and density) and the processing conditions (including die geometry). They suggested that the final MD and TD stresses in the bubble during film blowing at the freeze line are important parameters for determining the mechanical end-properties of the resulting blown film. More recently, Doufas and Mchugh (2001) used a two phase microstructural flow-induced crystallization (FIC) model, by using a “quasicylindrical” approximation for the momentum equations, to predict the locked-in system stresses at the frost line and correlated the stress to the physical and mechanical properties of the film.

It should be mentioned that the rate of deformation has been mostly measured by a tracer technique using a video camera. Tas (1994) and Michaeli and Schmitz (1995) have employed the laser Doppler velocimetry to measure the velocity profiles of the blown bubble during the film blowing. The stress field in the bubble has been determined via force balance by measuring the bubble drawing force at the nip rolls using mechanical transducers. However, the bubble force measurement is influenced by different frictional forces during flattening of the film bubble, pinching-off and taking-up. Ghaneh-Fard *et al.* (1997) introduced the flow birefringence technique to measure the stresses indirectly via stress-optical law.

### **1.1.2. Molecular Structure and Elongational Viscosities**

#### **1.1.2.1. Uniaxial Elongational Viscosity**

Han et al. (1983), Han and Kwack (1983) and Kwack and Han (1983) found that the blowability is increased as the resin's molecular weight distribution (MWD) becomes narrower and the degree of long chain branching (LCB) is less. They also concluded that a resin having lower elongational viscosity tends to give a better blowability. Moreover, they observed that a more uniform tensile strength in the MD and TD was achievable with a LLDPE resin than with a LDPE resin. This may be due to the absence of long side chain branching in LLDPE.

Ghijssels and Ente (1990) used the melt strength as an identifier to assess the bubble stability in film blowing process. A high melt strength is identified with a good bubble stability. They suggested that the molecular weight and the LCB are the two most important molecular structural factors governing the melt strength. The type of short chain branching (SCB) – both in terms of side-chain length and structure – has no significant effect, where the effect of molecular weight distribution is also considered to be small.

Fleissner (1988) suggested that the bubble stability in film blowing is related to rheological properties, from investigation of LDPE, HDPE, and LLDPE in film blowing on a commercial production line. They also suggested that shearing of the material in the palletization improves its stability. This improvement is partly due to the reduction in elongational viscosity and partly due to degradation of the polymer.

Ramesh and Malwitz (1997) used a simple rheological technique based on the entrance pressure drop method (Cogswell, 1994), which is used to obtain a value for the

elongational viscosity, to predict the behavior of new resins under film blowing conditions. They pointed out that an increased slope, followed by a flat elongational rheology curve is best for achieving stable bubble.

Mimic et al. (1998) investigated the transient elongational viscosity of LLDPE and its blends with 10% and 20% of LDPE at two temperatures. They suggested that the bubble behavior is mostly determined by the strain hardening characteristics of the polymer. Increasing strain-hardening characteristics could improve the bubble stability. Shear curves seem to be of limited use in predicting the bubble stability as a function of temperature in film blowing.

Beagan et al. (1999) suggested that shear viscosity of blends of mPE and LDPE increases with increasing mPE content and 100% mPE was shown to be less shear thinning than LDPE.

Bin Wadud and Baird (1999) have investigated three mPEs – One of the PE's is linear i.e. no LCB, while the other two have different amounts of LCB and suggested that the shear viscosity of the linear PE is reflective of the narrow molecular weight distribution of mPEs while the apparently branched PE's exhibit a higher viscosity and an earlier onset of shear thinning. The linear polymer exhibited lower activation energy than the branched PE with similar molecular weight.

Chai (1999) defined two new parameters:  $\delta(\text{MS})/\delta P$ , the melt strength pressure derivative and  $\delta(\text{MS})/\delta(\log \dot{\gamma})$ , the melt strength shear derivative to study the effects of molecular structure on melt rheology of different types of LLDPEs (one Zieler and three metallocenes) and their processabilities by using an improved Rheotens. Under the same processing conditions, the higher the values of the two parameters are, the more processable the resins will be.

More recently, Kim *et al.* (2003) studied bubble stability using PEs with different molecular structure and they claimed that the presence of LCB plays more important role than the broadening of the MWD. They also tried to use the plot of normalized tensile stress growth coefficient versus Hencky strain or normalized extensional viscosities versus extensional stress to correlate to the order of the bubble stability.

#### 1.1.2.2. Biaxial Elongational Viscosity

It was Han and Park (1975a) who first have attempted to determine the elongational viscosity in film blowing, namely, biaxial elongational viscosities. They suggested that the non-uniform biaxial elongational viscosity,  $\eta_{be}$ , may be represented as:

$$\eta_{be} = \frac{\sigma_{11}}{\dot{\gamma}_{11} - \dot{\gamma}_{22}} \quad (1.1)$$

or

$$\eta_{be} = \frac{\sigma_{33}}{\dot{\gamma}_{33} - \dot{\gamma}_{22}} \quad (1.2)$$

where  $\dot{\gamma}_{11}, \dot{\gamma}_{22}, \dot{\gamma}_{33}$  are strain rates in machine, normal and transverse directions respectively.  $\sigma_{11}$  and  $\sigma_{33}$  are stresses in machine and transverse directions respectively.

In order to avoid the influence of the non-isothermal bubble along the length, they used a special isothermal chamber with a glass window. However, their results are easily questionable due to the following reasons: (1) it is very difficult to avoid the influence of the non-isothermal bubble due to the existence of cooling effects. (2) the



quantitative determination of stress via classical mechanical method is a very difficult task, since the impact of the energy loss by frictional forces during flattening, pinching-off and taking-up of the film bubble on the drawing forces is difficult to evaluate. Han and Park suggested that the results calculated from equations (1.1) and (1.2) were acceptable, even though they are not identical. Ghaneh-Fard *et al.* (1997) have shown that the disagreement became worse for LDPE.

Kanai and White (1984) used only equation (1.1) to examine the apparent elongational viscosity in film blowing. Agassant *et al.* (1991) have suggested that  $\eta_{be}$  can be obtained by adding the two components of the stress tensor:

$$\eta_{be} = \frac{\sigma_{11} + \sigma_{33}}{\dot{\gamma}_{11} + \dot{\gamma}_{33}} \quad (1.3)$$

This suggestion has been adopted by Ghaneh-Fard *et al.* (1997) to calculate the non-uniform biaxial elongational viscosity. Moreover, Ghaneh-Fard *et al.* (1997) improved the technique, using birefringence measurement instead of the classical mechanical method, to determine the stress. However, he did not take the temperature effects into account by plotting biaxial elongational viscosity versus axial distance along the bubble.

## 1.2. Bubble Stability

The problem of bubble stability was first described by Ast (1974). Han and Park (1975c) and later Han and Shetty (1977) presented detailed description of the instability for a single layer film of LDPE and polystyrene (PS)/HDPE blends by recording the bubble behavior through still pictures. The stability results are compared to the so-called

“draw resonance” phenomenon observed in film casting from slit dies. They concluded that lowering the extrusion temperature improved the blown film stability for HDPE and LDPE. They observed pulsations of the bubble diameter as the stretch ratio increased under “uniaxial” deformation for small BUR less than unity and observed a wavy film under biaxial deformation for BUR larger than 1.5. Sweeney et al. (1992) have shown that using video analysis system is an effective way to quantify the bubble instabilities. The most extensive work was given by Kanai and White (1984), Minoshima and White (1986), White and Yamane (1987) and Ghaneh-Fard et al. (1996). Kanai and White (1984) investigated the kinematics and stability of the tubular film process over a wide range of BURs, TURs and FLHs for LLDPE, LDPE and HDPE and suggested that the stability should be in the following order: LDPE > HDPE > LLDPE. Minoshima and White (1986) have concluded that in tubular film extrusion, the LDPEs are most stable but the narrower distribution HDPEs and LLDPEs are much more unstable than the broader distribution HDPE. They also discussed the results in terms of convected Maxwell model representations. Yamane and White (1987) used a crystallization model to predict that the activation energy has a much greater effect on the bubble shape than variations in non-Newtonian characteristics. Both decreasing activation energy and power law exponent may produce narrow necked bubble. Following previous authors, Ghaneh-Fard et al. (1996) has extensively studied the bubble stabilities for LDPE, HDPE, LLDPE and PP by giving detailed definition of bubble instabilities and suggest that relative order of stability is: LDPE > HDPE > LLDPE > PP. LDPE is always the most stable in the polymers investigated during film blowing, it is due to the strain-hardening behavior of LDPE in elongational flow. Fleissner (1988) determined the critical drawdown speed as a criterion for the FLH instability of three high molecular weight HDPEs which were shown to have different extensional behaviors.

Ghijssels et al. (1990) suggested that a small axial take-up force is needed to stretch the low melt strength film in absence of strain-hardening for LLDPE, so a low-

tension bubble becomes sensitive to surrounding air flows and gravity forces, leading to bubble instabilities.

A theoretical stability analysis of instabilities due to axi-symmetric disturbances in an isothermal Newtonian fluid has been given by Yeow (1976). Based on his analysis, Cain and Denn (1988) have utilized an upper convected Maxwell model to analyze the bubble stability. They found that both the number of steady state solution branches and stability depended on the operating conditions represented by four variables such as axial velocity at the solidification point, the pressure inside the bubble, dimensionless tension, and a parameter relating inflating pressure to thickness and fluid viscosity. However, the models they have utilized do not show good agreement with experimental data. Yoon and Park (1999) evaluated the detailed effects of specific operating conditions on bubble instability based on the models developed by Cain and Denn. Their simulation results were compared with the experimental data obtained by Minoshima and White (1986).

### **1.3. Birefringence Measurements**

It is well-established that molecular orientation and stress-induced crystallization in a fabricated blown film influence its mechanical and physical properties. For semi-crystalline polymers like polyethylenes, the orientation of both the crystalline and amorphous phases is controlling the film properties.

Several techniques have been used by different researchers for off-line measurement of orientation in polymers. These techniques include birefringence, spectroscopy (FTIR, Raman, fluorescence, NMR, ...), X-ray scattering (XRS) (wide angle X-ray scattering (WAXS), small angle X-ray scattering (SAXS)), transmission electron microscopy (TEM), scanning electron microscopy (SEM), ultrasonic techniques

etc. Among these, the birefringence is the simplest and relatively quick. Moreover, it is a measurement of total molecular orientation in the sample and could also be very useful to determinate the stresses occurring in the melt zone during film blowing.

The techniques of birefringence measurement most widely used include refractometry, monochromatic polarized light retardation (Marsh et al. (1995) and Hoppler et al. (1995)), multiwavelength (Abel and Fuller (1990), Hongladarom and Burghardt (1993) and Beedmans and Boer (1996)) and some qualitative techniques (fringes and light scattering). Refractometry is limited by several factors: use of contact liquid is not appropriate in many cases, it is tedious and can not be applied for on-line monitoring. Monochromatic polarized light techniques are suitable for low orientation (low retardation) which are encountered in some cases, but are useless for moderately or highly oriented films, sheets or shapes. Takahashi and Fuller (1996) and Hongladarom and Burghardt (1994) have used this technique for biaxial orientation measurements in polymers with low degrees of orientation. The multi-wavelength technique on the other hand, has been limited to uniaxial orientation and monolayer materials. More recently, Ajji et al. (1998) and Ajji et al. (1999) have used a technique based on an incident multi-wavelength double beam and a photodiode array assembly, combined with in-house developed software to overcome the problems mentioned above.

#### **1.4. PE Blends**

Metallocene catalyzed polyethylenes are the latest addition to the polyethylene family and are reported to have superior mechanical properties over conventional polyethylenes, mainly due to their narrow molecular weight distribution and more uniform co-monomer distribution. However, these polymers are more difficult to process because of their relatively high viscosities encountered during melt processing.

In order to overcome some of these difficulties, mPEs may be blended or coextruded with other conventional polyethylenes.

Beagan et al. (1998) compared monolayer blended films of mPE and LDPE to three layer coextruded films of A:B:A structure where A is LDPE and B is mPE and found: (1). Incorporation of mPE into an LDPE film will result in an increase in tensile properties both for the monolayer blended film and the three layer coextruded film. (2). Generally the coextruded films exhibit higher break strengths than blended films for same percentage mPE. (3). Blending of even relatively small amounts of mPE into a LDPE film will lead to a significant decrease in crystallinity. Later (1999), they investigated the effect of blending two grades of mPEs with conventional LDPE for use in thin films, suitable as packaging materials and produced by the blown film process. Their work showed that increasing the percentage of mPE film improved the mechanical properties of the resultant film.

Due to the result of higher intermolecular entanglements, OH (1999) observed positive synergy effects of LLDPE/LDPE blends in the melt tension, elongation, Elmendorf tear strength, toughness and initial tear strength of blown film.

Castillo and Grossman (2000) investigated LDPE/FPO(flexible polyolefin resins) blends during film blowing process and found that the blends appear semicompatible. However, film extrusion processability increases, blocking decreases, along with better film appearance, and improvements in tensile strength without a decrease in flexibility. Alternatively, roughness, elongation and impact resistance increase.

Hong et al. (2000) found that through the addition of hyperbranched polymer (HBP), sharkskin was successfully eliminated without significantly changing the overall

physical properties of LLDPE films in the tubular film blowing process. They showed that HBP and LLDPE are immiscible, and HBP has a tendency to migrate to the surface to form a lubricating layer between the metal surfaces and the bulk material.

Determination of miscibility/immiscibility of a pair of blends is essential since immiscible blends may deteriorate the properties of final product. The techniques normally used are determination of glass transition temperature determined by thermal analysis, the morphology determined by optical and electron microscopy, and some trivial methods. Due to the low contrast, low and closer glass transition temperatures of PE blend, it is quite difficult to determine the blends miscibility using routine ways. The miscibility of PE blends has been investigated for a long time by different research groups using different techniques.

Alamo *et al.* (1997) reported that the branch content was the critical factor for HDPE/LDPE blends using small angle neutron scattering (SANS) technique, which was considered the most powerful technique. They found that when the branch content was more than 8 branches/100 backbone carbons the blends exhibited phase separation. However, the deuteration itself might have altered the chemistry and physics of individual component.

Cho *et al.* (1998) investigated LLDPE/LDPE, LLDPE/HDPE and HDPE/LDPE blends and found that they are all miscible in the melt state based on log additivity rule (LDR) and cole-cole plot. They also argued that LLDPE/LDPE and HDPE/LDPE blends show two crystallization and melting temperatures, which is an indication of phase separation upon cooling from the melt. It is worth noting that the mechanical properties showed that the LLDPE/LDPE blends were higher than calculated from a simple rule of mixtures while those of LLDPE/HDPE blend conformed to the rule of mixtures and the properties of HDPE/LDPE were less than the rule of mixtures prediction.

Chen *et al.* (2001) used different very low density polyethylenes (VLDPE) and LDPE to make blends. Based on thermal analysis, they concluded that the molar masses or melt flow indices of the PEs were not significant in controlling the morphology and only the distribution of branches along the chain was important.

Summarizing the literature review, numerous efforts have been put in modeling film blowing process and investigating the relationship between rheology and processability. However, we noticed many aspects have not been fully understood. The non-isothermal non-uniform biaxial elongational viscosity has not been studied yet and the bubble stability was limited to the traditional technique using camcorder. With respect to the speculated importance of rheological behaviors in discriminating between the impact of the polymer feedstock and the processing conditions on bubble stabilities and film properties, it is a pity that only a few of the theorists focused on predicting the inter-relationships. Many attempts have been made to describe the kinematics of the film in the bubble forming region, either with pure viscous model or viscoelastic plastic models. Although optimizing film blowing process is the final objective for all the researchers, one can only find some scattered data on the relationship between the rheological behavior of a polymer and its processability. So, it is safe to say that the relationship is still poorly understood, mostly because of lack of sufficient and reliable data. Therefore, this experimental study will be carried out to provide a better understanding of the process and to shed light on the different behaviors of various polyethylenes, especially for new members of polyethylene families – mPEs.

## CHAPTER 2. OBJECTIVES AND ORGANIZATION OF THE ARTICLES

### 2.1. Objectives

The ultimate objective is to optimize the film blowing process, that is to say, to obtain a maximum production rate with optimal physical and mechanical properties. From the practical point of view, it is highly desirable to have a criterion (or criteria) for the choice of resins that will give good tubular film processability, without having to perform a time-consuming tubular film blowing operation. Such a criterion, once established, will help the resin producers to tailor-make specific resins for certain applications and, also, will help the tubular film producers to conduct routine test of quality of the resin that they receive from the resin producers. So, our first objective is to establish such a criterion, that is to say, to study relationship between the rheological properties of various polyethylenes and their processabilities.

Due to the lack of reliable data in bubble stability measurement and non-isothermal non-uniform biaxial elongational viscosity (NNBEV) measurement during the past study, model development has been largely obstructed. Our second objective is to extensively study the bubble stability and determine the NNBEV during film blowing process using different polyethylenes with different molecular structures in order to provide reliable data for modeling purposes.

Since the application of mPE has been largely limited by its processability, the best solution to tailor the relationship between the bubble stability and the properties of final product is to make blends. Checking blend miscibility is always essential before making any blends. However, the similarity of PE molecular structure makes PE blends low contrast, low and closer glass transition temperatures, and thus make it difficult to determine the blends miscibility using routine ways, such as the glass transition



temperature determined by thermal analysis and the morphology determined by optical and electron microscopy, etc. Therefore, checking miscibility/immiscibility of PE blends is our third objective.

## 2.2. Organization of the Articles

In the first paper “Rheological Effects of Polyethylenes in Film Blowing”, the effects of rheology on the kinematics and dynamics of film blowing for different polyethylene resins, namely two low density polyethylenes (LDPEa, LDPEb), a high density (HDPE), a linear low density polyethylene (LLDPE), a metallocene-catalyzed polyethylene (mPE), were investigated. The aim of this article was to try to correlate the rheological behavior of different polyethylenes to their processabilities. The rheological properties (complex, shear, uniaxial elongational and non-uniform non-isothermal biaxial elongational viscosities) and bubble stability of the different PEs were studied. This paper is the first trial to calculate non-uniform non-isothermal biaxial elongational viscosity (NNBEV) using time-temperature superposition principle. The bubble stability of mPE have been studied and compared with the data of previous authors (Ghaneh-Fard et al, 1997) in our laboratory. The bubble of mPE and LLDPE are more unstable in comparison with LDPE and HDPE during film blowing. The uniaxial elongational viscosities of three resins, HDPE, LDPEb and mPE, have been studied using two convergent dies and two techniques, Cogswell and Binding analyses. The uniaxial elongational viscosity can not be correlated to the bubble stability. There is no simple equation relating stresses and strain rates in film blowing.  $\log G'$  versus  $\log G''$  plot was observed to be virtually independent of temperature for all the polymers investigated. The larger the  $G'$  value was, the more stable the bubble was during film blowing. The Trouton ratios for the HDPE, LLDPE, LDPEa, LDPEb and mPE versus deformation rate have been reported. In all cases, the ratio exceeds the limiting value of 3, expected for Newtonian fluids. The Trouton ratios of the LDPEa and LDPEb are

much larger than those of the HDPE, LLDPE and mPE. We believe that the high values of the Trouton ratio are closely related to the bubble stability in film blowing. Hence, it appears that information on the elongational viscosity is at least as important information as the shear flow properties.

Even though the first paper gave some qualitative conclusions, the results have to be evaluated in details to improve the quality of the data. Therefore, the second paper introduced a new way to quantitatively measure the bubble stability inline.

In the second paper entitled “Dynamics and Criteria for Bubble Instabilities in a Single Layer Film Blowing Extrusion”, the performance of a new in-line scanning camera system for the study of various bubble instabilities in film blowing extrusion was critically evaluated using three commercial film-grade polyethylenes, LmPE, LLDPE and LDPE. Reliable and objective criteria for differentiating various bubble instabilities such as draw resonance, helicoidal instability, frost line height instability are proposed by using the new device. Detailed dynamics of each bubble instability was carefully investigated as a function of time in a broad range of the take-up ratio (TUR), blow-up ratio (BUR) and frost line height (FLH). In addition, effects of melt temperature and mass flow rates on dynamics of the bubble instabilities are also discussed. It was found that the new system could capture the main characteristics of all bubble instabilities quantitatively.

In the paper 3 entitled “Thermal and Rheological Properties of mPE/LDPE Blends”, two types of metallocene catalyzed polyethylenes (mPEs) and two low density polyethylenes (LDPEs) as well as their blends were studied using DSC and rheometry. The aim of this paper is to try to determine the miscibility/immiscibility of different PEs and obtained reliable rheological data for NNBEV calculation. DSC results showed that the linear mPE (LmPE) based on hexene comonomer is immiscible with both LDPEs in crystalline states whereas the branched mPE (BmPE) based on octene comonomer is

miscible with the LDPEs. This suggests that increasing the length of short chains in mPEs can promote the miscibility of mPE/LDPE blends. The linear viscoelastic properties confirmed the immiscibility of the LmPE with the LDPEs in the molten state and miscibility of BmPE with LDPEs. In addition, the Palierne (1) emulsion model showed good predictions of the linear viscoelastic data for both miscible and immiscible polyethylene blends. However, as expected the low frequency data showed a clear influence of the interfacial tension on the elastic modulus of the blends for the immiscible blends.

After successfully evaluated the processabilities of different polyethylenes, we have to re-examine the technique proposed in the first article to determine the NNBEV. In addition, we have to confirm the miscibility/immiscibility of PE blends proposed by paper 3.

The last article entitled “Properties of mPE/LDPE Blends in Film Blowing” mainly focused on confirming the technique used for NNBEV calculation and miscibility/immiscibility of PE blends. The NNBEV at the reference temperature of 175°C has been evaluated using LDPE-1 at different BUR, TUR and FLH. The results show that NNBEV is approximately a unique function of the deformation rate, confirming the validity of the assumptions and technique used for NNBEV calculation. Hence, using film blowing unit as an inline rheometer is feasible. Paper 4 also presented the rheological data using inline measurement during film blowing for polyethylenes with different molecular structures and their blends. Experimental data show that before the crystallization starts the birefringence of the BmPE/LDPE-2 blends is a linear function of blend composition, suggesting miscibility of the BmPE/LDPE-2 blends. However, the birefringence of LmPE/LDPE-1 is not a linear function of blend composition, which indicates the existence of form birefringence, suggesting immiscibility of the LmPE/LDPE-1 blends.

In short, this work provides a useful technique to use extruder as an inline rheometer in order to better understand the rheology of polymer melt during film blowing process. We hope the experimental data we provided are reliable enough for different models to be compared with.

### CHAPTER 3. RHEOLOGICAL EFFECTS OF POLYETHYLENES IN FILM BLOWING\*

Yunli Fang, Pierre J. Carreau and Pierre G. Lafleur

Centre de Recherche Appliquée Sur les Polymères (CRASP), Dept. of Chemical Engineering, Ecole Polytechnique, Montreal, QC, H3C 3A7, Canada

#### Abstract

The aim of this work is to correlate the rheological properties and processability of various polyethylenes during film blowing process. The effect of rheology on the kinematics and dynamics of film blowing for five different polyethylene resins has been extensively studied using a fully instrumented laboratory unit. The complex viscosity, shear viscosity, uniaxial elongational viscosity and non-uniform biaxial elongational viscosity as well as the strain rates and stresses during film blowing have been determined and correlated to the bubble stability.  $G'$  versus  $G''$  plots were found to be virtually independent of temperature for all the polymers investigated. The more elastic polymers (larger  $G'$  values) were found to be the more stable in film blowing. Also the more stable polymer melts were found to be those possessing larger elongational properties.

Key word: film blowing, polyethylene(s), bubble stability, rheology, elongational viscosity

---

\* Published in *Polymer Engineering & Science*. **43(7)**, 1391-1406 (2003)

### 3.1. Introduction

Film blowing is one of the most major polymer processing operations, but yet the less understood process. This is largely due to the complex rheology of polymer melts in non-uniform biaxial, non-isothermal flow. From a practical point of view, it is highly desirable to have a criterion (or criteria) for the choice of resins that will give good tubular film processability, without having to perform a time-consuming film blowing operation. However, one can find only scattered data on the relationship between the rheological behavior of polymer and its processability (1,2,3). The relationship between rheology and processing is still poorly understood, mostly because of lack of sufficient and reliable data. The aim of this study is to fill partly this gap.

Two key parameters affecting the film blowing process are the bubble diameter and velocity. These parameters are used for almost all the calculations, thickness, strain rates, etc. Almost all the researchers in film blowing investigated both diameter and velocity profiles of the bubble as well as the bubble stability during film blowing using traditional video method. Dowd (4), and soon after Farber *et al.* (1) placed a piece of tape onto the molten stalk of the bubble and followed its progress with a movie camera. Kanai and White (5) used a similar technique in their kinematic study of polyethylene blown films. Huang and Campbell (6) placed a mark with a wax pencil on to the stalk of bubble and followed its progress. Based on the technique used by the previous authors, Simpson and Harrison (7) and Ghaneh-Fard *et al.* (8) used S-VHS video camera to record the process and treated the video signal by means of computer. New techniques and their advantages will be presented in this paper.

### 3.1.1. Determination of Stresses in Film

The force equilibrium equation in the normal direction, assuming thin membrane approximation and neglecting surface tension effects (9), is:

$$\frac{\Delta P}{h} = \frac{\sigma_{11}}{R_L} + \frac{\sigma_{33}}{R_H} - \rho g \sin \theta \quad (3.1)$$

where  $\sigma_{11}$ ,  $\sigma_{33}$  are normal stresses in machine and transverse direction, respectively;  $\rho$ , the density of the polymer melt;  $h$ , and  $\theta$ , the thickness of the bubble, bubble inflation angle at an axial distance  $z$ ;  $R_L$ ,  $R_H$  are the radii of curvature in machine and transverse direction, respectively given by:

$$R_L = -\frac{\sec^3 \theta}{d^2 r / dz^2} \quad (3.1)$$

and

$$R_H = r \sec \theta \quad (3.3)$$

where  $r$  is the radius of the bubble at axial distance  $z$ .

The force balance in the machine direction on a segment of bubble between an axial position  $z$  and nip-rolls ( $Z$ ) leads to the relation (9):

$$2\pi r h \sigma_{11} \cos \theta + \pi \Delta P (R^2 - r^2) + 2\pi \rho g \int_z^Z r h \sec \theta dz = F_z \quad (3.4)$$

where  $F_z$  is the drawdown force at nip rolls;  $\Delta P$  is the relative pressure inside the bubble.

The drawdown force was measured by a few authors (9,10) using mechanical transducers. However, the bubble force measurement is influenced by different frictional forces during flattening of the film bubble, pinching-off and taking-up. Hence, it is not accurate. We have preferred using the birefringence data to obtain the normal stress differences.

The flow birefringence technique is very useful to investigate the stresses occurring in film flow. This technique improves the classical mechanical methods in several aspects. Firstly, it does not disturb the flow field (11). Secondly, it responds faster and has higher sensitivity to dilute components. Thirdly, it has the ability to isolate the dynamics of separate constituents in the case of multi-components systems (12,13). However, since the birefringence is only an integrated effect along the direction of light beam, only birefringence data in two-dimensional fields without birefringence gradients in the direction of light beam can be collected. Moreover, optical methods require that the fluid under investigation be transparent (14).

The rheological application of the birefringence method is based on the stress-optical law, which gives proportionality between the components of the refractive index (polarizability) tensor and the stress tensor. In a wide range of conditions involving not too large stresses, the linear stress-optical law is expressed as:

$$\Delta n = C \Delta \sigma \quad (3.5)$$

where  $C$  is a material constant known as the stress-optical coefficient,  $\Delta n$  the birefringence, and  $\Delta \sigma$  the corresponding difference of the principal stresses.

Ghaneh-Fard *et al.* (14) were the first to apply the stress-optical law to calculate the normal stresses during film blowing. The stress-optical law, which can translate the birefringence data into stresses, is given by:



$$n_{11} - n_{33} = C(\sigma_{11} - \sigma_{33}) \quad (3.6)$$

In this work, the MD and TD stresses ( $\sigma_{11}, \sigma_{33}$ ) can be calculated via equations (3.1) and (3.6). The stress-optical coefficient,  $C$ , for all the PEs studied, was taken to be  $2.2 \times 10^{-9} \text{ m}^2 / \text{N}$  (15).

### 3.1.2. Determination of Non-uniform Biaxial Elongational Viscosity

The uniform biaxial elongational viscosity is defined as (16):

$$\eta_b = \frac{\sigma_{11} - \sigma_{22}}{\dot{\epsilon}_b} \quad (3.7)$$

where  $\dot{\epsilon}_b$  is the uniform biaxial deformation rate. For non-uniform biaxial deformation, as encountered in film blowing, we suggest to replace  $\dot{\epsilon}_b$  by the effective rate of deformation  $\bar{\dot{\gamma}}$ , defined as:

$$\bar{\dot{\gamma}} = \sqrt{\frac{1}{2} \text{II}_{\dot{\gamma}}} = \sqrt{\frac{1}{2} (\dot{\gamma}_{11}^2 + \dot{\gamma}_{22}^2 + \dot{\gamma}_{33}^2)} \quad (3.8)$$

where  $\dot{\gamma}_{11}$  and  $\dot{\gamma}_{33}$  are strain rates in machine and transverse direction, respectively, given by:

$$\dot{\gamma}_{11} = 2 \frac{dV_z}{dz} + 2V_z \left( \frac{dr}{dz} \right) \left( \frac{d\theta}{dz} \right) \quad (3.9)$$

and:

$$\dot{\gamma}_{33} = 2 \left( \frac{V_z}{r} \right) \frac{dr}{dz} \quad (3.10)$$

For an incompressible material,  $\sigma_{11} + \sigma_{22} + \sigma_{33} = 0$ , and we can define a non-uniform biaxial elongational viscosity for film blowing as:

$$\eta_{fb} = \frac{\sigma_{11} - \sigma_{22}}{\dot{\gamma}} = \frac{(2\sigma_{11} + \sigma_{33})}{\dot{\gamma}} \quad (3.11)$$

Equations (3.8) and (3.11) will be used to represent our experiment data.

### 3.1.3. Bubble Stability

Bubble stability plays a very important role in evaluating the processability of a polymer. A stable bubble is a requirement not only for the continuous operation of the process but also for the production of an acceptable film.

In order to represent the kinematics of the tubular film process in a global manner, we use three most important kinematical variables, the take-up ratio (TUR), the frost line height (FLH) and the blow-up ratio (BUR) under a certain mass flow rate and a fixed temperature at die exit. The former two quantities control the machine direction deformation rates and the latter the transverse direction deformation rates. Increasing values of TUR and BUR is explicitly desirable in a commercial film production. On the other hand, even though FLH does not control the film geometry, its effect on final film

properties cannot be denied, as it is a response to cooling conditions. The detailed criteria for the determination of bubble stability can be found elsewhere (17).

## **3.2. Experimental**

### **3.2.1. Materials**

Five different film-grade polyethylene resins: two low density polyethylenes (LDPEa, LDPEb), a high density (HDPE), a linear low density polyethylene (LLDPE) and a metallocene-catalyzed polyethylene (mPE) were used in this study. The main characteristics of the five resins are summarized in Table 3.1. The mPE has a small quantity of long chain branches.

### **3.2.2. Film Blowing In-line Measurements**

The film blowing experiments were conducted on a laboratory film unit, consisting of a 45mm Killion single screw extruder equipped with a helical blown film die (inner diameter = 60.44 mm, outer diameter = 63.49 mm). A double lip air ring, which has more efficient cooling than single lip, was used for cooling. Also this laboratory unit has no internal cooling system. The temperature of the cooling air was not regulated but at room temperature. The influence of the design and position of the movable lip was not investigated in this work.

An infrared pyrometer (IRCON 3400), which absorbs the infrared radiation in a wavelength of 3.43 $\mu$ m, was employed to obtain the bubble temperature profile. An optical train (14) and a Laser Doppler Anemometry (LDA) (Dantec, BSA-F50) were used for birefringence and instantaneous local velocity measurements, respectively.

Instead of using the traditional video method, a “line-scan” camera (18), which can catch line images from two perpendicular mirrors at certain axial distance and send the images to a PC with a pre-installed LabVIEW program, was used to obtain the bubble diameter profile in-line. The LDA, line-scan camera, infrared pyrometer, optical train were installed at the same height in a frame and could be moved simultaneously along the length of the bubble in order to collect the data at the same axial distance and the same time.

### 3.2.3. Rheological Measurements

The dynamic rheological properties, storage modulus ( $G'$ ), loss modulus ( $G''$ ) and complex viscosity ( $\eta^*$ ) were measured using a controlled stress rheometer (Bohlin CSM) at desired temperatures. The stabilities of all resins were verified at a low constant frequency (0.01Hz) under 200°C for periods of over 1.5 h. The linear viscoelastic properties were measured as a function of frequency in the frequency range of 0.01 to 30Hz and the applied stresses were adjusted to maintain the experiments in the linear domain. Each measurement was repeated at least three times. The final results were obtained from reproducible experiments and the data are believed to be within  $\pm 10\%$ . Activation energy (also shown in Table 3.1) for all the polyethylenes studied has been determined using the Arrhenius equation. The temperature shift factors were obtained via the time-temperature superposition principle (19).

The shear viscosity was determined using both a piston-driven capillary (Instron) rheometer and an in-line capillary rheometer (mounted on the extruder). The geometries of the dies of both piston-driven and in-line capillary rheometers can be seen in Table 3.2. A setup (20) was designed to measure shear viscosity from the in-line capillary rheometer, where a by-pass valve was employed in order to change the flow rate through the capillary die, while the total extruder flow rate remained constant and thus leaving

the extruder operating conditions unchanged. With this design, the polymer before extrusion die can be controlled by keeping the thermo-mechanical history unchanged. The melt temperature was kept at 200°C, which was the same as the extrusion temperature during the film blowing process, and the screw rotating speed was 75 rpm. The measurements were carried out at a temperature of 200°C for both piston-driven and in-line capillary rheometers. The shear viscosity was calculated following the Weissenberg-Rabinowitch procedure for both techniques and the Bagley correction was used to correct the wall shear stress for in-line capillary rheometer.

The apparent uniaxial elongational viscosity was determined using two different hyperbolic converging dies. Both dies have the same entry radius (12.7 mm) with different lengths and exit radii. The first die ( $D_1$ ) is 10 mm long with an exit radius of 1.995 mm whereas the second die ( $D_2$ ) is 20 mm long with an exit radius of 2.805 mm. The analyses of Cogswell (21) and Binding (22) were employed for the calculations.

### **3.3. Results and Discussion**

#### **3.3.1. Complex and Shear Viscosities**

The comparison of complex and steady shear viscosities for the five resins at 200°C are shown in Fig. 3.1. Not surprisingly, at low frequency, the HDPE shows the largest viscosity and no Newtonian plateau is reached within the investigated region; the viscosities of the other four resins seem to reach a plateau at low frequency. At high frequency, the LDPEa and LDPEb data almost overlap and show lower viscosity compared to the HDPE, LLDPE and mPE.

Both piston-driven and in-line capillary rheometer viscosity data show fairly good agreement. The shear and complex viscosities of the mPE, LLDPE, LDPEb and

HDPE match well at corresponding shear rate and frequency, indicating that the Cox-Merz rule is fairly satisfied for these polyethylenes within experimental error. However, for the LDPEa, the shear viscosity is larger than the complex viscosity. Shroff and Shida (23) showed that the differences between steady shear and dynamic viscosities increased with increasing branching for PE resins. However, it is worth noting that some results in the literature (24, 25) reported that linear polyethylenes violate the Cox-Merz rule while branched polyethylenes exhibit a better agreement. The zero shear viscosities ( $\eta_0$ ), as reported in Table 1, were determined using the Carreau-Yasuda model (16).

Fig. 3.2 shows the variation of shift factors  $a_T$  with temperature ( $1/T$ ), described by the Arrhenius equation:

$$a_T = \frac{\eta(T)}{\eta(T_0)} = \exp \left[ \frac{E_a}{R} \left( \frac{1}{T} - \frac{1}{T_0} \right) \right] \quad (3.12)$$

The values of the activation energy  $E_a$  for all the polyethylenes used are presented in Table 1. The values reported for the HDPE, LLDPE and LDPE are in agreement with literature data (26) while the mPE value corresponds to the data published by Bin Wadud and Baird (27).

### 3.3.2. Apparent Uniaxial Elongational Viscosity

The uniaxial elongational viscosity calculated is only an apparent one because as the polymer flows in the hyperbolic convergent die, it is not under steady-state stress conditions, although the elongational rate is approximately constant. The apparent uniaxial elongational viscosity for the LDPEb was calculated via the Cogswell and Binding analyses based on shear data and pressure drop in the converging dies. The

results are presented in Fig. 3.3a. Due to the different assumptions of the two analyses, the elongational viscosity calculated from the Binding method is slightly different from the one determined from the Cogswell method. Some discrepancies are observed between the two sets of data, obtained using the two dies,  $D_1$  and  $D_2$ . However, these data are acceptable considering the complexity of these measurements. Similar results have been obtained for the HDPE and the mPE. Fig. 3.3b compares the elongational viscosity of the three polyethylenes calculated from the Cogswell method using die  $D_1$ . They all exhibit strain-thinning behavior over the range studied. Unfortunately, we are unable to show the elongational behavior of the polymer melts under lower elongational rates due to apparatus limitations. Results of the elongational viscosity for the LDPEa and the LLDPE have been reported elsewhere (8). Different die geometries were used and the apparent elongational viscosity data are not comparable to our data.

### 3.3.3. Temperature, Diameter, Velocity and Thickness Profiles

The temperature profiles as a function of the vertical distance from the die exit ( $z$ ) for the mPE and LDPEb are shown in Fig. 3.4. The air ring, which was 90mm high, restricted the measurement of the temperature profile above that distance from the die. Fig. 3.4 shows that the temperature decays almost linearly along the bubble length and reaches a plateau, where the temperature of the LDPEa and mPE is 118°C and 102°C, respectively. The plateaus correspond to the stress induced crystallization temperatures of both polyethylenes, which are higher than the equilibrium crystallization temperatures, as expected.

A comparison of the bubble diameter profiles measured by the “line-scan” camera method (line plot) and the traditional (video camera) method (scatter plot) is shown in Fig.3.5 for a typical run of the LDPE containing 1% home-made white ( $\text{TiO}_2$ ) colorant. Fairly good agreement between the two sets of measurements is observed.

Moreover, the “line-scan” camera method has obviously the following advantages: (a) it is much faster and easier, both diameter profile and bubble stability can be determined in-line without any post tedious work. (b) It is more accurate than the traditional video method that neglects the view angle when the image of the whole bubble is taken. The “line-scan” camera is moved simultaneously with the whole system including LDA and the optical train for birefringence along the bubble. Thus, effects of the view angle and size of the mark can be eliminated and instantaneous information can be collected in-line. (c) Finally, the “line-scan” camera catches two perpendicular images and thus can quantitatively determine the uniformity of the bubble.

Fig. 3.6 shows the velocity profile of the bubble for a typical run for the LDPE measured by the traditional method (video method) using a marker onto the bubble. The figure shows the influence of the sampling frequency on the scatter of the data. Obviously, long sampling periods have to be used, but instantaneous information is lost when longer sampling periods are used. Fig. 3.7 (a, b) presents the bubble diameter and velocity profile along the axial distance for the mPE and LDPEb. The marked differences are the reflection of the different shapes of the bubble, the mPE having a much longer neck than the LDPEb.

#### 3.3.4. Strain Rates

The results of strain rates depend not only on accurate measurements of velocity and diameter profiles but also on regression techniques used. As far as we aware, different researchers used different regression techniques (1,5,8,9). The velocity profiles of both LDPEb and mPE were divided into two zones, below and above the FLH. A linear regression was used for the zone below the FLH. The diameter profiles of both LDPEb and mPE were divided into three zones, the neck zone, the expansion zone, and



above FLH. A fourth order polynomial expression was used for both resins in the expansion zone.

Fig. 3.8 compares the MD and TD strain rates of both mPE and LDPEb. The strain rates in TD for both LDPEb and mPE give similar trends. They remain close to zero at low axial distance (because of the existence of the neck zone), then increase sharply to their respective maximum in the expansion zone; and finally decrease drastically to zero again at FLH. The sudden jump for the LDPEb is due to the regression technique used. Because of a longer neck zone, the TD strain rate of the LDPEb starts to increase earlier than that of mPE. Also, the maximum in TD strain rate for mPE is larger and occurs at a higher distance than that of the LDPEb. The strain rates in MD for both LDPEb and mPE are quite similar, which remain almost constant, at low axial distances. As the axial distance increases, the MD strain rate for mPE increases slightly then decreases whereas the MD strain rate for the LDPEb decreases slightly. As expected, the strain rates in MD for both resins jump to zero above their respective FLH. The sudden jump is also due to the regression technique used. The MD strain rate for the mPE is always larger than that for the LDPEb except near FLH. As far as we aware, in the region of bubble expansion, almost all the published data showed that there is a peak for MD strain rates. Our data show that such a result is not necessarily true.

By comparing the strain rates in MD with those in TD, we may find the TD strain rates in the expansion zone exceed the MD strain rates for both LDPE and mPE. The same findings have been reported by other authors (1,8) for a LDPE.

### 3.3.5. Birefringence and Stresses

Fig. 3.9a presents the birefringence data for both mPE and LDPEb. Only the data of the LDPEb below the FLH are presented, since the birefringence increases dramatically above FLH and the trend could not be clearly shown. For the conditions investigated, the birefringence values are always positive and increase along the bubble indicating that the orientation in MD is always greater and increases faster than that in TD. In the vicinity of FLH, the birefringence for the mPE decreases slightly indicating that the orientation in MD increases slower than that in TD. This was also observed by Ghaneh-Fard et al. (14) for a LLDPE. They attributed it to the relaxation of molecular orientation, as originally proposed by Maddams and Preedy (28). The dramatic increase of birefringence near FLH during crystallization is due to the nucleation and growth processes and orientation of crystallites (29).

Based on the in-situ birefringence data and stress-optical law, the MD and TD stresses for the mPE and LDPEb were calculated using Equations 3.1 and 3.6 and the results are reported in Fig. 3.9b. Since the stress optical law is probably not valid when crystallites are present (30), only data below the height for which crystallization started are shown in the figure. For both mPE and LDPEb, the stresses in MD are always larger than those in TD and the differences, which are more pronounced for the LDPEb, increase with the axial distance. This is due to the increasing positive birefringence as mentioned before. By comparing the MD and TD stresses for the mPE and LDPEb, we see pronounced differences. The TD stress of the mPE almost overlaps with that of the LDPEb at lower axial distance and the differences become clear only at higher axial distance. The MD stress of the LDPEb increases faster than that of the mPE and the differences become more and more pronounced along the bubble.

### 3.3.6. Non-uniform Biaxial Elongational Viscosity and Deformation Rate

The non-uniform biaxial elongational viscosity and effective rate of deformation were calculated using Equations (8) and (11) and are reported in Fig. 3.10. The LDPEb exhibits a larger elongational viscosity and smaller deformation rates near FLH. Since this is a non-isothermal process, it is mandatory to compare the rheological parameters at the same temperature. We chose 170°C as the reference temperature. Plots of the non-uniform biaxial elongational viscosity versus deformation rate using the temperature shift factors at the reference temperature are presented in Fig. 3.11. Only data at lower axial distances (<250mm for mPE; < 260mm for LDPEb), that is only for films at higher temperature (>120°C for mPE; >140°C for LDPEb), are presented. The rheological behavior of both resins is quite different: the mPE only exhibits strain-thinning behavior whereas the LDPEb has almost a constant elongational viscosity (possibly exhibiting some strain-hardening at larger deformation rates).

### 3.3.7. Bubble Stability

Since the stability of polyethylenes (LDPE, HDPE and LLDPE) had been extensively studied in details previously (17) in our laboratory, the purpose the present study is to complement the previous investigation with mPE data.

Fig. 3.12 compares the bubble stability for the LLDPE and mPE at the same operation conditions (extrusion temperature and mass flow rate, etc.) for two TUR values, 4.7 (Fig.12a) and 6.2 (Fig.12b). Stable or unstable conditions are reported as functions of the frost line height (FLH), blow-up ratio (BUR) and take-up ratio (TUR). The definition for stability and the description of the three observed instabilities can be found in Ghaneh-Fard et al. (23). We see that the mPE appears slightly more stable than the LLDPE. LDPE is well known for its stability in film blowing due to its long chain

branches. LDPEa and HDPE instability data have been reported by Ghaneh-Fard et al. (23). The LDPEb has also been extensively studied and the results will be presented elsewhere. We propose the following relative order of stability (from stable to unstable) for the five polymers studied:

$$\text{LDPEa or LDPEb} > \text{HDPE} > \text{mPE} > \text{LLDPE}$$

### 3.3.8. The Role of Rheology in Film Blowing

Rheological properties play an important role in film blowing. They govern the shape and stability of the bubble and the onset of sharkskin (surface roughness). Because of the complexity of the flow involved, it is not generally possible to establish simple quantitative correlations between these phenomena and easily measured rheological properties. However, an understanding of how variations in the rheological behavior of melts can affect the processing and properties of blown films is essential if one is to achieve optimum results for this process.

### 3.3.9. $G'$ , $G''$ and Relationship to Bubble Stability

It is well-accepted fact that the storage modulus  $G'$  in oscillatory shear flow may be considered as the amount of energy stored in a viscoelastic liquid. So, the ratio of  $G'/G''$  may be interpreted as the ratio of the energy stored to the energy dissipated. In order to compare the elastic behavior of one fluid against others, Han and Lem (31) suggested to use logarithmic plots of  $G'$  and  $G''$ . They also used a simple dimensional analysis to show the relationship between  $G'$  and  $G''$  is virtually independent of temperature and molecular weight.

Fig. 3.13a presents the plot of  $\log G'$  versus  $\log G''$  for LDPEa at five different temperatures. As expected, all the data fall into a single curve, that is:  $G'$  versus  $G''$  is independent of temperature. The other four polymers, HDPE, LLDPE, LDPEa, and mPE, also exhibit the same behavior. It was also reported by Wong et al. (32) for a LDPE, a LLDPE and a mPE. Fig. 3.13b compares  $G'$  versus  $G''$  for the five polymers investigated. We observe that the two LDPEs are considerably more elastic than the HDPE, which is more elastic than the LLDPE and mPE. We note that the LLDPE and mPE show a comparable behavior at large values of  $G''$ , that is corresponding to the larger frequencies or strain rates relevant to the processing conditions. However, at low frequencies the mPE shows larger  $G'$  values. One interesting observation is that the larger the  $G'$  value (the more elastic the polymer) is, the more stable the bubble is during film blowing. That is to say, the order of elasticity for the five resins (in  $G'$  value), from high to low, coincides with that of bubble stability, from stable to unstable, although most authors believe that shear properties play an insignificant role on film blowing due to the fading memory of polymer melts. As pointed out by Wong et al. (32),  $G'$  is strongly dependent on MWD and molecular structure such as long chain branches. The broader the MWD, the larger the  $G'$ . It is well accepted that a polymer with broad molecular weight distribution (MWD) and long chain branches has good processability. Han and John (33) gave an extensive explanation with the aid of molecular theories. Nevertheless, the correlation of elasticity with film stability needs to be further assessed using different polymers.

### 3.3.10. Elongational Behavior

It is believed that the restrictiveness of shear data is their inability to provide direct relations with processing flows because the data only reflect the linear viscoelastic part of the material behavior. For this reason, uniaxial elongational rheology should be useful to complement the shear data as they capture the non-linear aspects of the melt

flow. The subtle shear rheology differences become more explicit when examining the elongational viscosity at different elongational rates.

It is well recognized that materials with pronounced strain-hardening behavior always reveal superior bubble stability. However, there was no strain-hardening behavior observed for any of the polymers and conditions investigated. Note the deformation rates involved during film extrusion range from 0.01 to 1 s<sup>-1</sup> depending on the take-up ratio and distance from the die to the freeze line. The lowest strain rate in the converging die we could obtain was larger than 1 s<sup>-1</sup>. Hence, the uniaxial elongational viscosity data cannot be directly related to the bubble stability. Alternatively, the Trouton ratio, which is ratio of the uniaxial elongational viscosity to the shear viscosity ( $\eta_e / \eta$ ), may be a useful parameter for correlating the bubble stability.

The Trouton ratios for the five polyethylenes calculated with the aid of the temperature shift factors are shown in Fig. 3.14. All the elongational data were based on the Cogswell technique from measurements using the hyperbolic converging dies for the HDPE, LDPEb and mPE and from a conical die (8) for the LLDPE and LDPEa. The figure shows that, for all the polymers investigated, the Trouton ratios far exceed 3, which is the theoretical value for Newtonian fluids. The LDPEa and LDPEb exhibit larger Trouton ratios than the HDPE, LLDPE and mPE.

### 3.4. Concluding Remarks

In order to get a better understanding of the effects of rheological properties on the processing performance of polyolefines in film blowing, different techniques have been used to measure the rheological properties of five polyethylenes: HDPE, LLDPE, LDPEa, LDPEb, mPE. The bubble velocity profiles have been determined using LDA and a “line-scan” camera was used to determine the bubble diameter profile and stability.

From our own experimental data and those of a previously published work (17), we propose the following relative decreasing order of stability for the polymers studied:

$$\text{LDPEa or LDPEb} > \text{HDPE} > \text{mPE} > \text{LLDPE}$$

Log  $G'$  versus Log  $G''$  plot was observed to be virtually independent of temperature for all the polymers investigated. The larger the  $G'$  value was, the more stable the bubble was during film blowing.

The Trouton ratios for the HDPE, LLDPE, LDPEa, LDPEb and mPE versus deformation rate have been reported. In all cases, the ratio exceeds the limiting value of 3, expected for Newtonian fluids. The Trouton ratios of the LDPEa and LDPEb are much larger than those of the HDPE, LLDPE and mPE. We believe that the high values of the Trouton ratio are closely related to the bubble stability in film blowing. Hence, it appears that information on the elongational viscosity is at least as important information as the shear flow properties.

### Acknowledgments

The authors wish to acknowledge the financial support received from NSERC (Natural Sciences and Engineering Research Council of Canada). They are also grateful to Mr. L. Parent for technical help and to Dow Chemical, Novacor and Union Carbide for providing the materials.

### 3.5. References

1. R. Farber, and J. Dealy, *Polym. Eng. Sci.* **14**, 435 (1974).
2. Ghijsels, J.J.S.M. Ente, and J. Raadsen, *Int. Polym. Process.* **4**, 284 (1990).
3. C.D. Han and H. Kwack, *J. Appl. Polym. Sci.* **28**, 3399 (1983).
4. L.E. Dowd, *SPE J.* **28**, 22 (1972).
5. T. Kanai and J.L. White, *Polym. Eng. Sci.* **24**, 1185 (1984).
6. T.A. Huang and G.A. Campbell, *J. Plastic Film and Sheeting* **2**, 30 (1986).
7. D.M. Simpson and I.R. Harrison, *SPE ANTEC'91* 203 (1991).
8. A. Ghaneh-Fard, P.J. Carreau, and P.G. Lafleur, *Polym. Eng. Sci.* **37**, 1856 (1997).
9. C.D. Han and J.Y. Park, *J. Appl. Polym. Sci.* **19**, 3257 (1975).
10. P.P. Tas, *Ph. D. Dissertation* Dept. Mech, Eng., Eindhoven University of Technology, The Netherlands (1993).
11. J.A. Van Aken and H. Janeschitz-kriegl, *Rheol. Acta* **19**, 744 (1980).
12. J.M. Dealy and K.F. Wissbrun, *Melt Rheology and Its Role in Plastics Processing: Theory and Applications* Van Nostrand Reinhold (1990).
13. G.G. Fuller, *J. Rheol.* **23**, 457 (1990).
14. Ghaneh-Fard, P.J. Carreau, and P.G. Lafleur, *J. Plastic Film and Sheeting* **12**, 68 (1996).
15. M. Okamoto, A. Kojima, and T. Kotaka, *Polym.* **39**, 2149 (1998).
16. P.J. Carreau, D. De Kee, and R.P. Chhabra, *Rheology of Polymeric Systems: Principle and Application* Hanser Publishers (1997).
17. A. Ghaneh-Fard, P.J. Carreau, and P.G. Lafleur, *AIChE J.* **42**, 1388 (1996).
18. J. Laffague, L. Parent, P.G. Lafleur, P.J. Carreau, Y. Demay, J.F. Agassant, Accepted for publication in *Intern. Polym. Process.* (2002).
19. J.D. Ferry, and M. L. Williams, , *J. Colloid. Sci.* **7**, 347 (1952).



20. C. Lacroix, M. Grmela, and P.J. Carreau, *J. of Non-Newt. Fluid Mech.* **80**, 183 (1999).
21. F.N. Cogswell, *Polym. Eng. Sci.* **12**, 64 (1972).
22. D.M. Binding, *J. of Non-Newt. Fluid Mech.* **27**, 173 (1988).
23. R.N. Shroff, and M. Shida, *J. Polym. Sci.* Part A-2, **2**, 1917 (1970).
24. L.A. Utracki, and R. Gendron, *J. Rheol.* **28**, 601 (1984).
25. S. Venkatraman, M. Okano, and A. Nixon, *Polym. Eng. Sci.* **30**, 308 (1990).
26. H. Mavridis, R.N. Shroff, *Polym. Eng. Sci.: Physics Ed.* **23**, 1778 (1992).
27. S.E. Bin Wadud and D.G. Baird, *SPE ANTEC'99* 1200 (1999).
28. W. F.Maddams, , and J.E. Preedy, *J. Appl. Polym.Sci.* **22**, 2739
29. Y. Shimonmura, , J.E. Spruiell, and J.L. White, *J. Appl. Polym. Sci.* **27**, 2663.
30. C.W. Macosko *Rheology: Principles, Measurements, and Applications* VCH Publishers (1994)
31. C.D. Han and K.W. Lem. *Polym. Eng. Rev.* **2**, 135 (1983).
32. C.M. Wong, H.H. Shih, and C.J. Huang, *J. Rein. Plast. Comp.* **17**, 945 (1998).
33. C.D. Han and M.S. John, *J. Appl. Polym. Sci.* **32**, 3809 (1986).

Table 3.1. Materials used in this study and main characteristics.

Polymer	Supplier	MI (dg/min)	Density (kg/m <sup>3</sup> )	$\eta_0^1$ (Pa.s)	$E_a$ (kJ/mol.K)
LDPEa	Novacor LF0219-A	2.0	919	11000 <sup>2</sup>	54.9
LDPEb	Dow Chemical 503A	1.9	923	10200 <sup>2</sup>	57.3
HDPE	Petromont DMDC-6400	0.7	960	96060 <sup>3</sup>	31.2
LLDPE	Union Carbide TUFLIN HS- 7028	1.0	924	10430 <sup>2</sup>	28.8
mPE	Dow Affinity <sup>®</sup> PL1880	1.0	902	12930	37.5

<sup>1</sup> Zero shear viscosity at 200°C.<sup>2</sup> Determined by fitting the data of complex viscosity to a Carreau-Yasuda equation.<sup>3</sup> Determined from Ghaneh-Fard *et al.* (8) using temperature shift factor.

Table 3.2. Geometries of the dies for the piston-driven capillary rheometer (INSTRON) and for the in-line capillary rheometer (mounted on a Killion extruder).

	In-line Capillary Rheometer			Piston-Driven Capillary Rheometer	
	$L/D = 8$	$L/D = 12$	$L/D = 16$	$L/D = 39.52$	$L/D = 24.61$
Diameter (mm)	1.6			1.27	
Length (mm)	12.8	19.2	25.6	50.04	31.25

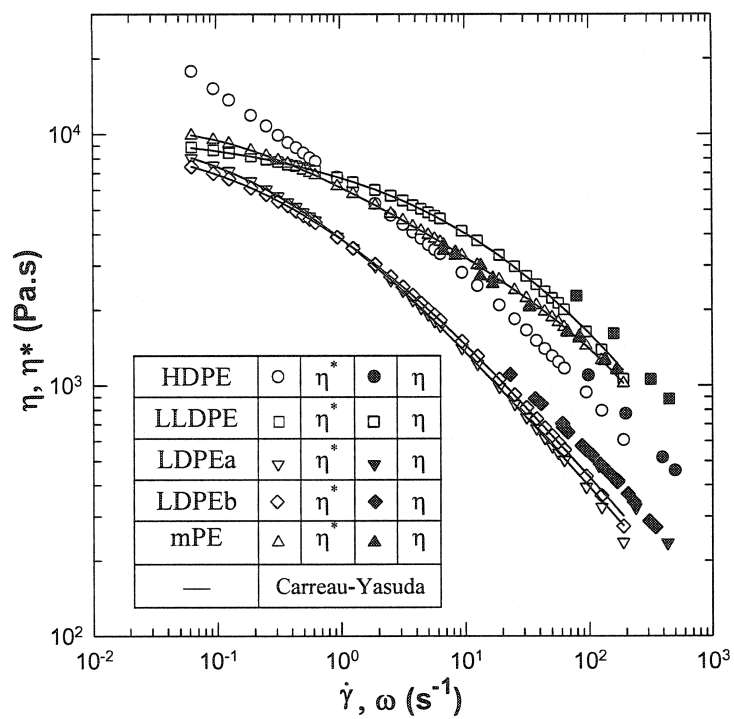


Figure 3. 1. Comparison of complex and steady shear viscosity data for five resins at 200°C.

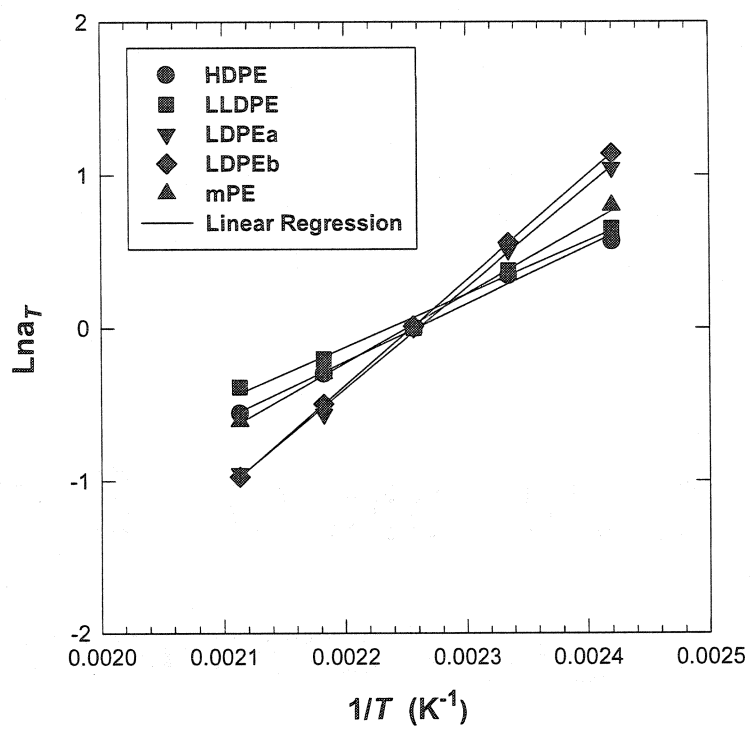


Figure 3. 2. Temperature shift factors at a reference temperature of 170°C.

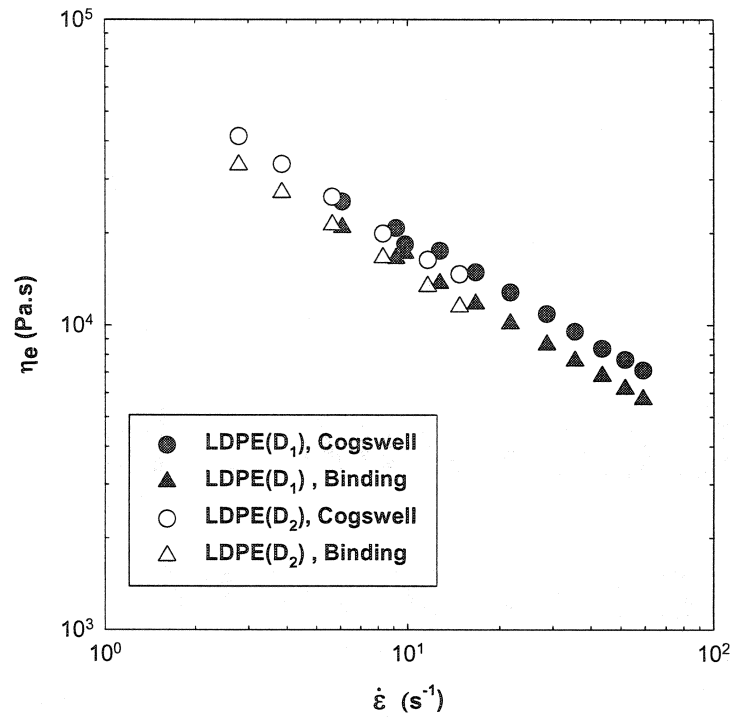
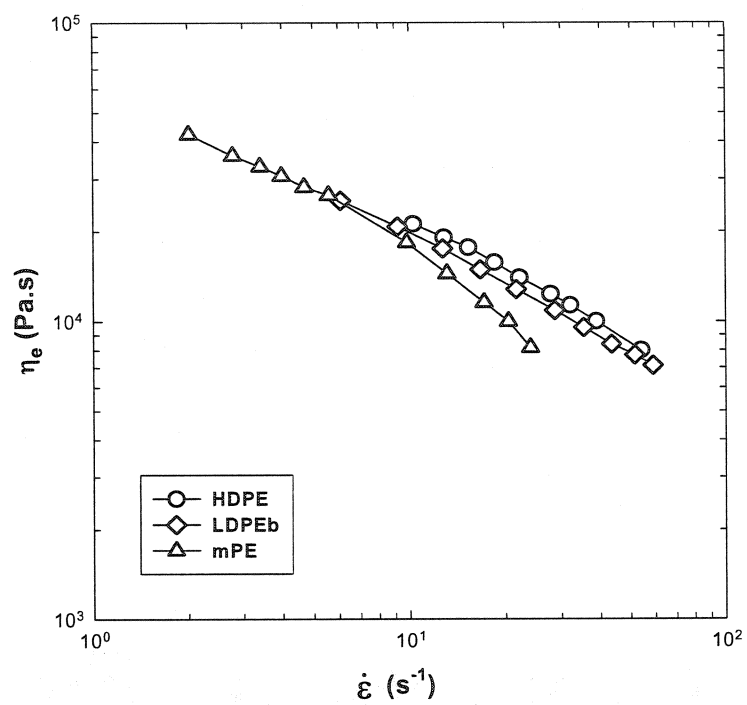


Figure 3. 3. Apparent uniaxial elongational viscosity versus elongational rate at 200°C.  
(a) calculated from two different techniques using two different dies for LDPEb.



(Continued) (b) Calculated from Cogswell method using die  $D_1$  for HDPE, LDPE and mPE.

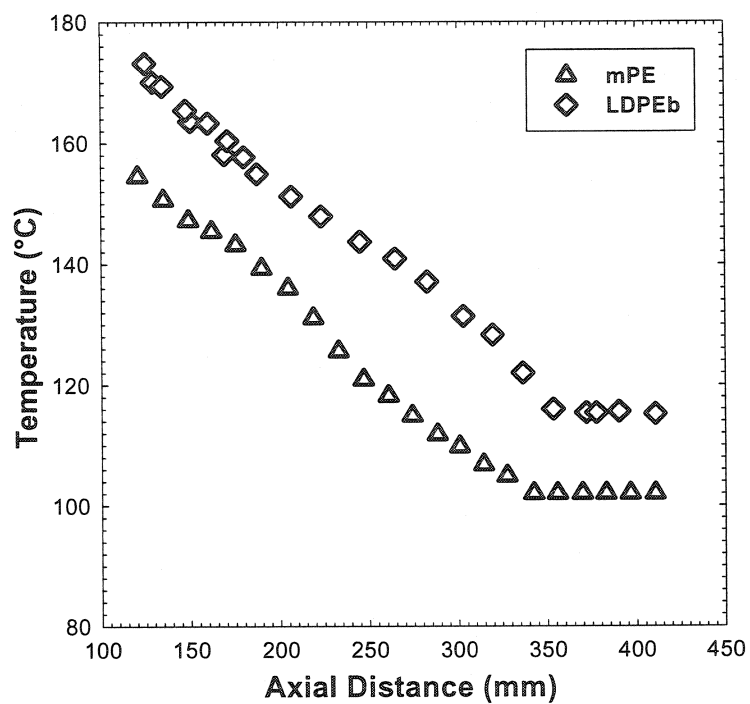


Figure 3. 4. Bubble temperature along the axial distance for mPE and LDPEb. The mass flow rate = 3.0 kg/h, TUR = 13.6, BUR = 2.0, temperature = 200°C.



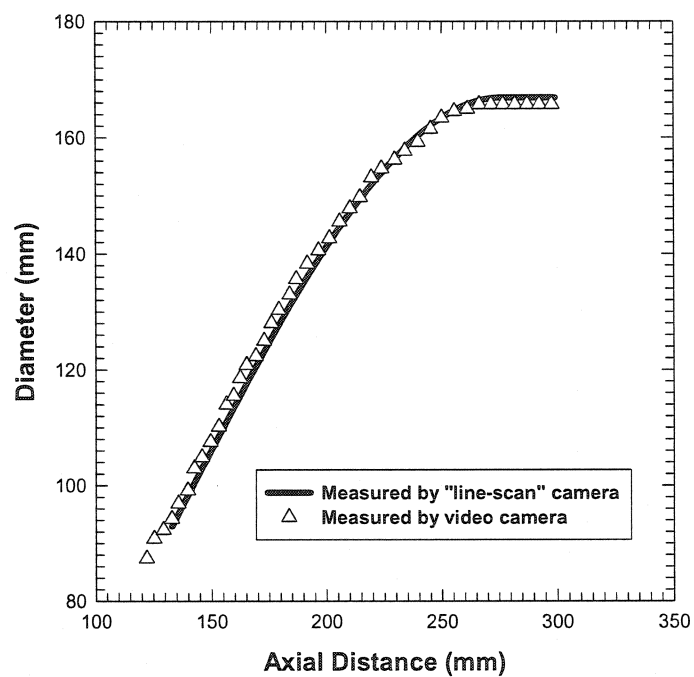


Figure 3. 5. Comparison of bubble diameter profile of LDPE with 1% colorant measured both by the line-scan camera method and by the traditional video method (operating conditions: mass flow rate = 5.0 kg/h, BUR = 2.7, TUR = 5.0, temperature = 200°C).

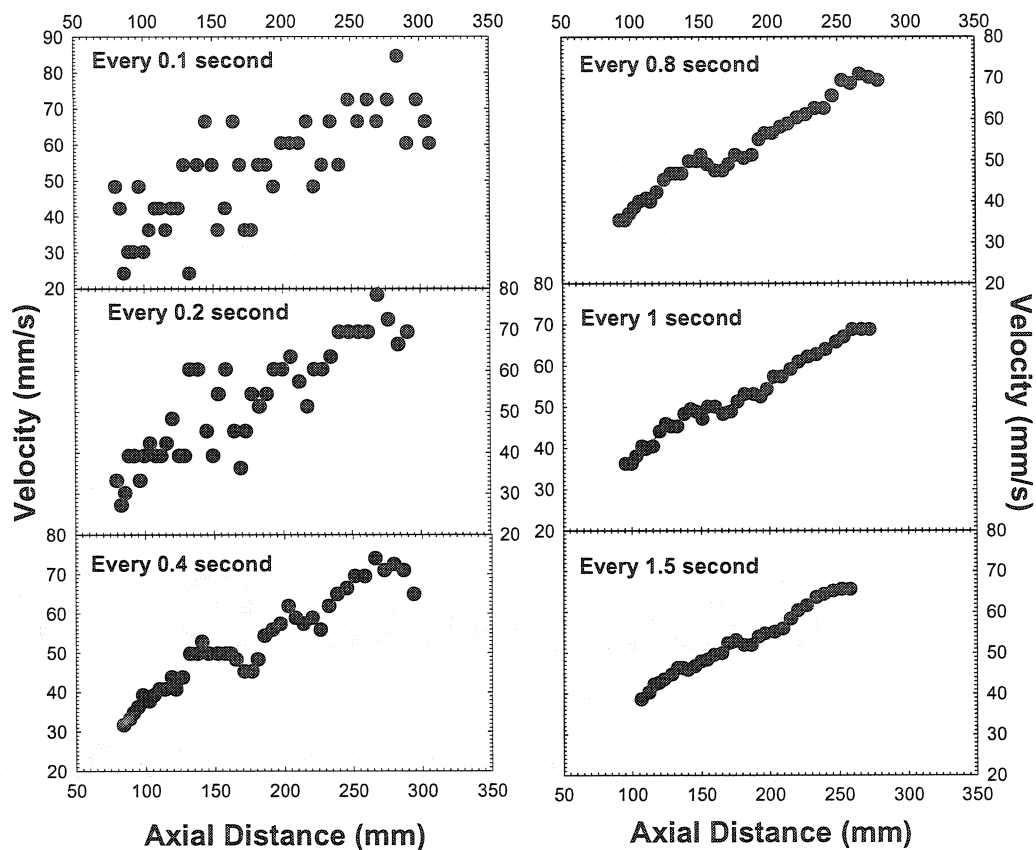
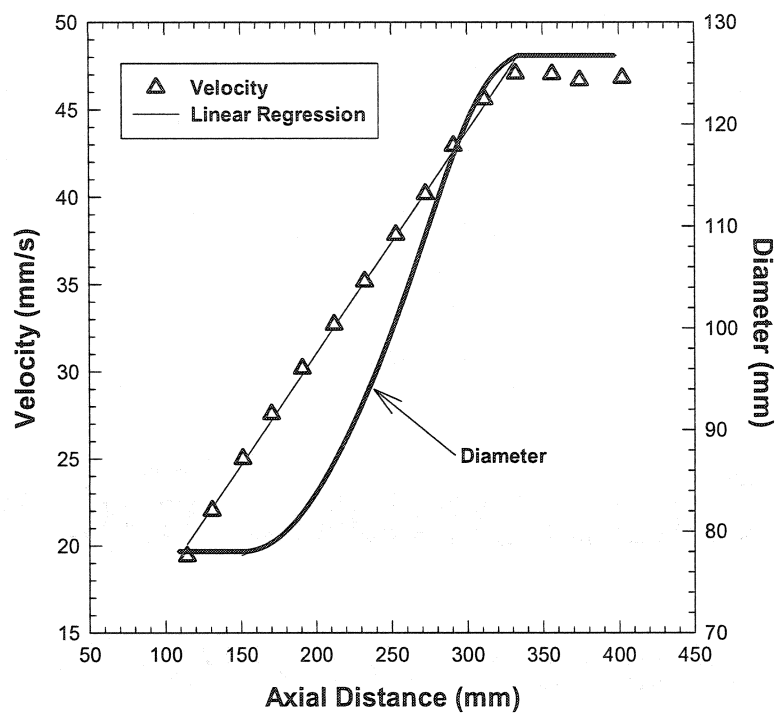


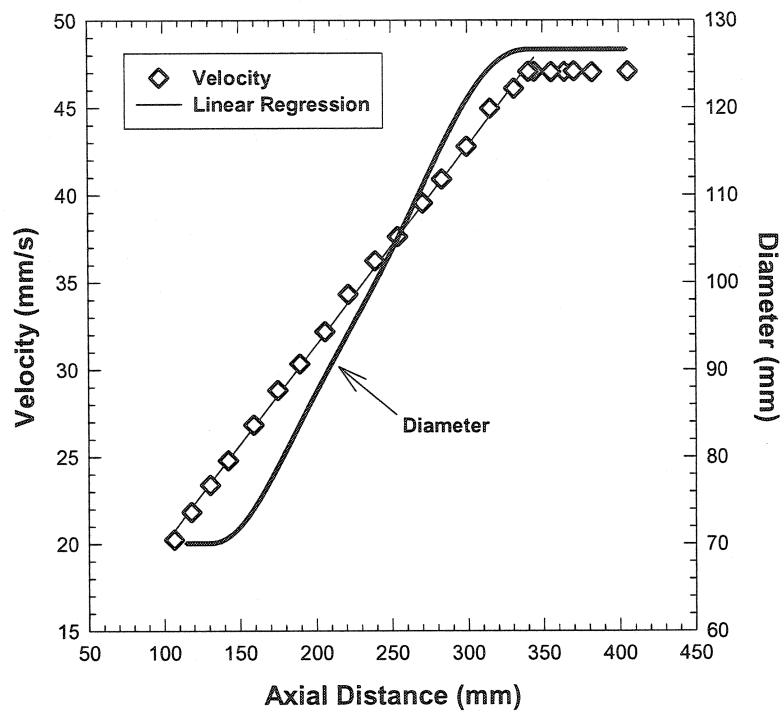
Figure 3. 6. Bubble velocity profiles measured by the video method for LDPE (operating conditions: mass flow rate = 5.0kg/h, BUR = 2.0, TUR = 10, temperature = 200°C).



(a)

Figure 3. 7. Bubble diameter and velocity profiles along the axial distance for (a) mPE.

The film blowing conditions are the same as in Figure 3.4.



(b)

(Continued) (b) LDPEb

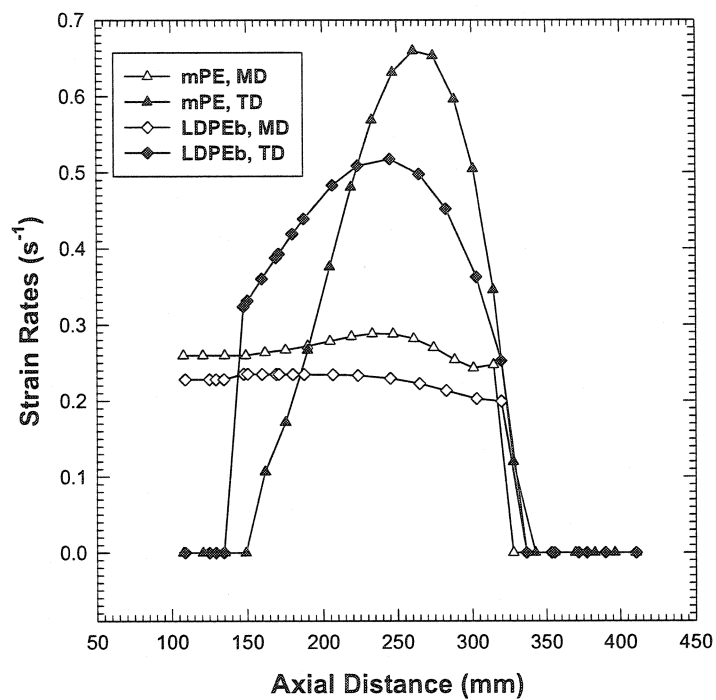


Figure 3. 8. Strain rates in MD and TD along the axial distance for mPE and LDPEb.

The film blowing conditions are the same as in Fig. 3.4.

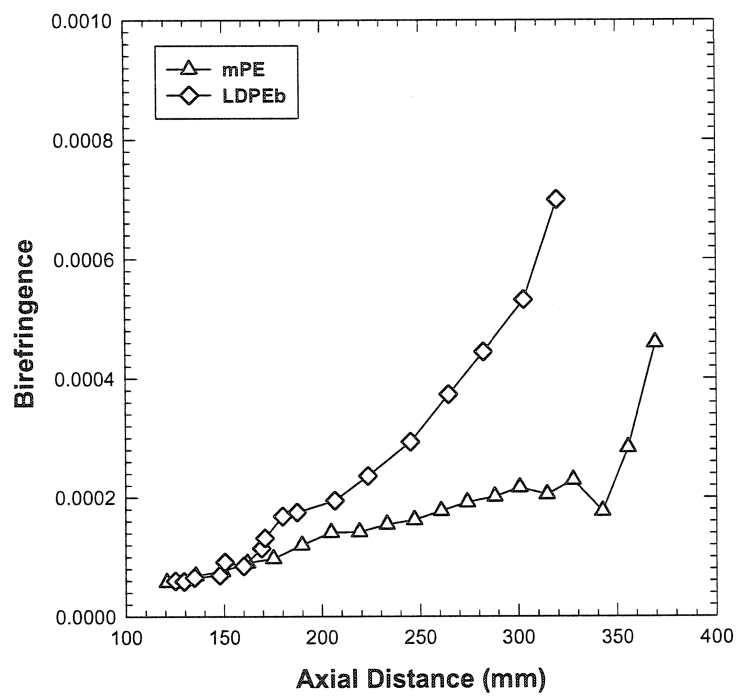
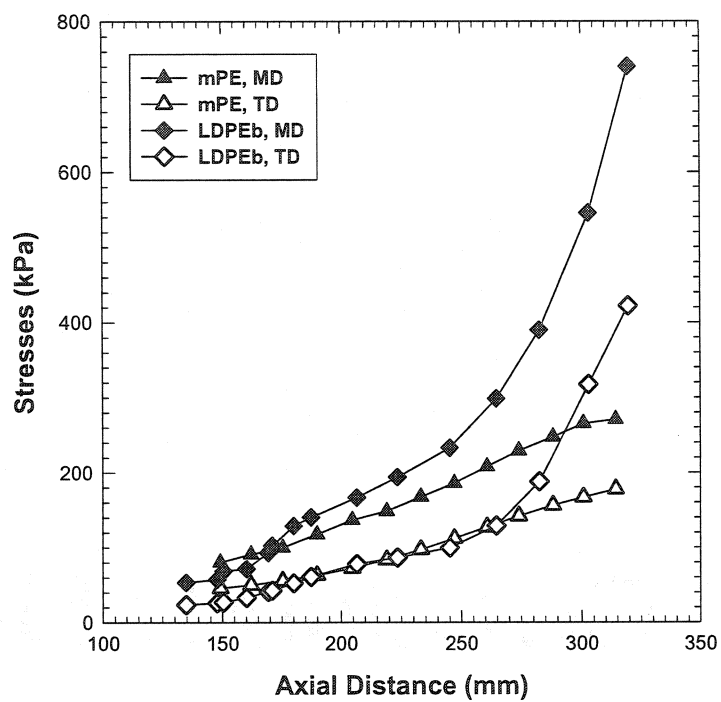


Figure 3. 9. (a) Birefringence along the axial distance for LDPEb and mPE. The film blowing conditions are the same as in Fig. 3.4.



(Continued) (b) Stress profiles along the axial distance for mPE and LDPEb. The film blowing conditions are the same as in Fig. 3.4.

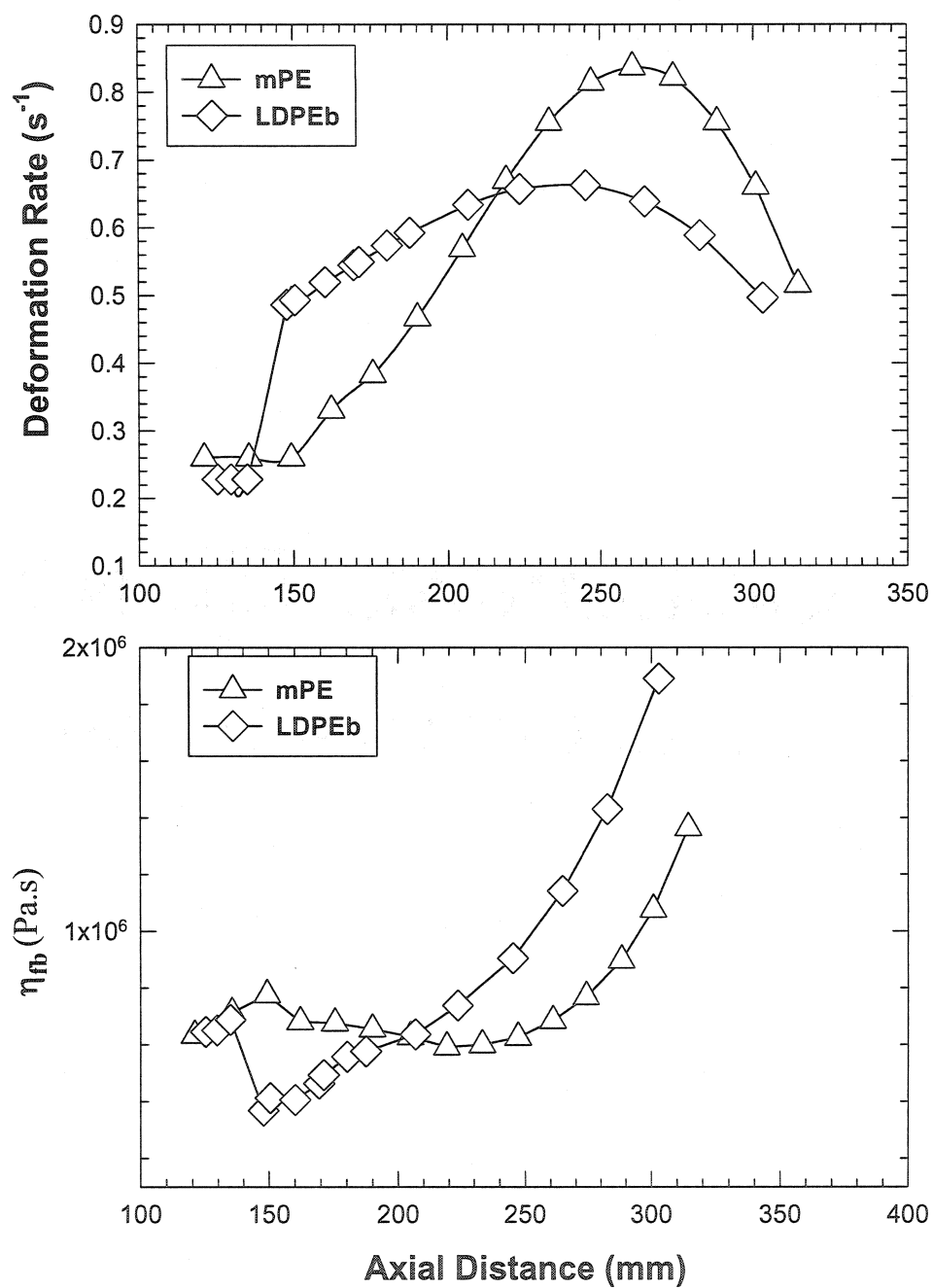


Figure 3. 10. Deformation rate and non-uniform biaxial elongational viscosity along the bubble for LDPEb and mPE. The film blowing conditions are the same as in Fig. 3.4.



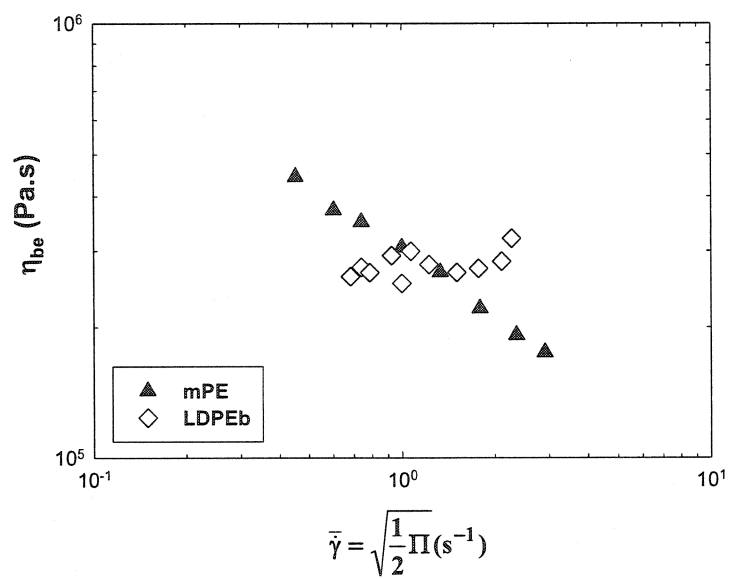


Figure 3.11. Biaxial elongational viscosity versus deformation rate for mPE and LDPEb at reference temperature of 170°C.

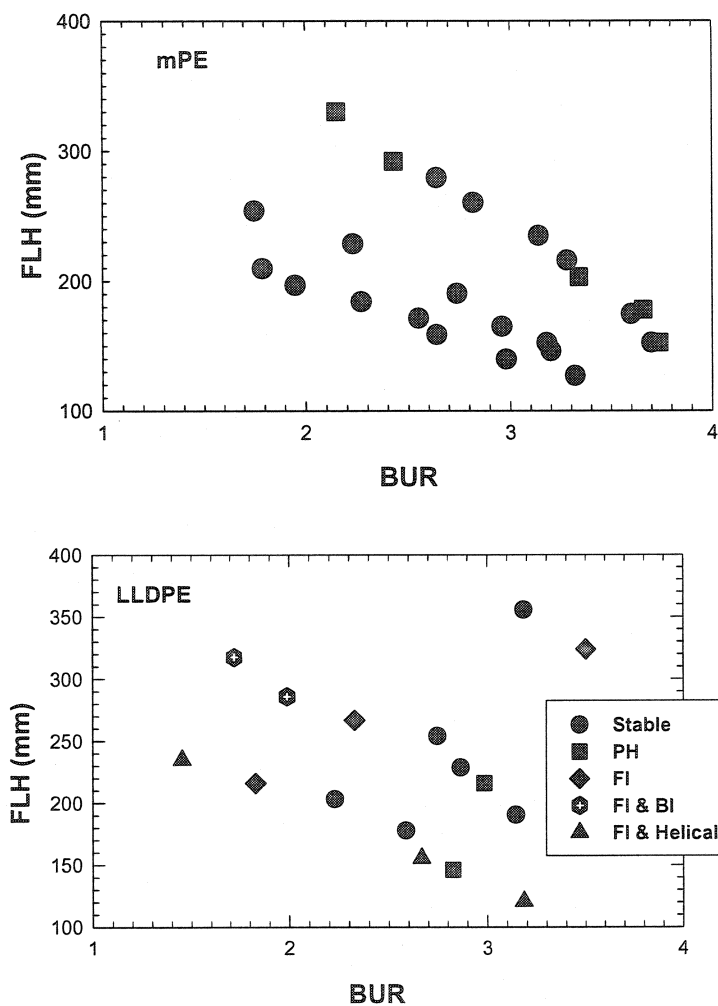
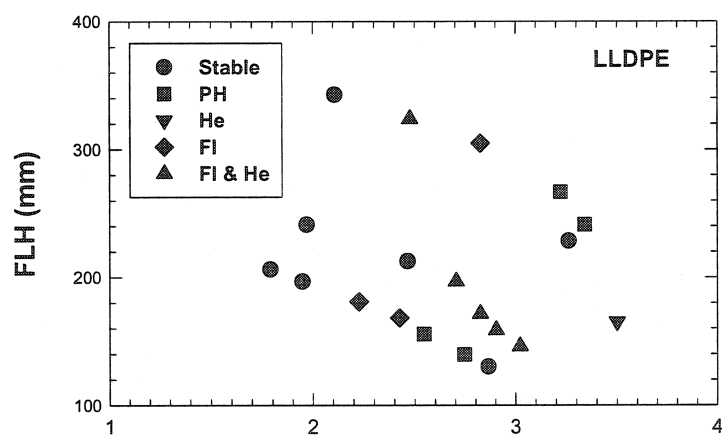
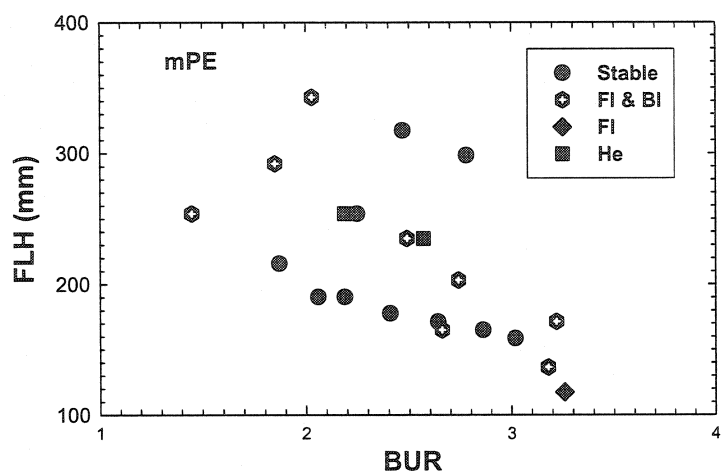


Figure 3.12. Bubble stability behavior of mPE and LLDPE under the extrusion temperature of 200°C, mass flow rate = 5.4 kg/h (He: Helical; PH: Partially Helical; FI: Frost Line Height Instable; BI: Bubble Instable); (a) TUR = 4.7



(Continued) (b) TUR = 6.2

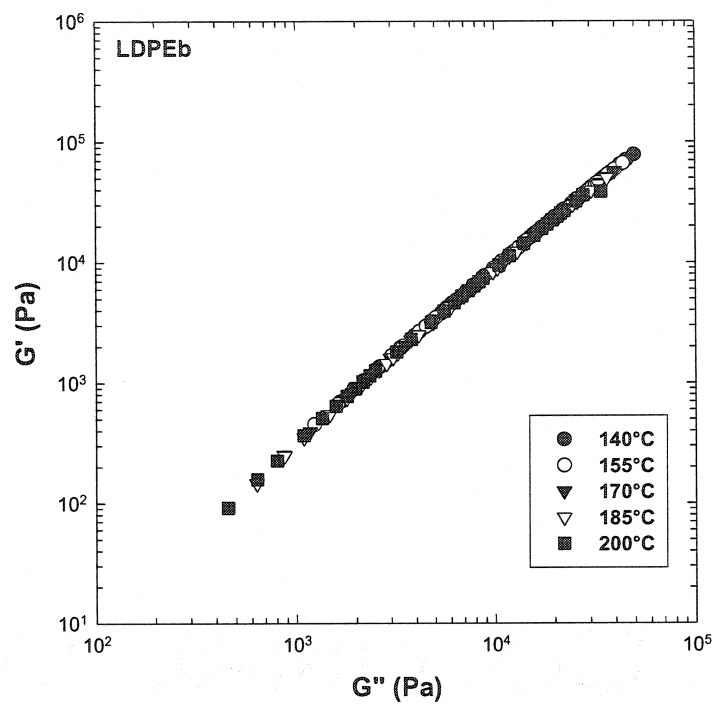
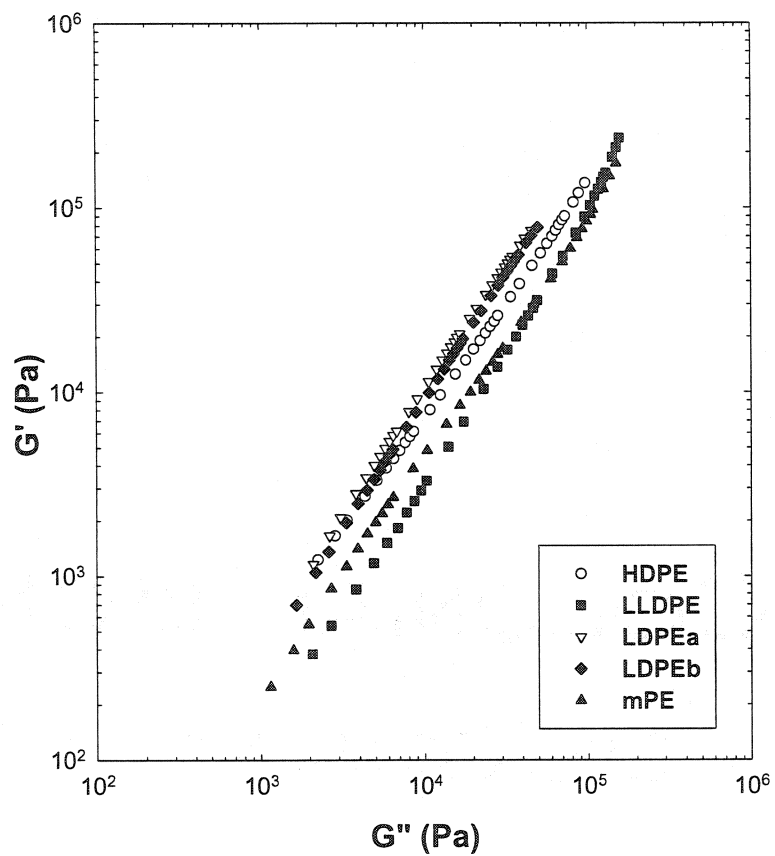


Figure 3.13.  $G'$  versus  $G''$  for all polyethylenes at five different temperatures: (a) LDPEb.



(Continued) (b) HDPE, LLDPE, LDPEa, LDPEb, and mPE.

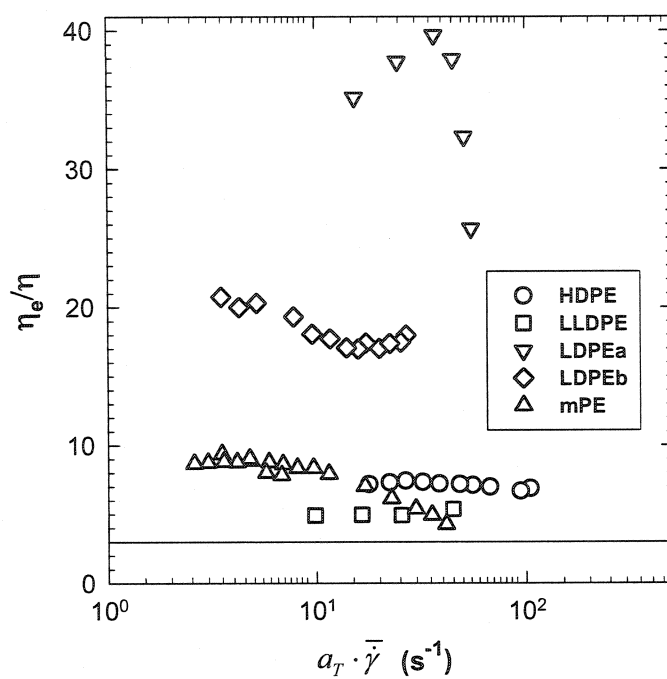


Figure 3. 14. Comparison of the Trouton ratio for five polyethylenes at a reference temperature of 170°C.

## CHAPTER 4. DYNAMICS AND CRITERIA FOR BUBBLE INSTABILITIES IN A SINGLE LAYER FILM BLOWING EXTRUSION<sup>†</sup>

S. Kim, Y. Fang, P.G. Lafleur and P.J. Carreau

Ecole Polytechnique de Montréal, Département de Génie Chimique, CRASP  
CP 6079, Succ. Centre-ville, Montreal, QC, H3C 3A7 Canada

### Abstract

In this paper, the performance of a new in-line scanning camera system for the study of various bubble instabilities in film blowing extrusion is critically evaluated. Three commercial film-grade polyethylenes, LmPE, LLDPE and LDPE, were used to generate the bubble instabilities. Reliable and objective criteria for differentiating various bubble instabilities such as draw resonance, helicoidal instability, frost line height instability are proposed by using the new device. Detailed dynamics of each bubble instability was carefully investigated as a function of time in a broad range of the take-up ratio (TUR), blow-up ratio (BUR) and frost line height (FLH). In addition, effects of melt temperature and mass flow rates on dynamics of the bubble instabilities are also discussed. It was found that the new system could capture the main characteristics of all bubble instabilities quantitatively. It was also found that magnitude and periodicity of radius variation during draw resonance of LmPE decreased as TUR increased at constant FLH and BUR. This implies that the origin of draw resonance in film blowing seems to be different from that observed in fiber spinning. In the case of helicoidal instability, eccentricity, which defines the deviation of the bubble center from the die center, decreased as TUR increased. However, the bubble could not be stabilized as expected. A graphical quantification approach to determine the stable zone in the bubble stability map is also discussed.

Keywords: film blowing, bubble instability, criteria, dynamics, polyethylenes

---

<sup>†</sup> Published in *Polymer Engineering & Science*. **44(2)**, 283-302 (2004).

#### 4.1. Introduction

Film blowing extrusion converts conventional polyethylenes such as high (HDPE), linear low (LLDPE) and high-pressure low density (LDPE) polyethylenes into thin plastic films. It is one of the most important forming processes in the plastic industry. Although this process is too complicated to be completely understood due to the complex deformation kinematics and non-isothermal cooling effects, for simplicity three important operating conditions have been frequently correlated with its performance. Firstly, the frost line height (FLH) characterized by a formation of certain solidification zone is used as an indication of cooling effects by external air directed to the molten bubble and strongly affects the shape of bubble. Two other operating conditions to be taken into account along with FLH are the blow-up ratio (BUR) and the take-up ratio (TUR). The BUR is defined as the ratio of the final film radius ( $R_f$ ) and the die radius ( $R_o$ ), thus  $R_f/R_o$ . The TUR, sometimes called the drawdown ratio, is defined as the ratio of the take-up velocity ( $V_f$ ) of the nip rolls and the extrudate velocity at the die exit ( $V_o$ ),  $V_f/V_o$ . Varying the speed of the nip rolls and the amount of the pressurized air inside the bubble controls the BUR and TUR, respectively. Both parameters strongly affect the thickness and final width of the film, thus the deformation kinematics of the molten bubble. The width of the final, flattened film is generally called layflat width in the film industry.

An ultimate goal in film blowing is to produce final film products with thin uniform gauge, good physical and optical properties at a maximum production rate. However, this is difficult to achieve due to technical restrictions. Two technical limitations related to materials have been frequently discussed in film blowing extrusion (1-4), which are presumed to have different origins: bubble instabilities and surface melt fracture (SMF, generally called sharkskin). While bubble instability can be observed even at very low flow rate due to a mismatch of various operating conditions in film



extrusion, SMF can be only observed at critical flow rates and is believed to originate from near the die exit. Thus, SMF is not directly relevant to the operating conditions of film blowing and has been the topic of a number of recent studies (5, 6).

Various types of bubble instability have been reported in the literature (7-12). Three phenomena are commonly discussed: 1) draw resonance (DR) characterized by a periodic oscillation of the bubble diameter, 2) helicoidal instability characterized by a helicoidal motion of bubble around its axial direction and 3) FLH instability characterized by variation in the location of FLH. Their schematic views are shown in Fig 1. Maintaining a stable bubble during the film blowing process is a necessary condition not only for the continuous operation but also for the production of acceptable film products. Non-uniform bubble diameter results in non-uniform layflat width and thickness of the film, which diminishes its performance in the following converting steps. Therefore, appearance of one of these bubble instabilities can greatly narrow down the stable operating ranges of commercial productions. These restrictions on stable conditions limit not only the production rate but also the working window for producing films of good physical properties since there is a strong interaction between processing conditions and physical properties of final films.

Han *et al.* (7,8) were the first to present the results of bubble instabilities for a single layer film of LDPE and polystyrene (PS)/HDPE blends by recording the bubble behavior through still pictures. They observed pulsations of the bubble diameter as the stretch ratio increased under uniaxial deformation for small BUR less than unity and observed a wavy film under biaxial deformation for BUR larger than 1.5. However, it is not clear what they observed under biaxial stretching was the helicoidal or the FLH instability. They also argued that lowering the melt temperature provided a more stable bubble for LDPE. Rather comprehensive studies of bubble instability were done by Kanai and White (9), White and Yamane (10), and Minoshima and White (11). They used LDPE, LLDPE and HDPE having different molecular structures in terms of long

chain branches (LCB) and molecular weight distribution (MWD). They tackled the problem by qualitatively assessing whether or not the bubble was stable based on visual observations at different operating conditions. They presented the data of the working space in a bubble stability map as functions of BUR, TUR and FLH with different symbols denoting stable, bubble instability (BI), meta-stable and helicoidal, which correspond to stable, DR, FLH instability and helicoidal instability, respectively. In addition, a plot of thickness reduction vs. BUR was also used to assess the effect of the molecular structure on the bubble instability. However, these results were mostly qualitative and bubble instabilities based on visual observations of the experimenter are rather subjective. Hence, a better tool has to be developed for studying bubble stability on a routine basis.

Despite the lack of detailed knowledge of the origin of various bubble instabilities, Wong *et al.* (13), Field *et al.*, (14), and Micic *et al.* (15) followed the method of White *et al.* and they compared the bubble stability of various PE's including two metallocene PE's (13) and LDPE/LLDPE blends (14,15). On the other hand, Fleissner (1) determined the critical drawdown speed as a criterion for the FLH instability of three high molecular weight HDPE's showing a different extensional rheological behavior. Obijeski and Puritt (16) used the variation of the layflat width as a criterion for classifying three instabilities such as FLH instability, DR and helicoidal instability of LDPE, LLDPE and their blends. Huang (17) used a pressure transducer to detect variations of pressure inside bubble and correlated them to the oscillation of various bubble instabilities. Recently Butler (12) has presented results of a comprehensive study by employing various tools: a gamma back-scatter gauge for measuring the film thickness variation in the machine direction (MD), a pressure transducer for detecting air pressure variation, a video camera for recording the layflat variation and finally an IR thermometer for scanning the temperature profile. However, all these methods, while useful in some cases, are indirect approaches and are not appropriate to capture quantitatively the characteristics of various bubble instabilities.

There is a strong need to develop a tool that can detect the onset of each instability and trace how it evolves as a function of time. This is a basic and necessary condition to understand the physics behind various bubble instabilities. The first quantitative approach of bubble instability was attempted by Sweeney *et al.* (18) by using a video camera along with a data analysis tool to convert the captured images on the video camera into analog voltage signal. This signal was fed to an analog filter to determine the relative positions of the bubble edges. The authors were able to capture the position of the bubble edges as a function of time and axial position, and quantify the bubble instabilities of LDPE and LLDPE blends. However, this technique is not easy to use and requires a post-data processing step to interpret the data. In addition, since a video camera was used as an image capturer, the three dimensional motion of unstable bubbles such as encountered in helicoidal instability could not be properly investigated.

Ghaned-Fard *et al.* (19) have also attempted to quantify the bubble instabilities by defining the degree of helicoidal instability (DHI), which takes into account the radius variation of the bubble captured by a video camera. However, they could not tell differences between various bubble instabilities, especially between helicoidal and FLH instabilities. Recently, Laffague *et al.* (20) developed a new system using an in-line scanning camera with seven mirrors. It has been shown that it can capture all features of the bubble instabilities as a function of time and axial distance. Detail of the system and preliminary results can be found in elsewhere (20). However, their results were limited to the study of LLDPE and the proposed definitions for some bubble instabilities need critical evaluation to verify their applicability to other polymers. Therefore, in this study we have extended their work and proposed reliable criteria for various bubble instabilities in terms of experimentally determined parameters.

While many attempts of mathematical modeling have recently been made to simulate the steady-state operation of the blown film process (21-25), only a few

theoretical investigations have been addressed to bubble instability (26-28). Yeow (26) was the first to try to predict various bubble instabilities by using a linear stability analysis for a Newtonian film under isothermal conditions. Cain and Denn (27) extended their analysis for a Newtonian and a viscoelastic upper-convected Maxwell fluid. Cain and Denn found that both the number of steady-state solution branches and stability depended on the operating conditions represented by four variables such as axial velocity at the solidification point ( $V_f$  in their paper), amount of pressure inside bubble ( $A$ ), dimensionless tension ( $T_z$ ), and a parameter ( $B$ ) relating inflating pressure to thickness and fluid viscosity. Based on their analysis they argued that their model can predict the draw resonance at the lower branch, *i.e.*, lower BUR near or less than unity where the thickness and the radius of bubble decreased as the bubble moved upward. Recently Yoon and Park (28) used the mathematical approach of Cain and Denn to evaluate the detailed effects of specific operating conditions on bubble instability. They have selected experimental data of LLDPE collected by Minoshima and White (10) to assess their theoretical results based on Newtonian and isothermal conditions. It is interesting to note that they reported for a case of a fixed amount of air and a given thickness reduction that there was an optimum FLH that exhibited the most stable region. However, while the previous theoretical approaches are partly successful in qualitatively predicting the occurrence of DR at low BUR, none of them provides a reasonable agreement with all experimental observations. On the other hand, there are not enough reliable experimental data on bubble instability to draw any solid consensus.

The objective of the present study was to propose reliable criteria, which can characterize quantitatively various bubble instabilities. We also present dynamics of unstable bubbles as a function of TUR and show how effective the new in-line system is in capturing the characteristics of unstable bubbles. In addition, a graphical approach is proposed to quantify the stable region in the bubble stability map. Finally, only one mass flow rate was used in previous work on bubble instability, for example 1.0 (7), 0.7 (9), 1.1 (10), 5.0 kg/h (20), which are sometimes unrealistic considering actual film blowing

processes. Thus, we also discuss the effects of the mass flow rate and melt temperature on the bubble stability map.

## **4.2. Experimental**

In this study the following procedure was used for all the measurements. At a given mass flow rate and a melt temperature, first the targeted BUR was attained for a given TUR by supplying the necessary amount of air and then the targeted location of FLH was adjusted by controlling the air cooling rate. If the required BUR was attained for a certain position of FLH, then TUR was slightly varied systematically to investigate the effect of TUR while simultaneously adjusting the cooling rate in order to keep a similar FLH position. Thus, the actual BUR was not exactly the same but quite close to the targeted value as shown in Fig. 4.2.

### **4.2.1. Film Blowing Unit**

A 45 mm Killion single-screw extruder with a standard screw was used. Its length to diameter ratio (L/D) is 24 and compression ratio is around 3. A helical annular die with an outer diameter of 63.5 mm and a gap of 3mm was installed at the exit of extruder with three electrical heating bands to achieve a good temperature profile within the die. The extrusion temperature profile from the hopper to the die was set as 165/195/200/200/200/200°C regardless of the polymer used, which results in melt temperature of 184 ~ 187°C at the die exit depending on the polymer. The mass flow rate of each polymer was maintained at  $2.0 \pm 0.1$  kg/h by adjusting the screw revolution speed depending on the polymer to relatively compare their bubble instabilities. However, for the evaluation of the mass flow rate and melt temperature effects on the bubble instabilities, two additional mass flow rates, 4.5 and 6.47 kg/h and two additional melt temperatures of 204 and 218°C were employed with LDPE. Cooling was performed

by using a dual-lip air ring, which is well known for its better cooling efficiency compared to that of a single-lip air ring. No internal cooling device was used. The air temperature was not regulated but was in the range of 20 ~ 23°C. The positions of upper and lower lips of air ring were set at the same level during the study to avoid any difficulty caused by variations of airflow due the lip position. Therefore, cooling of the molten bubble was controlled by air stream through mainly the lower air ring and partly the upper air ring. As a result, effect of cooling was taken into account only as a function of the air-cooling rate. Typical processing data for polymers used are summarized in Table 4.1.

#### 4.2.2. In-line Measurements

The optical system used in this study has been developed at CRASP-Ecole Polytechnique (Montreal) and the relevant mathematical derivation has been presented by Laffague *et al.* (20) in details. The schematic view of the new system and geometrical variables of the bubble and the die are shown in Figs. 4.3a and b, respectively. A summary relevant to this study is given here. The system includes seven mirrors which allow the line-scan camera (Dalsa, USA) to acquire two views of the bubble as two white stripes at the black back-ground on the same narrow image as shown in Fig. 3a. Synchronization of the two views is a result of the symmetry of the system. Three fluorescent lamps were placed above the mirrors as a light source and especially homemade designed black chambers were installed around the mirrors and the camera to avoid any parasite reflections and shadows and to get optimal contrast. The whole optical system can be used at a fixed position or with a frame movable in height by using a servomotor. The observations reported in this paper were made at a fixed position above FLH.

One of the important steps for successful measurements is an appropriate calibration. Through the calibration procedure, we can let the system know where the initial position of the die center is, which corresponds to the reference point of the system. In addition, there is a scaling factor to correlate the real dimension of the bubble to the number of pixels of the data from the acquisition system. Its correlation is:

$$\text{Scaling Factor: } \theta_1 = (P_4 + P_3)D_p/2, \quad \theta_2 = (P_1 + P_2)D_p/2 \quad (4.1)$$

where  $P_1$ - $P_4$  are the edge positions of two white stripes on the images of the in-line scanning camera (Fig.3a),  $\theta_1$  and  $\theta_2$  are the angles between the bubble center and two imaginary  $X$  and  $Y$  axes (Fig.3b), respectively, and  $D_p$  is a scaling factor.

Data acquisition rate was fixed at 0.26 s/data point for the whole measurements, which is short enough to detect a spontaneous response of the bubble to given conditions. This system gives four parameters as output: 1) **Eccentricity,  $d$** , describes how far a bubble moves away from the die center, 2) **Rotation angle,  $\alpha$** , is the reference angle of the bubble right side with respect to an arbitrary  $y$ -plane, as shown in Fig. 4.3b, 3) **Radii** of the left and right sides of the bubble ( $R_{Left}$  and  $R_{Right}$ ), and finally 4) **Ratio of the two radii**. Key relations of these parameters and geometrical variables are presented as follows:

$$\text{Rotation angle } (\alpha) = \arctan(Y_c/X_c) \quad (4.2)$$

$$\text{Eccentricity } (d) = \sqrt{X_c^2 + Y_c^2} \quad (4.3)$$

$$\text{Radius ratio} = R_{Left}/R_{Right} \quad (4.4)$$

where  $Y_c, X_c$  are the Cartesian coordinates that defines the bubble center.

Using these four experimentally observable parameters, we have studied the bubble instabilities as a function of time in a wide range of operating conditions. TUR was varied from 6 to 90 with a regular interval of 12 to detect any possible bubble instability. This range is broad enough to cover the typical TUR range used in the film industry of 50 ~ 60 (28, 29). However, the TUR value was slowly varied near critical conditions where a stable bubble became unstable in order to determine the precise stable/unstable transition. Within these operating conditions, LmPE and LLDPE did not exhibit any rupture behavior. However, the LDPE film bubble ruptured near TUR of 90 at the melt temperature of 186°C. The operating window for BUR was from 0.5 to 2.5. This range is slightly narrower than the typical BUR of 3 discussed in the literature (9-11). FLH was adjusted at values of 100, 180 and 250 mm from the surface of the die. These values are considered as high values for the size of our film-blowing unit. In addition, the variation of the air pressure inside the bubble was also recorded during the study of the bubble instabilities by using a manometer mounted on the die.

#### 4.2.3. Polymers Studied

Two conventional polyethylenes such as LLDPE, LDPE and a metallocene catalyzed linear polyethylene (LmPE) were selected in order to compare their typical bubble instabilities. LDPE is made by radical polymerization and known to possess a certain amount of long chain branches (LCB) in its main backbone and relatively broad MWD. LLDPE is produced using a multi-site Ziegler-Natta (Z-N) catalyst and contains a certain weight percent of octene as a co-monomer. On the other hand, LmPE, produced by using a single-site catalyst, has a narrow MWD and homogeneous short chain branch distribution. The molecular parameters for the PE's are tabulated in Table 4.2. Gas permeation chromatography (GPC) results in Table 2 were supplied by Dow Chemicals Co. and ExxonMobil Company. The melt indices and densities were determined by the resin suppliers by means of the ASTM-79 and 1683 method, respectively.



### 4.3. Characteristics of various bubbles

Most data discussed here were collected at melt temperature of 185 ~ 187°C and mass flow rate of  $2.0 \pm 0.1$  kg/h unless otherwise stated. It is worth noting how important the duration of an experiment is for assessing bubble instability. Although this was mostly ignored in previous work, it is one of the key factors when one of the processing conditions is varied near a critical point where a stable bubble becomes unstable or vice versa. Because small changes in the operating conditions near a critical condition can cause an immediate or slow response whether the bubble is stable or not, great care is needed. In this work, at least 5 min were allowed before judging the type of bubble instability. Meanwhile all results discussed in the next section were collected at conditions away from the transition region and the reproducibility has been verified.

#### A. Stable Bubble (Control)

Figures 4.4a-c show a typical stable bubble response recorded using the new system. These data were obtained for LDPE at BUR of 1.5, TUR of 42 and FLH of 180mm. Figure 4a exhibits the variations of both radii as a function of time. Both radii almost overlap each other implying that the bubble is axisymmetric. This is commonly observed for a stable bubble, and the variations of both radii are in the range of  $\pm 2.5\%$  of the radius as calculated by:

$$\text{Radius variation } (\Delta R) = (R_m - R_s) \times 100 / R_s \quad (4.5)$$

where  $R_m$  is the experimentally determined radius and  $R_s$  is the set radius. A radius variation of  $\pm 2.5\%$  is one of the two criteria previously proposed by Laffague *et al.* (20) for differentiating various instabilities based on experimentally determined bubble radius. This specific criterion was confirmed again in this study based on all our data collected for various operating conditions with different polymers. Figure 4b displays the

variations of  $\alpha$  and  $d$  for the same conditions as those of Fig. 4.4a. The variations of  $d$  describing how far the bubble center is away from the die center are within 10mm for this polymer and all the other polymers showing a stable bubble, confirming the other criterion proposed by Laffague *et al.* (20). On the other hand,  $\alpha$  remains within  $60^\circ$ , which is a typical value for most stable bubbles found in this study. Therefore, these two critical values,  $d = 10\text{mm}$  and  $\alpha = 60^\circ$ , along with  $\pm 2.5\%$  for radius variations and bubble symmetry characterized by the radius ratio were adopted as basic criteria for differentiating various bubble instabilities. It is also worth noting that the relative difference between the maximum and minimum  $\alpha$  is more meaningful than the absolute value, since the initial angle value is arbitrary. In addition, it is necessary to pay attention to periodic changes in  $\alpha$  since it is generally related with the development of certain instabilities. Although variations of this angle can be dramatically reduced as the external cooling rate or TUR is decreased, they cannot be avoided due to small perturbations caused by the cooling air. Figure 4c shows the variations of the pressure inside the bubble along with variations of  $\alpha$  for a stable LDPE film under different conditions (BUR of 1.5, TUR of 18.6 and FLH of 180mm). The variations of the air pressure inside the bubble are quite small, with an average pressure around  $26 \pm 0.4$  Pa, and no periodic pattern is observed. Meanwhile, the variations of  $\alpha$  are almost negligible in this case since a relatively low value of TUR results in a thick film and more resistance to imposed perturbations.

## B. Draw Resonance (DR)

Although the term DR originates from fiber spinning to describe the radius change of molten fibers along the stretching direction (30), similar phenomena have been reported for other processes such as cast film, extrusion coating and film blowing (3, 31). This phenomenon causes thickness variations as we can imagine easily due to different expansions in the transverse direction (TD). Figure 4.5a shows the radius variation and the radius ratio as functions of time for LDPE when draw resonance is

prevailing (BUR of 1.0, TUR of 18.6 and FLH of 100mm). At given conditions, this phenomenon has lasted longer than 15 min. As expected, the radius variation exceeds the critical value of  $\pm 2.5\%$  and reaches around  $\pm 25\%$  with a clear periodic pattern. Meanwhile, the radius ratio is quite close to unity implying that the bubble is still axisymmetric. Figure 4.5b shows the variations of  $\alpha$  and  $d$  for the same conditions as those of Fig. 4.5a. Although the bubble radius is changing with a sinusoidal pattern its center remains near the die center,  $d$  is less than 10mm, and  $\alpha$  shows small variations within  $60^\circ$  without periodicity. This phenomenon has been observed for all materials used in this study mainly at relatively low BUR near or less than 1.0 and sometimes at a large BUR of 2.0 for LmPE regardless of the FLH position, confirming the previous observations (9-11). The variations of the pressure inside the bubble and the radius values collected for another time interval are presented in Fig. 4.5c. Both the pressure and bubble radius vary periodically and in phase implying that the dynamics of the air inside the bubble plays a major role of this type of instability. This is in accordance with observations of Huang (17), who used a pressure transducer as a detecting device for bubble instability. The variations of the pressure are quite large for this instability with an average pressure of  $22.8 \pm 1.6$  Pa. The fluctuations represent about 7 % compared to 1.6% for a stable bubble. Meanwhile as DR was frequently combined with FLH instability as illustrated in Fig. 4.1b, it was sometimes difficult to observe the two phenomena separately.

### C. Helicoidal instability

This phenomenon has been observed for LDPE and LLDPE at relatively large values of BUR (higher than 1.5) but not for LmPE regardless of the FLH position. When this phenomenon was observed the bubble located at a position higher than the air ring was periodically rotating. Figure 6a shows  $\alpha$  and the radius variation as functions of time for LLDPE showing helicoidal instability (BUR of 2.0, TUR of 30.5 and FLH of 180mm). In this case,  $\alpha$  exhibits periodic changes in the range of 0 to  $360^\circ$  implying that

the bubble is rotating, while the radius variation is still within  $\pm 2.5\%$ . Figure 6b shows the variations of the eccentricity ( $d$ ) and radius ratio with time for the same conditions as in Fig. 6a). As expected  $d$  also shows deviations from that of a stable bubble and the variations are random. However, the radius ratio is close to unity with small perturbations implying that the bubble is still axisymmetric. Variations of the pressure inside the bubble and of  $d$  with time collected for another time interval are reported in Fig. 6c. The bubble pressure is fluctuating around an average value of  $33.1 \pm 4.7$  Pa showing a standard deviation of around 15%, that could not be correlated well with any other parameter. On the other hand, it should be noted that this typical behavior could be observable only at moderate conditions in terms of TUR and BUR. Any change of the operating conditions in this environment could cause catastrophic changes in the bubble shape and eventually provoke the bubble collapse. It has been reported that this helical instability is associated with improper set-up of the air ring (12). However, in our case no attempt was made to adjust the air ring in order to evaluate the effects of the helicoidal instability.

#### D. FLH instability

The FLH instability can be characterized by changes of the FLH position with time and it is frequently observed when the position of FLH is a little higher than that of the air ring. It was quite difficult to observe the FLH instability for a FLH of 100 mm in this study. For a FLH of 250 mm, BUR of 2.2 and TUR of 18.6 Figure 4.7a shows how  $d$  and  $\alpha$  respond to the FLH instability observed for LmPE. As seen in the figure, the values of  $d$  and  $\alpha$  fluctuate around critical values of 10 mm and  $60^\circ$ , respectively, randomly at the beginning then periodically near 1120 ~1200 s. Then, at longer time the motion becomes random and eventually the bubble touches the air ring at 1230 s and collapses. During the same time, the radius variation and the radius ratio, reported in Fig. 4.7b change randomly, meaning that the shape of the bubble is not symmetric any more. Fig. 4.7c shows the corresponding variation of the pressure inside the bubble. A periodic

pattern appears at the beginning with a long periodicity of 40 s and then periodicity is lost. Near 1230 s, the pressure drops suddenly due to the bubble collapse. The average pressure inside the bubble is around  $41.6 \pm 3.2$  Pa and the standard deviation of 7.63 % is quite close to that obtained in draw resonance. Therefore, the use of a single pressure transducer does not allow to distinguish between FLH instability and draw resonance.

The typical FLH instability described above was also observed for LLDPE at large BUR values of 2 and 2.5, and high positions of FLH but not for LDPE. On contrary to the description made by Minoshima and White (10), all parameters vary randomly with time or sometimes periodically. This can be easily understood taking into account the swirling motion of air trapped inside the bubble, affected by local cooling effect at the inner and outer surfaces of the bubble. Furthermore, periodic patterns were observable only at the beginning of this instability since the bubble could not hold its shape for a long time due to drastic changes of FLH. Despite the lack of knowledge on the origin of this phenomenon, heterogeneous cooling effects, unstable aerodynamics inside the bubble and non-uniform crystallization behavior of given polymer melt seem to be responsible for this phenomenon. Further study is needed to understand how FLH instability develops and elucidate the causes.

#### **E. Additional Observations**

An additional bubble instability has been observed for all the polymers used in this study at the very small TUR of 6 and large BUR of 1.8 ~ 2.0. Its schematic representation is shown in Fig. 4.8 and corresponding responses from the new system are shown in Fig. 4.9. While most previous instabilities are almost symmetric in their shape except a strong FLH instability, it is not the case for this instability as shown in Fig. 9a. The variation of the bubble shape with time is quite different depending on the viewpoint of the experimenter (Fig. 4.8). Thus, a visual inspection may lead to a misleading judgment. When this phenomenon is observed, the initial FLH remains

unchanged whereas all parameters show deviations from those of a stable bubble. However, as time evolves the FLH is moving slowly up and down while  $d$  and  $\alpha$  deviate from those of a stable bubble as shown in Fig. 9b. The deviations become larger and larger and eventually the bubble touches the air ring and collapses. The reason for this behavior has not been understood yet. However, we believe that this originates from a non-uniform thickness profile coupled with a non-uniform cooling rate around the air ring. It is worthwhile noting that although all parameters deviate from those of a stable bubble as in the case of FLH instability, all the variations are periodic contrary to those of FLH instability.

#### **F. Proposed Criteria for Typical Bubble Instabilities**

Based on the critical values for four parameters described in the previous section, we propose the criteria for differentiating the various bubble instabilities as shown in Table 4.3. Since the four parameters can be directly obtained from the in-line measurement and evaluated through Eqns. (4.2)-(4.5), each bubble instability can be characterized by a combination of these four parameters with their degree of variation denoted by two symbols, “O” and “X”. The symbol “O” means that the parameter is sensitive to a given instability. For example, the four parameters can be described as “O” in the following cases: 1) the relative difference between the maximum and minimum  $\alpha$  is greater than  $60^\circ$  with periodicity, 2) the value of  $d$  is larger than 10 mm, 3) the radius variation is larger than  $\pm 2.5\%$ , and 4) the radius ratio deviates from the unity and shows periodic changes. All the other cases can be expressed by use of a symbol “X”. Thus, a combination of all parameters should be all “X” for a stable bubble, which shows no change in all four parameters. DR can be characterized by radius variations only as expected. These criteria have been thoroughly evaluated by using three polymers under various conditions. The reproducibility of the results has also been verified.

## 4.4. Results and Discussion

### 4.4.1. Dynamics of Unstable Bubbles

One of the advantages of the new in-line scanning camera system is that it can give very valuable information for the transition between stable and unstable zones. This kind of information is not available in the literature. Therefore, we present some examples on how this system can capture the dynamics of an unstable bubble when it transits from unstable to stable, and vice versa.

#### A. Evolution of draw resonance at low BUR

Figure 4.10 shows an evolution of draw resonance as a function of TUR for LmPE. Initially, the bubble was unstable showing DR for the given processing conditions (BUR of 0.9, FLH of 180 mm, TUR of 6.8). Then, TUR was increased from 6.8 to 54.1 by steps of 12 and allowing a certain time interval in order to obtain a pseudo steady-state response of the bubble. As TUR increases, the radius variation is drastically reduced. Initially, the radius variation is  $\pm 45\%$  but it decreases to  $\pm 15\%$  at TUR of 42.3, and eventually it approaches  $\pm 2.5\%$  when TUR is further increased to 54.1, which meets one of the criteria for a stable bubble. Although not presented here for saving space, the variations of the other parameters such as  $d$  and  $\alpha$  are within the limits for a stable bubble. The amplitude and periodicity, denoted as  $\lambda$  in the Fig. 4.1a, are shown in Fig. 4.11 for this DR. The amplitude of DR was simply calculated by subtracting the set radius from the maximum radius at the given TUR. One interesting observation is that as TUR increases the amplitude is decreasing to zero, which means that the bubble becomes stable. The periodicity initially decreases and then approaches a plateau different from zero. This is, in fact, a quite different behavior compared to that of DR in fiber spinning, where the amplitude of the radius variations increases as TUR increases

beyond a critical value and then the fiber ruptures. Furthermore, DR in film blowing was frequently observed for a BUR of 1.0 or little larger value where the deformation kinematics is not uniaxial but planar or non-uniform biaxial implying that the origin of this phenomenon is not the same.

## **B. Evolution of Helicoidal Instability for Large BUR**

Figure 4.12 shows an evolution of the helicoidal instability for different values of TUR in the case of LLDPE. Initially, the bubble is stable under the given processing conditions (BUR of 2.0, FLH of 180 mm and TUR of 42.3). Then, TUR is decreased from 42.3 to 18.6 in steps of 12. While changing TUR enough time was allowed until the response of the bubble was almost independent of time and typical pattern was achieved. As TUR decreases from 42.3 to 30.5 as shown in the figure, the radius variation is maintained within  $\pm 2.5\%$ , but  $\alpha$  starts to oscillate between  $60^\circ$  and  $120^\circ$  implying that the bubble is rotating. Figure 13 reports the radius ratio and  $d$  as functions of time for various TUR under the same conditions as for Fig. 4.12. When TUR decreases from 42.3 to 30.5, the helicoidal instability appears. The shape of bubble remains axisymmetric; however, the center of the bubble is moving away from the die center. For example,  $d$  is smaller than 10mm when TUR is 42.3, but as TUR decreases from 42.3 to 30.5 it starts to grow beyond the critical value of 10mm. Further decrease of TUR from 30.5 to 24.5 and to 18.6 results in larger deviations of  $d$  as well as small oscillations in the radius ratio implying that the locus of the bubble circulating motion is getting worse and outward. Eventually, the bubble collapses due to a contact with a section of film blowing unit.



#### 4.4.2. Quantification of Stable Region in Bubble Stability Map

The other issue to be resolved in a bubble instability study is how we can quantify the stable region in the bubble stability map in order to evaluate the performance of different polymers. White *et al.* (9-11) used a plot of thickness reduction of film vs. BUR. However, up to now there has been no solid method that considers all effects of process conditions. Fielding *et al.* (15) and Micic *et al.* (16) recently proposed that the percent area of the stable zone within the whole working window could be used as a tool. Although this idea is good, their basis for selecting the working window is not clear enough. For this study we adopted their methodology and defined the working window as follows. Considering hardware limitations of our film unit in terms of maximum achievable TUR and BUR, a working window of TUR was selected from 6 to 90. The lower limit of TUR comes from the lowest speed of the nip rolls and the upper limit of TUR corresponds to the critical value where LDPE film ruptures. The range of BUR was selected between 0.5 and 2.5. At BUR lower than 0.5 it was difficult to produce a cylindrical bubble due to the low pressure inside the bubble. The upper limit of BUR was imposed by the air ring we used for the study since there was not enough space between the bubble outer radius and the lower lip of the air ring, especially at FLH of 100mm. However, much larger bubbles having BUR larger than 3 were produced at other FLH's.

Based on the proposed criteria within these operating windows, bubble stability maps were constructed for LDPE, LLDPE and LmPE at three FLH positions. Figures 4.14 and 4.15 show the bubble stability map at FLH of 180mm for LDPE and LLDPE, respectively. Various bubble instabilities discussed in the previous section were designated as symbols in the working windows and a guideline for bubble rupture was placed at high TUR region for LDPE in Fig. 4.14 but not for LLDPE. In addition, a critical transition zone where the stable bubble becomes unstable or vice versa due to changes of one of operating condition was found. Interestingly enough, the shape of the

transition zone is in accordance with that predicted by Yew (26) for a Newtonian fluid, based on the experimental observations of White *et al.* (9-11) for various polyethylenes. Fig. 4.16 shows another example of bubble stability map of LLDPE at FLH of 250 mm. The stable zone at FLH of 250mm is much narrower than that constructed at FLH of 180 mm (Fig. 4.15) implying that a more efficient cooling effect strongly stabilizes the LLDPE bubble. For quantification of the stable region, we generated small meshes in the map and calculated the shaded area corresponding to the stable region over all area surrounded by two limits, i.e., TUR of 0 to 90 and BUR of 0 to 2.5, as shown in Fig. 4.17 for LLDPE for the same conditions as in Fig. 16. Figure 4.18 reports the stability order for three polymers as a function of FLH. As expected, LDPE shows the most stable region within this working window confirming the previous observations for LDPE (10-15). However, its stable regime increases as FLH increases contrary to the previous observations (7,9). LLDPE shows a maximum stable region at FLH of 180 mm implying that there is an optimum FLH for exhibiting the best stable region as predicted by the stability analysis of Yoon and Park (28). Finally, LmPE is the most unstable polyethylene, and its stability decreases as FLH increases.

#### A. Effect of Mass Flow Rate on Bubble Stability Map

Figure 4.19 shows the bubble stability map of LDPE for a mass flow rate of 4.5 kg/h with melt temperature of 185°C at a FLH of 250 mm. Although extruder screw speed was varied to increase the mass flow rate, the melt temperature only increased by 1.0 ~ 1.5°C. When the mass flow rate was increased from 2.0 to 4.5 kg/h, the general trend of bubble instability map was almost the same, i.e., the various bubble instabilities observed for a mass flow rate of 2.0 kg/h were observed at the same location in the map for the larger mass flow rate. However, the maximum achievable TUR is decreased to 66 for 4.5 kg/h, to 38 for 6.47 kg/h, respectively, due to an increase of the melt velocity at the die exit. Figure 20 reports the effect of the mass flow rate on the bubble stability map for LDPE. The borderline that separates the stable and unstable regions at small

BUR moves drastically to the right direction whereas for BUR larger than 1 it remains about the same. This shift of the borderline to the right direction at small BUR seems to be related to bad cooling efficiency of air ring used for this study since no adjustment was made to enhance its capability. In fact, it was almost impossible to make a film bubble even near BUR of 1.0 with a mass flow rate of 6.47 kg/h and under maximum cooling rate, where film bubble could be made easily at lower mass flow rates with moderate cooling rate. We stress, however, that the use BUR of 1 or less has no practical interest for the film blowing process.

#### **B. Effect of Melt Temperature on Bubble Stability Map**

Two additional melt temperatures were selected for this evaluation. The temperature profile of the extruder and the die was changed in order to obtain melt temperatures of 204 and 218°C with a mass flow rate of 2.0 kg/h and a FLH of 250 mm. Figure 4.21 shows the typical bubble stability map for LDPE at a temperature of 204°C. Although melt temperature is increased by almost 20°C, the whole trend in the bubble stability map still remains the same as obtained for the lower temperature. However, the borderline between the stable and unstable regions is moved upward when the temperature is increased (compare Figs. 4.14 and 4.21). This trend can be seen clearly in Fig. 22 that reports the effect of the melt temperature on the bubble stability map for LDPE. The whole borderline shifts upward as the melt temperature increases from 185 to 218°C. The rupture behavior observed for the LDPE molten film at 185°C was not observed within the experimentally attainable TUR when the temperature was increased to 204 and 218°C. It is possible to conclude that decreasing the melt temperature stabilizes the bubble confirming the observations of Han *et al.* (4,5).

#### 4.5. Conclusions

The performance of a new in-line scanning camera system developed for the study of bubble instabilities in film blowing was critically evaluated by using LDPE, LLDPE and LmPE. Objective criteria for differentiating the various unstable bubbles are proposed based on four parameters, which can be directly determined by using the new device. It was shown that this new system could capture the dynamics of unstable bubbles quantitatively. It was also found that the amplitude and periodicity of the radius variations during draw resonance for LmPE decreased as TUR increased at a constant FLH and BUR implying that the origin of draw resonance in film blowing is not the same phenomenon observed in fiber spinning. Helicoidal instability and eccentricity decreased as TUR increased, however the bubble could not be stabilized as expected. A graphical quantification approach has been proposed to determine the stable zone in the bubble stability map. The order of bubble instability can be determined based on the total % area in BUR and TUR diagrams as a function of FLH. The order of bubble stability for the polymers used for this study is LDPE > LLDPE > LmPE. Lowering FLH stabilized the bubble for LmPEs and it was found for LLDPE that there was an optimum FLH that showed the most stable regions. The new in-line system along with other tools (*i.e.*, pressure inside bubble, infra-red thermometry) is suggested for investigating the origin of bubble instability.

#### ACKNOWLEDGEMENTS

The authors would like to thank Dr. Willem deGroot at Dow Chemical and Mr. Thomas Sun at ExxonMobil Company for supplying GPC results of the samples. The authors would like to extend our gratitude to Dow Chemical and ExxonMobil for supplying the samples used for this study. Finally, financial support of the National Science and Engineering Research Council of Canada (NSERC) in the form of strategic grant is acknowledged.

#### 4.6. References

1. M. Fleissner, Intern. Polym. Process., **2**, No.3/4, 229 (1988).
2. A. Ghijssels, J.J.S.M. Ente, J.Raadsen, Intern. Polym. Process., **5**, 4, 284 (1990).
3. R.G. Larson, Rheol. Acta, **31**, 213 (1992).
4. B. Debbaut *et al.*, Intern. Polym. Process., **13**, No.3, 262 (1999).
5. S.Q.Wang, Advances in Polymer Science, **138**, 229 (1999).
6. K.B. Migler, Y. Son, F. Qiao, K. Flynn, J. Rheology, **46**(2), 229 (2002).
7. C. D. Han, J.Y. Park, J. Applied. Polym. Sci., **19**, 3291 (1975).
8. C.D. Han, R. Shetty, Ind. Eng. Chem. Fund., **16**, 49 (1977).
9. T. Kanai, J.L. White, Polym. Eng. Sci., **24** (5), 1185 (1984).
10. W. Minoshima, J.L. White, J. Non-Newt. Fluid Mech., **19**, 275 (1986).
11. J.L. White, H. Yamane, Pure & Applied Chem., **59** (2), 193 (1987).
12. T.I. Butler, SPE Antec Tech. Paper, **1**, 156 (2000).
13. T.J. Obijeski, K.R. Pruitt, SPE Antec Tech. Paper, **1**, 150 (1992).
14. C.M. Wong, H.H. Shih, C.J. Huang, J. of Reinf. Plas. and Comp., **17** (10), 945 (1998).
15. G.J. Field, P. Micic, S.N. Bhattacharya, Polymer International, **48**, 461 (1999).
16. P. Micic, S.N. Bhattacharya, G.J. Field, Polym. Eng. Sci., **38**, 1685 (1998).
17. T.A.Huang, Advances in polymer technology, **8**(1), 65 (1988).
18. P.A. Sweeney, G. A. Campbell, F.A. Feeney, Intern. Polym. Process., **7**, 229 (1992)
19. A. Ghaneh-Fard, P.J. Carreau, P.G. Lafleur, AIChE J., **42**, 1388 (1996)
20. J. Laffague, L. Parent, P.G. Lafleur, P.J. Carreau, Y. Demay, J.F. Agassant,  
Accepted for publication in Intern. Polym. Process. (2002)
21. P.P. Tas, Doctoral thesis, Technical University of Eindhoven (1994).
22. S.J. Kurtz, Intern. Polym. Process., **10** (2), 148 (1995)
23. Liu, C.-C., Bogue, D.C., Spruiell, J.E., Intern. Polym. Process., **10**, 230 (1995b)

24. J.M. Andre, J.F. Agassant, Y.Demay, J.m. Haudin, B. Monasse, Intern. J. of Forming Process, **1** (2), 187 (1998)
25. A.K. Doufa, A.J. Mchugh, J. Rheology, **45** (5), 1085 (2001)
26. Y.L.Yeow, J. of Fluid Mech., **75** (part 3), 577 (1976)
27. J.J. Cain and M.M. Denn, Polym. Eng. Sci., **28**, 1527 (1988)
28. K.S. Yoon, C.W. Park, Intern. Polym. Process. **14** (3), 342 (1999)
29. S. Milner *et al.*, NSF Annual Report, "Interdisiplinary macromolecular science and engineering", Material Science Division, 43 (1998)
30. R.E. Christensen, SPE J., **18**, 751 (1962)
31. C.J.S. Petrie, M.M. Denn, AIChE J., **22**, 209 (1976)

Table 4.1. Processing conditions for a mass flow rate of 2.0 kg/h.

Polymer	RPM	Torque (Amp.)	Die pressure (MPa)	Melt temp. (°C)
LmPE	9.5 ~ 9.8	6 ~ 6.5	33.1 ~ 33.8	187
LLDPE	9.4 ~ 9.7	5 ~ 5.5	27.6~ 29.6	185
LDPE	12.4 ~ 12.7	1.5 ~ 2.0	12.4 ~ 13.1	185

Table 4.2. Molecular parameters of polymers used

Polymer	$\rho$ (g/cm <sup>3</sup> )	$MI$ (g/10min)	$M_w$	$PI$ ( $=M_w/M_n$ )	Comonomer
LmPE	0.918	1.0	111 918	2.36	C <sub>6</sub>
LLDPE	0.920	1.0	119 600	3.8	C <sub>8</sub>
LDPE	0.923	1.9	80 900	5.2	N/A



Table 4.3. Summary of proposed criteria for bubble instabilities

Type of instability	Alpha ( $\alpha$ )	Eccentricity ( $d$ )	Radius variation ( $\Delta R$ )	Radius ratio ( $R_o/R_i$ )
Stable	X	X	X	X
Pure DR	X	X	O	X
FLH only	O	O	O	O
Helicoidal	O	O	X	X

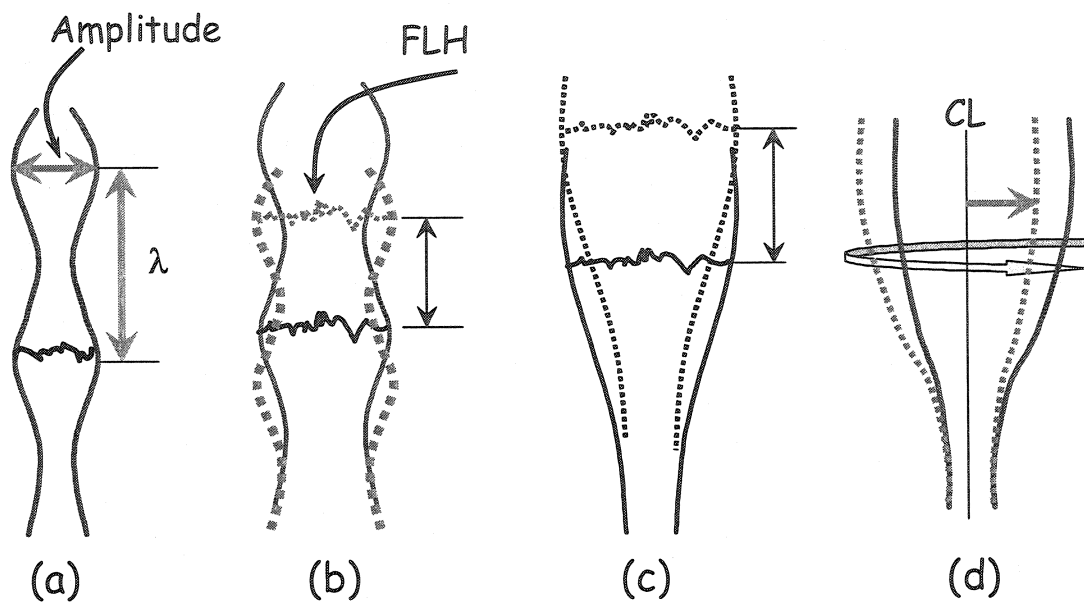


Figure 4. 1. Schematic views of typical bubble instabilities (a) draw resonance (DR), (b) FLH combined with DR, (c) FLH instability, (d) Helicoidal instability.

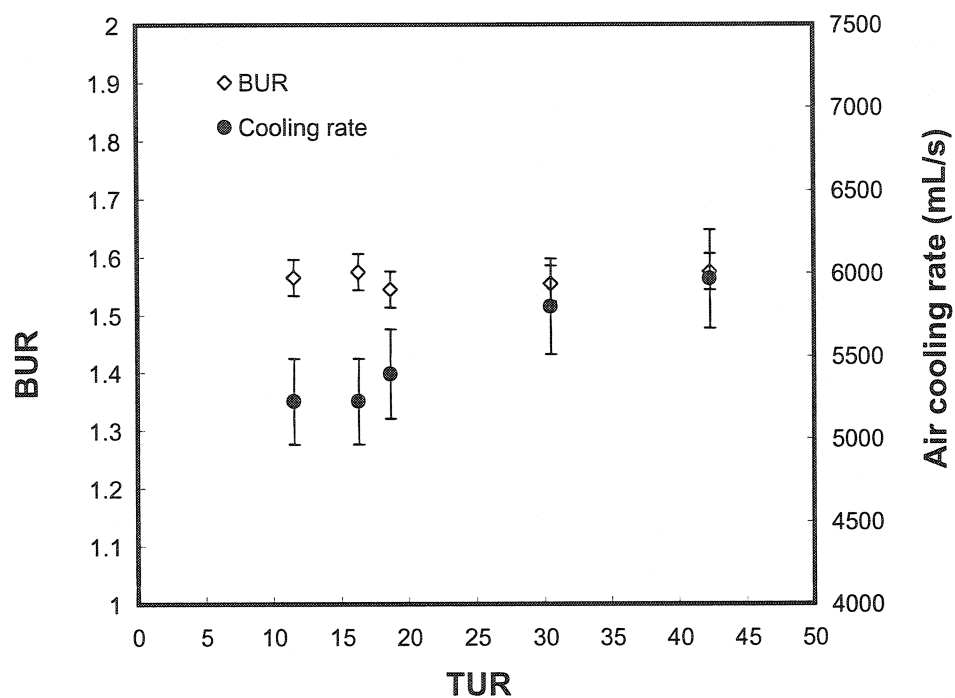
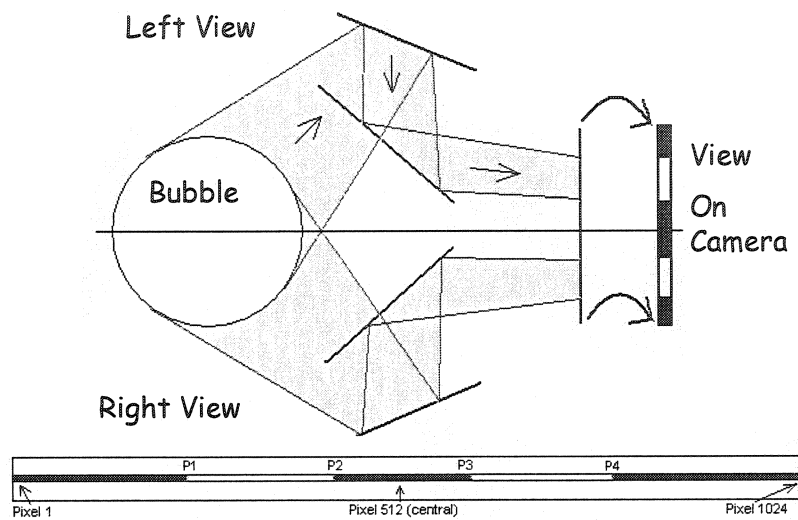
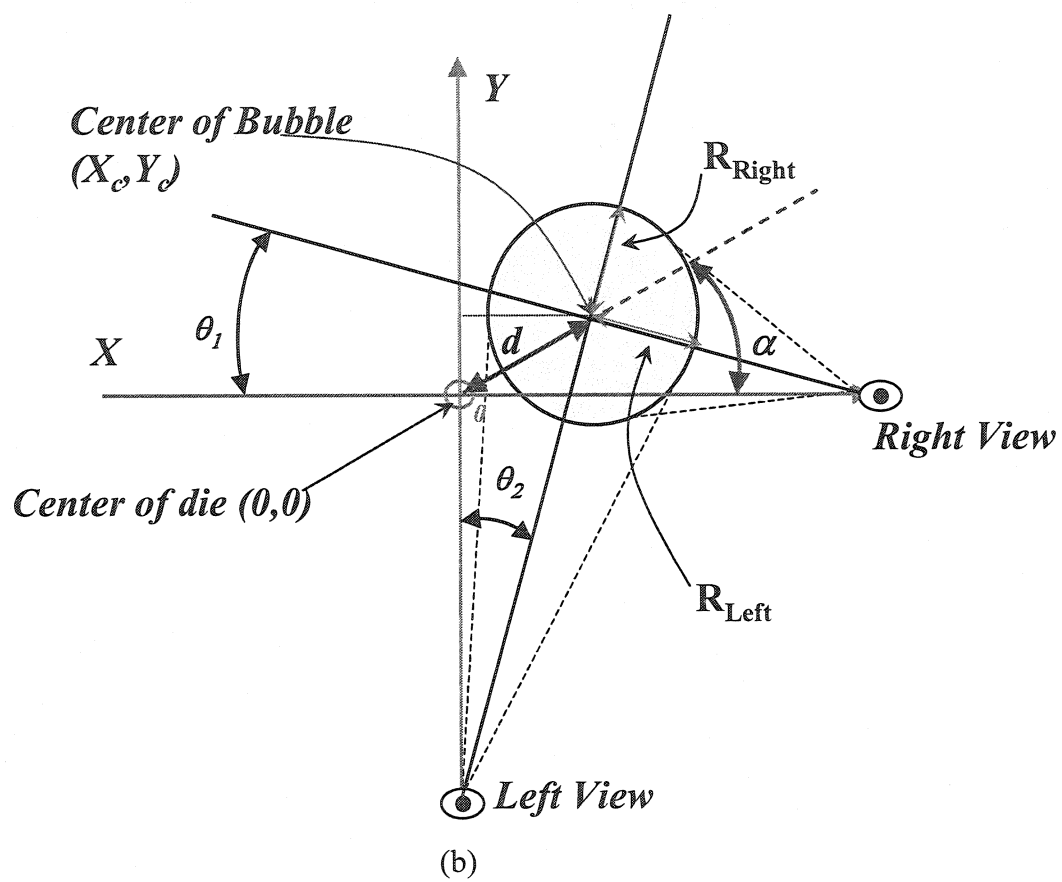


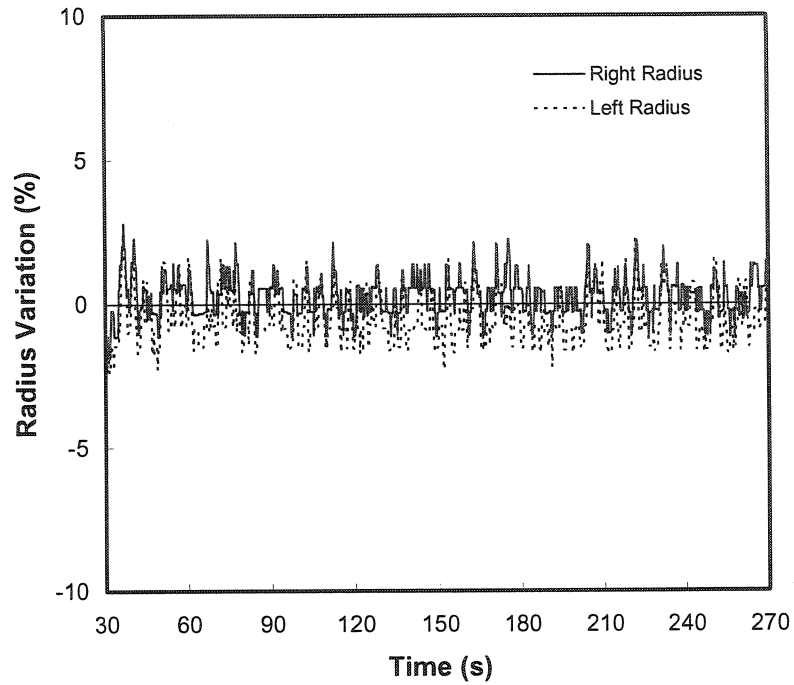
Figure 4. 2. Variations of BUR and air cooling rate as functions of TUR while holding an approximately constant similar FLH of 180mm (LDPE, targeted BUR around 1.5).



(a)

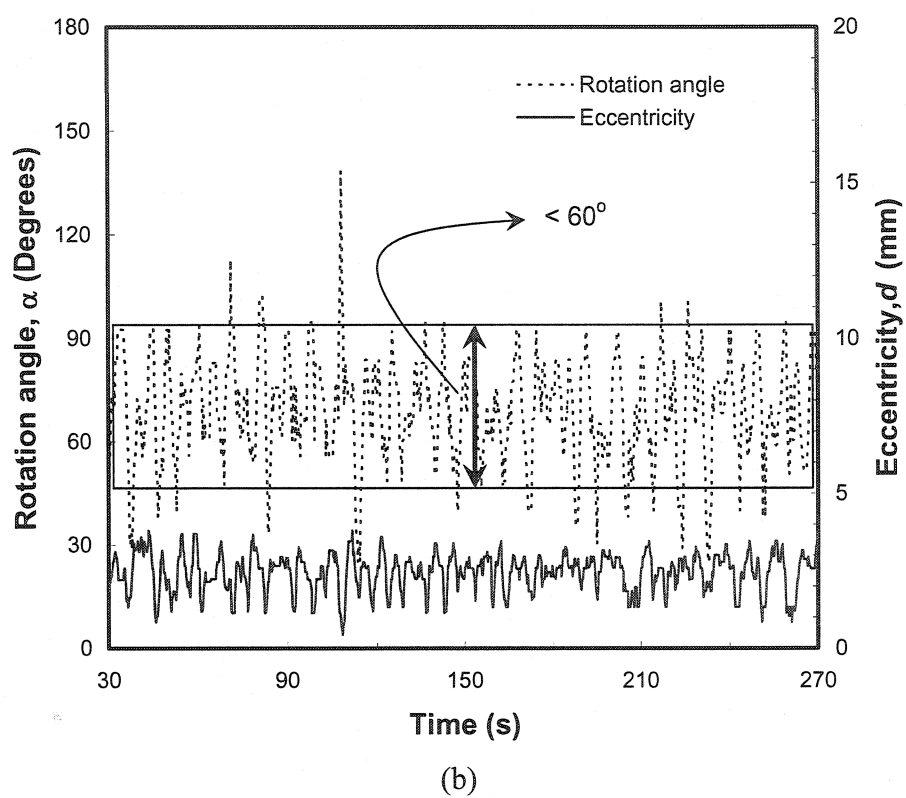
Figure 4. 3. (a) Schematic view of the new system and (b) geometrical variables of bubble and die.

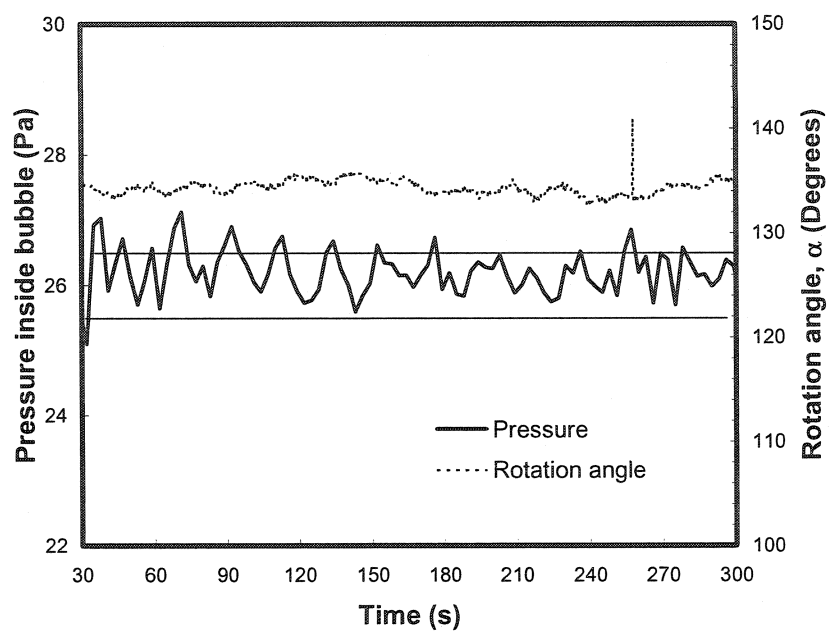




(a)

Figure 4. 4. Typical responses for a stable bubble of LmPE (FLH = 180 mm, BUR = 1.5, TUR = 42); a) radius variations, b) variations of eccentricity and rotation angle, c) variations of pressure inside the bubble and radius ratio as a function of time. (FLH = 180 mm, BUR = 1.5, TUR = 18.6).





(c)



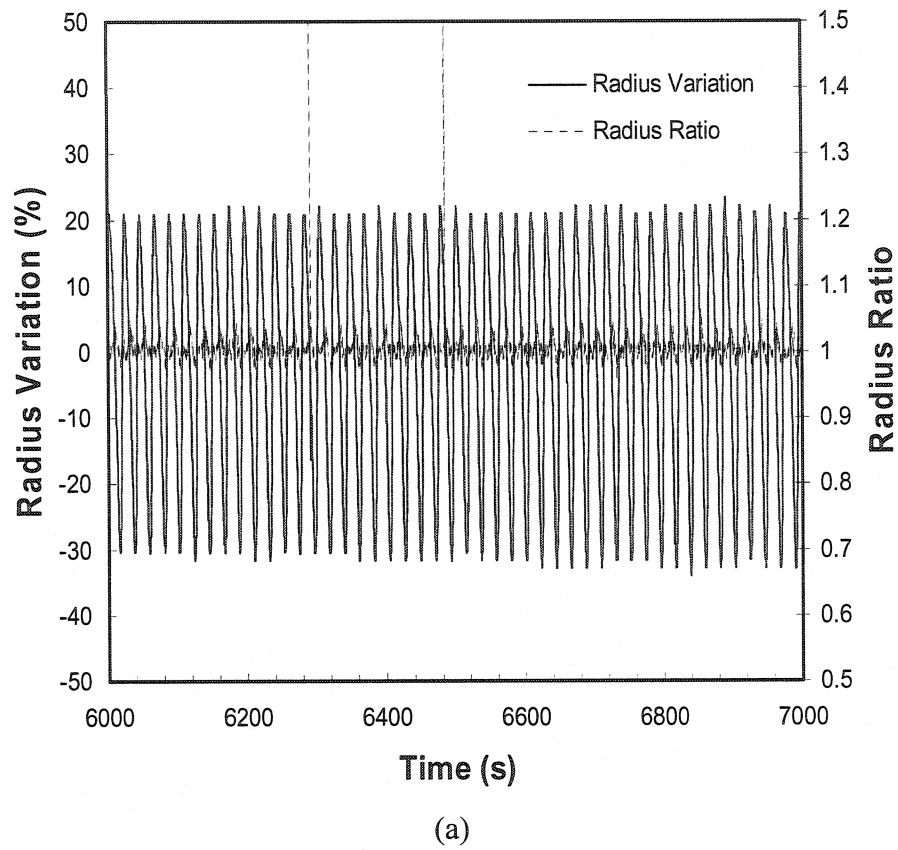
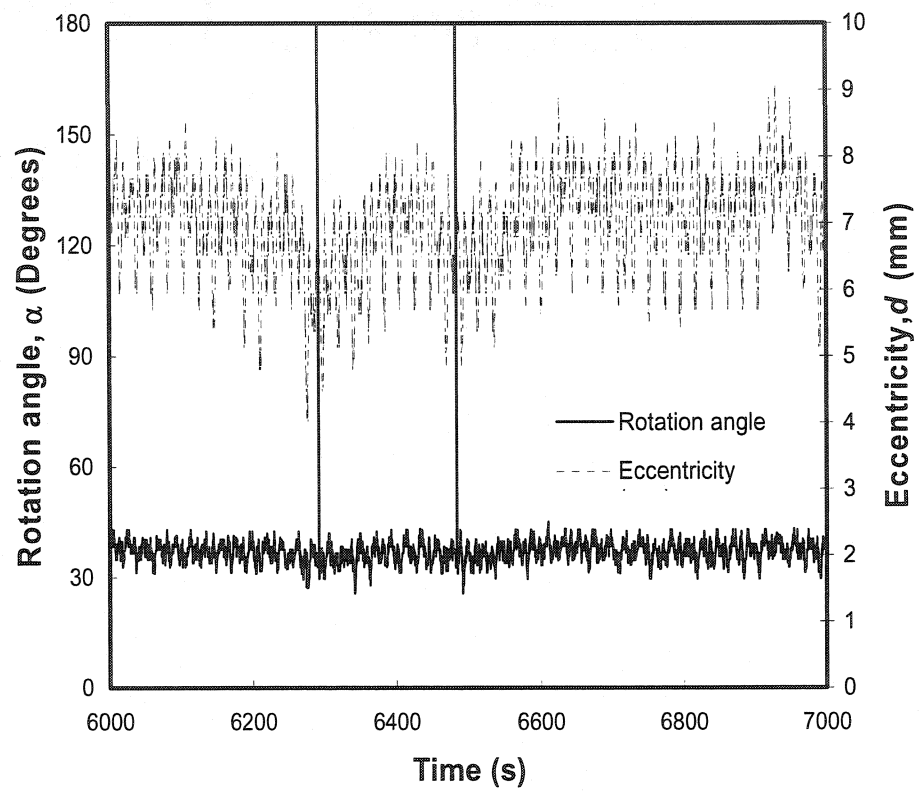
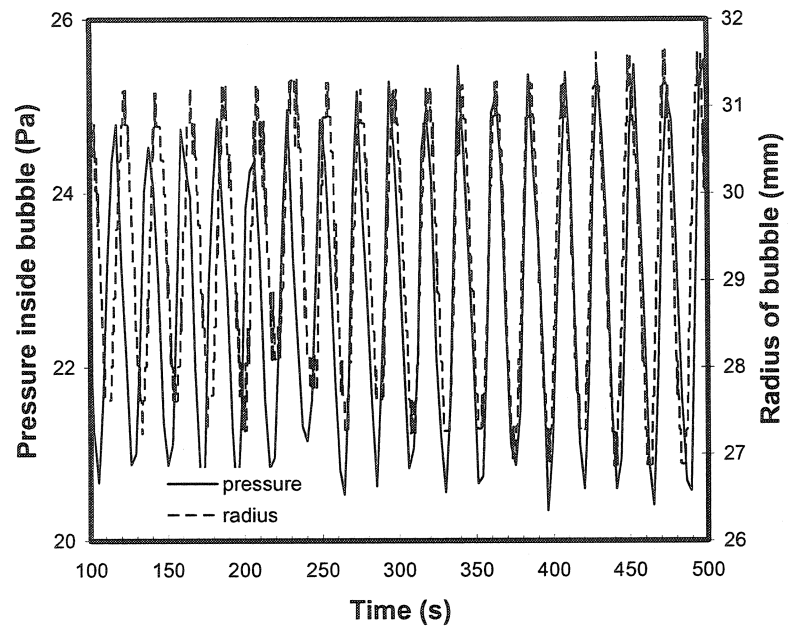


Figure 4. 5. Typical responses for draw resonance of LDPE (FLH = 100 mm, BUR = 1.0, TUR = 18.6); a) radius variations and radius ratio, b) variations of eccentricity and rotation angle, c) variations of pressure inside the bubble and radius as a function of time.



(b)



(c)

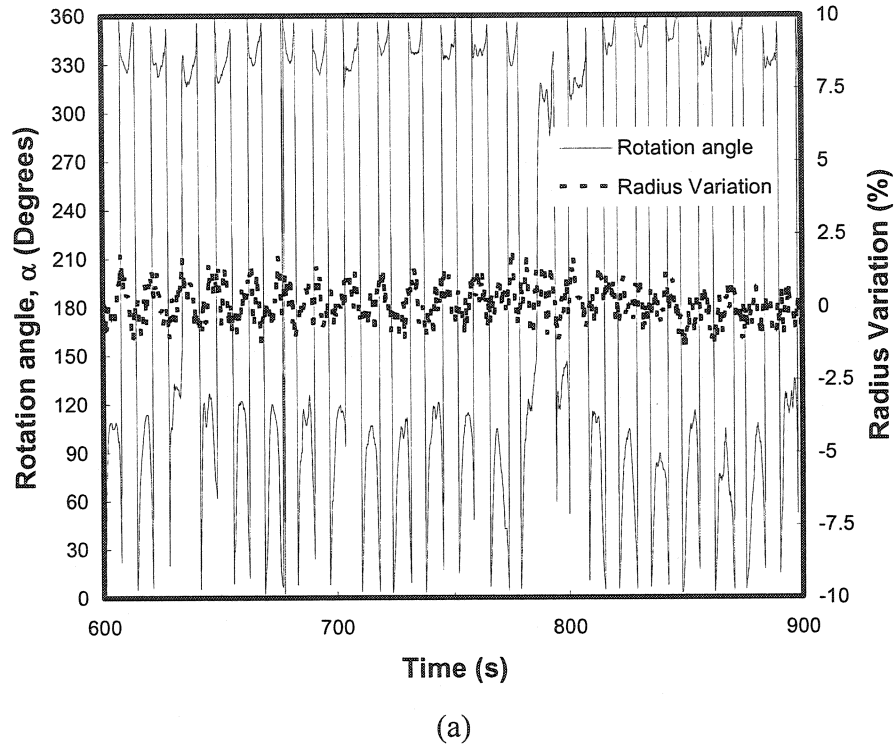
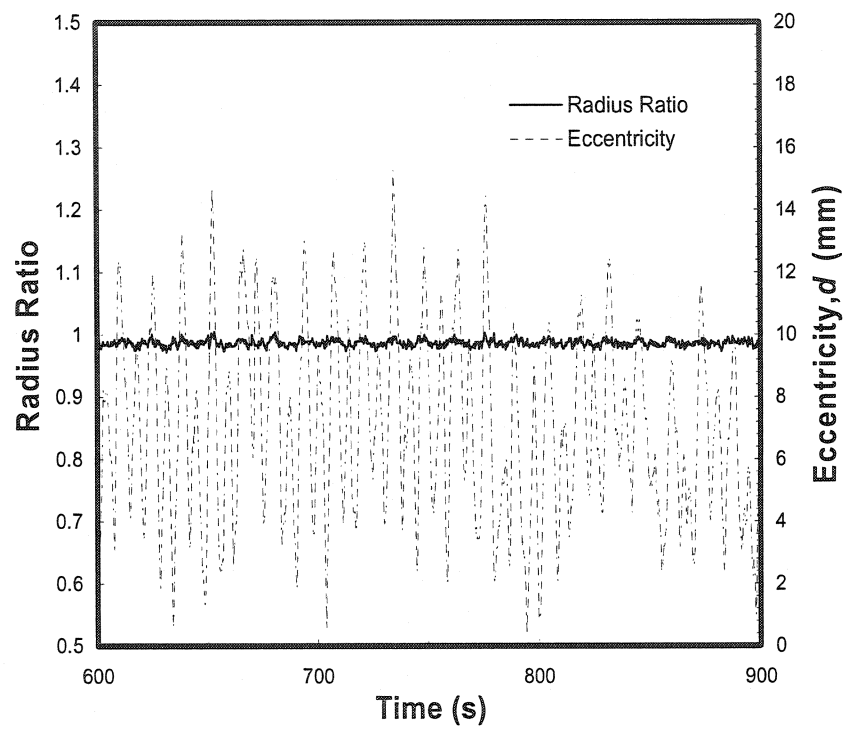
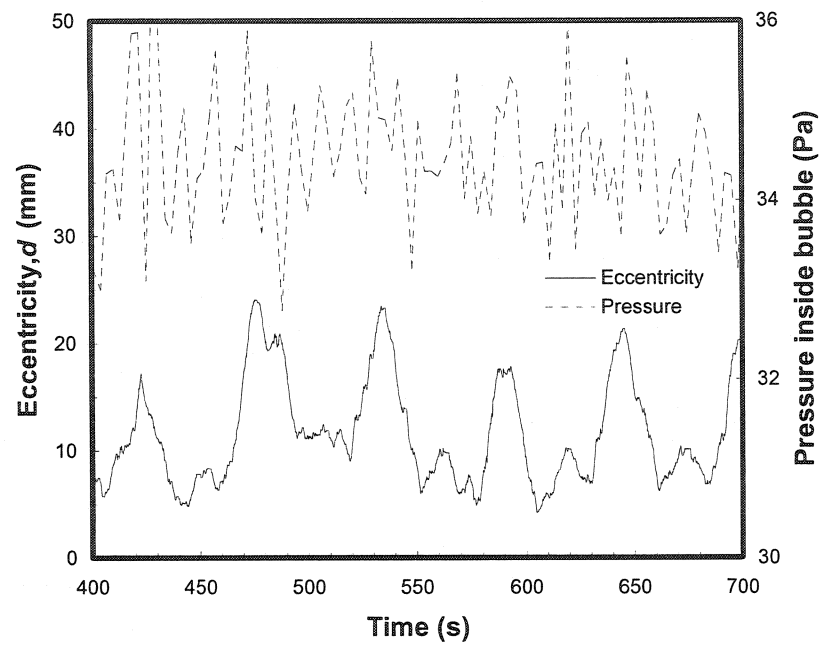


Figure 4. 6. Typical responses for helicoidal instability of LLDPE (FLH = 180 mm, BUR = 2.0, TUR = 30.5); a) radius variations and rotation angle, b) eccentricity and radius ratio, c) variations of pressure inside the bubble and eccentricity as a function of time.



(b)



(c)

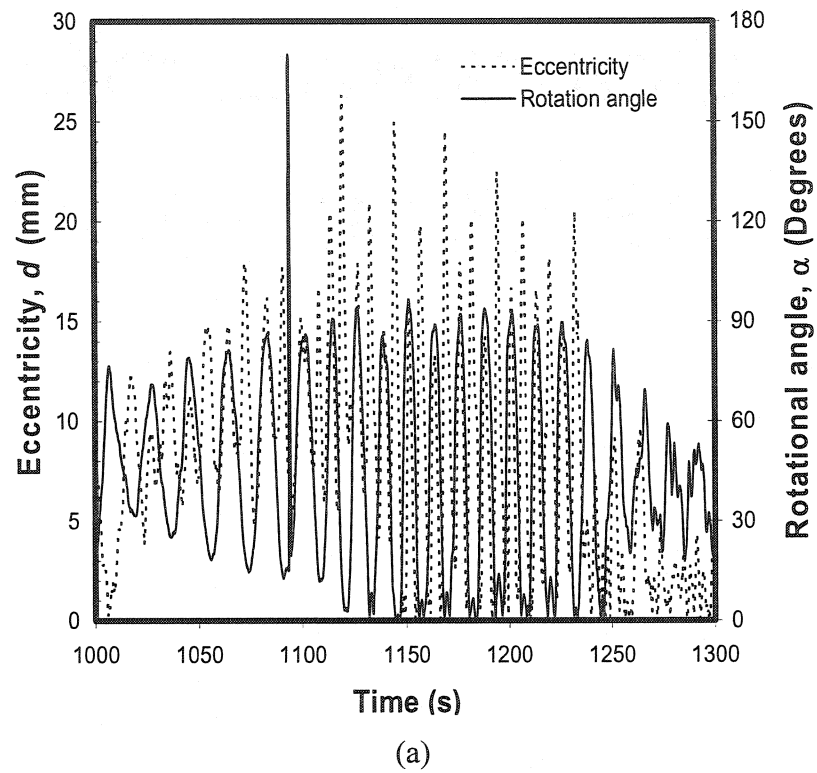
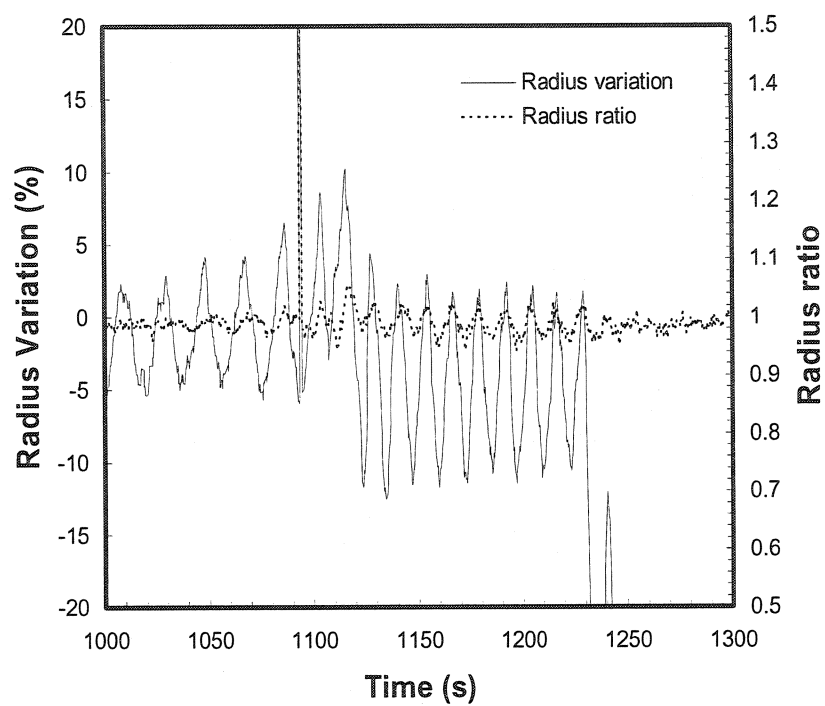
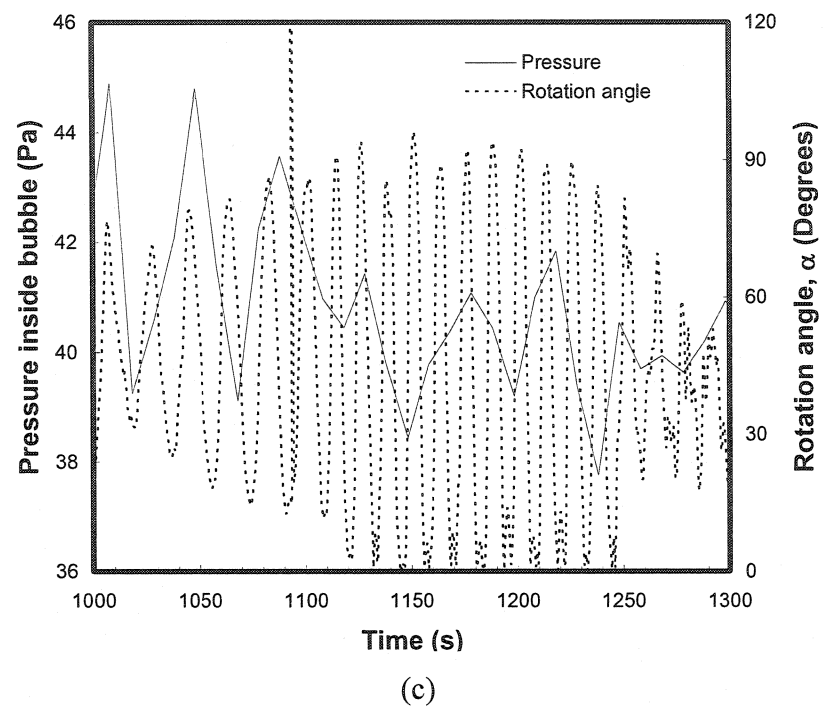


Figure 4. 7. Typical responses for FLH instability of LmPE (FLH = 250 mm, BUR = 2.2, TUR = 18.6); a) variations of eccentricity and rotation angle, b) radius variations and radius ratio, c) variations of pressure inside the bubble and rotational angle as functions of time.

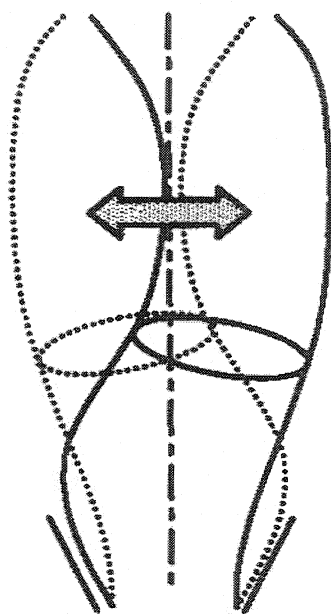


(b)





Side View



Front View

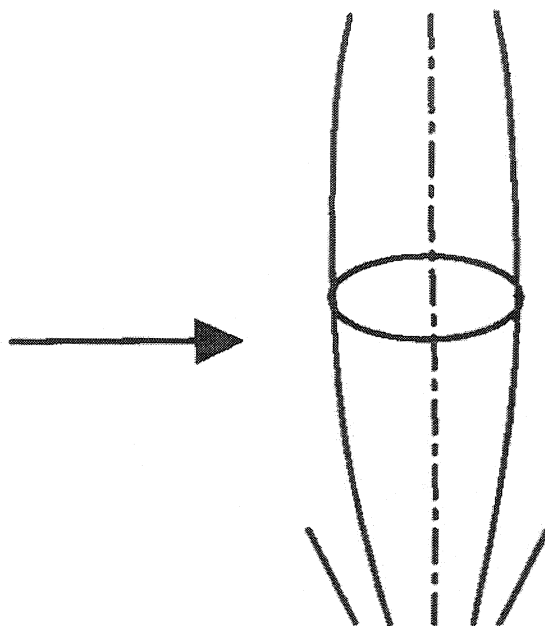


Figure 4. 8. Schematic views of additional bubble instability from two different points of view.

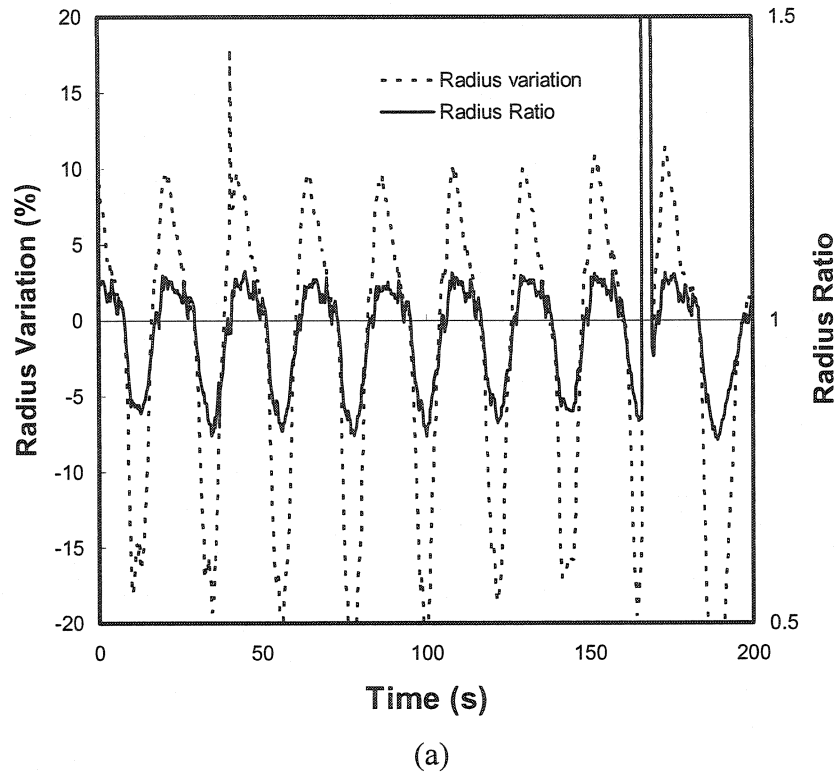
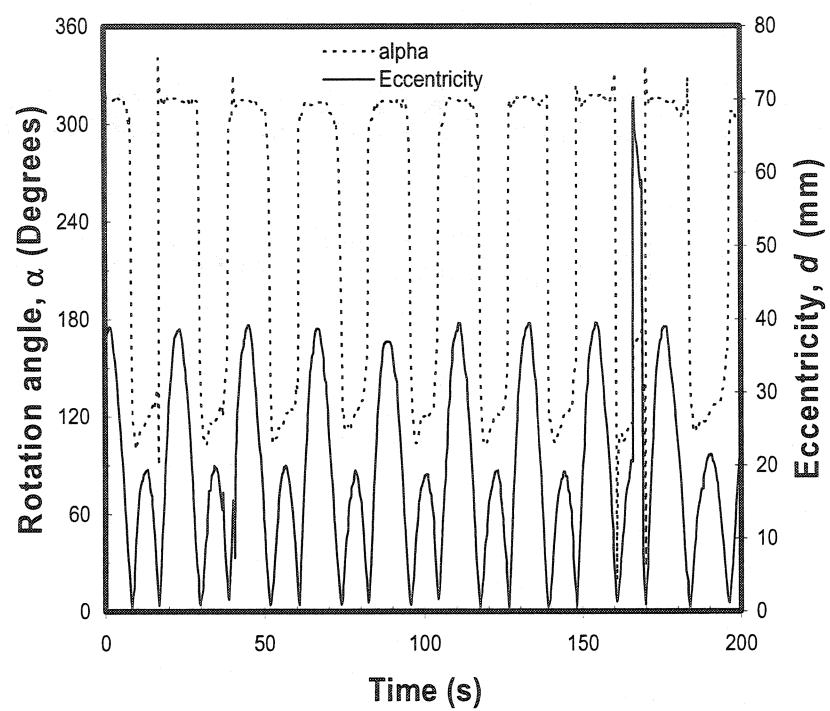


Figure 4. 9. Responses for additional bubble instability of LmPE (FLH = 180 mm, BUR = 1.98, TUR = 6); a) radius variations and radius ratio, b) variations of eccentricity and rotation angle as functions of time.



(b)

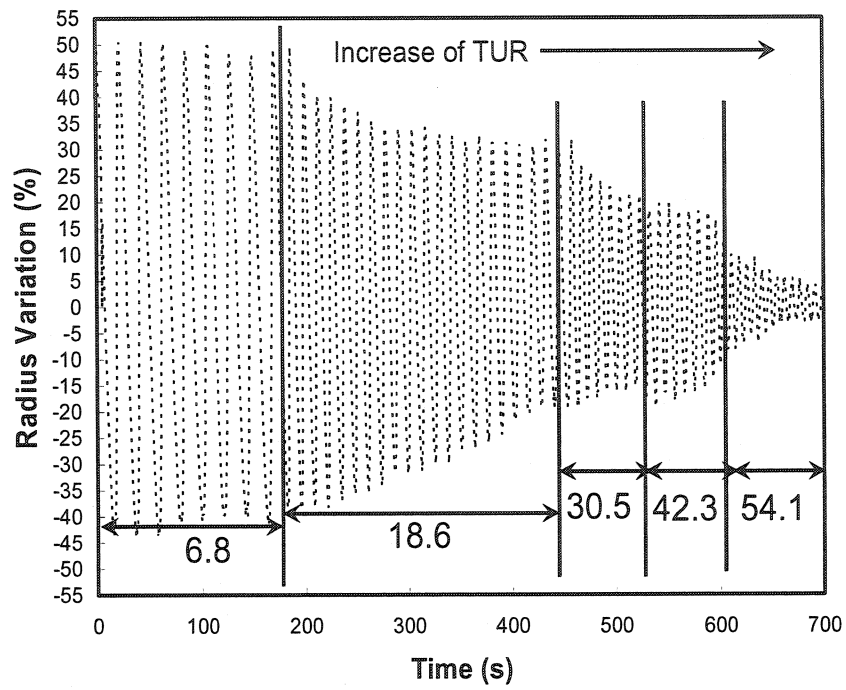


Figure 4. 10. Evolution of draw resonance as a function of TUR of LDPE (FLH = 100 mm, BUR = 0.9,  $Q = 2.0 \pm 0.1$  kg/h,  $T_{melt} = 185^{\circ}\text{C}$ ).

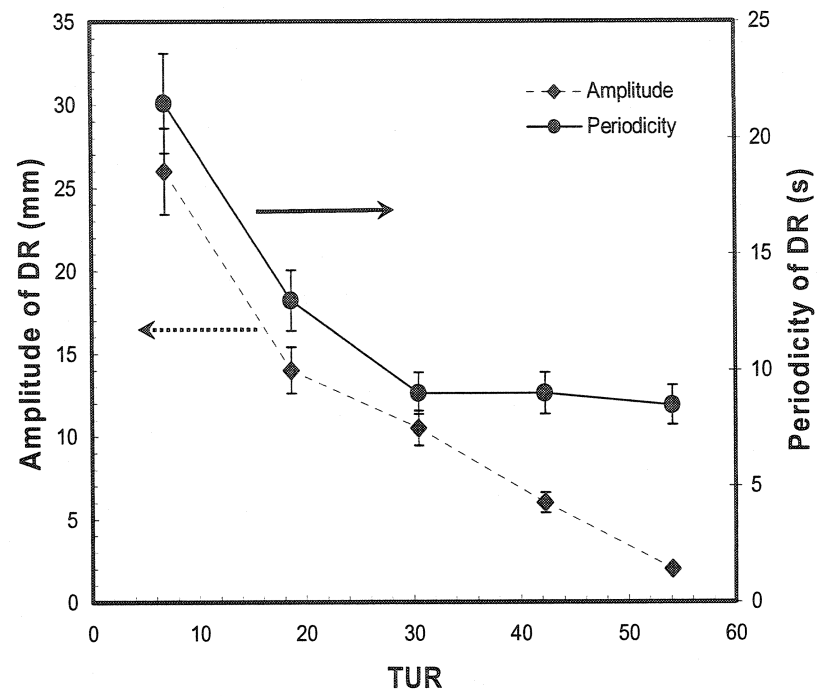


Figure 4. 11. Variations of amplitude and periodicity for draw resonance as functions of TUR. All conditions are the same as in Fig. 4.10.

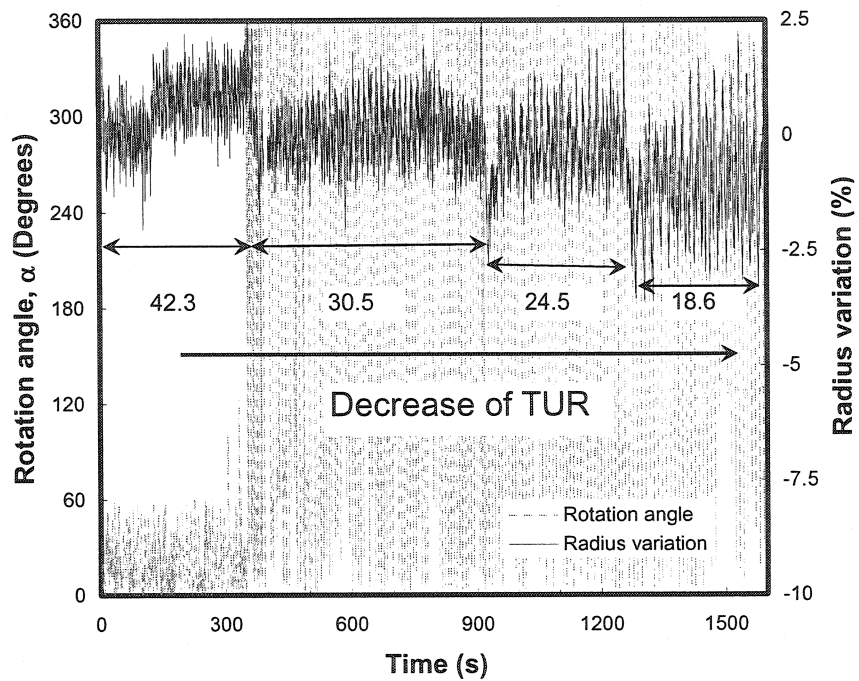


Figure 4. 12. Radius ratio and eccentricity as functions of time with various TUR values under helicoidal instability of LLDPE. (FLH = 180 mm, BUR = 2.0,  $Q = 2.0 \pm 0.1$  kg/h,  $T_{melt} = 186^\circ\text{C}$ )

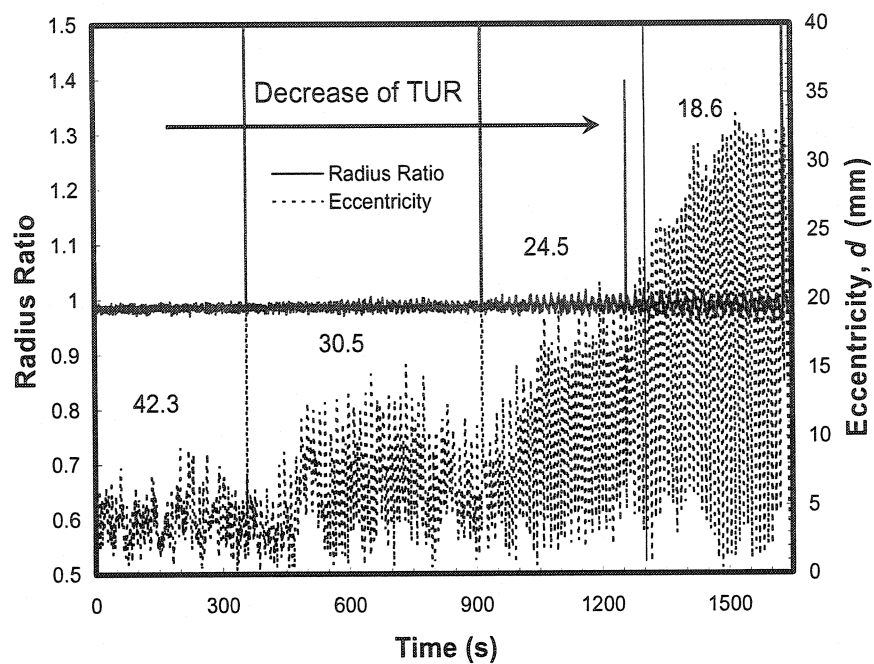


Figure 4. 13. Rotational angle and radius variations as functions of TUR under helicoidal instability of LDPE. All conditions are the same as in Fig. 4.12.



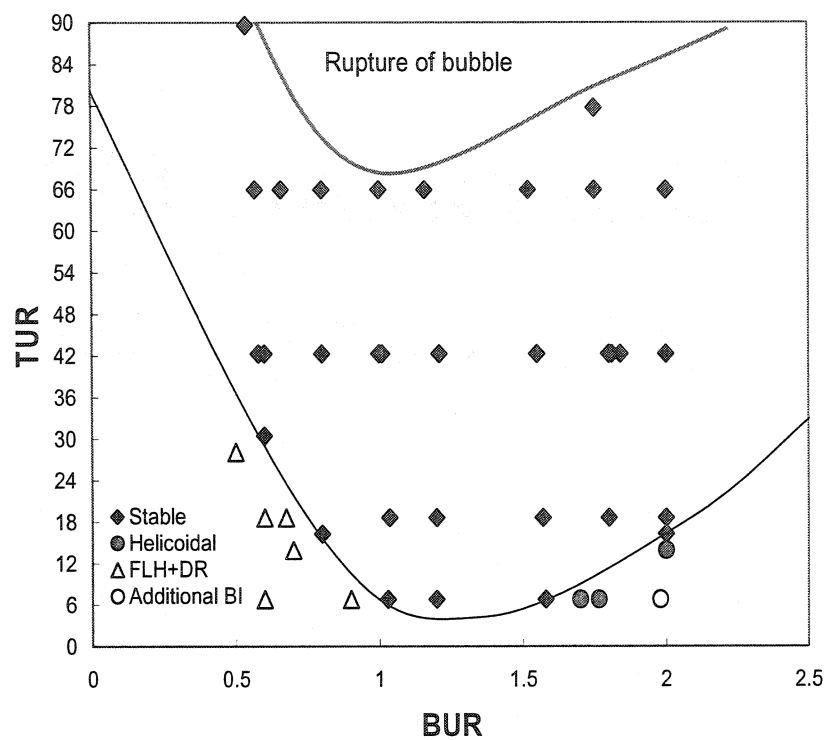


Figure 4. 14. Bubble stability map for LDPE as functions of BUR and TUR (FLH = 180 mm,  $Q = 2.0 \pm 0.1$  kg/h,  $T_{melt} = 185$  °C).

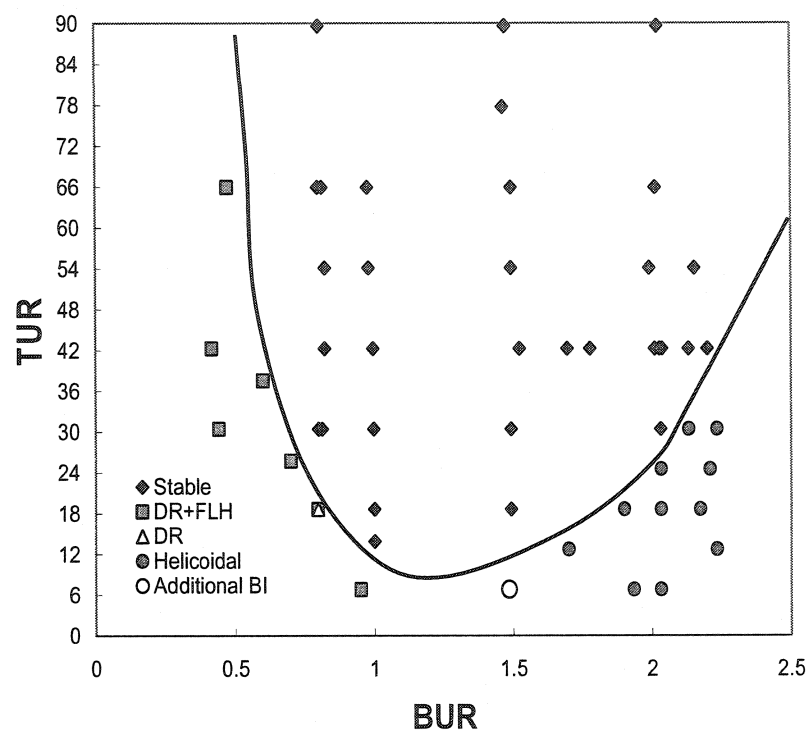


Figure 4. 15. Bubble stability map for LLDPE as functions of BUR and TUR (FLH = 180 mm,  $Q = 2.0 \pm 0.1$  kg/h,  $T_{melt} = 186$  °C).

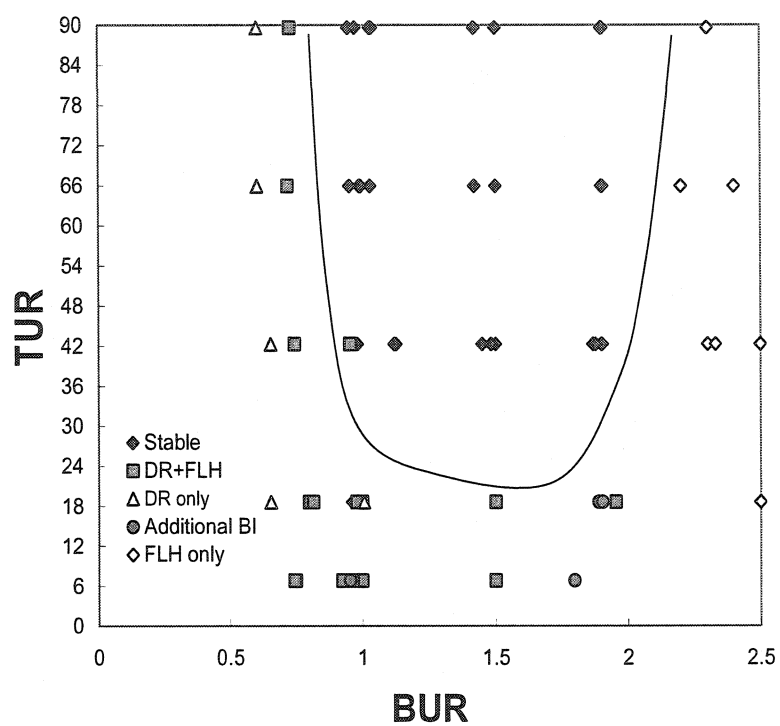


Figure 4. 16. Bubble stability map for LLDPE as functions of BUR and TUR (FLH = 250 mm,  $Q = 2.0 \pm 0.1$  kg/h,  $T_{melt} = 187^{\circ}\text{C}$ ).

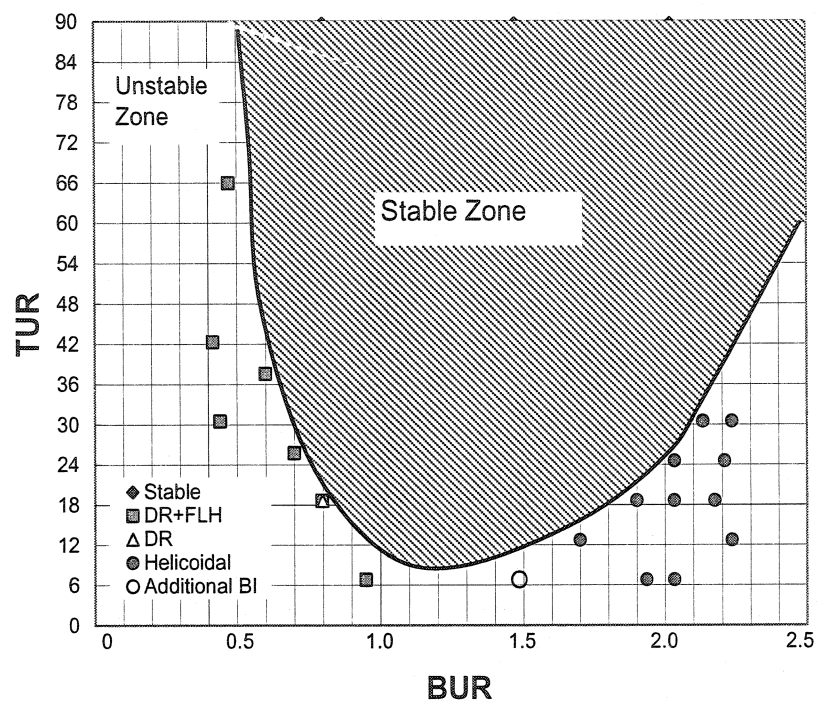


Figure 4. 17. Typical example of graphical quantification of stable region in the bubble stability map of LLDPE. All conditions are the same as in Fig. 4.15.

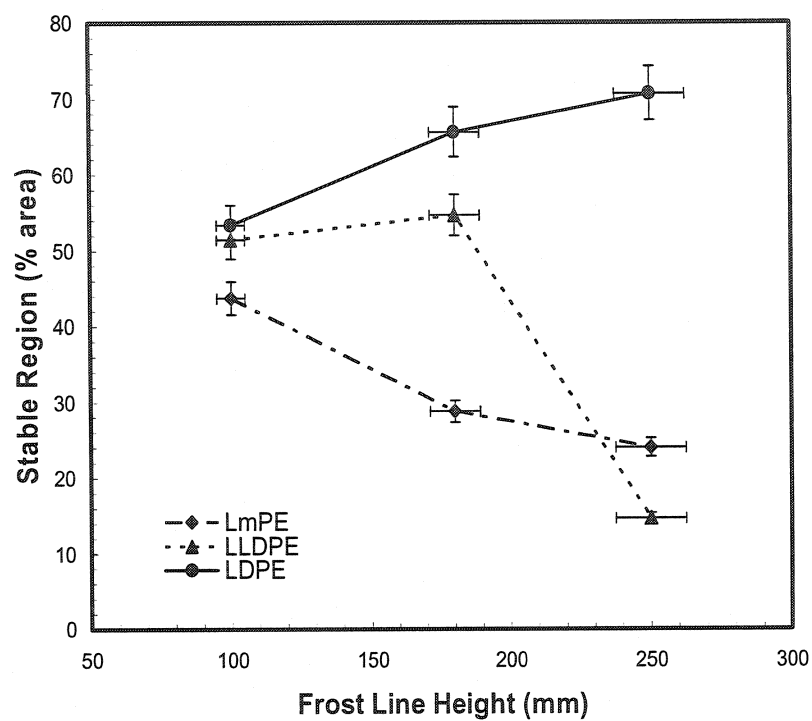


Figure 4. 18. Summary of bubble stability of samples used as a function of FLH ( $Q = 2.0 \pm 0.1$  kg/h,  $T_{\text{melt}} = 186 \sim 187^\circ\text{C}$ ).

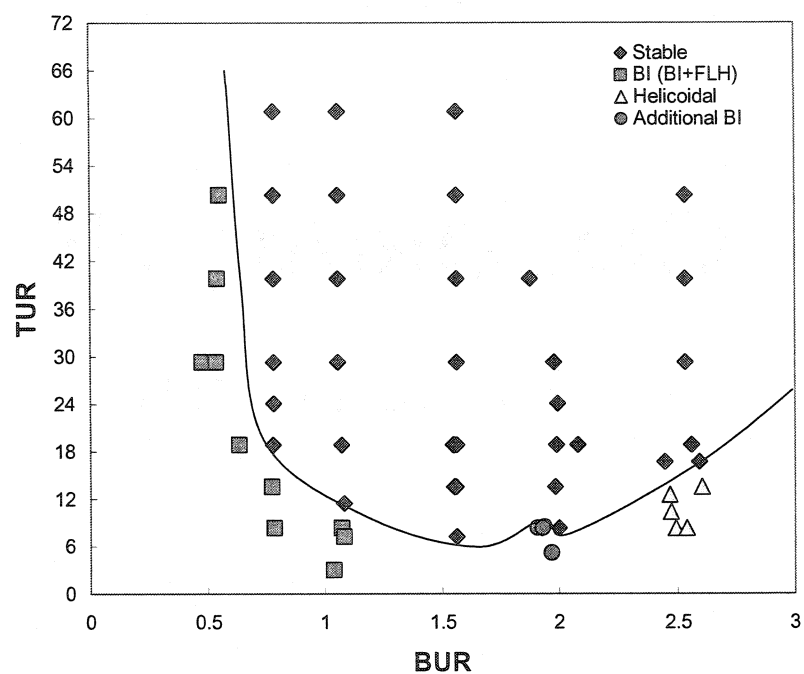


Figure 4. 19. Bubble stability map of LDPE as functions of BUR and TUR (FLH = 250mm,  $Q = 4.5 \pm 0.1$  kg/h,  $T_{\text{melt}} = 185^{\circ}\text{C}$ ).

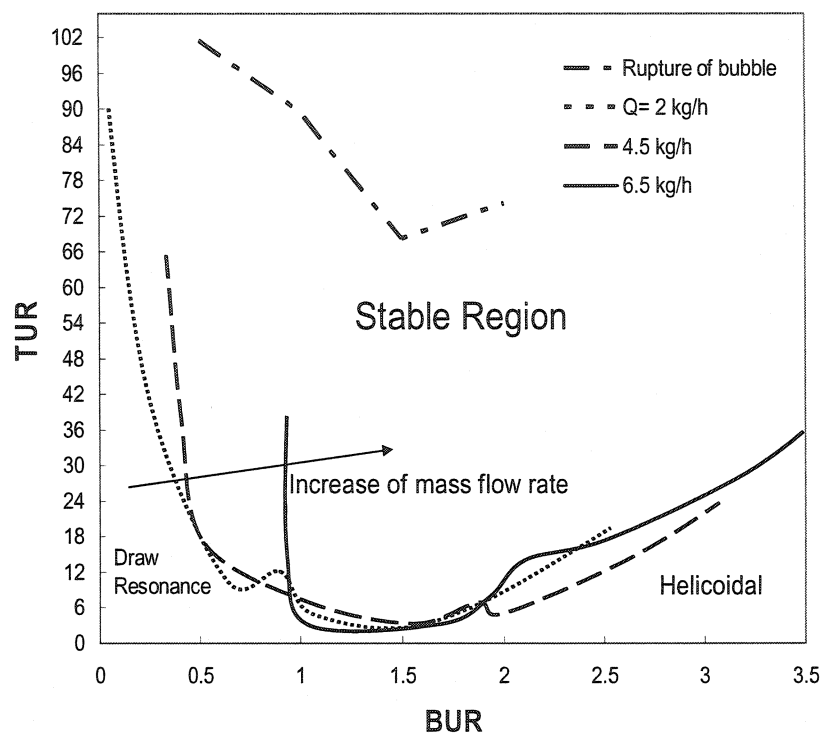


Figure 4. 20. Summary of bubble stability map of LDPE as a function of mass flow rate (FLH = 250 mm,  $T_{melt} = 185^{\circ}\text{C}$ ).

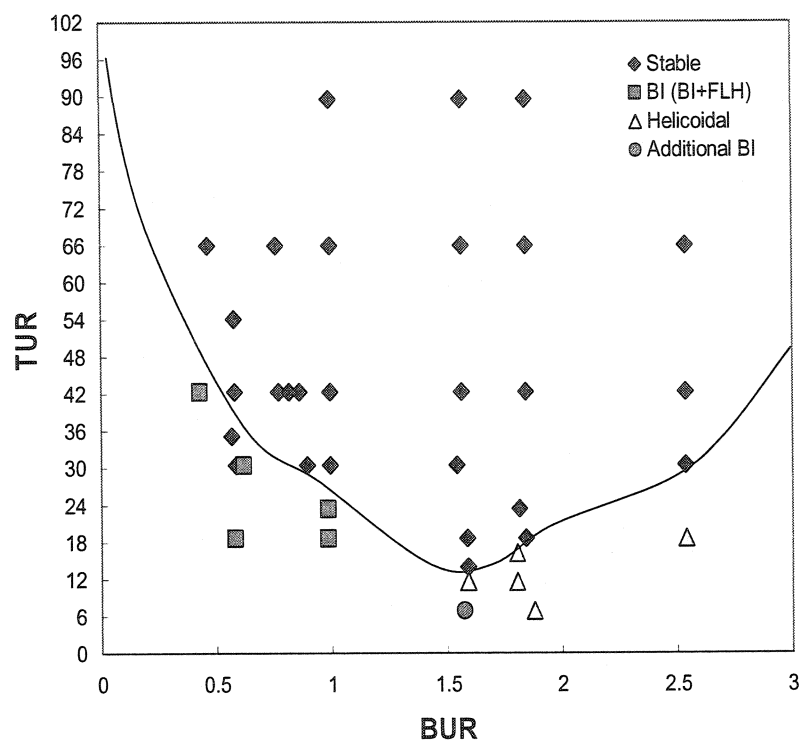


Figure 4. 21. Bubble stability map of LDPE as functions of BUR and TUR (FLH = 250 mm,  $Q = 2.0 \pm 0.1$  kg/h,  $T_{melt} = 204$  °C).



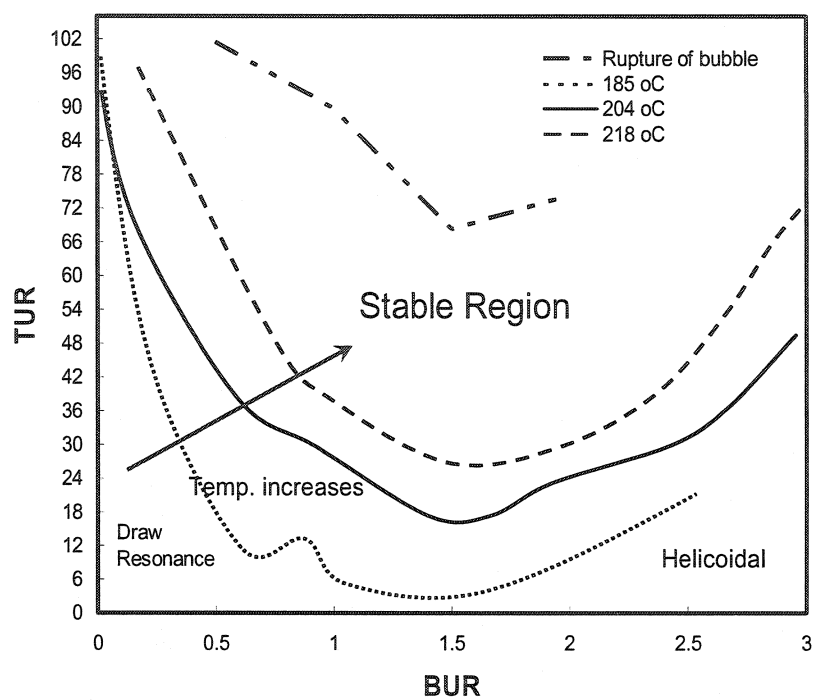


Figure 4. 22. Summary of bubble stability map of LDPE as a function of melt temperature (FLH = 250 mm,  $Q = 2.0 \pm 0.1$  kg/h).

## CHAPTER 5. THERMAL AND RHEOLOGICAL PROPERTIES OF mPE/LDPE BLENDS<sup>‡</sup>

Yunli Fang, Pierre J. Carreau and Pierre G. Lafleur

Centre de Recherche Appliquée Sur les Polymères (CRASP), Dept. of Chemical  
Engineering, Ecole Polytechnique  
Montreal, QC, H3C 3A7, Canada

### Abstract

The thermal and rheological properties of two types of metallocene catalyzed polyethylenes (mPEs) and two low density polyethylenes (LDPEs) as well as their blends were studied using DSC and rheometry. DSC results showed that the linear mPE (LmPE) based on hexene comonomer is immiscible with both LDPEs in crystalline states whereas the branched mPE (BmPE) based on octene comonomer is miscible with the LDPEs. This suggests that increasing the length of short chains in mPEs can promote the miscibility of mPE/LDPE blends. The linear viscoelastic properties confirmed the immiscibility of the LmPE with the LDPEs in the molten state and miscibility of BmPE with LDPEs. In addition, the Palierne emulsion model showed good predictions of the linear viscoelastic data for both miscible and immiscible polyethylene blends. However, as expected the low frequency data showed a clear influence of the interfacial tension on the elastic modulus of the blends for the immiscible blends.

**Key Words:** metallocene catalyzed polyethylene(s), miscibility/immiscibility, rheology, DSC

---

<sup>‡</sup> Submitted to *Polymer Engineering & Science* (2004)

## 5.1. Introduction

The new member of polyethylene families made by metallocene catalysts offers opportunities in the area of product development for plastics. Due to its tailored structure, with narrow molecular weight distribution (MWD) and sparse long-chain branch (LCB), metallocene-catalyzed polyethylenes (mPEs) exhibit the combined properties of LLDPE and LDPE. LLDPE has superior mechanical properties but relatively poor processability due to its MWD and lack of LCB whereas LDPE has very good processability but relatively poor mechanical properties due to its broad MWD and a large amount of LCB. However, the amount of LCB in mPEs is not sufficient to give good processability even though the superior properties of mPE have been widely recognized. Hence, the use of mPEs has been largely limited. Blending mPE with LDPE is a good way to solve this problem.

The miscibility of PE blends has been investigated for a long time by different research groups using different techniques. They reported that PE blends were either immiscible or partially miscible [2-8]. The low contrast, low and closer glass transition temperatures of PE blend components make it difficult to determine the blend miscibility using routine ways, such as glass transition temperature determined by thermal analysis and morphology determined by optical and electron microscopy, etc.. Alamo *et al.* [9] reported that the branch content was the critical factor for HDPE/LDPE blends using small angle neutron scattering (SANS) technique, which was considered the most powerful technique. They found that when the branch content was more than 8 branches/100 backbone carbons the blends exhibited phase separation. However, the deuteration itself might have altered the chemistry and physics of the individual components. Okamoto *et al.* [10] tried to determinate the immiscibility of LDPE/UHMWPE (ultra high molecular weight polyethylene) and LLDPE/HDPE via birefringence based on the stress optical rule (SOR) using elongational flow opto-

rheometry (EFOR). They showed that LDPE/UHMWPE blends obeyed SOR whereas LLDPE/HDPE violated the rule due to form birefringence. Datta and Birley [11] used thermal analysis to prove that LLDPE/LDPE blends were incompatible while Lee *et al.* [12] also showed LLDPE/LDPE blends are immiscible in the crystalline state.

Using rheometry as a technique to study the immiscibility of blends is getting more and more popular since the rheological properties of polymers are not only sensitive to the molecular structure but also to the phase behavior. A lot of techniques have been developed by different groups. The most well accepted method is log-additivity rule, which is a semi-log relation between zero shear viscosity and the compositions of the blends. Miscibility is expected to exhibit a linear relation if the blend components do not interact specifically. If blends are miscible, their zero shear viscosity as a function of blend composition would be linear relation. However, Yang *et al.* [13] showed a negative deviation behavior (NDB) for miscible PMMA/poly(vinylidene fluoride) whereas miscible PMMA/poly(styrene-co-acrylonitrile) blends showed a positive deviation behavior (PDB). As far as we aware, there is no report for miscible PE blends showing PDB, NDB or positive-negative deviation behavior (PNDB). Also, there is no observation for immiscible PE blends that obey log-additivity rule. Kwag *et al.* [5] used revised log-additivity rule by plotting the complex viscosity as a function of composition for different frequencies to determine the immiscibility of mPE blended with HDPE, PP, poly(propylene-co-ethylene) and (propylene-co-ethylene-co-1-butylene). More recently, Liu *et al.* [8] reported the immiscibility of mPE/LDPE based on log-additivity rule. Cole-Cole plots of the dynamic rigidity ( $\eta''$ ) versus dynamic viscosity ( $\eta'$ ) of the blends as well as the pure resins on a linear scale, has also been used by different groups to determine the immiscibility of the blends [5, 14]. If the blend is miscible, the curve should form a semicircular relationship. Han *et al.* [15] revised the Cole-Cole plot by plotting the storage modulus ( $G'$ ) versus the loss modulus ( $G''$ ) on logarithmic scales. For a miscible blend, the same slope was observed for the blends and the pure components;

otherwise, changing slopes indicated poor miscibility and immiscible or phase separated blends. Kwag *et al.* [5] also used this technique for their immiscibility study.

Palierne [1] introduced a model which could predict the linear viscoelastic properties of immiscible emulsion-type blends. Under favorable conditions the Palierne model can be used to determine the interfacial tension of immiscible polymer components using rheological data [16]. Recently, Hameed and Hussein [17] determined the immiscibility of mLLDPE/LDPE blends based on log-additivity rule and Palierne model and reported that mLLDPE/LDPE were immiscible for all the compositions and increasing the mLLDPE branch length from butene comonomer to hexene did not influence the immiscibility.

The objective of this work was to study the thermal and rheological properties and try to determine immiscibility of mPE/LDPE blends with different molecular structures, mainly with different lengths of short chain branches and different melt index (*MI*). The miscibility/immiscibility of LmPE/LDPE-1, BmPE/LDPE-2 blends will be further investigated by inline measurements during film blowing in an upcoming paper.

## **5.2. Experimental**

### **5.2.1. Materials and Blend Preparation**

The polymers used in this study were commercial grade blown film resins and were chosen based on their different molecular structures and melt index. Two metallocene-catalyzed mPEs with the same melt index and similar molecular weight (MW) and molecular weight distribution (MWD) but different lengths of short chain branches have been selected: a linear mPE (LmPE) based on 1-hexene comonomer

(Exxon Mobile) and a branched mPE (BmPE), based on octene from Dow Chemical. Two low density polyethylenes with different melt indices have been chosen: LDPE-1 and LDPE-2, also from Dow Chemical. The polymers used and their main characteristics are reported in Table 5.1. The values for MW and MWD were determined by Dr. Shuqin, Bo (Changchun Institute of Applied Chemistry, Chinese Academy of Sciences) using gel permeation chromatography (GPC).

Five different blend combinations, 90/10, 80/20, 50/50, 20/80, 10/90, were chosen for all the blends (LmPE/LDPE-1, LmPE/LDPE-2, BmPE/LDPE-1, BmPE/LDPE-2). 0.5% antioxidant was added to prevent degradation or cross-linking during melt blending and testing. The blends including the pure resins have been prepared using a Haake (Rheocord 90) internal mixer. The initial set temperature of the mixing chamber was 195°C and the blend was mixed for 10 min under constant flow of dry nitrogen.

### 5.2.2. Thermal Analysis

Differential scanning calorimetry (DSC) measurements were performed using a Perkin-Elmer DSC (Pyris-7). The temperature scale of calorimeter was calibrated from the melting points of indium and tin and the thermal response from the enthalpy of indium. The experiments were carried out with about 13 mg of samples sealed in aluminum pans under dry nitrogen. All the samples were first heated from 70°C to 150°C at a scanning rate of 40°C/min, held at 150°C for 5 min, and then cooled at a rate of 5°C/min to 70°C and held at 70°C for 5 min and finally heated again from 70°C to 150°C at 5°C. The cooling scans and the second heating scans were used to obtain the crystallization and melting temperatures.

### 5.2.3. Rheological Measurements

Dynamic rheological measurement was carried out on a Rheometric SR5000 stress controlled rheometer. The samples from the internal mixer were melt pressed in a Carver laboratory hot press at 190°C for 5 min under  $5 \times 10^5$  Pa, then pressed under  $1 \times 10^6$  Pa for another 5 min and cooled using a cold press. The measurements were then carried out using a 25 mm parallel plate geometry and a 1 mm sample gap. Time sweep under 0.01 rad/s was performed over 5 h to check the thermal stability for all the blends and pure polyethylenes. The dynamic viscoelastic properties were determined with frequencies ranging from 0.001 to 500 rad/s depending on the temperature, using strain and stress values determined to lie within the linear viscoelastic regime. Three/four different steps of stress or strain sweeps were used to investigate the linear regions under different frequencies (0.01, 0.05, 0.5 and 5 rad/s). Four/five different steps, 0.001-0.01 rad/s, 0.01-0.05 rad/s, 0.05-0.5 rad/s, 0.5-5 rad/s, 5-500 rad/s, were used for the frequency sweeps. The rheological data under overlapped frequencies can also be used to evaluate the quality of the data acquired. All the measurements were carried out under nitrogen atmosphere at three different temperatures: 150, 175, and 200°C. All the frequency sweeps were repeated at least three times to confirm the reproducibility.

## 5.3. Results and Discussion

### 5.3.1. Thermal Properties

The curves of the DSC melting and cooling scans of LmPE/LDPE-1, LmPE/LDPE-2 blends are shown in Figs. 5.1 and 5.2, respectively. From these figures, we see that the melting point of the LmPE is higher than those of LDPEs, which can be explained by the different lamellar thicknesses, as reported by Wunderlich [18] for LLDPE and LDPE. We also observe that the melting peak of the LmPE is less intense

and broader than those of the LDPEs, which is due to a large amount and heterogeneous distribution of short chain branches (SCBs) in the LmPE. Furthermore, the LmPE, the LmPE/LDPE-1 (90/10, 80/20, 50/50) blends and the LmPE/LDPE-2 (90/10, 80/20, 50/50, 20/80) blends exhibit two distinct peaks during both heating and cooling scans, whereas the LDPEs and the LmPE/LDPE-1(20/80, 10/90) blends and the LmPE/LDPE-2 (10/90) blends show only one peak. Munstedt *et al.* [19] showed that LLDPE cannot be generally regarded as a homogeneous material. Mirabella *et al.* [20] also reported that LLDPE itself shows phase separation in the melt, which is also due to the heterogeneous distribution of SCBs giving rise to a broad range of lamellae thicknesses during crystallization, thus leading to multiple melting behaviors. This is also the case for the LmPE used in this study. Unfortunately, the first crystallization and melting peaks for the LmPE are quite close to those of the LDPEs. Nevertheless, the two separated peaks for most of these blends suggest immiscibility. Fig. 5.3 reports the crystallization and the melting peaks as functions of the blend composition for these two families of blends. The error bar denotes the estimated accuracy of  $\pm 2.5\%$  error. The main crystallization and melting peaks (peaks 2) for the LmPE keeps almost unchanged, indicating that the crystallization of the LmPE is not influenced by the presence of the LDPE. We may also see that with the addition of LmPE, the position of the first peaks for the blends do not get closer to the main peaks of the LmPE. This may be due to existence of firstly solidified phase may obstruct the growth of lamellar crystallites of the rest of polymers and eventually lead to liquid-solid phase separation for the blends [21].

Figs. 5.4 and 5.5 show melting and cooling scans of BmPE/LDPE-1 and BmPE/LDPE-2 blends, respectively. The composition dependence of the melting temperature,  $T_m$ , and the crystallization temperature,  $T_c$ , for BmPE/LDPE-1 and BmPE/LDPE-2 blends are plotted in Fig. 5.6 (a) and (b), respectively. These blends show a totally different thermal behavior compared to the blends based on the LmPE. The BmPE shows broader melting peak than those of both LDPEs and the melting temperature of BmPE is considerably lower ( $101.3^\circ\text{C}$ ) than those of LDPEs ( $110.6^\circ\text{C}$ ).



The same trend is observed for the crystallization temperatures and only one peak is observed for all the compositions of both blend systems, suggesting total miscibility of these blends. Also, the composition dependence of the melting points and crystallization temperatures of both blend systems almost follow linear relations, indicative of co-crystallization of the blend components. Under cooling, the LDPE crystallizes first and acts as nucleating agent for the crystallization of the rest of the polymer components. When co-crystallization happens, the thermal and physical properties of the blend system would be intermediate properties with respect to those of the individual components [22].

### 5.3.2. Rheological Properties

Fig. 5.7 shows the complex viscosity versus frequency for the LmPE/LDPE-1 blends at 175°C. The LmPE depicts a very long Newtonian viscosity plateau at low frequencies and then a pronounced shear-thinning at high frequencies. The complex viscosity of the LDPE-1 at low frequencies is much larger than that of the LmPE, and the zero-shear plateau is not reached for the LDPE-1 at the lowest frequencies. At very high frequencies, the complex viscosity of the LmPE is much larger than that of the LDPE-1. All the blends show an intermediate behavior except 10/90 and 20/80 LmPE/LDPE-1 blends that depict at low frequencies viscosity values greater than that of the major component (LDPE-1). This is indicative of immiscibility of the polymer components as discussed below using the log-additivity rule, relaxation spectra and Palierne model predictions.

The log-additivity rule based on zero shear viscosity ( $\eta_0$ ) is well-known and has been discussed by many authors. Miscible blends are expected to follow the log-additivity rule even though some authors have reported notable exceptions. Recently, Kwag *et al.* [5] reported that the complex viscosity also followed the log additivity rule

at any frequencies for LLDPE/LDPE, LLDPE/HDPE and HDPE/LDPE blends. Munoz-Escalona *et al.* [23] explained the PDB by the decrease of the free volume of the blends whereas Lin [24] described the NDB by telescopic flow with an interlayer slip. To describe the PDB, NDB and PNDB, Utracki [25] proposed the following expression for the blend viscosity:

$$\log \eta = \log \eta_L + \Delta \log \eta^E \quad (5.1)$$

in which the first and second terms on the right hand side denotes the NDB and PDB, respectively, and are given by:

$$\eta_L = \frac{1}{\left[1 + \beta \sqrt{(\phi_1 \phi_2)}\right] (\phi_1 / \eta_1 + \phi_2 / \eta_2)} \quad (5.2)$$

$$\Delta \log \eta^E = \eta_{max} \left(1 - \left[ (\phi_1 - \phi_{1I})^2 / (\phi_1 \phi_{2I}^2 + \phi_2 \phi_{1I}^2) \right]\right) \quad (5.3)$$

where  $\phi_1$ ,  $\phi_2$ ,  $\eta_1$  and  $\eta_2$  are the volume fractions and the viscosities, respectively, of components 1 and 2;  $\phi_{1I}$  and  $\phi_{2I}$  are the phase inversion concentrations of components 1 and 2;  $\beta$  is the interlayer slip factor and  $\eta_{max}$  is a parameter determining the magnitude of the PDB effect.

The composition dependence on the zero-shear viscosity and the complex viscosity at different frequencies for LmPE/LDPE-1, BmPE/LDPE-1, LmPE/LDPE-2, BmPE/LDPE-2 blends are plotted in Fig. 8 for data obtained at 150°C.  $\eta_0$  was obtained by fitting the viscosity curve using the Carreau-Yasuda model [26] and verified by the calculation of the relaxation spectrum. Due to the large viscosity of LDPE-2 at 150°C

and limitations of the rheometer, the  $\eta_0$  of LmPE/LDPE-2 and BmPE/LDPE-2 blends is not presented. The lines in Fig. 8 are the best fits for the Utracki expression (Eqs. 2 and 3). From Fig. 5.8a, we observe that the LmPE/LDPE-1 blends exhibits strong PDB for all frequency data. The PDB is not affected by the frequency. However, the BmPE/LDPE-1 blends (Fig. 5.8c) show weak PDB for the zero-shear viscosity and the PDB for the LmPE/LDPE-2 (Fig. 5.8b) and BmPE/LDPE-1 blends increases with frequency. The BmPE/LDPE-2 blends (Fig. 8d) almost perfectly follow the log-additivity rule. These results suggest immiscibility of the LmPE/LDPE-1 blends, partial miscibility of the LmPE/LDPE-2 and BmPE/LDPE-1 blends and miscibility of the BmPE/LDPE-2 blends. Similar results obtained for the same blends at 175°C are not presented here, but in Fig. 5.9 we report the zero-shear viscosity for these blends obtained at 200°C as a function of composition. All blends show a PDB except BmPE/LDPE-2 blends that follow the log-additivity rule. Clearly, an increase of 50°C did not improve the miscibility of the other blends.

Weighted relaxation spectra can offer another efficient way to determine if blend components are immiscible. If so, there should be an additional relaxation mechanism associated with the deformation of dispersed droplets in a matrix as reported by Carreau *et al.* [16], Bousmina and Muller [26], Gramespacher and Meissner [27], Lacroix *et al.* [28]. The relationship between the relaxation spectrum  $H(\tau)$  and dynamic moduli  $G'$ ,  $G''$  can be expressed by [26]:

$$G'(\omega) = \int_{-\infty}^{+\infty} H(\tau) \frac{\omega^2 \tau^2}{1 + \omega^2 \tau^2} d \ln \tau \quad (5.4)$$

$$G''(\omega) = \int_{-\infty}^{+\infty} H(\tau) \frac{\omega \tau^2}{1 + \omega^2 \tau^2} d \ln \tau \quad (5.5)$$

The relaxation spectrum can be calculated by several methods. In this work, the relaxation spectrum was calculated using a modified Tikhonov regularization method developed by Honerkamp and Weese [29].

Figs. 5.10 (a) and (b) show the weighted relaxation spectra of the LmPE/LDPE-1 at 150°C and BmPE/LDPE-2 blends at 175°C, respectively. From Fig. 5.10(a), we see that the relaxation spectra of both unblended components depict a single peak that is a characteristic relaxation time. The characteristic time for the LDPE-1 is about four decades longer than that of the LmPE. The 90/10, 80/20 and 50/50 LmPE/LDPE-1 blends depict two peaks, which correspond to the average relaxation times of the LmPE and LDPE-1, respectively, suggesting that the LmPE governs the rheological behavior of the blend at high frequency whereas LDPE-1 governs the behavior of the blend at low frequency. We also observe that the 10/90 and 20/80 LmPE/LDPE-1 blends exhibit only one peak which is higher than that of LDPE-1. The behavior described by Fig. 5.10a implies immiscibility of the LmPE and LDPE-1 components and is associated with the shape relaxation and deformation of the droplets. In contrast, as seen in Fig. 5.10(b) all the spectrum curves for the BmPE/LDPE-2 blends have a single peak for all the compositions and the peak transits smoothly from that of the BmPE to that of the LDPE-2. This behavior implies miscibility of the BmPE/LDPE-2 blend components. We note that the relaxation times for both unblended components are much closer than for the LmPE and LDPE-1 as expected from their respective molecular weights (see Table 5.1). However, the small differences in the molecular weight can not explain the immiscibility of the LmPE/LDPE-1 system. The relaxation spectra for the other two blend systems were not as clear, probably because of partial miscibility and, hence, they are not shown here. Also, similar relaxation spectra were obtained for the data at 175 and 200°C and are not reported.

The storage moduli of the LmPE/LDPE-1 and BmPE/LDPE-2 blends at 175°C are plotted in Figs. 5.11 (a) and (b), respectively. From Fig. 5.11(a), we see that the storage modulus of the LmPE depicts a long terminal zone (slope of 2 at low frequencies) corresponding to the long Newtonian plateau for the complex viscosity (Fig. 5.7). The storage modulus of the LDPE-1 is much larger than that of the LmPE at low frequencies, but the trend is reversed at high frequencies. The values of the storage modulus of the 10/90 and 20/80 LmPE/LDPE-1 blends are somewhat larger than that of the LDPE-1 in the terminal zone, which is due to the deformability of the dispersed phase, as reported by other authors [16, 25] for multiphase systems. At high frequency, the storage modulus of the LDPE/LmPE blends decreases slowly with the addition of LDPE. Fig. 5.11 (b) shows that the values of the storage modulus for all the BmPE/LDPE-2 blends are intermediate of those of the BmPE and the LDPE-2 in both terminal and high frequency zones.

Palierne [1] developed a model to predict the linear viscoelastic properties of immiscible, emulsion-type blends. If the simpler case of a narrow distribution of droplet diameters [31] and constant interfacial tension,  $\alpha$ , the complex modulus of the blend is given by:

$$G_B^*(\omega) = \frac{1 + 3\phi H^*(\omega)}{1 - 2\phi H^*(\omega)} \quad (5.6)$$

with  $H^*$  is defined as:

$$H^*(\omega) = \frac{4 \left( \frac{\alpha}{R_V} \right) (2G_m^*(\omega) + 5G_d^*(\omega)) + (G_d^*(\omega) - G_m^*(\omega)) (16G_m^*(\omega) + 19G_d^*(\omega))}{40 \left( \frac{\alpha}{R_V} \right) (G_m^*(\omega) + G_d^*(\omega)) + (2G_d^*(\omega) + 3G_m^*(\omega)) (16G_m^*(\omega) + 19G_d^*(\omega))} \quad (5.7)$$

where  $\phi$  is the volume fraction of droplets with of volume-average radius  $R_V$ .  $G_m^*$  and  $G_d^*$  are the complex moduli of the matrix and droplets, respectively. The storage and loss moduli for the blends can be easily calculated from simple algebraic equations (see Marguerat *et al.* [32]). This model has been widely used and has been modified by many authors. Due to the low optical contrast between PE components, it is virtually impossible to obtain dimensions of droplets in PE blends and hence,  $R_V$ . As done by Hussein *et al.* [7] we consider  $\alpha/R_V$  as a single parameter in Eq. 7 and use the Palierne model to obtain the best fits of the experimental data for the blends.

Fig. 5.12 shows the influence of  $\alpha/R_V$  (0 and 3000) on the storage and loss moduli predicted by the Palierne model for the 10/90 LmPE/LDPE blend. From this figure, we see that the  $G''$  values predicted by Palierne model are in good agreement with the experimental data for both values of the  $\alpha/R_V$ . In other words,  $G''$  is not sensitive to the value of  $\alpha/R_V$ . However, the value of  $\alpha/R_V$  affects significantly the storage modulus,  $G'$ , at low frequencies and the best fit was obtained for  $\alpha/R_V = 3000$ . Assuming an interfacial tension of 0.1 mN/m for this highly compatible PE pair, the corresponding droplet radius would be 30 nm, which is quite close to the radius of gyration of PE macromolecules and virtually impossible to measure by usual techniques. In the following figure, we restrict the comparison of the simulation results to the  $G'$  data for the 20/80 blends that are the most sensitive to droplet deformation.

Fig. 5.13 shows the influence of  $\alpha/R_V$  on the storage modulus predicted by Palierne model for the 20/80 LmPE/LDPE-1, LmPE/LDPE-2, BmPE/LDPE-1, and BmPE/LDPE-2 blends at 175°C. From this figure, we see that the predictions by the Palierne model are in good agreement with the experimental data for all the blends. However, the fits for the low frequency data depend on the value of  $\alpha/R_V$ , which is a more sensitive parameter for the LmPE/LDPE blends (Figs. 5.13a and b) than for the other blends. As observed in Fig. 5.12 for the (10/90) blend, the best fit for the (20/80) LmPE/LDPE-1blend is obtained for a value close to 3000. The values of  $\alpha/R_V$  which can

give best simulation for Palierne model are summarized in Table 5.2. We see that the  $\alpha/R_V$  value decreases to 500 and 0 for the BmPE/LDPE-1 and BmPE/LDPE-2 blends, respectively. A value of the interfacial tension,  $\alpha$ , equal to 0 is indicative of total miscibility of the BmPE/LDPE-2 blends as shown previously from DSC. It is interesting to note that the Palierne model developed for immiscible blends yields a good fit of the linear viscoelastic properties of these miscible polymer blends. Obviously, for  $\alpha = 0$ , the model predicts no influence of a dispersed phase on the dynamic moduli as it can be deduced from Eqs. 5.6 and 5.7.

#### 5.4. Conclusions

The thermal and rheological properties of four polyethylenes with different molecular structure and their blends have been studied. Also, the immiscibility of all the blend systems has been determined both in the crystalline and melt states using different techniques. DSC and rheological results suggest that the increase of the length of short chains in mPEs and comparable MW can promote miscibility of mPE/LDPE blends. In summary:

1. From DSC, the LmPE/LDPE-1 and LmPE/LDPE-2 blends are immiscible whereas BmPE/LDPE-1 and BmPE/LDPE-2 blends are miscible in the crystalline state.
2. Based on the log-additivity rule for the complex viscosity and the weighted relaxation spectra, LmPE/LDPE-1 blends are believed to be immiscible whereas BmPE/LDPE-2 blends are miscible and the miscibility is not improved by increasing temperature. The situation is not as clear for the other two blends, possibly due to partial miscibility.
3. The sensitivity of the Palierne model predictions was tested considering  $\alpha/R_V$  (ratio of interfacial tension and average radius of dispersed phase) as one parameter. The

Palierne model predictions are in good agreement with experimental data of all the blends investigated. However, the low frequency  $G'$  data for LmPE/LDPE blends are well described for  $\alpha/R_V=3000$ , indicative of the presence of a dispersed phase. For the BmPE/LDPE blends, the best fits were obtained for  $\alpha/R_V \approx 0$ , suggesting miscibility.

### Acknowledgments

This work has been funded through a strategic grant from the National Science and Engineering Research Council of Canada, for which we are grateful. We also wish to thank Dr. Shuqin, Bo (Changchun Institute of Applied Chemistry, Chinese Academy of Sciences) kindly offer GPC data.



## 5.5. References

1. J. F. Palierne, *Rheol. Acta* **29**, 204(1990).
2. L. A. Utracki and B. Schlund, *Polym. Eng. Sci.* **27**, 1512 (1987).
3. P. Micic, S. N. Bhattacharya and G. Field, *Int. Polym. Proc.* **12**, 110 (1997).
4. M. Yamaguchi and S. ABE, *J. Appl. Polym. Sci.* **74**, 3153 (1999).
5. H. Kwag, D. Rana, K. R. J. Cho, T. Woo, B. Lee, S. Choe, *Polym. Eng. Sci.* **40**, 1672 (2000).
6. F. Chen, R. Shanks, G. Amarasinghe, *J. Appl. Polym. Sci.* **81**, 2227 (2001).
7. I. A. Hussein and M. C. Williams, *Polym. Eng. Sci.* **41**, 696 (2001).
8. C. Liu, J. Wang, J. He, *Polym.* **43**, 3811 (2002).
9. R. G. Alamo, W. W. Graessley, R. Krishnamoorti, D. J. Lohse, J. D. Londono, L. Mandelkern, F. C. Stehling, G. D. Wignall, *Macromolecules* **30**, 561 (1997).
10. M. Okamoto, A. Kojima, T. Kotaka, *Macromolecules* **31**, 5158 (1998).
11. N. K. Datta and A. W. Birley *Plastic Rubber Process Application* **27**, 1512 (1983).
12. H. Lee, K. Cho, T. K. Ahn, S. Choe, I. J. Kim, I. Park, B. H. Lee, *J. Polym. Sci.: Polym. Phy.* **35**, 1633 (1997).
13. H. H. Yang, C. D. Han, J. K. Kim, *Polym.* **35**, 1503 (1994).
14. L. A. Utracki, *Polymer Alloys and Blends: Two-Phase Polymer Systems*, Hanser Publishers, (1991)
15. C. D. Han and J. Kim, *J. Polym. Sci.: Polym. Phy.* **35**, 1633 (1997).
16. P. J. Carreau, M. Bousmina, and A. Ajji, (invited), *Rheological Properties of Blends: Facts and Challenges*, in *Progress in Pacific Polymer Science 3*, K. P. G. Ghiggino, Ed., pp. 25-39, Springer-Verlag, (1994).
17. T. Hameed and I. A. Hussein, *Polym.* **43**, 6911 (2002).
18. B. Wunderlich, *Macromolecular physics*, Vol. 2, Academic Press, New York (1976).
19. H. Munstedt, S. Kurzbeck, L. Egersdorfer, *Rheol. Acta* **37**, 21(1998).

20. F. M. Mirabella, S. P. Westphal, P. L. Fernando, E. A. Ford, J. G. Williams, *J Polym. Sci. Part B: Polym. Phys. Ed.* **26**, 1995 (1988).
21. N.K. Datta and A.W. Birtay, *Plast. Rubber Process Appl.* **2**, 237 (1982).
22. D. Rana, C. H. Lee, K. Cho, B. H. Lee, and S. Choe, *J. Appl. Polym. Sci.* **69**, 2441 (1998)
23. A. Munoz-Escalona, P. Lafuente, J. F. Vega, M. E. Muoz, A. Santamaria, *Polym.* **38**, 589 (1997).
24. C.C. Lin, *Polym. J.* **11**, 185 (1979).
25. L. A. Utracki, *J. Rheol.* **35**, 1615, (1991).
26. P. J. Carreau, D. De Kee, and R. P. Chhabra, *Rheology of Polymeric Systems: Principle and Application*, Hanser Publishers (1997).
27. H. Gramespacher and J. Meissner, *J. Rheol.* **36**, 1127 (1992).
28. C. Lacroix, M. Aressy, P. J. Carreau, *Rheol. Acta* **36**, 416 (1997).
29. J. Honerkamp and J. Weese *Rheol. Acta* **32**, 65 (1993).
30. C. Lacroix, Bousmina, P. J. Carreau, B. D. Favis, *Polym.* **37**, 2939 (1996).
31. M. Bousmina, P. Bataille, S. Sapiéha and H. P. Schreiber, *J. Rheol.* **39**, 499 (1995).
32. F. Marguerat, P. J. Carreau and A. Michel *Polym. Eng. Sci.* **42**, 1941 (2002)

Table 5.1. Polymers used in this study and their main characteristics.

Sample	LmPE	BmPE	LDPE-1	LDPE-2
Producer	Exxon Mobile	Dow Chemical	Dow Chemical	Dow Chemical
Density [g/cm <sup>3</sup> ]	0.918	0.902	0.923	0.923
<i>MI</i> [g/10min]	1	1	1.9	0.22
$M_w$	111,920	116,400	80,900	119,400
$M_w/M_n$	2.36	2.11	5.2	7.6
Comonomer	C <sub>6</sub>	C <sub>8</sub>	N/A	N/A
Long Chain Branches [1/10 <sup>4</sup> C]	N/A	0.1773	-	-

Table 5.2. Values of  $\alpha/R_v$  for the best fits of the Palierne model predictions.

Composition	LmPE/LDPE-1	LmPE/LDPE-2	BmPE/LDPE-1	BmPE/LDPE-2
10/90	$\approx 3000$	$\approx 1000$	$\approx 500$	$\approx 0$
20/80	$> 3000$	$\approx 3000$	$\approx 500$	$\approx 0$

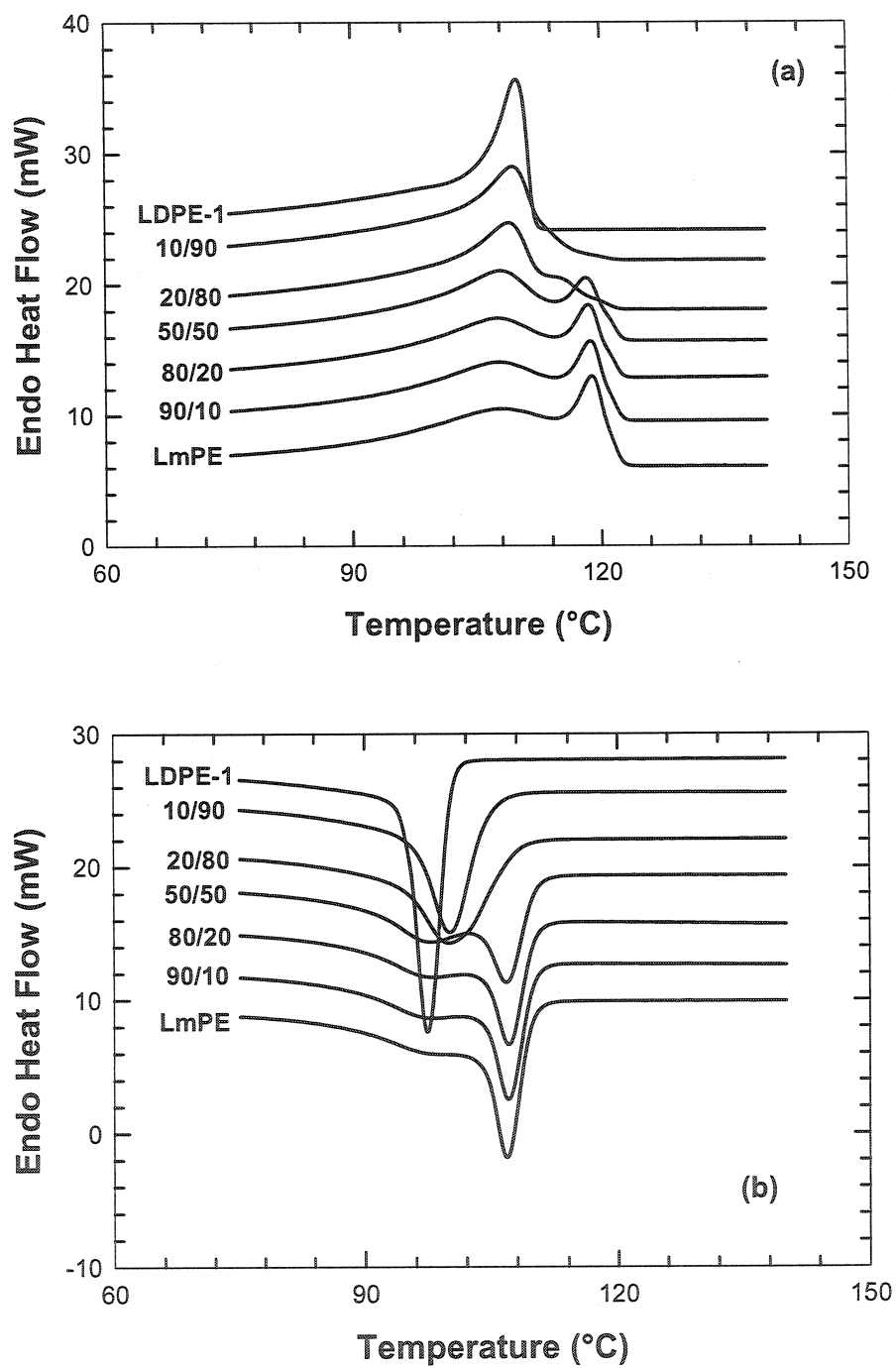


Figure 5. 1. DSC thermograms for the LmPE, LDPE-1 and their blends: (a) Heating, (b) Cooling. Both heating and cooling rates were 5°C/min.

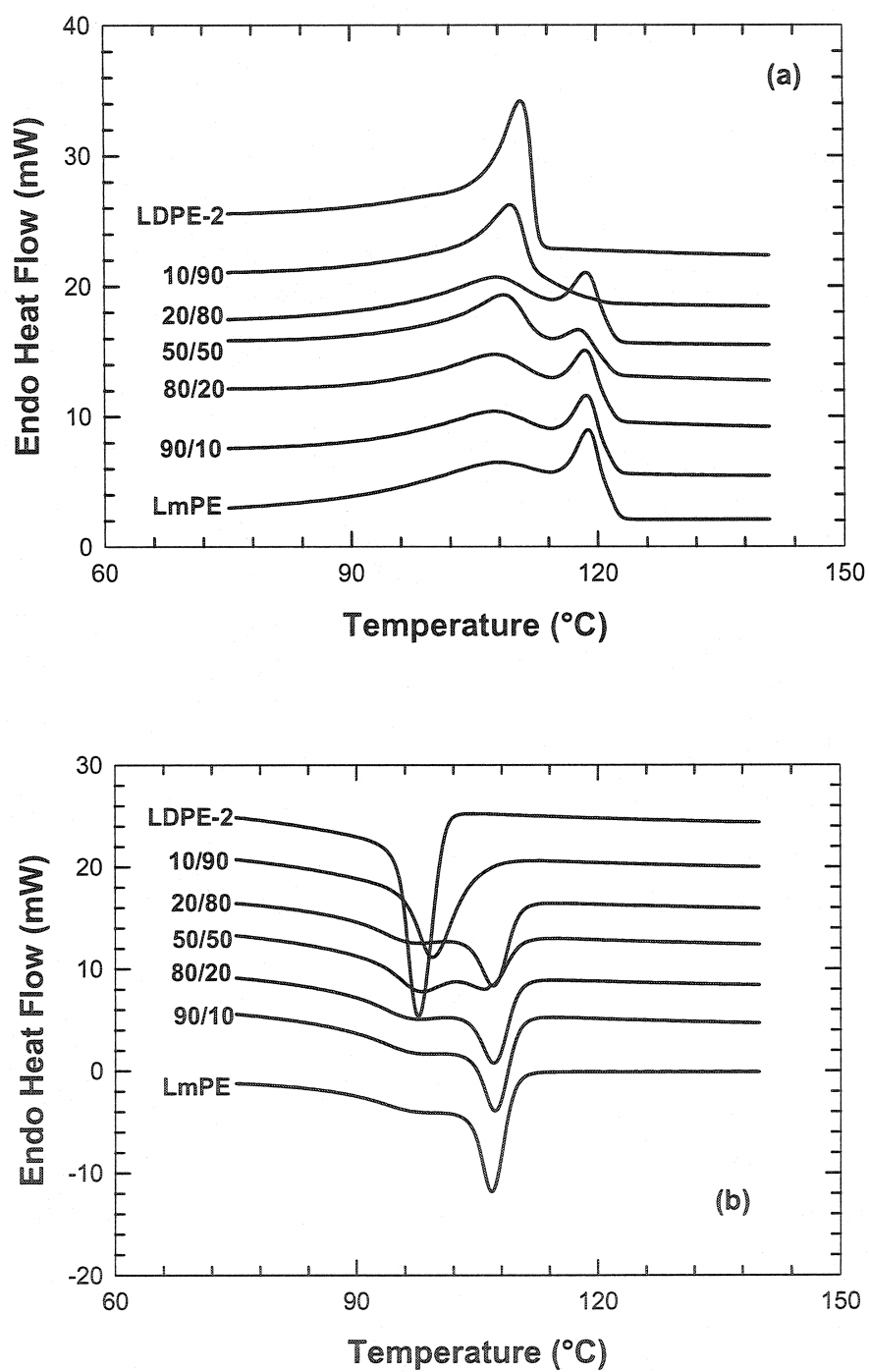


Figure 5. 2. DSC thermograms for the LmPE, LDPE-2 and their blends: (a) Heating, (b) Cooling. Both heating and cooling rates were 5°C/min.

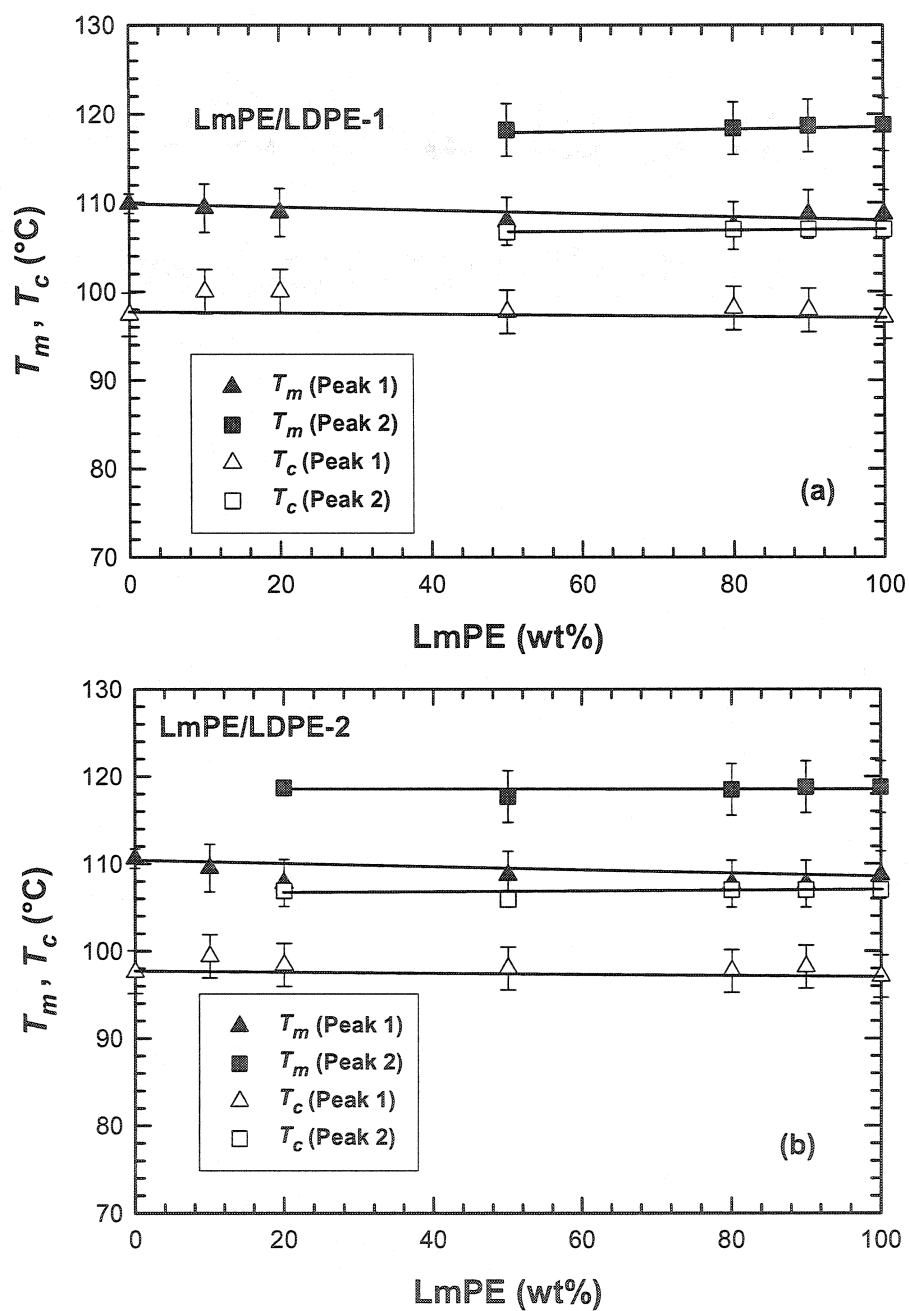


Figure 5.3. Composition dependence of the melting temperature,  $T_m$ , and the crystallization temperature,  $T_c$ , for (a) LmPE/LDPE-1, (b) LmPE/LDPE-2 blends.

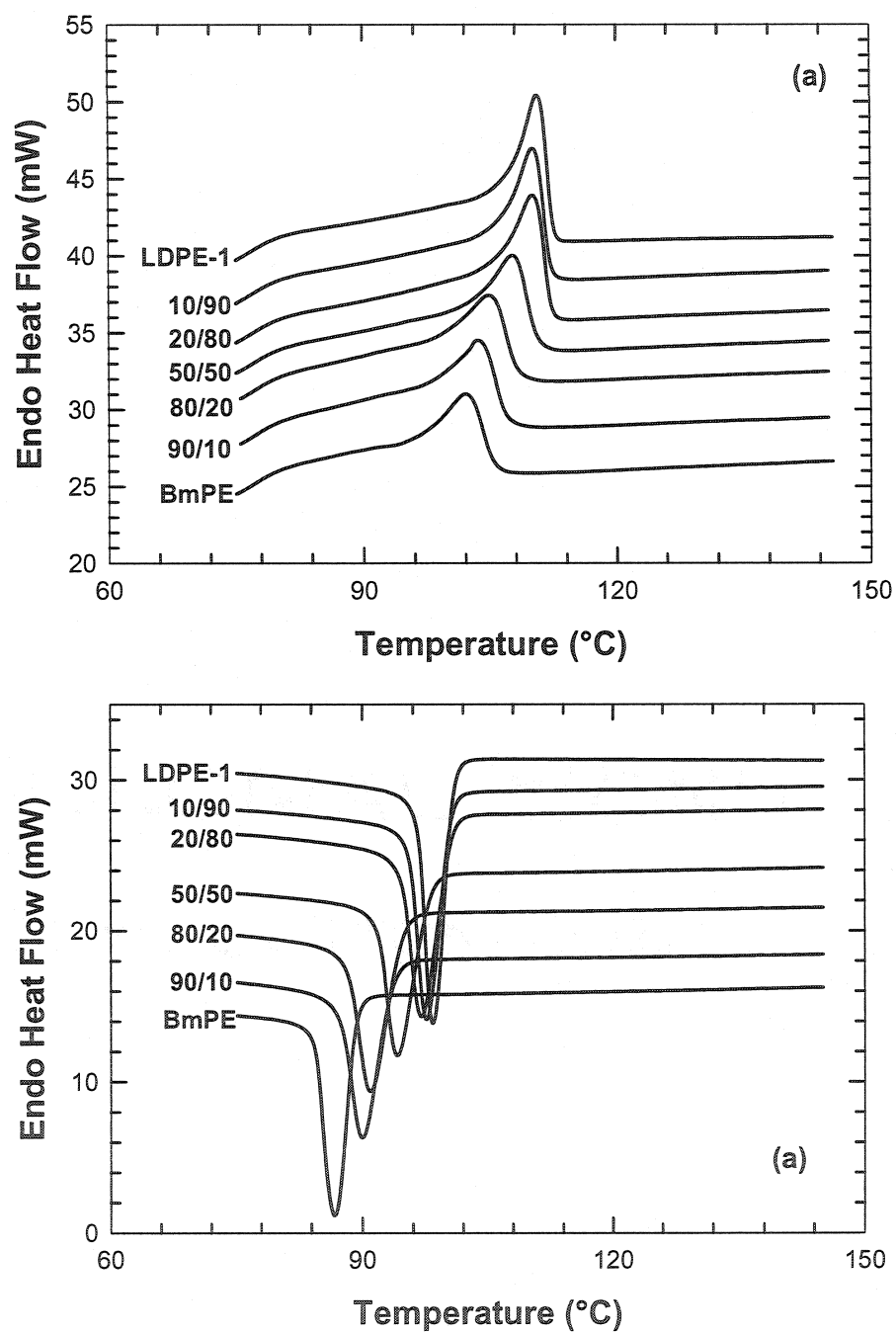


Figure 5. 4. DSC thermograms for the BmPE, LDPE-1 and their blends: (a) Heating, (b) Cooling. Both heating and cooling rates were 5°C/min.



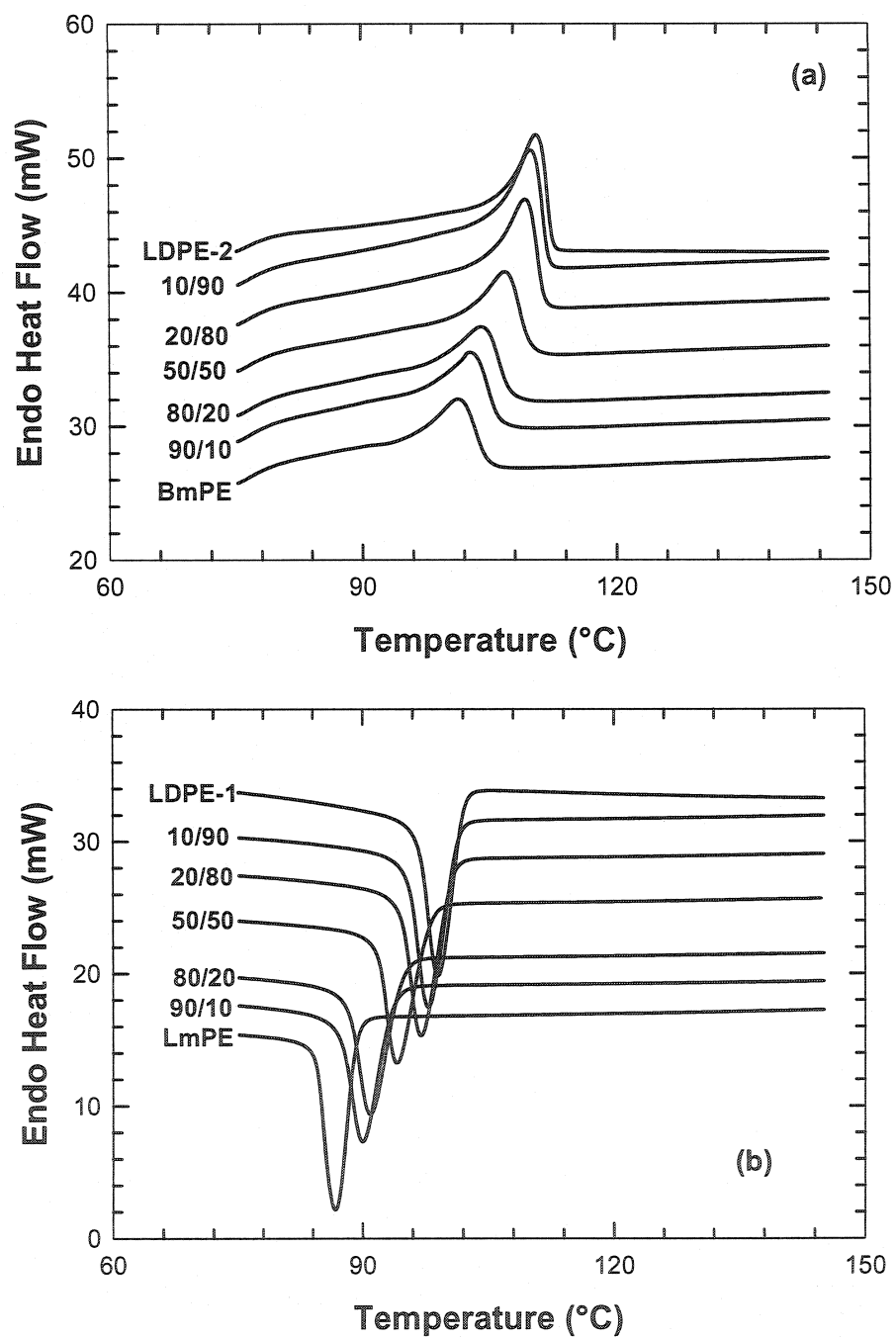


Figure 5. 5. DSC thermograms for the BmPE, LDPE-2 and their blends: (a) Heating, (b) Cooling. Both heating and cooling rates were 5°C/min.

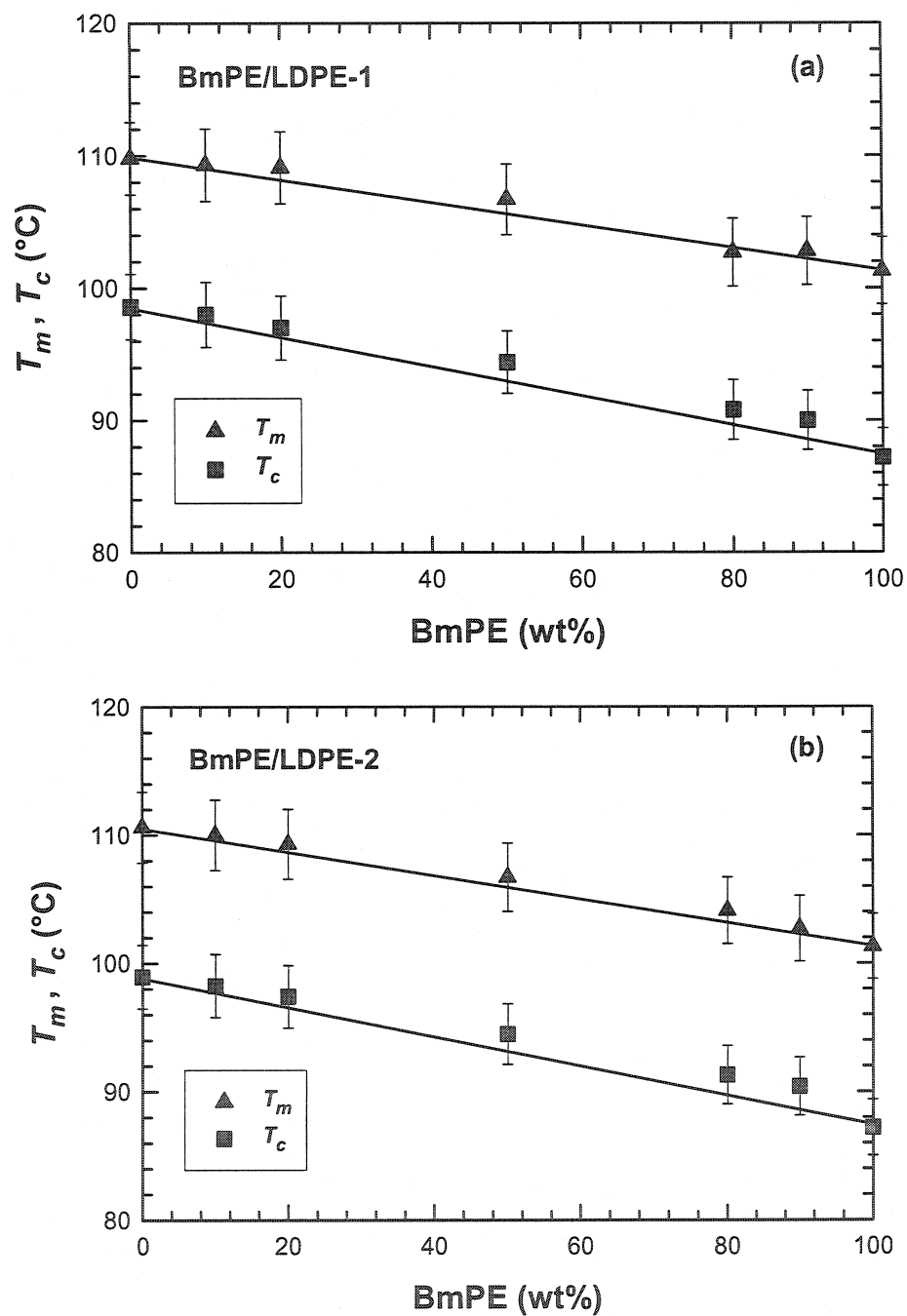


Figure 5.6. Composition dependence of the melting temperature,  $T_m$ , and the crystallization temperature,  $T_c$ , for (a) BmPE/LDPE-1 blends and (b) BmPE/LDPE-2 blends.

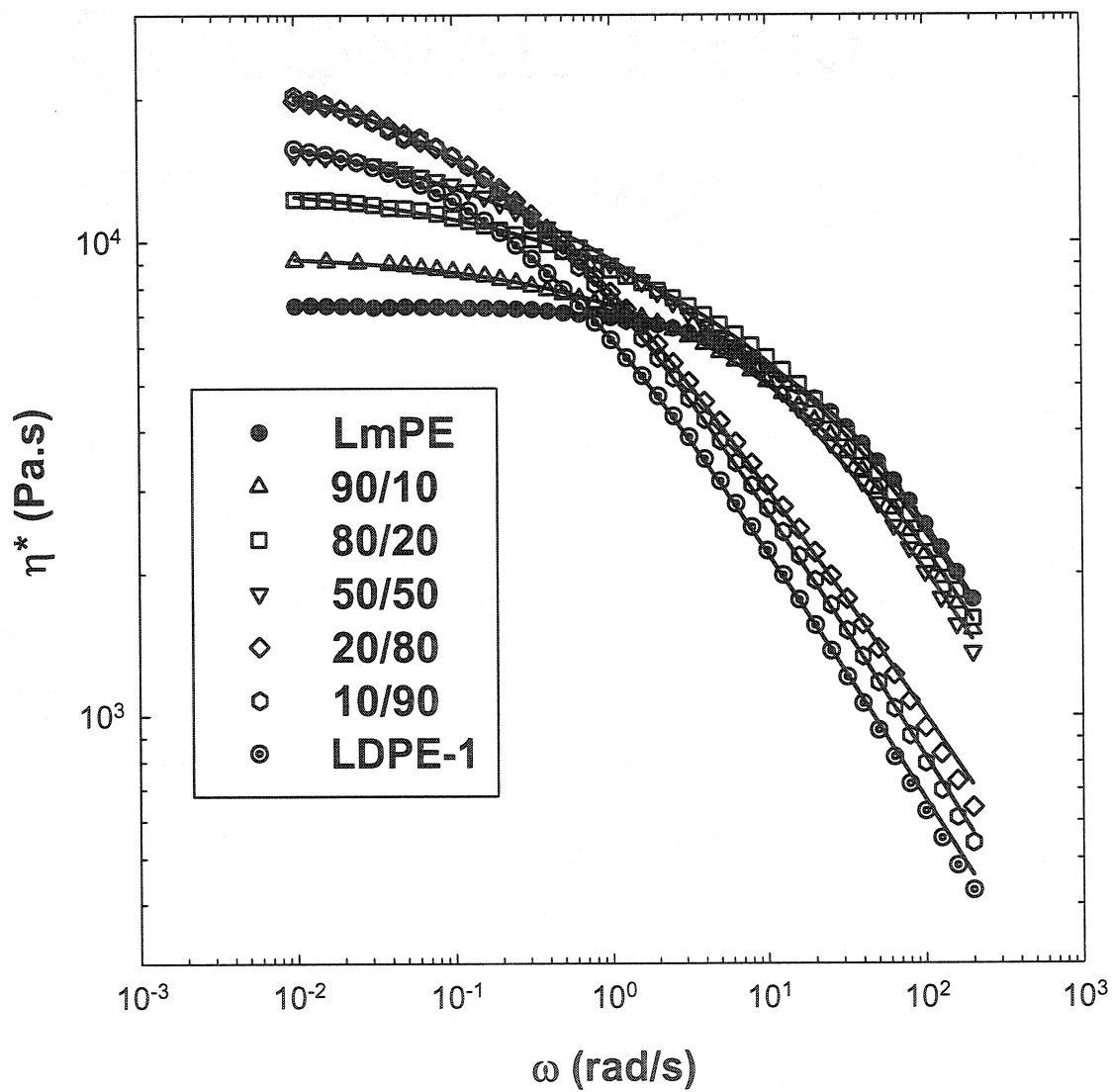


Figure 5.7. Complex viscosity versus frequency for LmPE/LDPE-1 blends at 175°C (solid line is curve fitting using Carreau-Yasuda model).

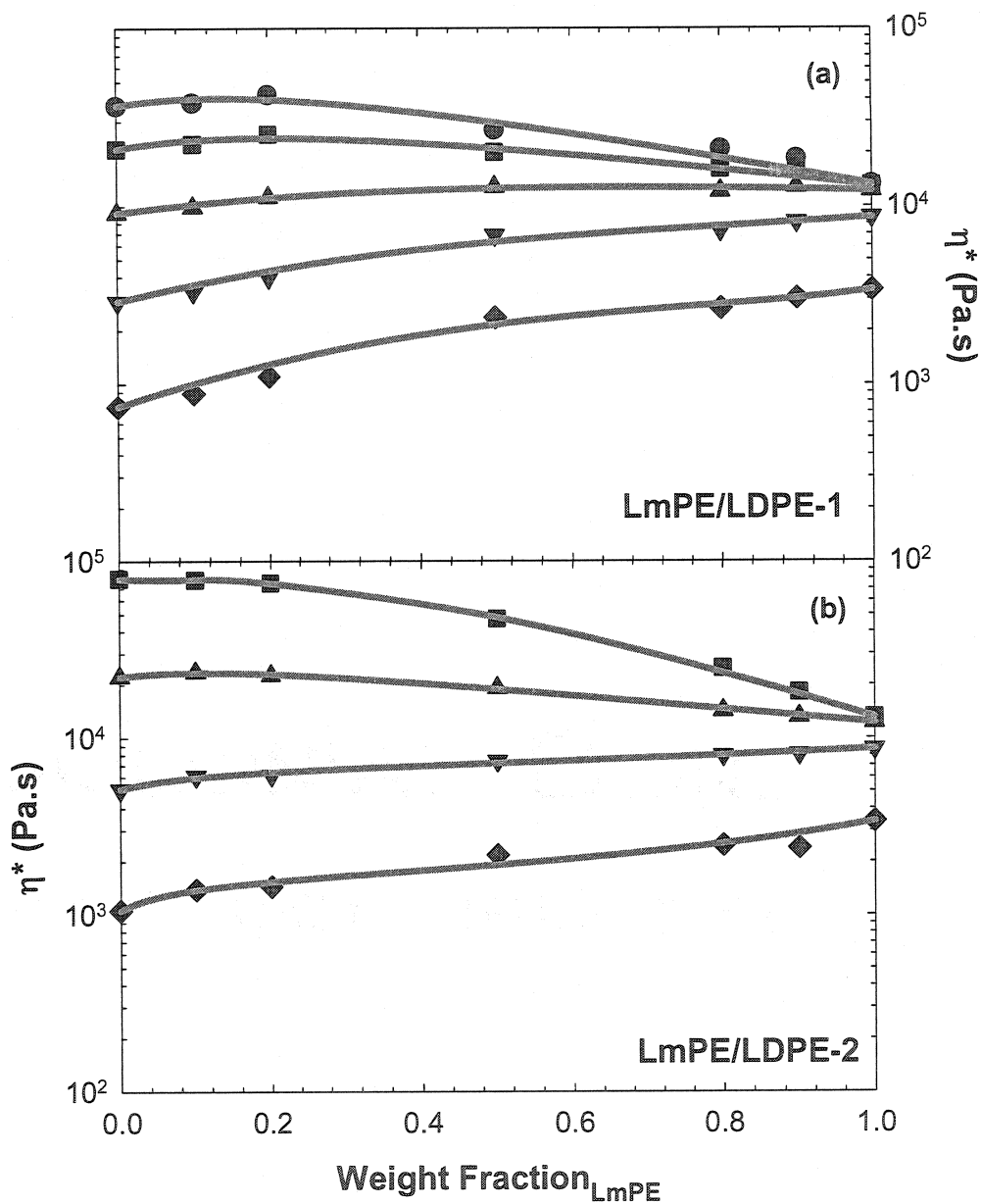
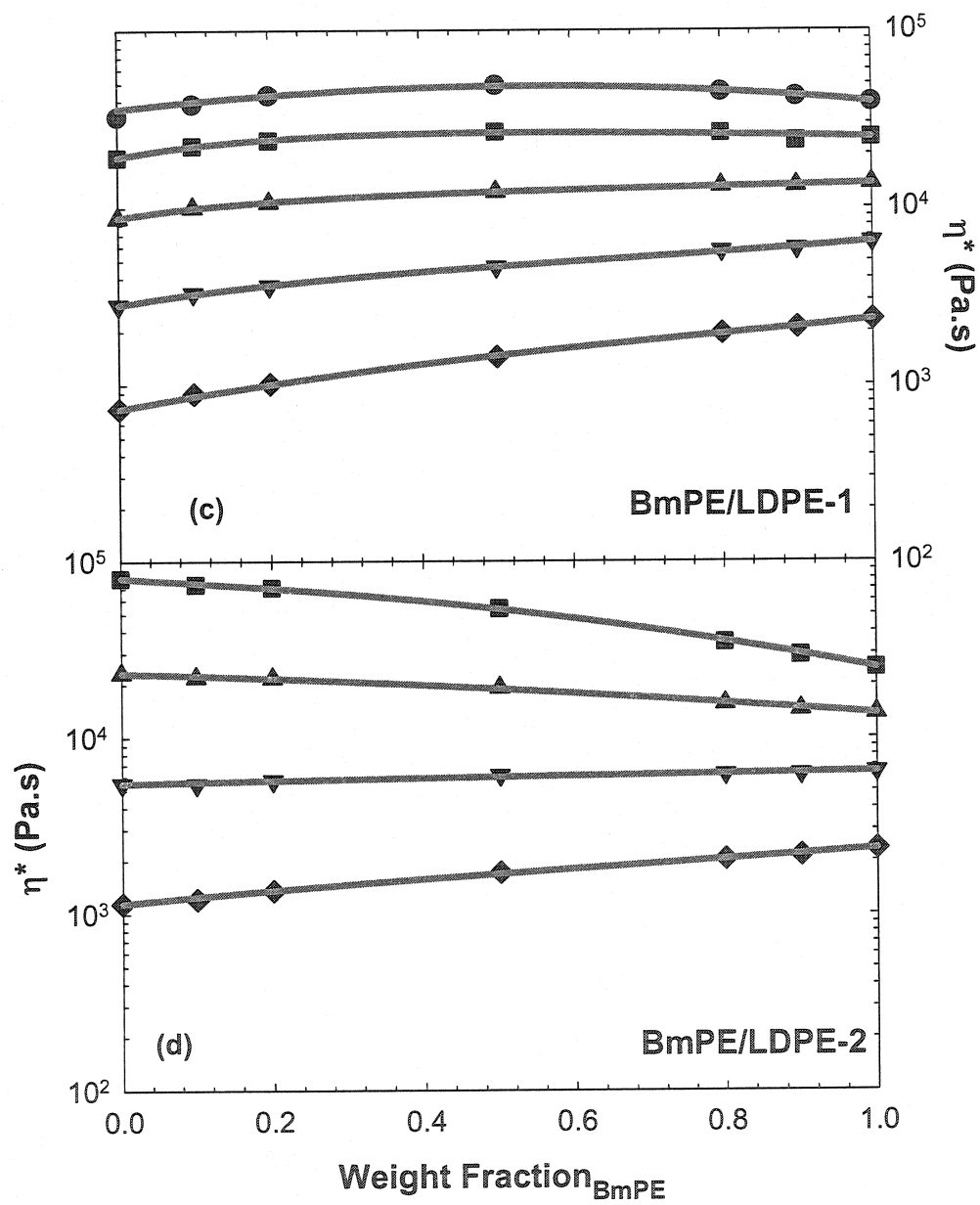


Figure 5. 8. Composition dependence on complex viscosity at different frequencies for: (a) LmPE/LDPE-1, (b) LmPE/LDPE-2, (c) BmPE/LDPE-1 and (d) BmPE/LDPE-2 blends at 150°C. (● Zero shear viscosity, ■  $\omega = 0.1$  rad/s, ▲  $\omega = 1.0$  rad/s, ▼  $\omega = 10.0$  rad/s, ◆  $\omega = 100.0$  rad/s).



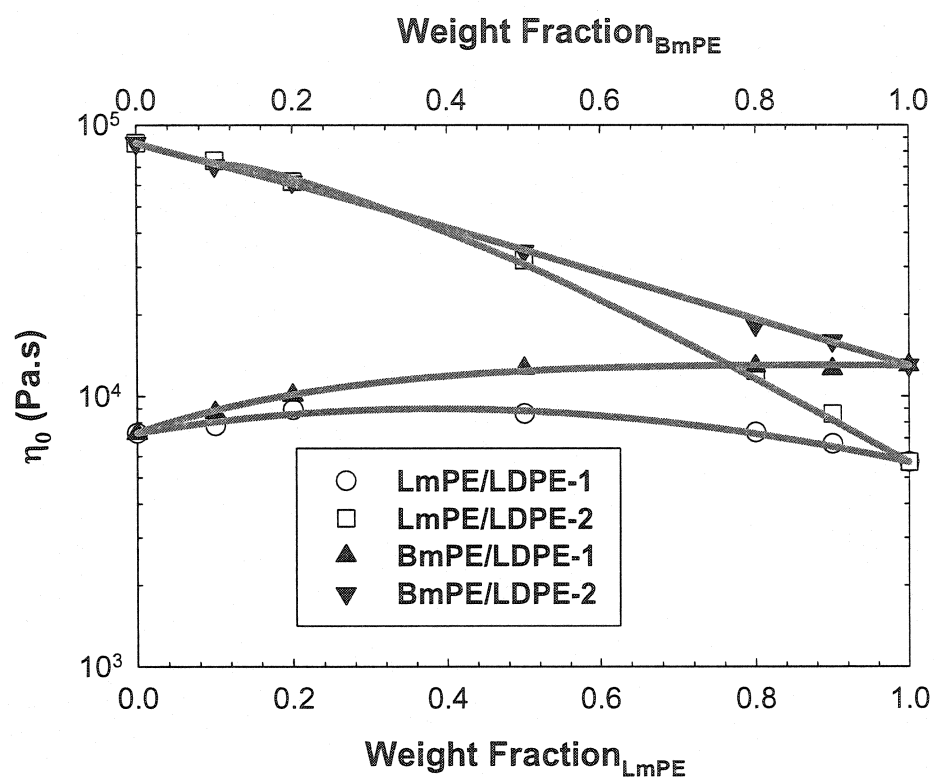


Figure 5.9. Zero-shear viscosity versus blend composition for the LmPE/LDPE-1, LmPE/LDPE-2, BmPE/LDPE-1, BmPE/LDPE-2 blends at 200°C.

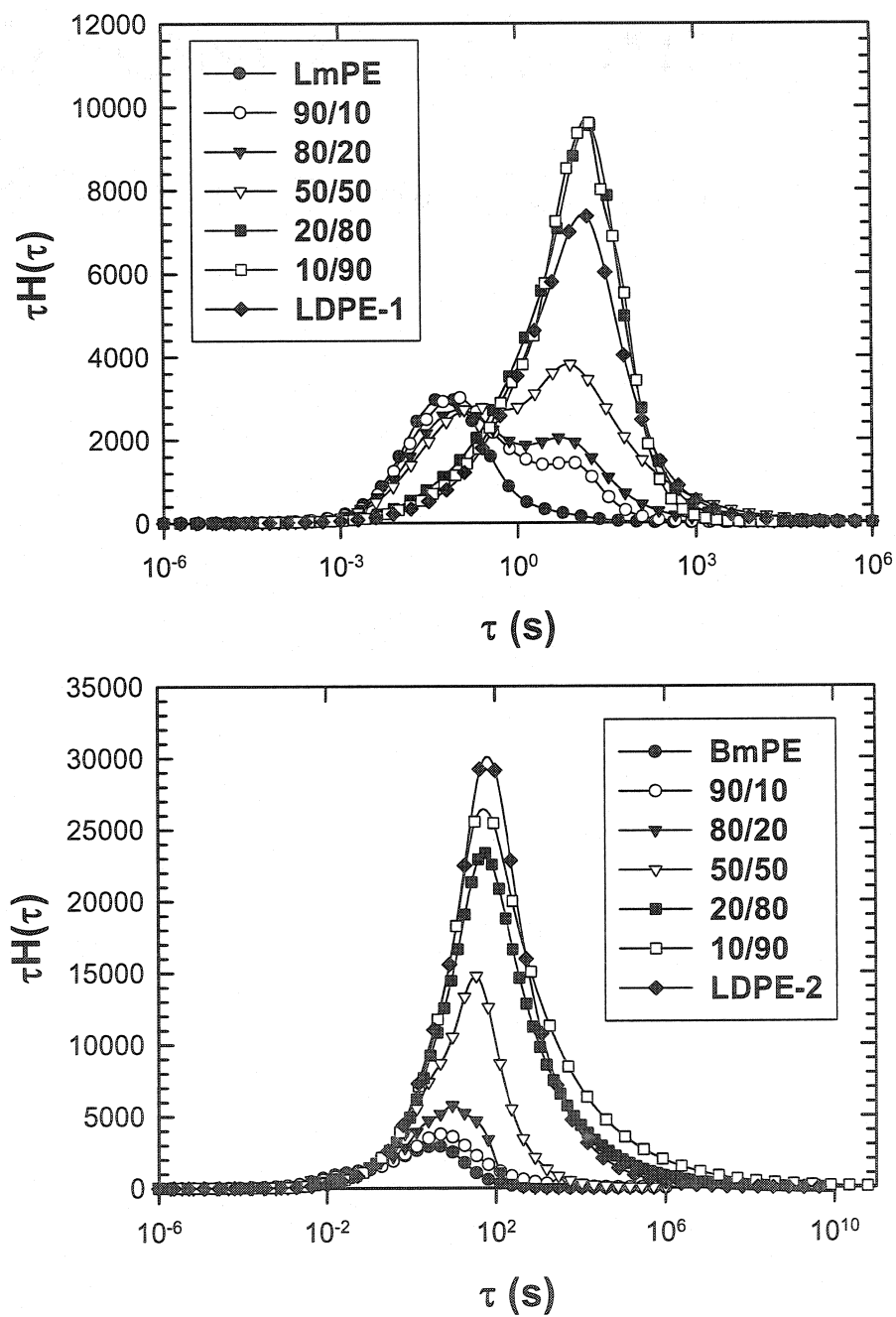


Figure 5. 10. Weighted relaxation spectra of (a) LmPE/LDPE-1 blends at 150°C (b) BmPE/LDPE-1 blends at 175°C.

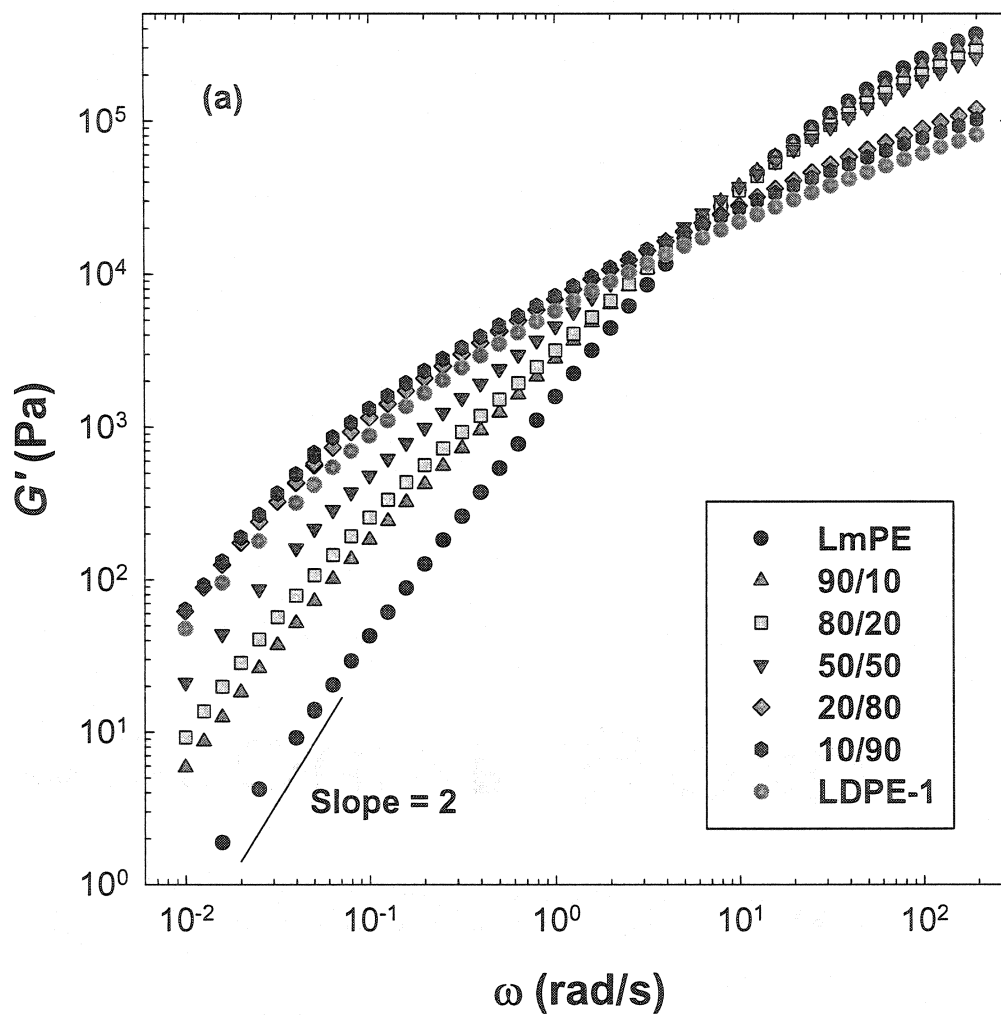
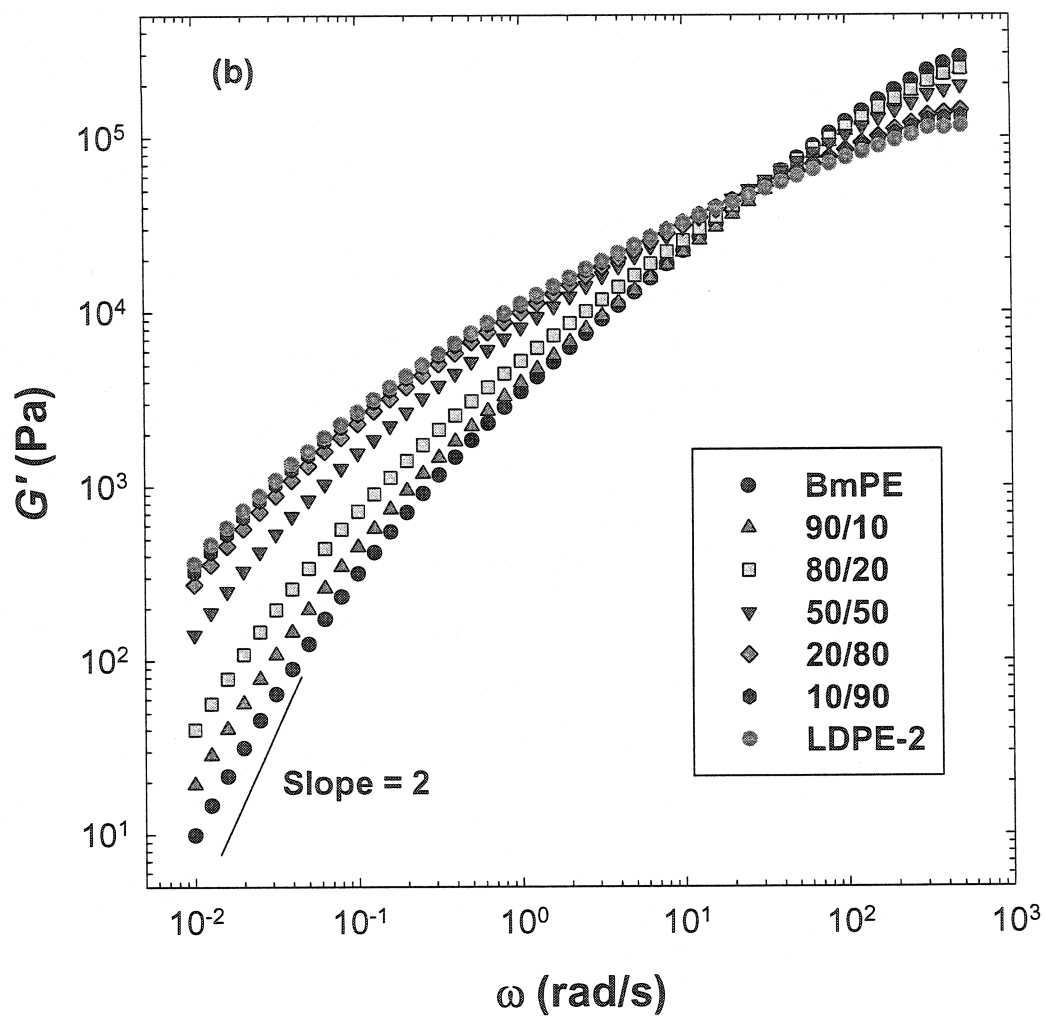


Figure 5. 11. Storage modulus  $G'$  versus frequency of (a) LmPE/LDPE-1, (b) BmPE/LDPE-2 blends at 175°C.





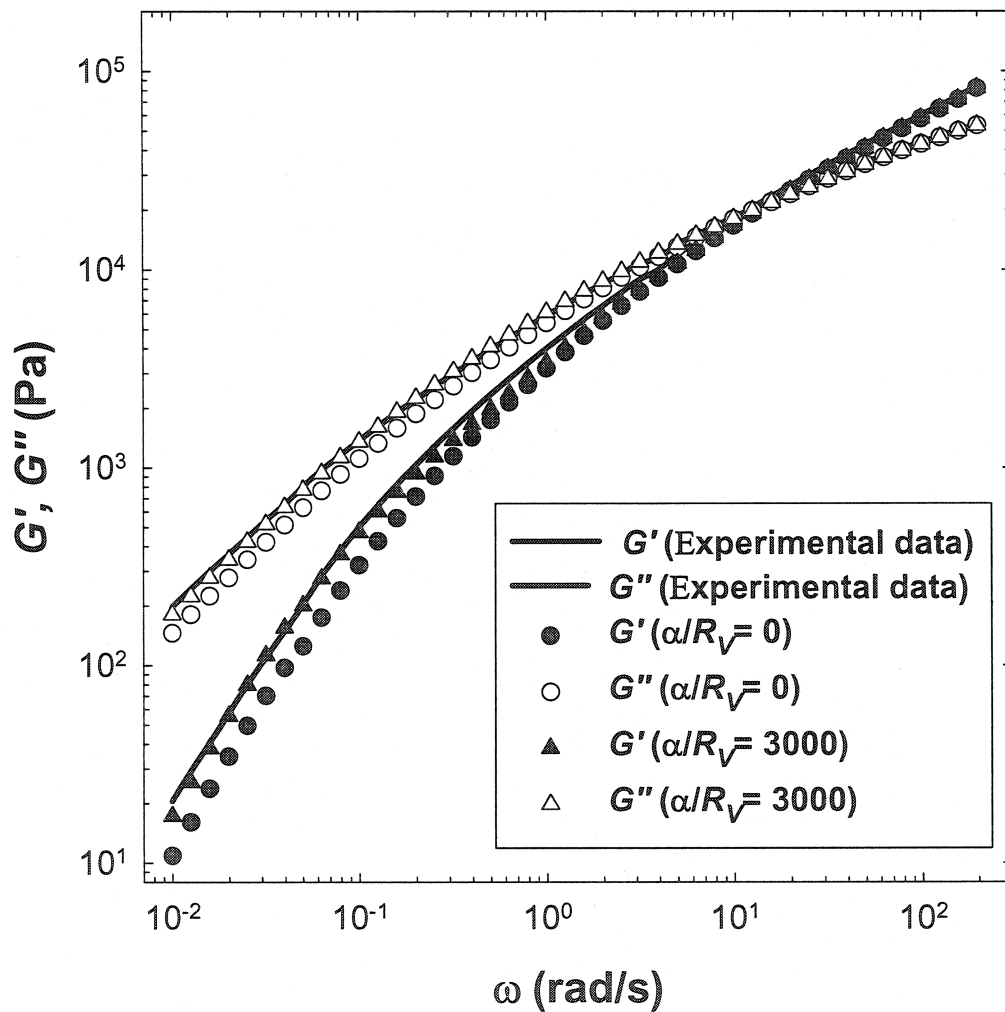


Figure 5. 12. Sensitivity of Palierne model predictions of  $G'$  for the (10/90)LmPE/LDPE-1 blend to different values of  $\alpha/R_V$  at 175°C.

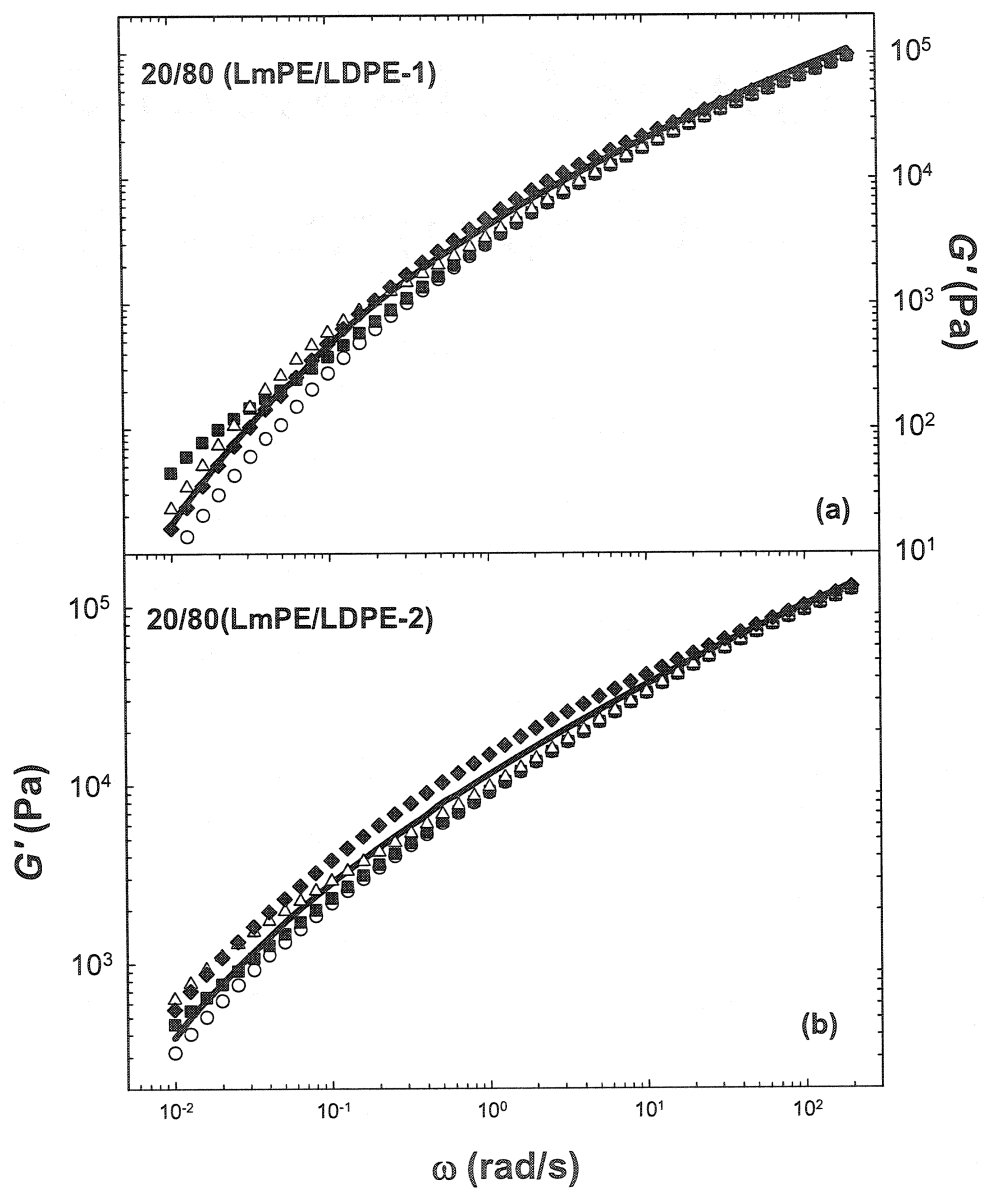
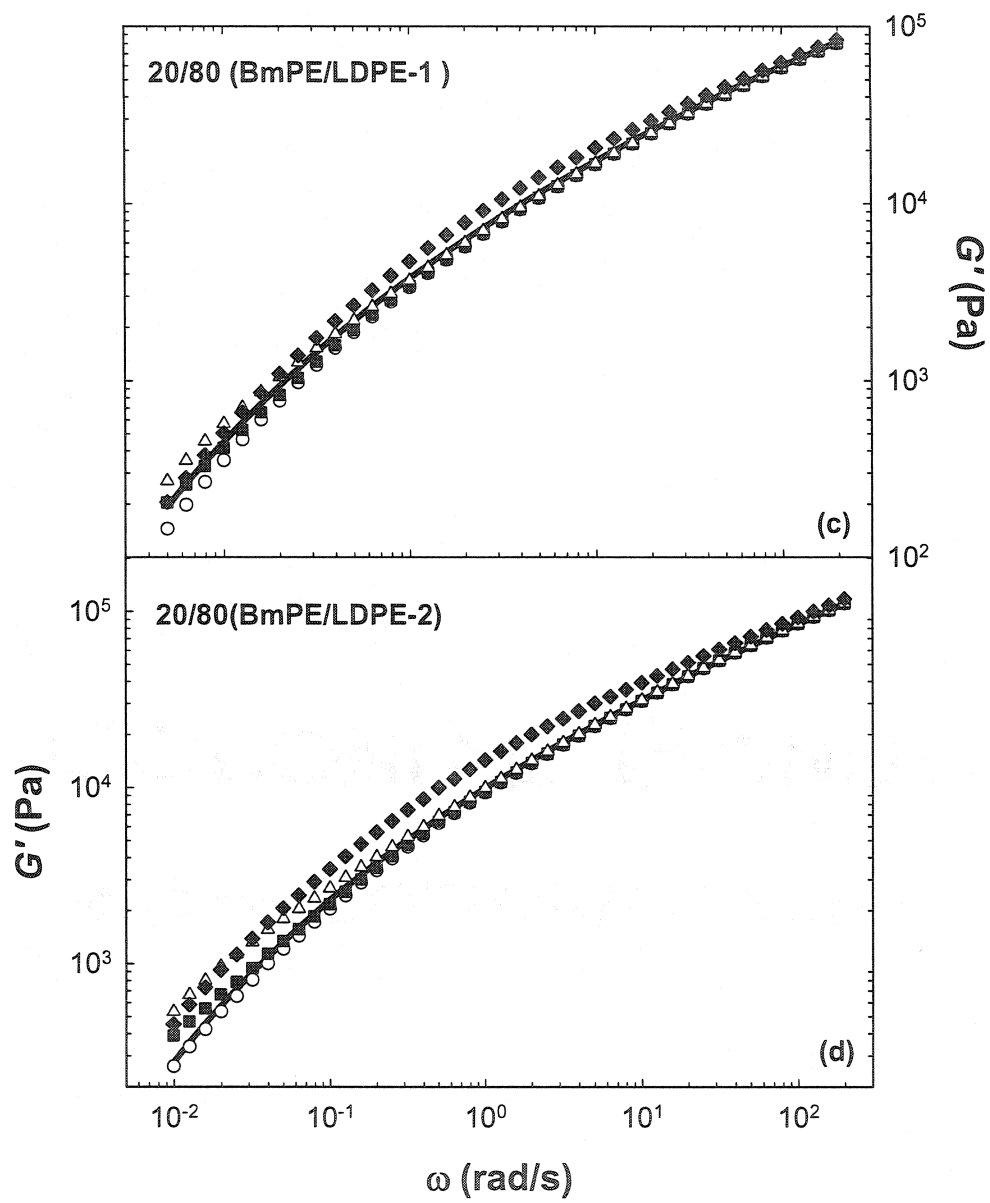


Figure 5. 13. Sensitivity of Palierne model predictions of  $G'$  for the 20/80 blends to different values of  $\alpha/R_V$  at 175°C: (a) LmPE/LDPE-1, (b) LmPE/LDPE-2, (c) BmPE/LDPE-1 and (d) BmPE/LDPE-2 blends.

(  $\circ$   $\alpha/R_V = 0$   $\blacksquare$   $\alpha/R_V = 500$   $\triangle$   $\alpha/R_V = 3000$   $\blacklozenge$   $\alpha/R_V = 100000$  — Experimental data)



## CHAPTER 6. PROPERTIES OF mPE/LDPE BLENDS IN FILM BLOWING<sup>§</sup>

Yunli Fang, Pierre J. Carreau, Pierre G. Lafleur and Salah Ymmel

Centre de Recherche Appliquée Sur les Polymères (CRASP),

Dept. of Chemical Engineering, Ecole Polytechnique

Montreal, QC, H3C 3A7, Canada

### Abstract

In this paper, the inline birefringence of two blend systems, LmPE/LDPE-1 and BmPE/LDPE-2, has been evaluated in film blowing. Experimental data show that before the crystallization starts the birefringence of the BmPE/LDPE-2 blends is a linear function of blend composition, suggesting miscibility of the BmPE/LDPE-2 blends. However, the birefringence of the LmPE/LDPE-1 blends shows positive deviations with respect to a linear function of blend composition. This is caused by the existence of form birefringence, suggesting immiscibility of the LmPE/LDPE-1 blends. The non-uniform, non-isothermal biaxial elongational viscosity (NNBEV) at the reference temperature of 175°C for the LDPE-1 was evaluated for different operating conditions. The results show that NNBEV is approximately a unique function of the deformation rate, confirming the validity of the assumptions and technique used for the NNBEV calculation. The NNBEV and the non-uniform non-isothermal biaxial Trouton ratio (NNBT) of the BmPE/LDPE-2 blends was also evaluated using the same technique. The NNBEV of all BmPE/LDPE-2 blends shows a strain-thinning behavior within the deformation rates investigated. Furthermore, the NNBT results show that the LDPE-2 deviates largely from the Newtonian fluid behavior whereas the BmPE is quite close to the Newtonian behavior. Nevertheless, the NNBT of the BmPE/LDPE-2 blends is almost a linear function of blend composition.

**Keywords:** polyethylene (PE), blends, birefringence, elongational viscosity, stress optical rule (SOR), miscibility/immiscibility

---

<sup>§</sup> Submitted to *Polymer Engineering & Science* (2004)

## 6.1. Introduction

Film blowing is the main process for polyethylene. During the past decades, numerous efforts have been devoted to the modeling. However, there is no model that can successfully predict the film blowing process so far. First of all, film blowing is a very complex process with simultaneous effects of heat transfer, melt rheology, aerodynamics and free surface kinematics. Secondly, one needs complete and reliable data to assess the different models; these are rather sparse in the open literature.

From a rheological point of view, the film blowing process can be divided into various stages. From the hopper to the annular die, the polymer flows under a pressure gradient; upon leaving the die, the molten polymer is suddenly free of the stress imposed by the die wall and it is subjected to uniaxial elongational flow; with increasing axial distance, the polymer melt is non-uniformly biaxially stretched due to the drag force of the nip roll and air pressure inside the bubble; as the axial distance further increases, the biaxially stretched film starts to crystallize. Furthermore, due to the cooling effects from the cooling air and heat exchange with the environment, this process is highly non-isothermal.

Film blowing is a non-uniform, biaxial elongational, non-isothermal flow. Hence, the determination of the elongational (or extensional) viscosity is essential to evaluate the relationship between structure, processability and properties. Uniaxial elongational flow has been studied by many researchers [1-2] and different types of elongational rheometers have been built over the past decades. Among the different rheometers, Meissner's elongational rheometer is one of the most reliable equipment to measure the uniaxial elongational viscosity. However, the elongational viscosity can only be measured for low strain rates due to limitations of the apparatus. There have been many attempts [3-6] to obtain the uniaxial elongational viscosity by indirect methods. As far as we are aware, only few authors have attempted to measure the non-uniform, non-

isothermal biaxial elongational viscosity (NNBEV) in the film blowing process. Han and Park [7] were the first to try to determine the elongational viscosity in film blowing. They suggested that the non-uniform biaxial elongational viscosity,  $\eta_{be}$ , may be represented as:

$$\eta_{be} = \frac{\sigma_{11}}{\dot{\gamma}_{11} - \dot{\gamma}_{22}} \quad (6.1)$$

or

$$\eta_{be} = \frac{\sigma_{33}}{\dot{\gamma}_{33} - \dot{\gamma}_{22}} \quad (6.2)$$

where  $\dot{\gamma}_{11}, \dot{\gamma}_{22}, \dot{\gamma}_{33}$  are strain rates in the machine, normal and transverse directions, respectively.  $\sigma_{11}$  and  $\sigma_{33}$  are the normal stresses in the machine and transverse directions, respectively.

The strain rates in film blowing can be defined as:

$$\dot{\gamma}_{11} = 2 \frac{dV_z}{dz} + 2V_z \left( \frac{dr}{dz} \right) \left( \frac{d\theta}{dz} \right) \quad (6.3)$$

and

$$\dot{\gamma}_{33} = 2 \left( \frac{V_z}{r} \right) \frac{dr}{dz} \quad (6.4)$$

Also from the continuity equation for incompressible material:

$$\dot{\gamma}_{22} = -(\dot{\gamma}_{11} + \dot{\gamma}_{33}) \quad (6.5)$$

To avoid the effect of heat transfer, Han and Park [7] used a special isothermal chamber with a glass window. However, their results are questionable since they could not avoid totally cooling effects and their determination of the stresses based on drawing force measurements was not accurate. Han and Park [7] concluded that the results calculated from Eqs. (6.1) and (6.2) were acceptable, even though they were not identical. Ghaneh-Fard *et al.* [8] have shown that the disagreement between Eqs. (6.1) and (6.2) became worse for LDPE.

Kanai and White [9] used only Eq. (6.1) to examine the apparent elongational viscosity in film blowing. Agassant *et al.* [10] have suggested that  $\eta_{be}$  can be obtained by adding the two components of the stress tensor:

$$\eta_{be} = \frac{\sigma_{11} + \sigma_{33}}{\dot{\gamma}_{11} + \dot{\gamma}_{33}} \quad (6.6)$$

This suggestion has been adopted by Ghaneh-Fard *et al.* [8] to calculate the non-uniform biaxial elongational viscosity. Moreover, Ghaneh-Fard *et al.* [11] improved the technique, using birefringence measurements, instead of the classical force balance, to determine the stresses. However, they reported the elongational viscosity as a function of the axial distance, without taking into accounting of cooling effects. More recently, Fang *et al.* [12] suggested the following equation for the NNBEV calculation:

$$\eta_{fb} = \frac{\sigma_{11} - \sigma_{22}}{\bar{\dot{\gamma}}} = \frac{(2\sigma_{11} + \sigma_{33})}{\bar{\dot{\gamma}}} \quad (6.7)$$

where  $\bar{\dot{\gamma}}$  is the effective rate of deformation, defined with respect to the second invariant of the rate-of-deformation tensor,  $\mathbf{\dot{\gamma}}$ , as:



$$\bar{\dot{\gamma}} = \sqrt{\frac{1}{2} \Pi_{\dot{\gamma}}} = \sqrt{\frac{1}{2} (\dot{\gamma}_{11}^2 + \dot{\gamma}_{22}^2 + \dot{\gamma}_{33}^2)} \quad (6.8)$$

To solve the temperature issue, they used the time temperature superposition principle to shift all the viscosity and deformation rate data at different axial distances (different temperatures) to the same reference temperature based on the results calculated from inline birefringence measurements.

Rheo-optical techniques, especially birefringence, have become a standard method in the study of polymer rheology to supplement the mechanical methods [13-15]. Okamoto *et al.* [17,18] used the stress-optical law (SOR) to evaluate the miscibility/immiscibility of the PE blends using elongational flow opto-rheometry (EFOR). If the SOR was found to be valid for a blend, they considered the blend to be miscible. Otherwise, the SOR was violated due to the contribution of form birefringence in the case of immiscible blends.

This paper mainly focuses on inline birefringence measurements to evaluate the miscibility/immiscibility of mPE/LDPE blends and to determine the NNBEV of miscible blends.

## 6.2. Experimental

### 6.2.1. Materials

The main characteristics of the four polyethylenes used to make the blends and inline measurements and are listed in Table 6.1. Two low density polyethylenes (LDPE) with different molecular weight distribution (MWD) and different molecular weight (MW) and two metallocene catalyzed polyethylenes have been investigated. One is a

linear metallocene catalyzed polyethylene (LmPE), which is a hexene based copolymer and another one is metallocene catalyzed polyethylene with sparse long chain branched (BmPE), which is an octene based copolymer.

### 6.2.2. Blending Procedure

Five combinations, 90/10, 80/20, 50/50, 20/80, 10/90 per weight, were chosen for the LmPE/LDPE-1 and BmPE/LDPE-2 blend systems. The polymers were first dry mixed in a WEIGHT SCALE blender for 5 min and then were fed to a Leistritz AG 34 mm co-rotating twin-screw extruder (TSE). The temperature profiles were 170, 180, 190 and 200°C for the feed zone, the compression zone, the metering zone and the die end, respectively. The screw speed was held at 100 rpm and the extruded materials were palletized after passing through water at room temperature. The unblended resins were also processed in the twin screw extruder under the same conditions to give them the identical thermo-mechanical history as the blends.

### 6.2.3. Film Blowing Unit

The film blowing experiments were performed on a lab film unit fed by a single screw extruder. The details can be found elsewhere [12]. The temperature of the bubble as a function of vertical distance from the die ( $z$  direction) was measured using an infrared pyrometer (IRCON 3400). This instrument absorbs the infrared radiation in a wavelength of 3.43  $\mu\text{m}$ . The frame with the infrared pyrometer and the optical train (for birefringence measurements) was moved along the bubble upward and downward at low speed (1.0 mm/s) at least 3 times to get temperature and birefringence profiles. The velocity profiles were obtained via Laser Doppler Velocimetry (LDV) with the equipment installed on the same frame as mentioned above. Three measurements of the velocity of both sides of the bubble as a function of the axial distance have been made.

The bubble diameter profiles were determined by taking photos using a high resolution digital camera.

#### 6.2.4. Birefringence and Stress Optical Rule (SOR)

The details of the birefringence measurement technique can be found elsewhere [11]. The birefringence can be defined as:

$$\Delta n = \frac{\delta \lambda}{2\pi h} \quad (6.9)$$

where  $\delta$  is the retardation angle,  $h$ , the thickness of the film,  $\lambda$ , the wave length (632.8nm) and  $\Delta n$ , the birefringence. Also,  $\sin \delta$  is defined as anisotropy in this experiment [19].

The birefringence of polymer blends may be formulated by [16]:

$$\Delta n = \Delta n_A^0 f_A \phi_A + \Delta n_B^0 f_B \phi_B + \Delta n_F \quad (6.10)$$

where  $\Delta n_i^0$  is the intrinsic birefringence of the  $i$ -polymer,  $\phi_i$  is the volume fraction,  $f_i$  is the orientation function and  $\Delta n_F$  is the form birefringence. The orientation function  $f$  is defined by:

$$f = \frac{3 \langle \cos^2 \theta \rangle - 1}{2} \quad (6.11)$$

where  $\theta$  is the angle between the axis of the molecular chain and the stretching direction and the brackets represent an average over all orientation. By assuming  $f_A = f_B$  and

$\rho_A = \rho_B$ , we may evaluate the birefringence of the blends. Normally,  $\Delta n_F$  is assumed to be zero for miscible blends. However, for immiscible blends, the non-trivial form birefringence will play an important role.

The polymer flows under shear stress before it leaves the die. After leaving the die, it flows under elongational stresses. To investigate the birefringence under elongational flow, it is not as complicated as in shear flow since the principal axes are well defined. The stress optical rule can be written as:

$$(n_{11} - n_{33}) = C(\sigma_{11} - \sigma_{33}) \quad (6.12)$$

where  $(n_{11} - n_{33})$  is the in-plane birefringence and  $C$  is the SOR coefficient that can be derived from the theory of ideal rubber [14]:

$$C = \frac{2\pi}{45kT} \left( \frac{(n^2 + 2)^2}{n} \right) (\alpha_1 - \alpha_2) \quad (6.13)$$

where  $n$  is the average refractive index of the material,  $k$  the Boltzmann constant,  $T$  the temperature and  $\alpha_1 - \alpha_2$  the difference in the polarizability of the polymeric chains. From Eq. (6.13), we see that  $C$  depends on the chemical structure of the polymer and should be independent of the molecular weight and its distribution [20, 21]. The range of the SOR validity has been reported by Macosko [22].

Immiscible blends do not obey the stress-optical law [17, 18]. This can be explained in terms of the different values for  $C$  as well as the existence of form birefringence. Nevertheless, we still assume that the SOR is valid for all our blend systems to calculate the non-uniform biaxial elongational viscosity even though the

LmPE/LDPE-1 blends are suspected to be immiscible as reported in a previous paper [23].

### 6.3. Results and Discussion

#### 6.3.1. LDPE-1

The rheological properties of polymers should be independent of the technique used for the measurement. In other words, the non-uniform non-isothermal biaxial elongational viscosity (NNBEV) measured in film blowing should be a unique function of deformation rate and temperature. Therefore, if the method is valid, the elongational viscosity data of a given polymer calculated from different operation conditions using the same reference temperature should superpose. For this reason, the LDPE-1, which has the largest stable working window during film blowing process, was chosen at a mass flow rate of 2.0 kg/h and die temperature of 200°C. The four following different operation conditions (take-up ratio, TUR, blow-up ratio, BUR, frost line height, FLH) were investigated:

1. TUR = 60, BUR = 1.5, FLH  $\approx$  180 ( $\pm$ 5mm)
2. TUR = 80, BUR = 2.0, FLH  $\approx$  180 ( $\pm$ 5mm)
3. TUR = 80, BUR = 1.5, FLH  $\approx$  220 ( $\pm$ 5mm)
4. TUR = 80, BUR = 1.5, FLH  $\approx$  180 ( $\pm$ 5mm).

The diameter and temperature profiles along the axial distance are reported in Fig.6.1. In order to make the figure clearer the data for the temperature measurements have been replaced by 4<sup>th</sup> order polynomial regressions. The symbols are used only for identifying the different curves. The same presentation of the results will also be used for the LmPE/LDPE-1 and BmPE/LDPE-2 blends. We observe that the plateaus in the temperature profiles, where the exothermic heat of crystallization is removed, are almost

the same for all the conditions. This indicates that the crystallization temperature is not very sensitive to the operation conditions within the range investigated. This observation was also reported by other authors [24]. We may also observe that the BUR and TUR have small effects on the temperature profiles.

Fig. 6.2 shows the velocity profile for both sides of the LDPE-1 bubble under the same different operating conditions. Some discrepancy is observed between the velocity for both sides of the bubble and this comes from various sources. (1) The stability of the bubble, since it is only relatively stable. Details on the stability definition can be found elsewhere [25]. (2) The non-uniform thickness of the bubble caused by non-uniform temperature and die gap before leaving the die as well as non-uniform cooling. The discrepancy gets smaller with increasing TUR and decreasing FLH. This implies that cooling effects plays a major role on the uniformity of the bubble. Higher cooling rate leads to a more uniform and more stable bubble. We may also observe that the velocity above the FLH decreases slightly for all the operating conditions investigated. This is due to the density changes of the polymer. A second-order polynomial regression was used to fit the data below the FLH for all the operating conditions, which will be used for the calculations.

Fig. 6.3 reports the strain rates in both machine and transverse directions of the LDPE-1 for the same different operation conditions, using Eqs. (6.3) and (6.4). The jumps observed at larger axial distances in the figure are due to the regression technique used. For conditions 1, 3 and 4 we observe that strain rates in machine direction (MD) are always larger than those in transverse direction (TD). The differences in strain rates become larger with increasing TUR or FLH while keeping the other parameters constant. By comparing conditions 1 and 4, we see that the differences of MD and TD strain rates become smaller with increasing BUR. Unfortunately, the strain rates for the lower axial position could not be observed due to limitations imposed by the air ring of the apparatus.

Fig. 6.4 shows the anisotropy profile of LDPE-1 for the same different operating conditions. Also, due to the motion of the bubble, some oscillations at the same axial distance are observed, especially in the transition zone. These oscillations correspond to the discrepancies observed in the velocity measurements of both sides of the bubble. From this figure, we see that the anisotropy increases with increasing TUR in both melt and solid states and decreases with increasing FLH with keeping the other parameters constant. All the anisotropy data are positive, indicating that the orientation in the machine direction is always larger than that in the transverse direction. With increasing TUR and decreasing of BUR and FLH, the anisotropy increases faster along the bubble below the FLH. In the vicinity of the FLH, where the polymer under stress starts to crystallize, the anisotropy increases drastically and finally reaches a plateau for all the conditions except when  $FLH \approx 220$  mm where a plateau has not been observed due to the limits of the equipment.

If we neglect density changes with temperature (by assuming:  $\rho = 800 \text{ kg/m}^3$ ) and take third order and second order polynomial regressions for diameter and velocity profiles, respectively, below FLH, the thickness profile can be calculated to determine the birefringence using Eq. (6.9).

In addition, the anisotropy data were smoothed by using the Loess regression technique, which is a local smoothing technique with tri-cube weighting and polynomial regression. Both thickness and birefringence calculated data for the different operating conditions are reported in Fig. 6.5. We observe that the birefringence is always positive, confirming that the orientation in the machine direction is larger than that in the transverse direction. We also note that the birefringence increases rapidly as the film starts to crystallize.

Based on the birefringence data and the pressure inside the bubble, the stress profile can be obtained using the SOR and the force equilibrium equation in the normal direction, which can be approximated by the thin membrane equation, neglecting surface tension effects [7]:

$$\frac{\Delta P}{h} = \frac{\sigma_{11}}{R_L} + \frac{\sigma_{33}}{R_H} - \rho g \sin \theta \quad (6.14)$$

where  $\Delta P$  denotes the pressure inside the bubble,  $R_L$  and  $R_H$  are the radii of curvature in the machine and transverse directions, respectively.

The pressures inside the bubble measured for the LmPE/LDPE-1 and BmPE/LDPE-2 blends are listed in Table 6.2 and the non-uniform biaxial elongational viscosity can be easily calculated from Eq. (6.7) by solving Eqs. (6.12) and (6.14).

As we are dealing with non-isothermal conditions, we have to compare the rheological properties at the same temperature. In order to fulfill this requirement, we shifted the non-uniform, non-isothermal biaxial elongational viscosity versus effective deformation rate to a reference temperature of 175°C using the time temperature superposition principle. The activation energies for the LDPE-1, LmPE/LDPE-1 and BmPE/LDPE-2 were obtained based on the rheological measurements reported in a previous article and are also reported in Table 6.2. Furthermore, since the stress-optical law and the time-temperature superposition principle are not valid when a polymer melt goes through a phase transition, only data for which the temperature were 10°C higher than the crystallization temperature were used for the calculations.

Fig. 6.6 shows the NNBEV versus effective deformation rate for the LDPE-1 at 175°C under different operation conditions. The NNBEV for all the operating conditions show strain-thinning behavior within the range of deformation rate investigated. We also



observe that the NNBEV shows some deviations for the data calculated from the different operating conditions. However, they are acceptable considering the various sources of errors, non-uniformity of the bubble, temperature difference across the film thickness, oscillations of the bubble during the measurement, the assumption of a constant density and regression technique used, etc. In summary, the NNBEV calculated for the different operation conditions are consistent and acceptable considering the difficulty of the experiment and the various sources of error.

### 6.3.2. LmPE/LDPE-1 Blends

From our previous work [23], the LmPE/LDPE-1 blends are suspected to be immiscible. During film blowing experiments, it was quite difficult to get stable bubbles, with a constant FLH and film thickness. Figs. 6.7 and 6.8 show the diameter, velocity and temperature profiles for LmPE/LDPE-1 blends for a same mass flow rate of 2.0 kg/h, die temperature of 200°C, BUR of 1.5, TUR of  $\approx 40$  and FLH of  $\approx 180$ mm. From the diameter profiles, we see that the LmPE bubble exhibits a longer neck than that of the LDPE-1 and the velocity profiles show a similar trend as the diameter profiles. Furthermore, the appearance of plateau for velocity profiles starts at larger axial distance than that for diameter profiles for all the blends investigated. In other words, the deformation of the polymer is changed from non-uniform biaxial to planar extension. This is because the stress level in machine direction (MD) is much larger than that in transverse direction (TD) when crystallization starts. The higher level of stress in MD stretches the polymer and the velocity keeps increasing until most of the molecules are crystallized. It is worth noting that the frost line height (FLH) is defined as the line where the bubble becomes translucent. Morris (26) refers to the onset of the plateau as the crystallization line height (CLH) and the end of the plateau as the freeze line (FZH). The frost line height (FLH) falls in between the CLH and FZH.

The temperature profiles of the LmPE and the LDPE-1 are quite similar and this explains why similar temperature profiles were observed for all blends. In addition, the 90/10 blend gives slower decreases due to the large non-uniformity of the FLH. Non-uniform FLH was observed during all experiments for this blend and the repeatability of the results was not good. Therefore, we do not report the subsequent results for the 90/10 (LmPE/LDPE-1).

Fig. 6.9 shows the MD and TD strain rates for LmPE/LDPE-1 blends. The MD strain rates for all the LmPE/LDPE-1 blends show the same trend: they decrease rapidly to reach zero at the FLH. We may see that the LmPE shows the largest MD strain rate whereas the LDPE-1 shows the smallest and the blends are intermediate.

Fig. 6.10 reports the birefringence profiles for LmPE/LDPE-1 blends. Because it is of more interest to investigate the birefringence of the blends in the amorphous phase in order to see the effect of the form birefringence, only the data before crystallization starts are shown. From the figure we see that the values of birefringence for all the blends are always positive and increase with the axial distance, indicating that the orientation in the machine direction is higher than that in the transverse direction. We may also see that the values for the blend birefringence do not follow the blend composition. At low axial distances, the order of the birefringence values for blend LmPE/LDPE-1 is: 10/90, 20/80, 50/50, 0/100, 80/20, 100/0. At high axial distances, the order is: 10/90, 20/80, 0/100, 50/50, 80/20, 100/0. The birefringence data of the LmPE/LDPE-1 blends imply the existence of form birefringence, which gives another indication of the immiscibility of LmPE/LDPE-1 blends.

Assuming that the SOR were valid, the NNBEV for the LmPE/LDPE-1 blends was calculated using the time temperature principle and the results are reported in Fig. 11. We see that the NNBEV of the LmPE and the 80/20 blend is almost constant under the deformation rate investigated whereas the other blends and the LDPE-1 show strain-

thinning behavior. We also observe that viscosity of the blends do not follow the semi-log additivity rule.

### 6.3.3. BmPE/LDPE-2 Blends

The diameter, velocity and temperature profiles for the BmPE/LDPE-2 blends are reported in Figs. 6.12 and 6.13 for the same mass flow rate of 2.0 kg/h, die temperature of 200°C, BUR of 1.5, TUR of  $\approx 40$  and FLH of  $\approx 180$ mm. We observe in Fig. 12 that the velocity profiles of the blends are intermediate with respect to those of both components. The situation is more complex for the diameter profiles where the data for the 80/20 BmPE/LDPE-2 blend cross over those of the other blends, indicating that this blend has a shorter neck than the other blends and both components. We see in Fig. 6.13 that the BmPE depicts a lower crystallization temperature whereas the LDPE-2 shows a higher one. In addition, in the crystallization region, the temperature profile of the BmPE shows a clear plateau whereas that of the LDPE-2 decreases smoothly. In comparison to the BmPE, the LDPE-2 film shows a higher surface temperature. The sequence of temperature profiles for the BmPE/LDPE-2 blends changes with blend composition. The results for the temperature profiles confirm our DSC results [23] for the blends although in film blowing the crystallization is induced by stresses.

The strain rates in MD and TD for BmPE/LDPE-2 blends are presented in Fig.6.14. The MD strain rates show the same trend as for the LmPE/LDPE-1 blends: they decrease rapidly to reach zero at FLH and there is no maximum within the range investigated. The jump is due to the regression technique used. However, except for the BmPE, which shows a maximum at the axial distance around 135mm, the BmPE/LDPE-2 blends and LDPE-2 show rapid decreases of the TD strain rates to reach zero at FLH.

Fig. 6.15 reports the birefringence profiles along the bubble below the FLH for the BmPE/LDPE-2 blends. We see that the birefringence of the LDPE-2 is larger than that of the BmPE and increases with axial distance whereas the birefringence of the BmPE remains almost constant. The birefringence of the blends changes accordingly to the blend composition, i.e. the form birefringence is zero, suggesting miscibility of the BmPE/LDPE-2 blends as discussed elsewhere [23].

The NNBEb and the biaxial Trouton ratio versus effective deformation rate at the reference temperature of 175°C are presented in Fig. 6.16. We observe that all the BmPE/LDPE-2 blends show strain-thinning behavior. Moreover, the viscosity order from low to high is: BmPE, 90/10, 80/20, 50/50, 20/80, 10/90 and LDPE-2, which is corresponding to the blend composition. However, the elongational viscosity versus blend composition curve (data not shown here) does not exactly follow the semi-log additivity rule, possibly due to various sources of errors as mentioned before. The biaxial Trouton ratio (BTR) can be defined as the ratio of the biaxial elongational viscosity over the shear viscosity. For Newtonian fluids, the BTR should be 6. Although the film blowing is not a uniform biaxial elongation flow, we report in Fig. 6.16 the BTR for all BmPE/LDPE-2 blends. We observe that the BTR values are larger than 6 and, as expected, the larger values are obtained for the LDPE-2. The BTR of the blends correlated fairly well with the blend composition. The BTR for the BmPE is quite close to the theoretical value of 6.

#### 6.4. Concluding Remarks

The behavior of two families of polyethylene blends has been investigated using a fully instrumented film blowing unit in order to offer more reliable data for modeling purposes and confirm the miscibility/immiscibility of BmPE/LDPE-2 and LmPE/LDPE-1 blends as reported in a previous paper [23].

A laser Doppler velocimetry method was used to determine the local film velocity. It was shown to be a more reliable technique, although the data collected showed considerable scatter due to the non-uniformity of the bubble. In-situ birefringence measurements of the molten film were used to determine the stresses via the SOR and calculate the non-uniform, non-isothermal biaxial elongational viscosity (NNBEV). The NNBEV of the LDPE-1 under different operating conditions has been evaluated. The qualitative agreement obtained for the various conditions confirmed the technique used for the calculation of the NNBEV.

The inline birefringence of the LmPE/LDPE-1 and the BmPE/LDPE-2 blends below FLH has been studied. Experimental trials showed the existence of form birefringence for the LmPE/LDPE-1 blend. This confirms the assumption that the LmPE/LDPE-1 blends are immiscible as reported in a previous paper [23]. On the other hand, the birefringence of the BmPE/LDPE-2 blends was shown to be closely related to the blend composition, suggesting miscibility of these blends. The non-uniform, non-isothermal biaxial elongational viscosity (NNBEV) of all BmPE/LDPE-2 blends showed a strain-thinning behavior within the deformation rates investigated. Furthermore, the results showed that the LDPE-2 deviated largely from the Newtonian fluid behavior whereas the BmPE was quite close to the Newtonian behavior.

### **Acknowledgements**

This work was funded through a strategic grant from NSERC (Natural Science and Engineering Research council of Canada), for which we are grateful.

## 6.5. References

1. J. Meissner, *Rheologica Acta* **8**, 78 (1969).
2. J. Meissner, *Pure and Applied Chemistry* **43**, 553 (1975).
3. F. N. Cogswell, *Polym. Eng. Sci.* **12**, 64 (1972).
4. D. M. Binding, *J. of Non-Newt. Fluid Mech.* **27**, 173 (1988).
5. M. E. Mackay and G. Astarita, *J. of Non-Newt. Fluid Mech.* **70**, 219 (1997).
6. C. Lacroix, M. Grmela, and P. J. Carreau, *J. of Non-Newt. Fluid Mech.* **80**, 183 (1999).
7. C.D. Han and J.Y. Park, *J. Appl. Polym. Sci.* **19**, 3257 (1975)
8. A. Ghaneh-Fard, P. J. Carreau, and P. G. Lafleur, *Polym. Eng. Sci.* **37**, 1856 (1997)
9. T. Kanai and J. L. White, *Polym. Eng. Sci.* **24**, 1185 (1984)
10. J.-F. Agassant, P. Avenas, J.-Ph. Sergent, and P. J. Carreau, *Polymer Processing: Principles and Modeling* Hanser Publishers, New York (1991)
11. A. Ghaneh-Fard, P. J. Carreau, and P. G. Lafleur, *Int. Polym. Process.* **2**, 136 (1997)
12. Y. Fang, P. J. Carreau, and P. G. Lafleur, *Polymer Engineering & Science.* **43**, 1391 (2003)
13. J. L. S. Wales, *The Application of Flow Birefringence to Rheological Studies of Polymers* Delft University, Rotterdam, (1976)
14. H. Janeschitz-Kriegl, *Polymer melt Rheology and Flow Birefringence* Springer, New York (1983)
15. A.W. Chow and G.G. Fuller, *J. Rheol.*, **28**, 23 (1984)
16. L. A. Utrachi, *Two-Phase Polymer Systems* Hanser Publishers, New York (1991).
17. M. Okamoto, A. Kojima, and T. Kotaka, *Polymer*, **39**, 2149 (1998).
18. M. Okamoto, A. Kojima, and T. Kotaka, *Macromolecules*, **31**, 5158 (1998)
19. Documentation for LabVIEW Rheo-Optical Analyzer v1.8b (for LabVIEW 3.0).

20. B.E. Zebrowshki, and G.G. Fuller, *J. Polym. Sci., Polym. Phys. Ed.*, **19**, 531 (1981)
21. J.M. Dealy, and K. F. Wissbrun, *Melt Rheology and Its Role in Plastics Processing: Theory and Applications* Van Nostrand Reinhold, New York, (1990).
22. C.W. Macosko, *Rheology, Principles, Measurements, and Applications* VCH, USA (1994)
23. Y. Fang, P. J. Carreau, and P. G. Lafleur, submitted to *Polym. Eng. Sci.* (2004).
24. T. Kanai, G. Campbell, and W. Baker, *Film Processing* Hanser Publishers (1999).
25. S. Kim, Y. Fang, P. J. Carreau, and P. G. Lafleur, *Polym. Eng. Sci.* **44**, 283 (2004).
26. B. A. Morris, *SPE ANTEC'98* 1006 (1998)

Table 6.1. Polymers used and their main characteristics

Sample	Density [g/cm <sup>3</sup> ]	$MI$ [g/10min]	$M_w$	$M_w/M_n$		$LCB$ [1/10 <sup>4</sup> C]
LmPE	0.918	1.0	111 920	2.36	C <sub>6</sub>	N/A
BmPE	0.902	1.0	116 400	2.11	C <sub>8</sub>	0.1773
LDPE-1	0.923	1.9	80 900	5.02	-	-
LDPE-2	0.923	0.22	119 400	7.60	-	-



Table 6.2. Activation energy and pressure inside the bubble of LmPE, BmPE, LDPE-1, LDPE-2 and their blends.

Blends	LmPE	LmPE/LDPE-1 blends					LDPE-1
		10/90	20/80	50/50	80/20	90/10	
$E_a$ (kJ/mol.K)	28.3	32.9	29.1	34.4	42.1	40.6	45.8
Pressure <sup>1</sup> (Pa)	37.3	25.4	25.0	32.7	38.9	37.6	20.1
Blends	BmPE	BmPE/LDPE-2 blends					LDPE-2
		10/90	20/80	50/50	80/20	90/10	
$E_a$ (kJ/mol.K)	40.4	42.8	44.5	50	54.7	56.4	58.1
Pressure <sup>2</sup> (Pa)	41.8	59.1	58.3	51.6	46.4	43.0	59.4

<sup>1</sup> The operating conditions for LmPE, LDPE-1 and their blends are mass flow rate = 2.0kg/h, BUR = 1.5, TUR  $\approx$  60, FLH  $\approx$  180mm, die temperature = 200°C.

<sup>2</sup> the operating conditions for BmPE, LDPE-2 and their blends are: mass flow rate = 2.0kg/h, BUR = 1.5, TUR  $\approx$  40, FLH  $\approx$  180mm, die temperature = 200°C.

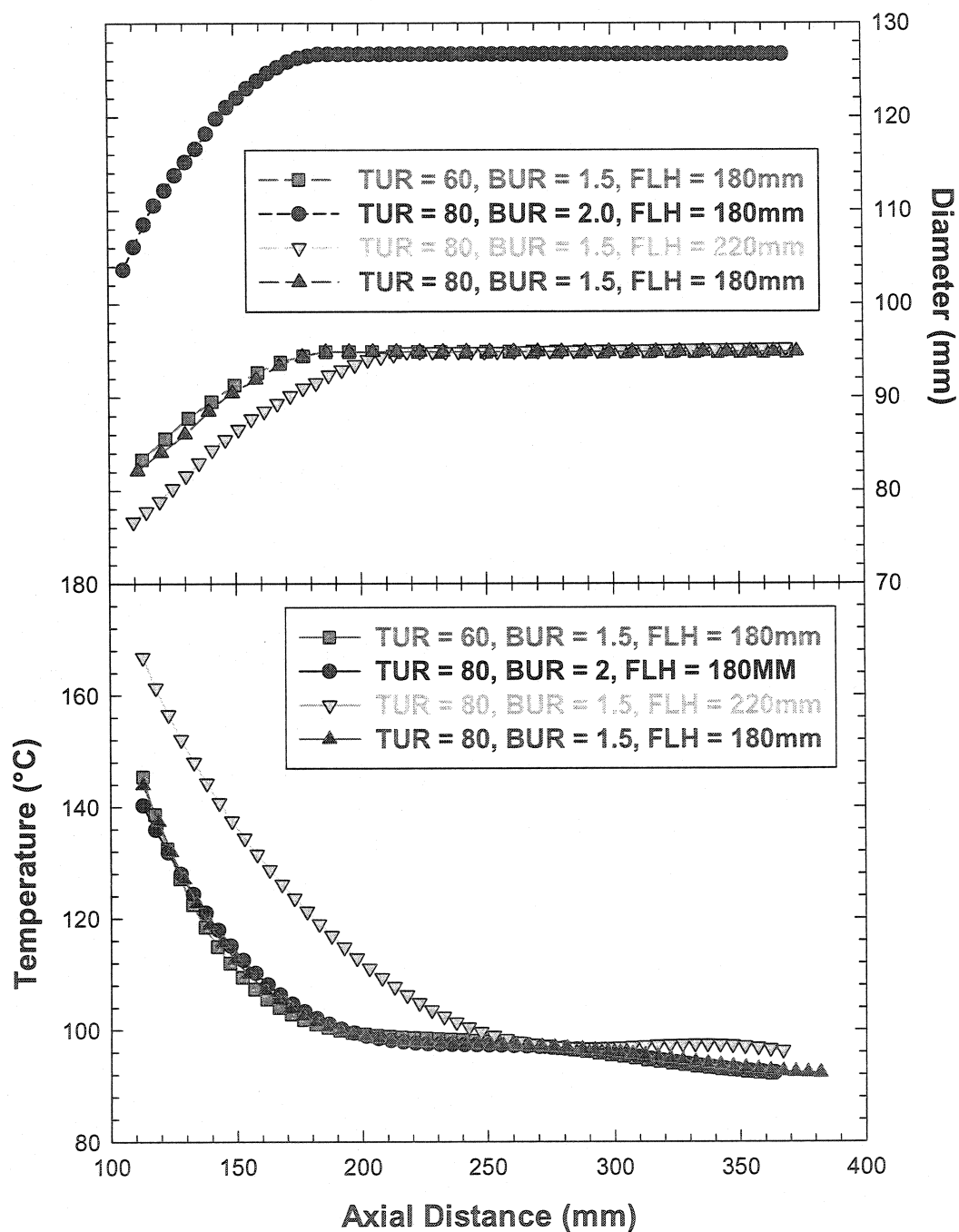


Figure 6. 1. Diameter and temperature profiles of the LDPE-1 at a mass flow rate of 2.0 kg/h and die temperature of 200°C for different other operation conditions.

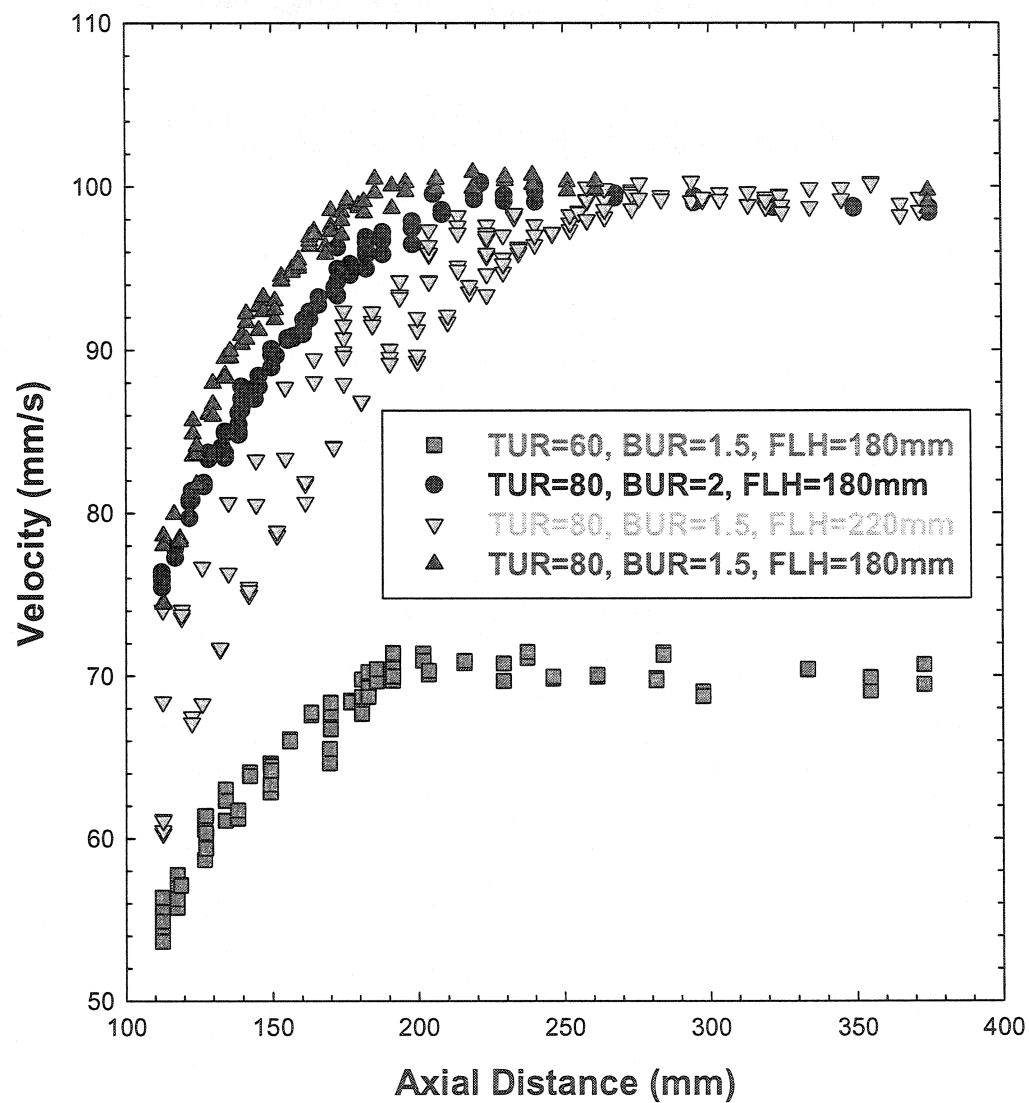


Figure 6. 2. Velocity profiles of the LDPE-1 for the conditions indicated in Fig. 6.1.

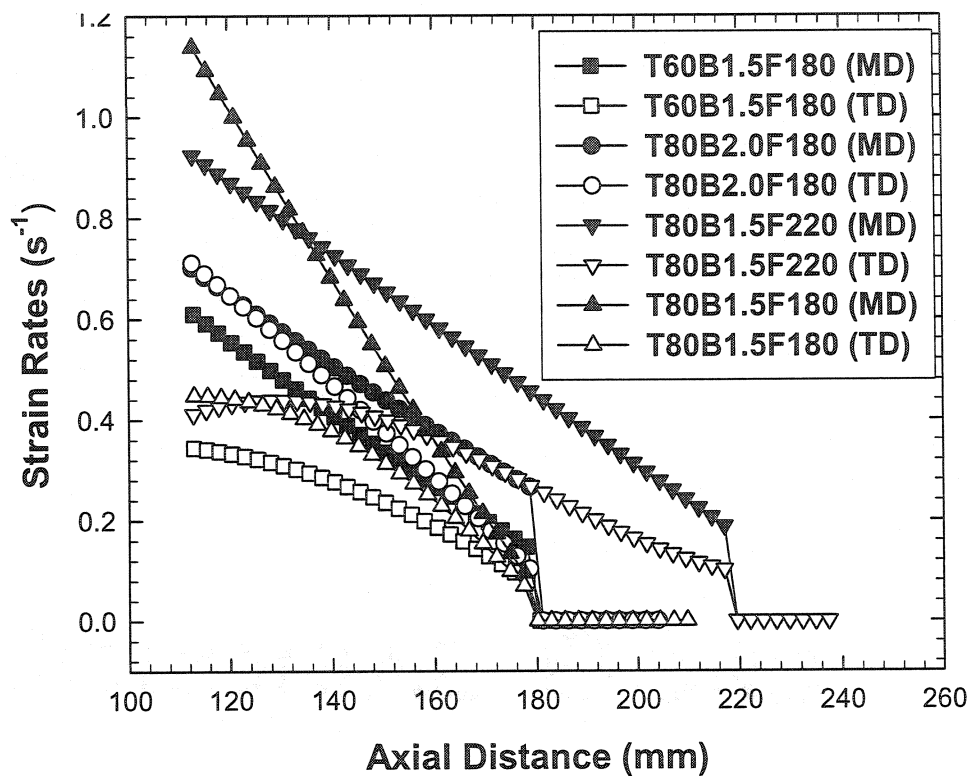


Figure 6.3. Strain rates of the LDPE-1 in machine and transverse directions for the conditions indicated in Fig. 6.1 (T = TUR, B = BUR, F = FLH).

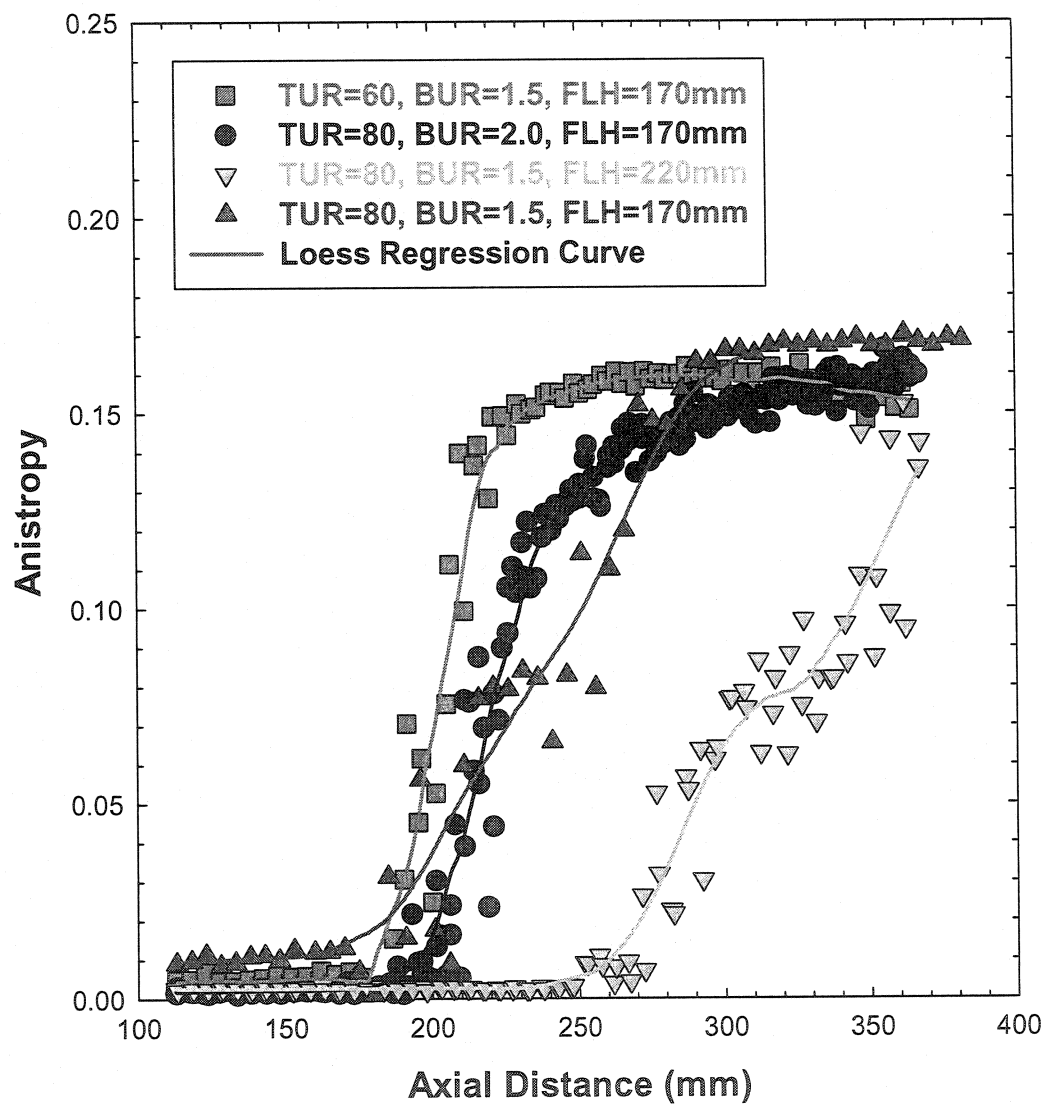


Figure 6. 4. Anisotropy profiles of the LDPE-1 for the conditions indicated in Fig. 6.1.

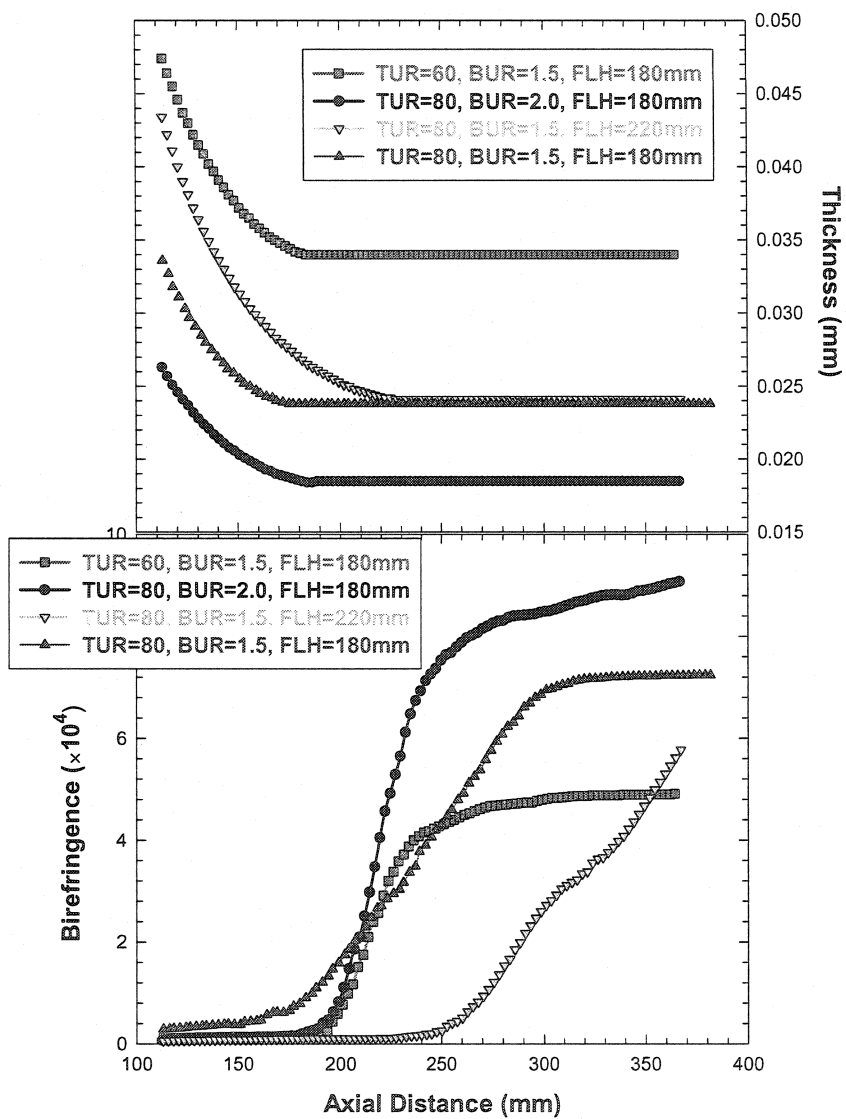


Figure 6.5. Thickness and birefringence profiles of the LDPE-1 for the conditions indicated in Fig. 6.1.

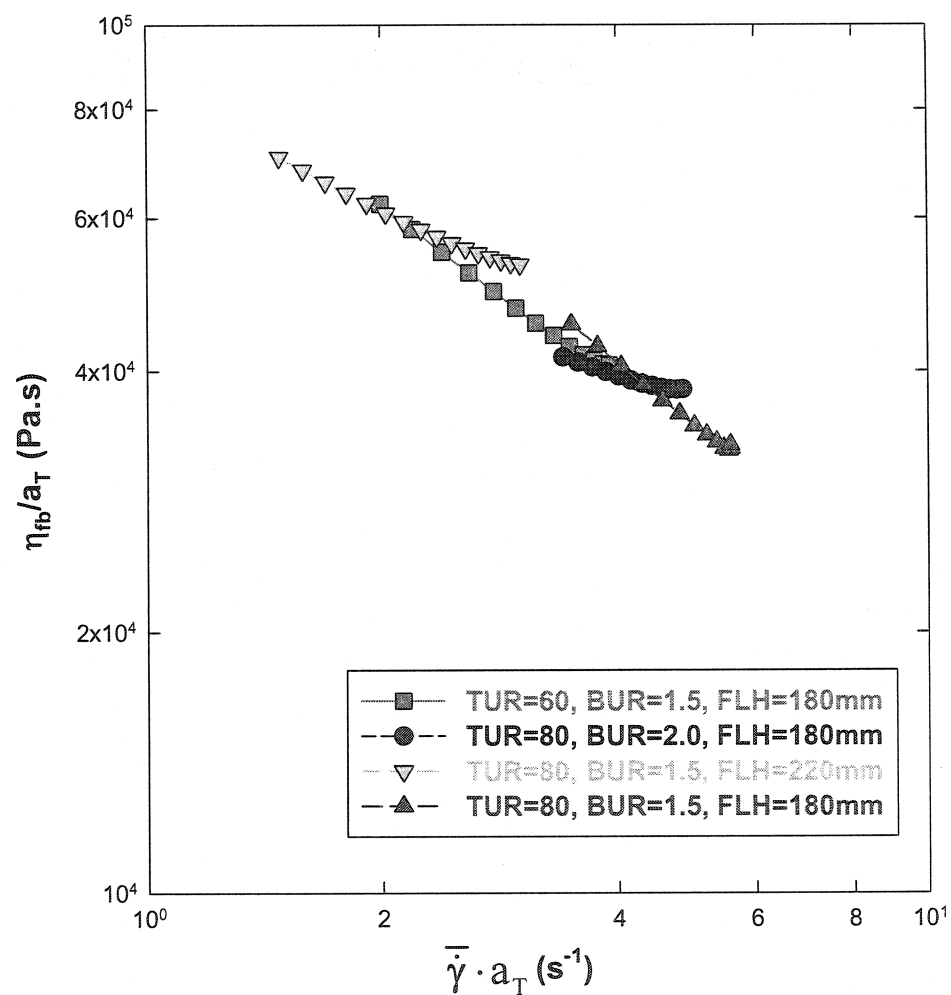


Figure 6.6. Non-uniform, non-isothermal biaxial elongational viscosity versus effective deformation rate for the LDPE-1 at 175°C for the conditions indicated in Fig.6.1.

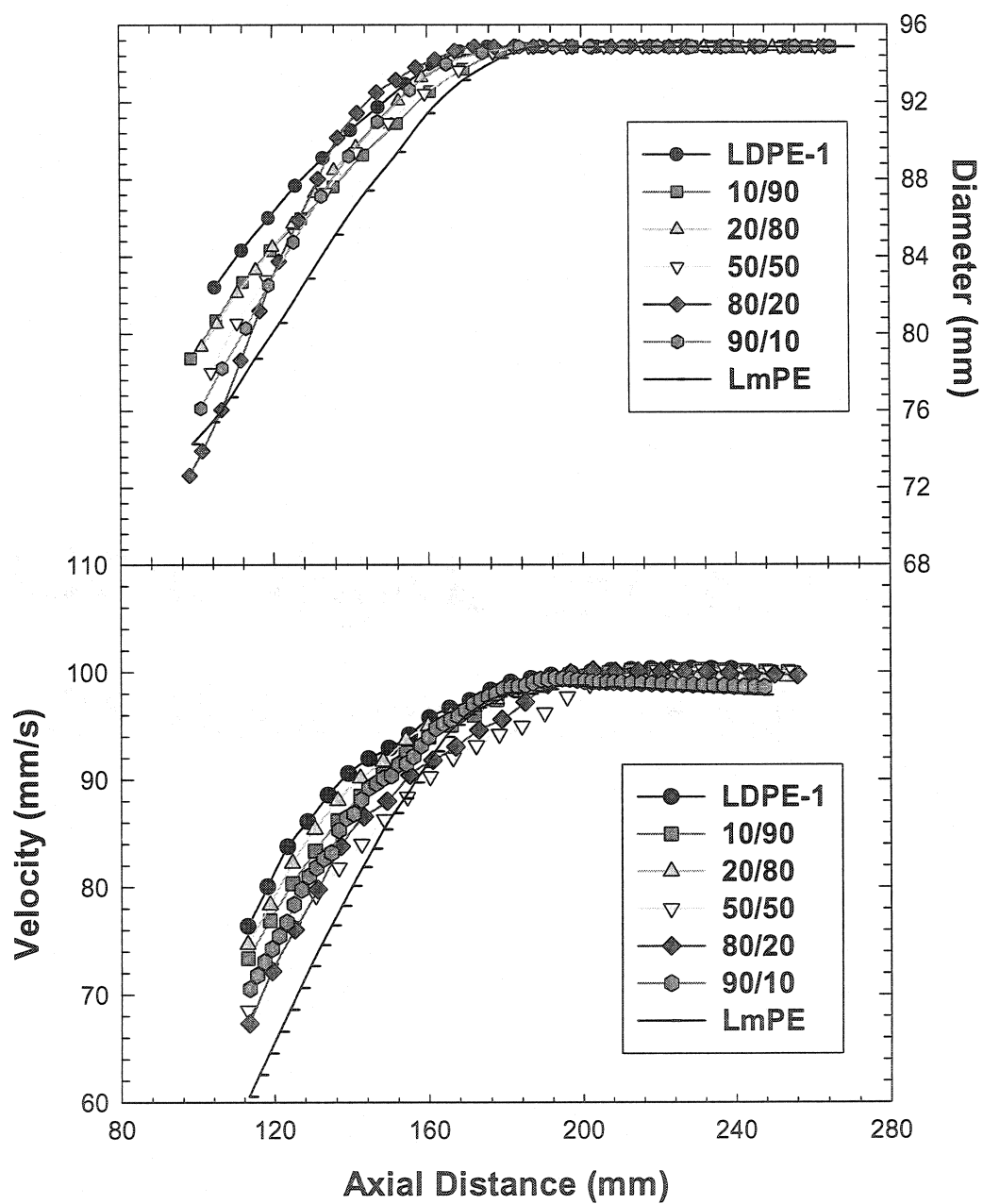


Figure 6. 7. Diameter and velocity profiles for the LmPE/LDPE-1 blends at a mass flow rate = 2.0kg/h, BUR = 1.5, TUR  $\approx$  60, FLH  $\approx$  180mm, die temperature = 200°C.



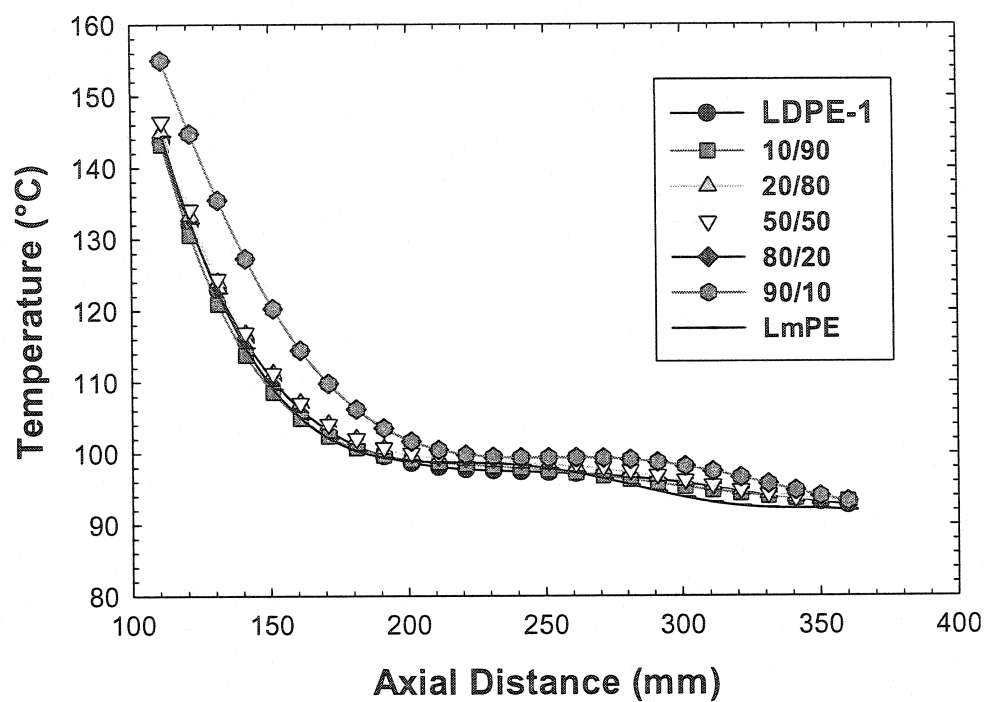


Figure 6. 8. Temperature profiles for the LmPE/LDPE-1 blends. The operating conditions are the same as for Fig. 6.7.

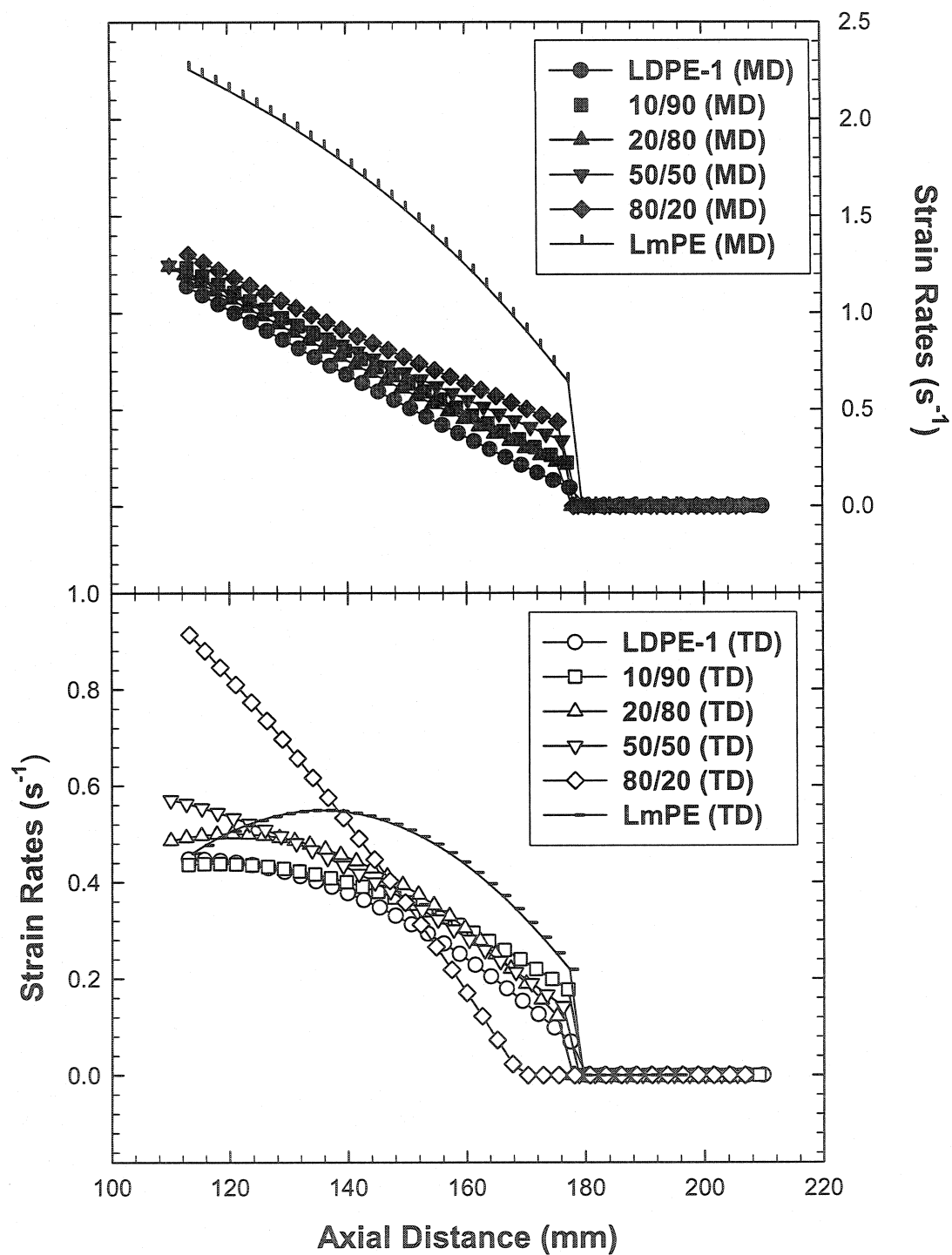


Figure 6. 9. Strain rates along the bubble for the LmPE/LDPE-1 blends in machine and transverse directions. The operating conditions are the same as for Fig. 6.7.

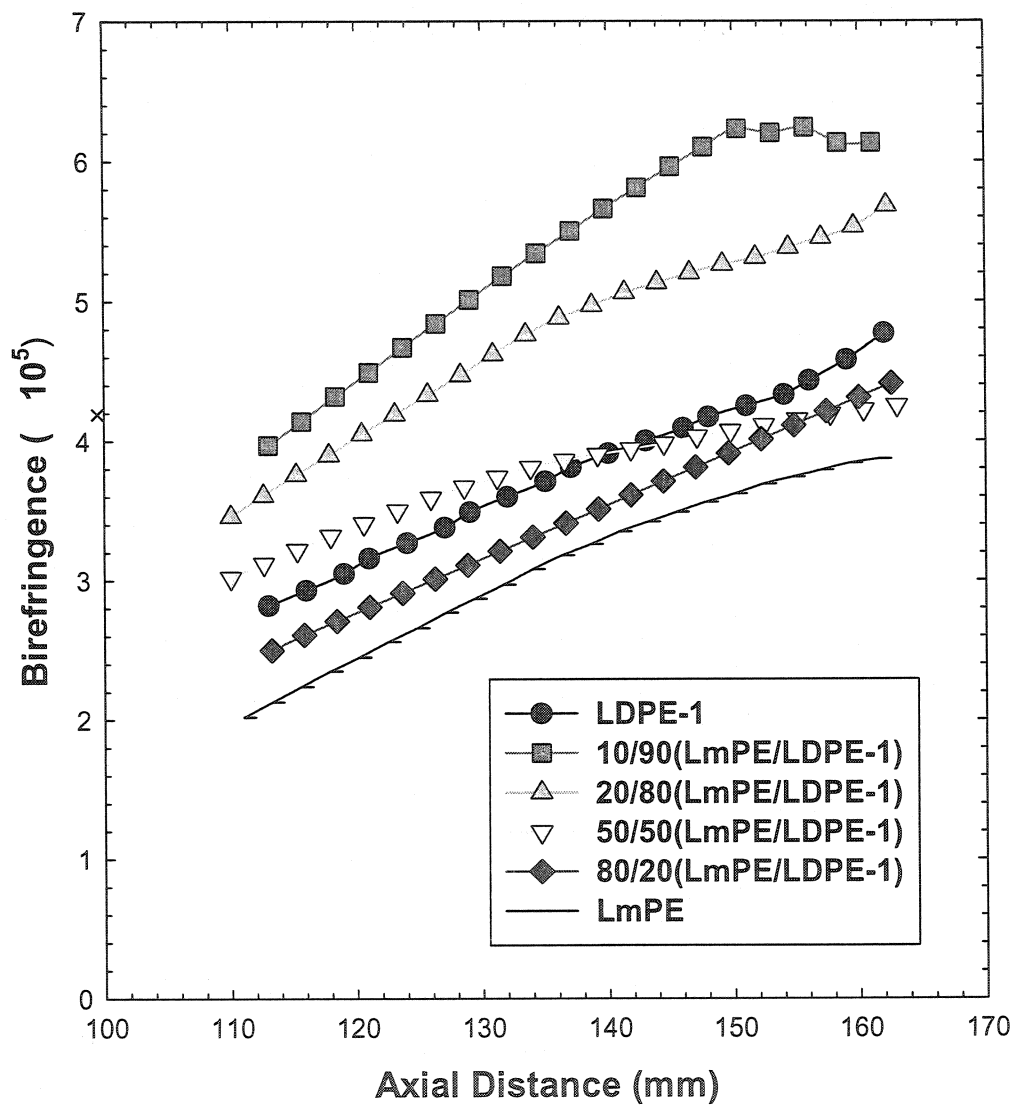


Figure 6.10. Birefringence profile for the LmPE/LDPE-1 blends. The operating conditions are the same as for Fig. 6.7.

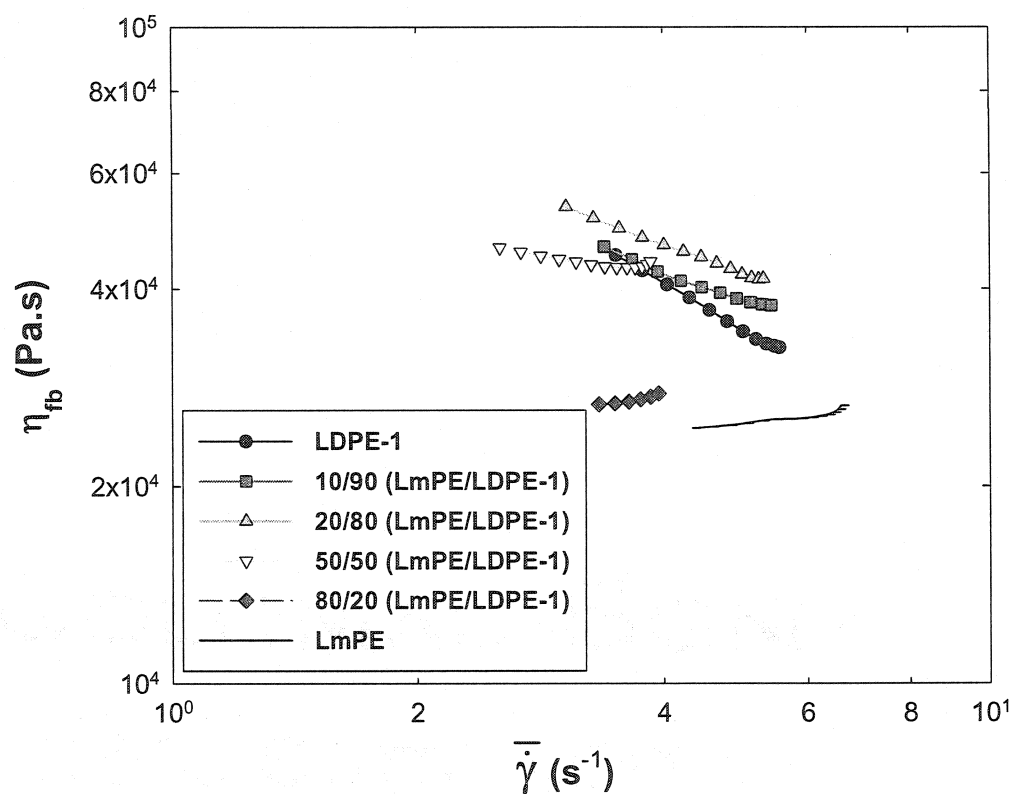


Figure 6.11. Non-uniform, non-isothermal, biaxial elongational viscosity versus effective deformation rate at the reference temperature of 175°C for the LmPE/LDPE-1 blends. The operating conditions are the same as for Fig. 6.7.

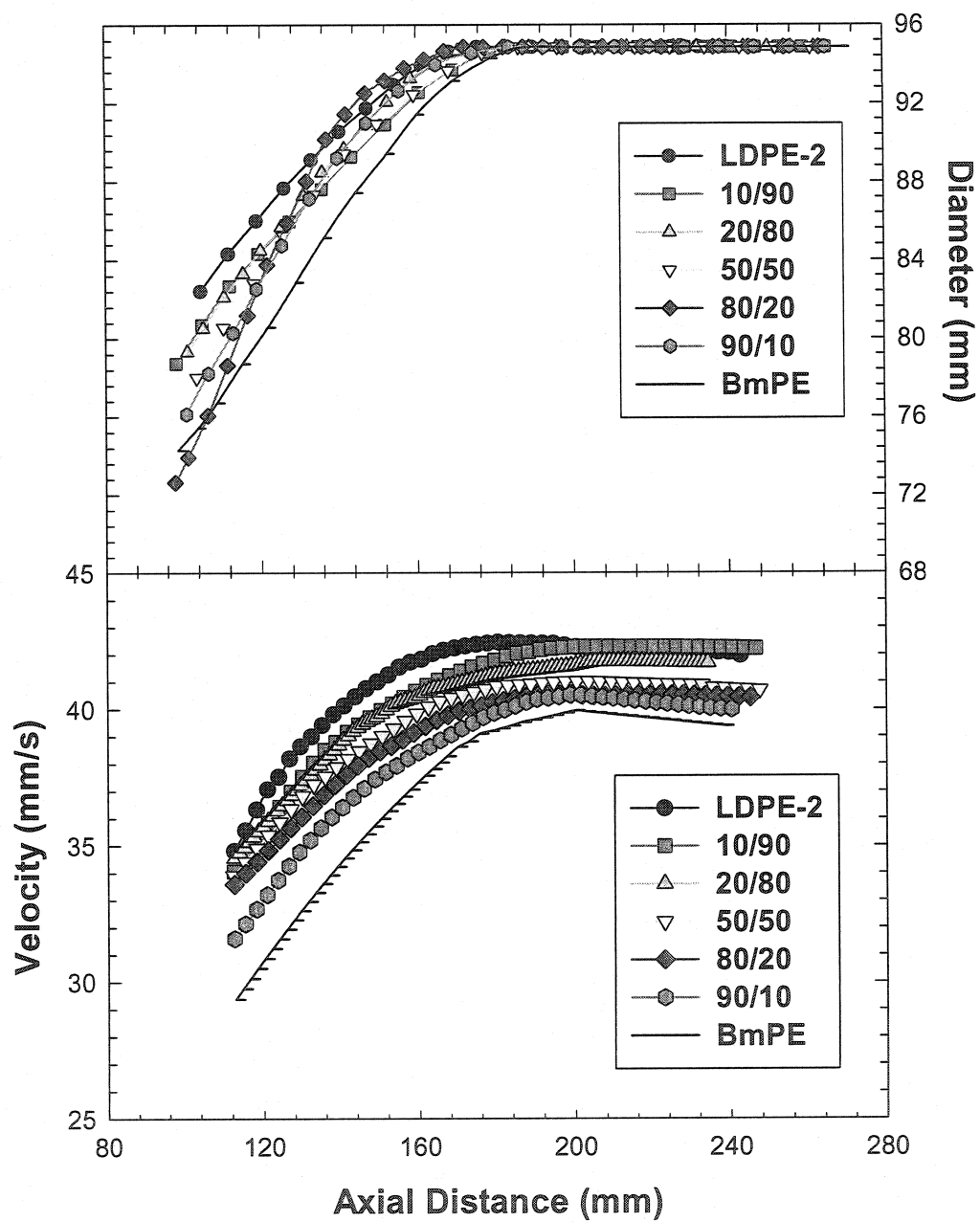


Figure 6.12. Diameter and velocity profiles for the BmPE/LDPE-2 blends at a mass flow rate = 2.0kg/h, BUR = 1.5, TUR  $\approx$  40, FLH  $\approx$  180mm, and die temperature = 200°C.

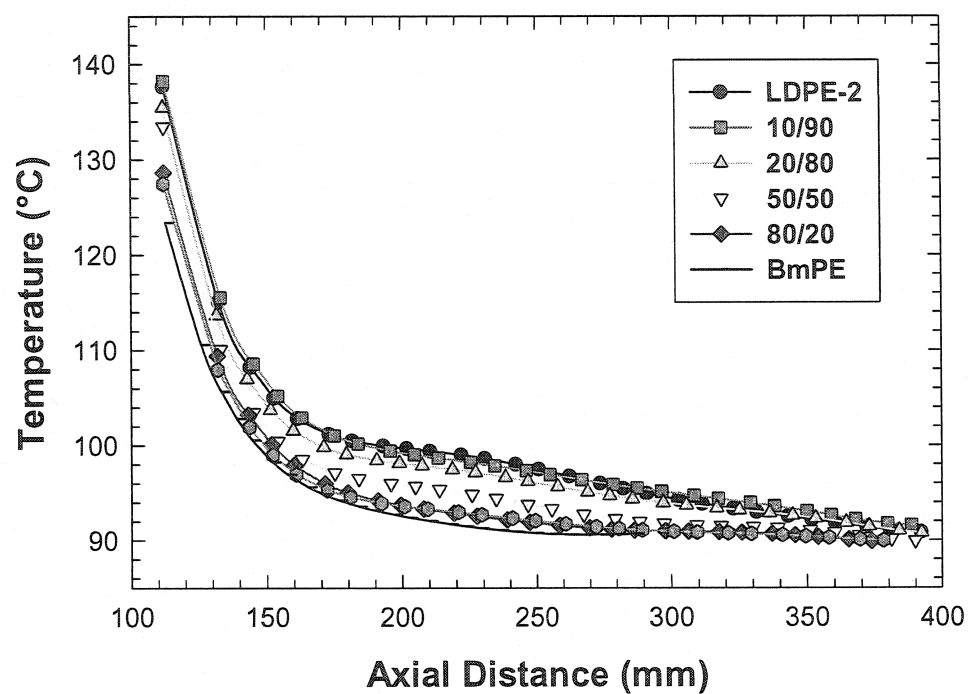


Figure 6.13. Temperature profiles for the BmPE/LDPE-2 blends. The operation conditions are the same as shown in Fig. 6.12.

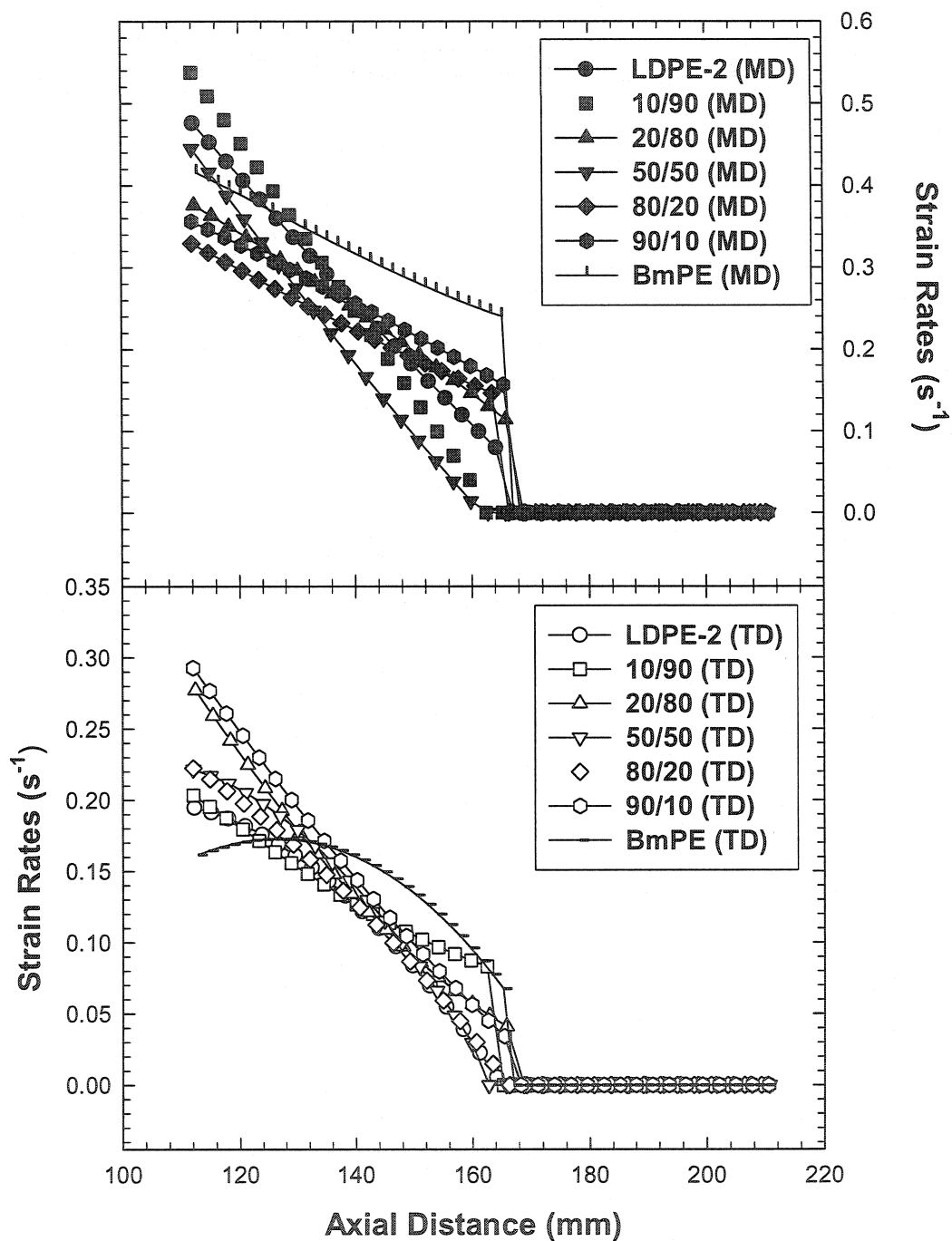


Figure 6.14. Strain rates in machine and transverse directions for the BmPE/LDPE-2 blends along the bubble. The operation conditions are the same as shown in Fig. 6. 12.

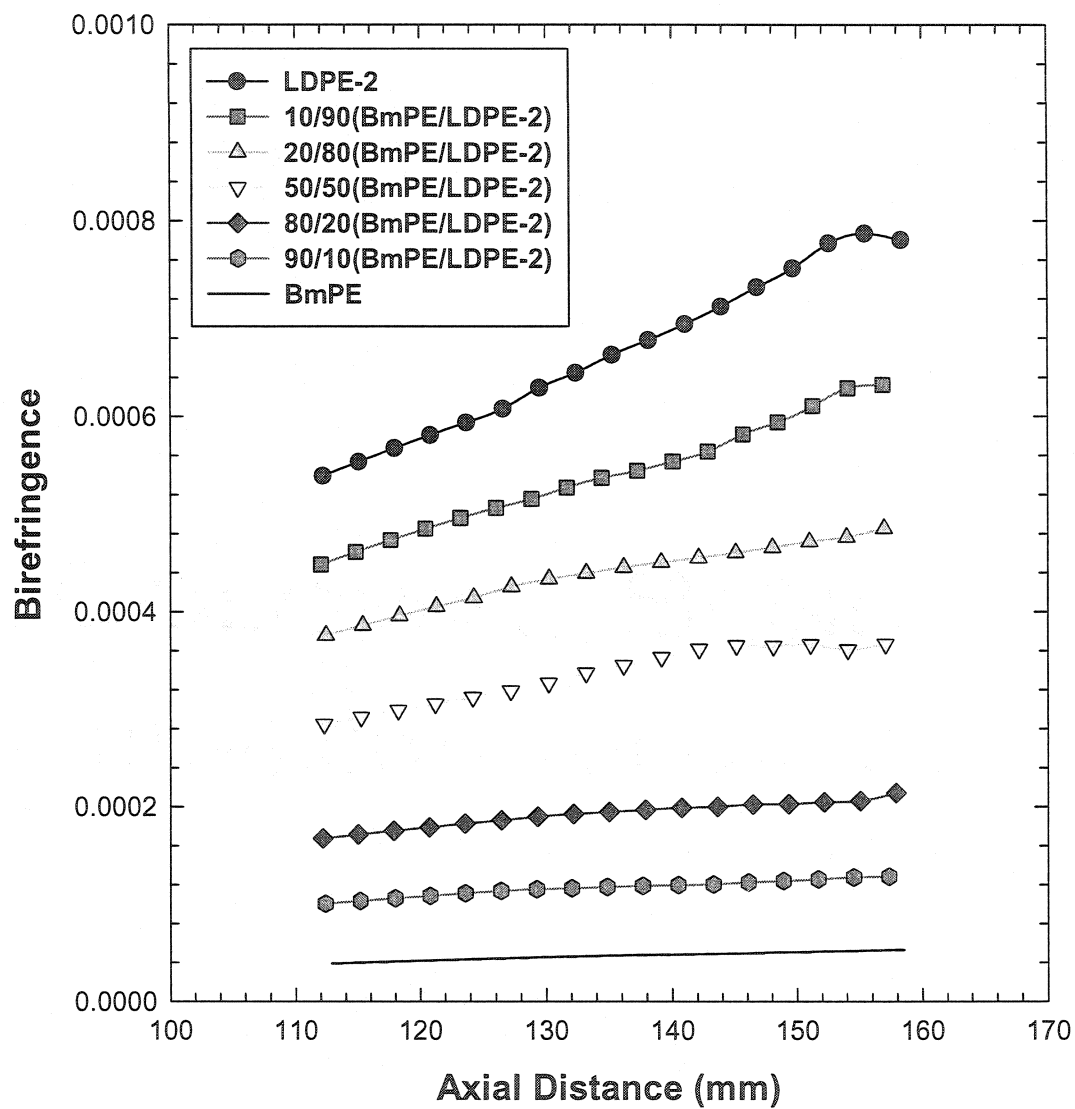


Figure 6.15. Birefringence profile for the BmPE/LDPE-2 blends. The operating conditions are the same as in Fig. 6.12.



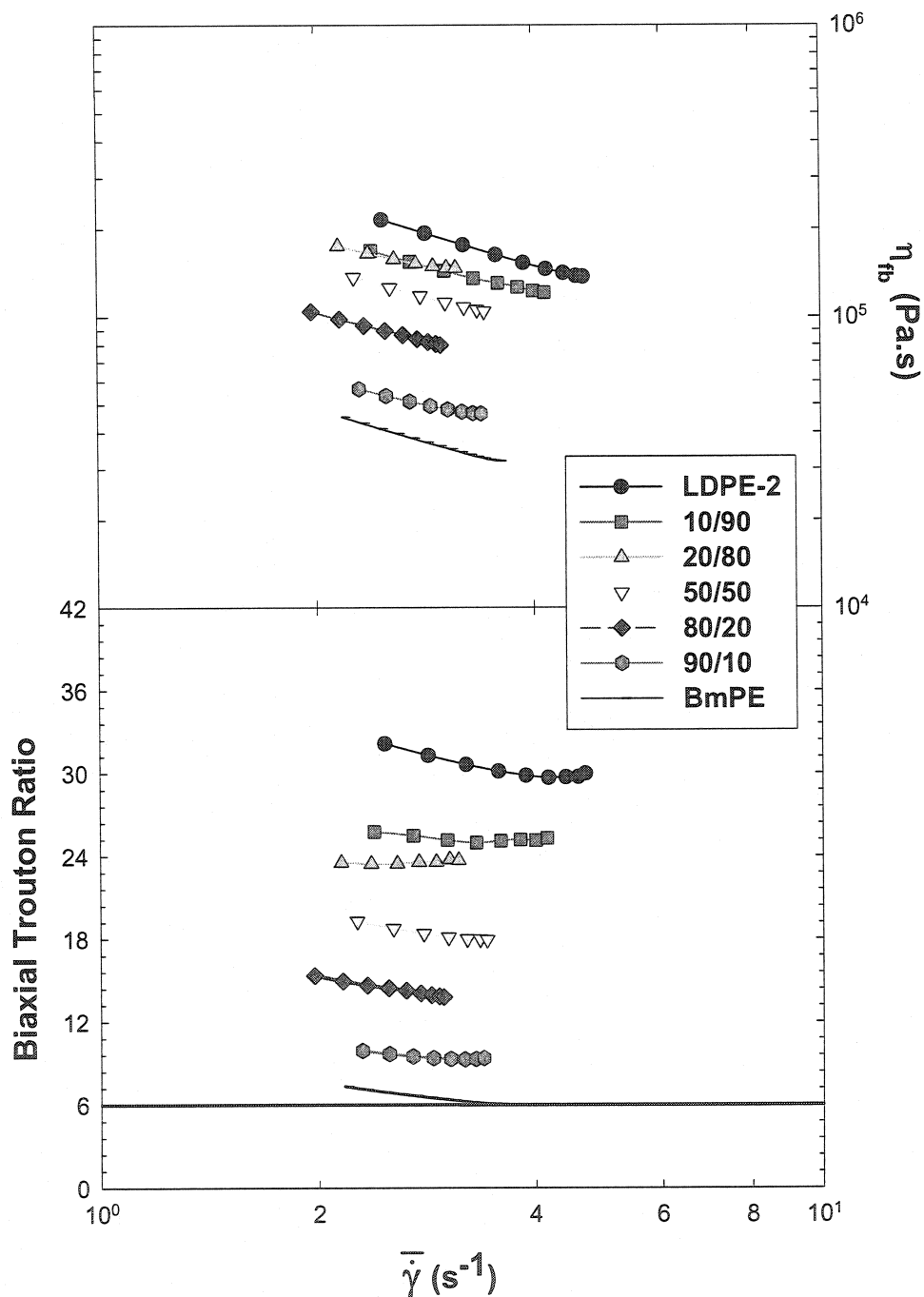


Figure 6.16. Non-uniform, non-isothermal, biaxial elongational viscosity and Biaxial Trouton ratio versus effective deformation rate at a reference temperature of 175°C for the BmPE/LDPE-2 blends. The operating conditions are the same as in Fig. 6.12.

## CHAPTER 7. SCIENTIFIC CONTRIBUTIONS

**Contribution 1.** Film blowing process is a very complex process with melt rheology, heat transfer and aerodynamics being involved. With the aid of time-temperature superposition principle, the isothermal non-uniform biaxial elongational viscosity (NNBEV) can be calculated and compared at the same reference temperature. This technique filled the gap of lack of NNBEV data, which is quite useful for modeling purpose and understanding the structure-processability-property relationship.

**Contribution 2.** By extensively evaluating the performance of a new in-line scanning camera system developed for the study of bubble instabilities during film blowing, we may quantitatively differentiate the various bubble instabilities, especially during the transition from stable to unstable bubble, or *vice versa*. Based on the parameters which can be directly determined using the new device, objective criteria have been defined. The data we obtained are quite reliable and useful for modeling purpose.

**Contribution 3.** Due to the lack of morphology data, the miscibility/immiscibility of mPE/LDPE blends have been critically evaluated using rheometry as DSC. Furthermore, it was shown that inline birefringence measurement is a powerful tool to confirm the existence of form birefringence for immiscible blend.

## CHAPTER 8. CONCLUSIONS AND RECOMMENDATIONS

### 8.1. Conclusions

From our own experimental data and those of a previously published work (17), we propose the following relative decreasing order of stability for the polymers studied:

$$\text{LDPEa or LDPEb} > \text{HDPE} > \text{mPE} > \text{LLDPE}$$

Log  $G'$  versus Log  $G''$  plot was observed to be virtually independent of temperature for all the polymers investigated. The larger the  $G'$  value was, the more stable the bubble was during film blowing.

The Trouton ratios for the HDPE, LLDPE, LDPEa, LDPEb and mPE versus deformation rate have been reported. In all cases, the ratio exceeds the limiting value of 3, expected for Newtonian fluids. The Trouton ratios of the LDPEa and LDPEb are much larger than those of the HDPE, LLDPE and mPE. We believe that the high values of the Trouton ratio are closely related to the bubble stability in film blowing.

The NNBEV has been calculated based on inline birefringence measurement and time-temperature principle for the five resins and the calculation technique was further confirmed using LDPE-1 under different operation conditions.

A new in-line scanning camera system developed for the study of bubble instabilities during film blowing has been shown to be able to capture the dynamics of unstable bubbles quantitatively. Objective criteria for differentiating the various unstable bubbles are proposed based on four parameters, which can be directly determined by

using the new device. It was also found that the amplitude and periodicity of the radius variations during draw resonance for LmPE decreased as TUR increased at a constant FLH and BUR implying that the origin of draw resonance in film blowing is not the same phenomenon observed in fiber spinning. Helicoidal instability and eccentricity decreased as TUR increased, however the bubble could not be stabilized as expected. A graphical quantification approach has been proposed to determine the stable zone in the bubble stability map. The order of bubble instability can be determined based on the total % area in BUR and TUR diagrams as a function of FLH. The order of bubble stability for the polymers used for this study is LDPE > LLDPE > LmPE. Lowering FLH stabilized the bubble for LmPEs and it was found for LLDPE that there was an optimum FLH that showed the most stable regions.

The immiscibility of mPE/LDPE blends has been determined both in the crystalline and melt states using different techniques. DSC and rheological results suggest that the increase of the length of short chains in mPEs and comparable MW can promote miscibility of mPE/LDPE blends. From DSC, the LmPE/LDPE-1 and LmPE/LDPE-2 blends are immiscible whereas BmPE/LDPE-1 and BmPE/LDPE-2 blends are miscible in the crystalline state. Based on the log-additivity rule for the complex viscosity and the weighted relaxation spectra, LmPE/LDPE-1 blends are believed to be immiscible whereas BmPE/LDPE-2 blends are miscible and the miscibility is not improved by increasing temperature. The situation is not as clear for the other two blends, possibly due to partial miscibility.

The miscibility/immiscibility results are further confirmed by inline measurement during film blowing. The inline birefringence of LmPE/LDPE-1 and BmPE/LDPE-2 blends below FLH has been studied. Experimental trials showed the existence of form birefringence for LmPE/LDPE-1 blend. On the other hand, the birefringence of the BmPE/LDPE-2 blends was shown to be closely related to the blend composition, suggesting miscibility of these blends.

## 8.2. Recommendations for Future Work

- The rheological properties of the polymer melt for different PEs and their blends should be correlated to the mechanical and optical properties of the final product film.
- The compatibility of LmPE/LDPE-1 blend can be further confirmed by investigating the optical and mechanical properties of the final product.
- Since the applicability of the (stress-optical rule) SOR does not rest on fundamental physical laws, it has to be validated at least within the range of film blowing. Moreover, the constant  $C$  has to be specified for specific polymers under different temperatures in order to get more reliable stress data.
- Complement uniaxial elongational viscosity data by improving the equipment, in order to get the lower elongational rates, and by improving the technique, in order to get more reliable data.

## REFERENCES

AGASSANT, J.-F., AVENAS, P., SERGENT, J.-PH. and CARREAU, P. J. (1991). Polymer Processing: Principles and Modeling New York, Hanser Publishers.

AJJI, A. GUÈVREMONT, J. MATTEWS, R. G. and DUMOULIN, M. M. (1999). Orientation Determination Using Birefringence and Spectroscopic Techniques. SPE ANTEC'99 2361.

AJJI, A., COLE. K. C. and BEN DALI, H. (1998). Measurements of Absolute Birefringence of Biaxially Orientation Films and Sheets On-line or Off-line. SPE ANTEC'98 1534.

ALAIE, S. M. AND PAPANASTASIOU (1993). Modeling of Non-isothermal Film Blowing with Integral Constitutive Equations. Int. Polym. Process. 8, 51.

ALFREY, T. (1965). Plastics Processing and Fabrication Problems Involving Membranes and Rotational Symmetry. SPW Transactions 5, 68.

ALMO RG, GRAESSLEY WW, KRISHNAMOORTI R, LOHSE DJ, LONDONO JD, MANDELKERN L, STEHLING FC, WIGNALL, GD (1997). Macromolecules 30, 561.

ASHOK, B. K. AND CAMPBELL, G. A. (1992). Two-phase Simulation of Tubular Film Blowing of Crystalline Polymers. Int. Polym. Process. 7, 240.

AST, W. (1974). Air Cooling on Blown Film Lines. Kunststoffe 64, 146

BABEL, A. K. and CAMPBELL, G. A. (1993a). Correlating the Plastic Strain with the Properties of the Low Density Polyethylene Blown Film. J. Plastic Film & Sheeting 9, 246.

BABEL, A. K. and CAMPBELL, G. A. (1993b). Metallocene Catalysed Polyethylene in Blown Film Applications – A Comparison Between Monoextruded Blended Films and Coextruded Films. SPE ANTEC'93 444.

BABEL, A. K. and CAMPBELL, G. A. (1995). A Model Linking Process Variables to the Strength of Blown Films Produced from LDPE and LLDPE. Tappi J. 78, 199.

BEAGAN, C. M., MC NALLY G. M. and MURPHY, W. R. (1998). Metallocene Catalysed Polyethylene in Blown Film Application Between Monoextruded Blended Films and Coextruded Films. SPE ANTEC'98 511.

BEAGAN, C. M., MC NALLY G. M. and MURPHY, W. R. (1999). The Blending and Coextrusion of Metallocene Catalyzed Polyethylene in Blown Film Applications. Journal of Plastic Film & sheeting 15, 329.

BERNABEU, E. and BOIX J. M. (1996). Optical Properties of Extruded Polyethylene Thin Films Related to Anisotropy and Inhomogeneous Microstructure. Polym. Eng. Sci. 26, 1203.

BINDING, D. M. (1988). An Approximate Analysis for Contraction and Converging Flows. J. of Non-Newt. Fluid Mech. 27, 173.

BIN WADUD, S. E. and BAIRD, D. G. (1999). Rheology of Metallocene-catalyzed Polyethylenes – The effect of Branching. SPE ANTEC'99 1200.

CAIN, J. J. and DENN, M. M. (1988). Multiplicities and Instabilities in Film Blowing. Polym. Eng. Sci. **28**, 1527.

CAMPBELL, G. A. and CAO, B. (1987) J. Plastic Film and Sheeting **3**, 158.

CAMBELL, G. A. and HUANG, T. A. (1985). Deformational History of LLDPE/LDPE blends on Blown Film Equipment. Advances in Polymer Technology **5**, 181.

CAO, B., SWEENEY, P. and CAMPBELL, G. A. (1990). Viscoplastic-Elastic Modeling of Tubular Blown Film Processing. AIChE J. **36**, 420.

CAO, B., SWEENEY, P. and CAMPBELL, G. A. (1990). Simultaneous Surface and Bulk Temperature Measurement of Polyethylene during Film Blowing. J. Plastic Film and Sheeting **6**, 117.

CARREAU, P. J., DE KEE, D. and CHHABRA, R. P. (1997) Rheology of Polymeric Systems: Principle and Application New York, Hanser.

CHAI, C. K. (1999). Melt Rheology and Processability of Conventional and Metallocene Polyethylenes. SPE ANTEC'99 1210.

CHEN F., SHANKS, R. and AMARASINGHE, G. (2001). Miscibility Behavior of Metallocene Polyethylene Blends. J. of Appl. Polym. Sci. **81**, 2227.

CHO, K., LEE, B. H., HWANG, K. LEE, H. and CHOE, S. (1998). Rheological and Mechanical Properties in Polyethylene Blends. Polym. Eng. Sci. **38**, 1969.



CHOI, K., SPRUIELL, J. E. and WHITE, J. L. (1982). Orientation and Morphology of High Density Polyethylene Film Produced by the Tubular Blowing Method and Its Relationship to Process Conditions. J. Polym. Sci.: Polymer Physics Edition 20, 27.

COGSWELL, F. N. Converging Flow of Polymer Melts in Extrusion Dies (1972). Polym. Eng. Sci. 12, 64.

COGSWELL, F. N. (1994). Polymer Melt Rheology George Dodwin Limited, Abington, Cambridge.

COLLYER, A. A. and UTRACKI, L. A. (1990). Polymer Rheology and Processing England, Elsevier Science Publishers.

COVAS, J. A. and CARNEIRO, O. S. (1990). Assessing the Convergent Flow Analysis as a Technique for Characterizing the Extensional Flow of Polymer Melts. Polymer Testing 9, 181.

DEALY, J. M. and WISSBRUN, K. F. (1990) Melt Rheology and Its Role in Plastics Processing: Theory and Applications New York, Van Nostrand Reinhold.

DEBBAUT, B., GOUBLomme, A., HOMERIN, O., KOOPMANS, R., LIEMAN, D., MEISSNER, J., SCHROETER, B., RECKMANN, B., DAPONTE, T., VERSCHAEREN, P., AGASSANT, J.-F., VERGNES, B. and VENET, C. (1998). Development of High Quality LLDPE and Optimised Processing for Film Blowing. Int. Polym. Process. 13, 262.

DOUFAS, A. K. and MCHUGH, A. J. (2001). Simulation of Film Blowing Including Flow-induced crystallization. J. Rheol. 45, 1085.

DOWD, L. E. (1972). What Happens When You Cool and Draw Blown Films. SPE J. 28, 22.

FANG, Y., CARREAU, P.J., and LAFLEUR, P.G. (2003). Rheological Effects of Polyethylenes in Film Blowing. Polym. Eng. & Sci. 43, 1391.

FARBER, R. and DEALY, J. (1974). Strain History of Melt in Film Blowing. Polym. Eng. Sci. 14, 435.

FLEISSNER, M. (1988) Elongational Flow of HDPE Samples and Bubble Instability in Film Blowing Int. Polym. Process. 2, 229.

FLORY, P. J. (1969). Statistical Mechanics of Chain Molecules. Interscience New York.

FURUMIYA, A., AKANA, Y., USHIDA, Y., MASUDA, T. and NAKAJIMA, A. (1985). Relationship between Molecular Characteristics and Physical Properties of Linear Low Density Polyethylenes. Pure & Appl. Chem 57, 823.

Fuller, G. G. (1990). Optical Theometry. J. Rheol. 23, 457.

GHIJSELS, A., ENTE, J.J.S.M. and RAADSEN, J. (1990). Melt Strength Behavior of PE and its Relation to Bubble Stability in Film Blowing. Int. Polym. Process. 4, 284.

GHANEH-FARD, A., CARREAU, P. J. and LAFLEUR, P. G. (1996a). Application of Birefringence to Film Blowing. J. Plastic Film and Sheeting 12, 68.

GHANEH-FARD, A., CARREAU, P. J. and LAFLEUR, P. G. (1996b). Study of Instabilities in Film Blowing. AIChE J. 42, 1388.

GHANEH-FARD, A., CARREAU, P. J. and LAFLEUR, P. G. (1997a). On-Line Birefringence Measurement in Film Blowing of a Linear Low Density Polyethylene. Int. Polym. Process. 2, 136.

GHANEH-FARD, A., CARREAU, P. J. and LAFLEUR, P. G. (1997b). Study of Kinematics and Dynamics of Film Blowing of Different Polyethylenes. Polym. Eng. Sci. 37, 1856.

GHANEH-FARD, A. (1997c). Study of the Film Blowing Process and On-line Measurements of Birefringence. Ph.D. Dissertation Dept. Chem, Eng., École Polytechnique de Montréal, Canada.

GIBERT, M. LIU, Z. and HITT, D. J. (1997). Biaxial Orientation of Poly (Vinyl Chloride) Compounds: Interaction Between Drawing, Structure, and Properties. Polym. Eng. Sci. 37, 1858.

GRAESSLEY, W. W. (1984). Viscoelasticity and Flow of Polymer Melts and Concentrated Solutions. Physical Principles of Polymers Edited by Mark, J. E., Amerr. Chem. Soc., Wash. D. C.

GREENER, J. and EVANS, J. R. G. (1998). Uniaxial Elongational Flow of Particle-Filled Polymer Melts. J. Rheol. 42, 697.

GUPTA, R. K., METZNER, A. B. and WISSBRUN, K. F. (1982). Modeling of Polymeric Film-Blowing Processes. Polym. Eng. Sci. 22, 172.

HAN, C.D. and JOHN, M. S. (1986). Correlations of the First Normal Stress Difference with Shear Stress and of the Storage Modulus with Loss Modulus for Homopolymers. J. Appl. Polym. Sci. 32, 3809

Han, C.D., Kim, Y. J., Chuang, H.-K. and Kwack, H. (1983). Rheological Properties of Branched Low-Density Polyethylene. J. Appl. Polym. Sci. 28, 3435.

Han, C.D. and Kim, Y. W. (1974). Studies on Melt Spinning. V. Elongational Viscosity and Spinnability of Two-Phase System. J. Appl. Polym. Sci. 18, 2589.

HAN, C.D. and KWACK, H. (1983). Rheology-Processing-Property Relationships in Tubular Blown Film Extrusion. I. High-Pressure Low-Density Polyethylene J. Appl. Polym. Sci. 28, 3399.

HAN, C.D. and LEM. K. W. (1983). Polym. Eng. Rev. 2, 135.

HAN, C.D. And PARK, J. Y. (1975a). Studies on Blown Film Extrusion. I Experimental Determination of Elongational Viscosity. J. Appl. Polym. Sci. 19, 3257.

HAN, C.D. and PARK, J. Y. (1975b). Studies on Blown Film Extrusion. II. Analysis of the Deformation and Heat Transfer Process. J. Appl. Polym. Sci. 19, 3277.

HAN, C.D. and PARK, J. Y (1975c). Studies on Blown Film Extrusion. III. Bubble Instability. J. Appl. Polym. Sci. 19, 3291.

HAN, C.D and SHETTY, R. (1977). Flow Instability in Tubular Film Blowing. I. Experimental Study. IEC Fundam. 16, 49.

HOPPLER, H. U., DINKEL, A. and TOMKA, I. (1995). Polymer 36, 3809.

HUANG, T. A. and CAMPBELL, G. A. (1985). Deformational History of LLDPE/LDPE blends on Blown Film Equipment. Advances in Polymer Technology 5, 181.

HUANG, T. A. and CAMPBELL, G. A. (1986). Deformational and Temperature History Comparison for LLDPE and LDPE Elements in the bubble Expansion Region of Blown Films. J. Plastic Film and Sheeting 2, 30.

IDE, Y. And WHITE, J. L. (1978). Experimental Study of Elongational Flow and Failure of Polymer Melts. J. Appl. Polym. Sci. 22, 1061.

JANESCHITZ-KRIEGL, K. (1983). Polymer Melt Rheology and Flow Birefringence Berlin, Springer-Verlag.

KANG, H. J., WHITE, J. L. and CAKMAK, M. (1990). Single and Double Bubble Tubular Film Extrusion of Polyethylene Terephthalate. Int. Polym. Process. 5, 62.

KANAI, T., KIMURA, M., and ASANO, Y. (1986). Studies on Scale-Up of Tubular Film Extrusion. SPE ANTEC'86 912.

KANAI, T. and WHITE, J. L. (1984). Kinematics, Dynamics and Stability of Tubular Film Extrusion of Various Polyethylenes Polym. Eng. Sci. 24, 1185.

KANAI, T. and WHITE, J. L. (1985). Dynamics, Heat Transfer and Structure Development in Tubular Film Extrusion of Polymer Melts. J. Polym. Eng. 5, 135.

KAINAI, T. and CAMPBELL, G. A. (1999). Film Processing Munich, Hanser Publisher.

KIM, H. C., PENDSE, A. and COLLIER, J. R. (1994). Polymer melt Lubricated Elongational Flow. J. Rheol. 38, 831.

KIM, S., FANG, Y., LAFLEUR, P. G, and CARREAU, P. J. (2004). Dynamics and Criteria for Bubble Instabilities in A Single Layer Film Blowing Extrusion. Polym. Eng. Sci. 44, 283.

KIM, S., LAFLEUR, P. G., SAMMUR, P. and MICHEL, H. A. (2003). Effects of Molecular Structure of Polyethylenes on Their Bubble Instabilities in Film Blowing Extrusion. SPE ANTEC'2003 361.

KIMURA, S. OSAKI, K. and KURATA, M. (1981). Stress Relaxation of Polybutadiene at Large Deformation. Measurement of Stress and Birefringence in Shear and Elongation. J. Polym. Sci. 19, 151.

KITANO, T. and KATAOKA, T. (1980). The Effect of the Mixing Methods on Viscous Properties of Polyethylene Melts with Fiber. Rheol. Acta 19, 753.

KOYAMA, K. and ISHIZUKA, O. (1989). Birefringence of Polyethylene Melt in Transient Elongational Flow at Constant Strain Rate. J. Polym. Sci. 27, 297.

KUIJK, E. W. TAS, P. P., and NEUTEBOOM, P. (1998). A Rheological Model for the Prediction of Polyethylene Blown Film Properties. SPE ANTEC'98 3001.

KURTZ, S. J. (1995). Relationship of Stress in Blown-film Process. Int. Polym. Process. 10, 148.

KWACK, T. H. and HAN, C. D. (1983). Rheology-Processing-Property Relationships in Tubular Blown Film Extrusion. II. Low-Pressure Low-Density Polyethylene. J. Appl. Polym. Sci. 28, 3419.

KWACK, T. H. AND HAN, C. D. (1988). Development of Crystalline Structure during Tubular Film Blowing of Low-Density Polyethylene. J. Appl. Polym. Sci. 35, 363.

LACROIX, C., GRMELA, M. and CAREAU, P. J. (1999). Morphological Evolution of Immiscible Polymer Blends in Simple Shear and Elongational Flows. J. of Non-Newt. Fluid Mech. 80, 183.

LA MANTIA, F. P. and ACIERNO, D. (1985). Influence of the Molecular Structure on the Melt Strength and Extensibility of Polyethylenes. Polym. Eng. Sci. 25, 279.

LAUN H. M. and SCHUCH, H. (1989). Transient Elongational Viscosity and Drawability of Polymer Melts. J. Rheol. 33, 119.

LAWLER, J. V., MULLER, S. J., BROWN, R. A. and ARMSTRONG, R. C (1986). LaserDoppler Velocimetry of Velocity Fields and Transitions in Viscoelastic Fluids. J. Non-Newt Fl. Mech. 20, 51.

LEE, K. Y. AND HAN, C. D. (1990) Polym. Eng. Sci. 30, 665.

LEGROS, N., GHANEH-FARD, A., COLE, K. C., AJJI, A., and DUMOULIN, M.M (1998). Tensile Properties and Orientation Evolution with Processing Conditions in Polyethylene Blown Films. SPE ANTEC'98 729.

LIU, C.-C., BOGUE, D. C. and SPRUIELL, J. E. (1995a). Tubular Film Blowing: Part 1, On-line Experimental Studies Int. Polym. Process. 10, 226.

LIU, C.-C., BOGUE, D. C. and SPRUIELL, J. E. (1995b). Tubular Film Blowing: Part 2, Theoretical Modeling. Int. Polym. Process. 10, 230.

LUO, X-L. and TANNER, R. I. (1985). A Computer Study of Film Blowing J. Polym. Sci. 25, 621.

MACKAY, M. E. and ASTARITA, G. (1997). Analysis of Entry Flow to Determine Elongational Properties Revisited. J. of Non-Newt. Fluid Mech. 70, 219.

MADDAMS, W. F. and PREDDY, J. E. (1978) X-Ray Diffraction Orientation Studies on Blown Polyethylene Films. II. Measurements on Films from a Commercial Blowing Unit. J. Appl. Polym. Sci. 22, 2739.

MARSH, R. D. L., DUNCAN, J. C. and BRISTER, S. (1995). J. Thermal Analysis 45, 891.

MAVRIDIS, H. (1998). A New High-Performance LLDPE for Blown Film Applications. SPE ANTEC'98 1006.

MEISSNER J. (1975). Basic Parameters, Melt Rheology, Processing and End-use Properties of Three Similar Low Density Polyethylene Samples Pure Appl. Chem. 42, 553.

MICHAELI, W and SCHMITZ, G. (1995). Investigation of Blown Film Extrusion Using the Laser Doppler Velocimetry. SPE ANTEC'95 181.

MICIC, P., BHATTACHARYA, S.N. and FIELD, G. (1998). Transient Elongational Viscosity of LLDPE/LDPE Blends and Its Relevance to Bubble Stability in the Film Blowing Process. Polym. Eng. Sci. 38, 1685.



MINOSHIMA, W. and WHITE, J. L. (1986). Instability Phenomena in Tubular Film, and Melt Spinning of Rheological Characterized High Density, Low Density and Linear Low Density Polyethylenes. J. of Non-Newt. Fluid Mech. 19, 275.

MACOSKO, C.W. (1994). Rheology, Principles, Measurements, and Applications VCH, USA.

MORRIS, B. A. (1998). The Effect of Coextrusion on Bubble Kinematics, Temperature Distribution and Property Development in the Blown Film Process SPE ANTEC'98 1006.

MUNSTEDT, H. and LAUN, H. M. (1979). Elongational Behavior of a Low Density Polyethylene Melt II. Transient Behavior on Constant Stretching Rate and Tensile Creep Experiments. Comparison with Shear Data. Temperature Dependence of the Elongational Properties. Rheol. Acta. 18, 492.

NAOTOVE, H. H. and SCHUT, J. H. (1993). Plastics Technology 41, 10.

OH, J. (1999). Blown Film Extrusion of LLDPE/LDPE Blends Journal of Reinforced and Composites 18, 662.

OKAMOTO, M. KOJIMA, A. and KOTAKA, T. (1998). Elongational Flow and Birefringence of Low Density Polyethylene and its Blends with Ultrahigh Molecular Weight Polyethylene. Polym. 39, 2149.

OSAKI, K. AND BESSHO, N., KOJIMOTO, T. and KURATA, M. (1979). Flow Birefringence of Polymer Solutions in Time-Dependent Field. J. Rheol. 23, 457.

PEARSON, J. R. A. and PETTRIE, C. J. S. (1970a). The Flow of a Tubular Film Part 1. Formal Mathematical Representation. J. of Fluid Mech. 40, 1.

PEARSON, J. R. A. and PETTRIE, C. J. S. (1970b). The Flow of a Tubular Film Part 2. Interpretation of the Model and Discussion of Solutions. J. of Fluid Mech. 42, 609.

PEARSON, J. R. A. and PETTRIE, C. J. S. (1970c). Plast. Polym. 38, 85.

PETRIE, C. J. S. (1973a). Memory Effects in a Non-Uniform Flow: A Study of the Behavior of a Tubular Film of Viscoelastic Fluid. Rheol. Acta 12, 8.

PETRIE, C. J. S. (1973b). Memory Effects on a Non-uniform Flow: A Study of the Behavior of a Tubular Film of Viscoelastic Fluid. Rheol. Acta 12, 92.

PETRIE, C. J. S. (1975). A Comparison of Theoretical Predictions with Published Experimental Measurements on the Blown Film Process. AICHE J. 21, 275.

RAMESH, N. S. and MALWITZ, N. (1997). Innovative Approach to Understand Metallocene Based Polyolefins and Thermoplastic Resins for Film Applications. SPE ANTEC'97 1954.

REDNER, A. S. (1998). On-line Birefringence Measurements in Production of Biaxially Oriented Polymers. SPE ANTEC'98 1598.

RYU, D. S., INOUE, T., and OSAKI, K. (1998). A birefringence study of polymer crystallization in the process of elongation of films. Polym. 39, 2515.

SEO, Y. and WISSLER, E. H. (1989). The Effect of Extrude Swell on Modeling the Film Blowing Process. Polym. Eng. Sci. 29, 722

- SHIMOMURA, Y., SPRUIELL, J. E., and WHITE, J. L. (1982). Orientation Development in the Tubular Film Extrusion of Polypropylene J. Appl. Polym. Sci. 27, 2663.
- SHROFF, R. N. and SHIDA, M. (1970). Effect of Long-Chain Branching on the Relation between Steady –Flow and Dynamic Viscosity of Polyethylene Melts. J. Polym. Sci. Part A-2, 2, 1917.
- SIMPSON, D. M. and HARRISON, I. R. (1991). The use of Deformation Rates in the Scale-Up of Polyethylene Blown Film. SPE ANTEC'91 203.
- SWEENEY, P. A. and CAMPBELL, G. A. (1992). Real Time Video Techniques in the Analysis of Blown Film Instability. Int. Polym. Process. 7, 229.
- TAKAHASHI, T. and FULLER, G. (1996). Stress Tensor Measurement Using Birefringence in Oblique Transmission. Rheol. Acta 35, 97.
- TAS, P. P. (1993). Film Blowing: from Polymer to Product. Ph.D Dissertation Dept. Mech, Eng., Eindhoven University of Technology, The Netherlands.
- TERRY, B. W. and YANG, K. (1964). A New Method for Determine Melt Density as a Function of Pressure and Temperature SPE J. 20, 540.
- UTRACKI, L. A. and GENDRON, R. (1984). Pressure Oscillation During Extrusion of Polyethylenes. II. J. Rheol. 28, 601.
- VAN AKEN, J. A. and JANESCHITZ-KRIEGL H. (1980). New Apparatus for the Simultaneous of Stresses and Flow Birefringence in Biaxial Extension of Polymer Melts. Rheol. Acta 19, 744.

VENKATRAMAN, S., OKANO, M. and NIXON, A. (1990). A Comparison of Torsional and Capillary Rheometry for Polymer Melts: the Cox-Merz Rule Revised. Polym. Eng. Sci. **30**, 308.

WHITE, J. L. and YAMANE, H. (1987). A collaborative Study of the Stability of Extrusion, Melt Spinning and Tubular Film Extrusion of Three high Density, Two Low Density and a Linear Density Polyethylene Samples. Pure Appl. Chem. **59**, 193.

WONG, C. M., SHIH, H. H. and HUANG, C. J. (1998). Effect of Various Polyethylene Structure on Film Extrusion. J. Rein. Plast. Comp. **17**, 945.

XU, J, XU, X, ZHENG, Q, FENG, L, and CHEN, W. (2002). Dynamic Rheological Behaviors of Metallocene-based ethylene-butene copolymers and their blends with low-density polyethylene. European Polymer Journal **38**, 365.

YAMANE, H., and WHITE, J. L. (1987). Simulation of Tubular Film Extrusion of Polymer Melts. Int. Polym. Process. **2**, 107.

YEOW, Y. L. (1976). Stability of Tubular Film Blow: A Model of the Film-Blowing Process. J. of Fluid Mech. **75**, 577.

ZEBROWSKI, B.E., and FULLER, G. G. (1981) J. Polym. Sci., Polym. Phys. Ed., **19**, 531.